Near field optical spectroscopy of hybrid nanoparticles for biosensor application and confocal microscopy of single silicon nanocrystals

Nayla El-Kork Kork El-

▶ **To cite this version:**

Nayla El-Kork Kork El-. Near field optical spectroscopy of hybrid nanoparticles for biosensor application and confocal microscopy of single silicon nanocrystals. Other [cond-mat.other]. Université Claude Bernard - Lyon I, 2009. English. NNT : 2009LYO10108 . tel-00692395

HAL Id: tel-00692395
https://theses.hal.science/tel-00692395

Submitted on 4 May 2012

Acknowledgement

This work has mainly taken place at the Laboratoire de Physico –Chimie des Materiaux Luminescents (LPCML), Université Claude Bernard Lyon 1, which has been successively under   direction of Mr. Christian Pedrini, and Mrs. Marie France Joubert. I am deeply thankful for   their having kindly received me even as part of the 'Big team '.

I would like to address my most sincere gratitude to Mr. Paul Moretti , for having been there all through the way, and knowing how to lift me up and encourage me , especially in the hardest moments of the work. His warm smile and personality were sometimes enough to face the bad surprises of experimental research. With him, I have realized how much a simple 'idea' can be of tremendous importance. I hope that he will find in this work the results he was hoping we would reach.

A special credit also to Mr. Bernard Jacquier, who has played a major role in the advancement, and direction of this thesis. I have learned from him the art of patience, hard work and the importance of curiosity when working with science. Through his help, I have had the rare chance work in an international research team. For this, and much more,   I am very grateful.

Half of this work   has been done within a collaboration between members of the European   Research Group NANOLUM. Through it, I have had the chance to experience working in Germany, at Chemnitz University of Technology, under the financial support of Max Plank institute. I would like to thank the persons which were responsible of offering me such a chance:

Mr. Freidrich Huisken, whose devotion, and understading   helped me go through the most difficult moments. The discussions we have had always made me realize how small we were in front of science, still it was possible for humans to try to understand, and handle it in one way or another.

Mr. Christian von Borczyskowski and his group, who received me both, at work and at heart. Not only was I amazed by the importance of the work, and immense amount of scientific research going on in his group, but I was also happily surprised to know that the human touch was one main generator beyond such advancements. I would like to express how grateful   I am, for I feel now as part of the OSMP family.

I would like to express my deep gratitude toward the members of my jury for their helpful and constructive remarks, particularly Mrs. Callard for near field optical microscopy measurements, and Mrs.Herlin , Mr. Huisken and Mr.Borczyskowski for silicon nanocrystal studies.

My experience at the Laboratoire de Physico- Chimie des Materiaux Luminescents was one of the most unforgettable ones. Thanking all the persons and staff that helped me with an advice, an explanation or even with a simple ' bonjour'…(YES it counts) would have to take another thesis by itself. This is why I refer to all the professors, researchers, and staff of LPCML when I say '. Those are invisible hands that pushed me little by little to where I am right now'.

I would also like to thank Alexandra , Cecile , Bruno and Aude for their sharing hopeful and desperate moments of SNOM tip fabrication, characterization and of course…breakage with me. Each moment was a pleasure with you guys.

I would like to wish the best of luck for the Dr.'s and Dr.'s to be which I have encountered during my journey, and which turned out to be very dear and close friends: Anna, Antoine, Bruno, Camille, Delphine, Gaelle, Hakim, Julien, Philippe, Theo, Vincent. The family is so big; I hope I have cited everyone. If not, due to a clumsiness of mine, I am sure that the reader would recognize himself (or herself).

As to my Lebanese family in Lyon (or as one of my friends had once said: the 'Lebanese contingent' in Lyon), I think they already know how important they are to me, and how much in dept I am toward them. Without them I'm sure my stay in Lyon wouldn't have been the same. Gadys, Maya, Rand, Yara, Nadine, Jinane, Rachid, Doreid, Salem, Myriam, Abbas, Rami, Ramy, Maria, Khaled, Mosaab, Mehdi, zeinab, Chawki and all the rest, thank you for being there when I needed you.

I hope the Monteil family and Zelmi acknowledge how important their help was to me during the last 5 years. I express to them with these few words my deepest sympathy.

Last but not least, come the persons who made sure I was 'good' (In all of the ways possible) 24/7, even when I childishly thought I didn't need it. My work is dedicated to these three names: Leila, Mahmoud, Iman.

General Introduction

The domains of nanoscience and nanotechnology have known in the last decades a remarkable advance in practically all the branches of science. The expectations and emergences of such a new field have been subject to important debates and controversies. For example whether scientists really do have a secure control in the manipulation of objects on such a small scale has been the cause of many interrogations. More specifically, a fear of an uncontrolled development of nanotechnology in military applications has risen from possible dangers of biological weapons and microrobots[1]. Others consider that the claims of this domain are only of speculative nature, where such an area of study is referred to in some journals as being only a scale-bound area who's lack of charisma has been fortified by 'remarkable dreams and alluring promises that spark excitement for nanotechnology[2]. However, in spite of all these fears and suspicions, one cannot deny the tremendous improvements that have taken place in many fields thanks to the advancement of this small scaled science. These include electronic applications,[3] new chemical synthesis methods,[4] and of course most importantly biological,[5,6] and medical applications. One example of medical applications is the use of nanoparticles for diagnostic and screening purposes[7].

The subject of this work will mostly deal with such kind of nanoscaled objects. Specifically, we will be interested by two kinds of nanoparticles: Chemically synthesised nanoparticles and laser pyrolised silicon nanocrystals. The first finds numerous applications in the biological domain, while the second constitutes an excellent candidate for the improvement of opto-electronic devices. We will perform our investigations with the use of new emerging optical microscopy techniques, which are the near-field optical microscopy and confocal microscopy. These tools permit us to reach such small scales

---

[1] Jurgen Altmann, "Military Uses of Nanotechnology: Perspectives and Concerns," *Security Dialogue* 35, no. 1 (Mars 1, 2004): 61-79.

[2] Cynthia Selin, "Expectations and the Emergence of Nanotechnology," *Science Technology Human Values* 32, no. 2 (Mars 1, 2007): 196-220.

[3] M.T. Bohr, "Nanotechnology goals and challenges for electronic applications," *Nanotechnology, IEEE Transactions on* 1, no. 1 (2002): 56-62.

[4] Harold H. Kung et Mayfair C. Kung, "Nanotechnology: applications and potentials for heterogeneous catalysis," *Catalysis Today* 97, no. 4 (Novembre 2004): 219-224.

[5] J M Wilkinson, "Nanotechnology applications in medicine," *Medical Device Technology* 14, no. 5 (Juin 2003): 29-31.

[6] Shuming Nie et coll., "Nanotechnology Applications in Cancer," review-article, Juillet 25, 2007, http://arjournals.annualreviews.org/doi/abs/10.1146/annurev.bioeng.9.060906.152025

[7] OV Salata, "Applications of nanoparticles in biology and medicine," *Journal of Nanobiotechnology* 2, no. 1 (2004): 3

that a global view of the nanoparticle's optical properties can be easily accessed. For the case of hybrid nanoparticles we will be specifically interested in imaging these nano-objects, comparing their properties in the near and far field, and seeing how they can be used for biological applications when used in combination with near field optical microscopy. For the silicon nanocrystals, we will be more interested in the spectroscopic properties of such nanocrystals, when they are surrounded by media having differing dielectric nature.

Our studies will be organized in this thesis in following way:

A first chapter will serve as an introduction to the concepts of near field and far field microscopy, where we present a general description of the different principles and techniques of two kinds of microscopes, that is the confocal and near field optical microscopes.

The second chapter deals with the different experimental setups and configurations which we used for our measurements, whether concerning far and near field spectroscopy, or confocal and near field imaging. It is important to understand that, unlike conventional optical microscopes, many configurations exist in Near Field Optical Microscopy, in function of the different phenomena or properties of the samples, to be studied. We will thus present a general aspect of the Omicron Twin SNOM, and its different configurations, which served us in collecting various kinds of information about hybrid nanoparticles. We have processed and characterised all of the SNOM tips we used during our measurements. A part of this chapter will thus be devoted for the presentation of such fabrication and characterisation processes. Finally, a global view on the confocal microscope which we used for the single silicon nanocrystal spectroscopy is presented in the last section.

One major chapter will then be about the main characteristics and results obtained concerning the chemically synthesized hybrid nanoparticles. Our main goal concerning these nano-hybrids was to have an idea about their emission properties, and to prove their importance as biological actors, in a near field optical aspect. This would also prove the SNOM to be an essential new tool that could play a crucial role in the detection of biological nano-composites. In fact, these fluorescent nanohybrids have been produced in such a way that their surface could be functionalized with biological elements; by

proving such a functionalisation possible through the detection of their fluorescence with the near field probe, we are able to confirm the importance of both the technique and the studied nanoparticles. But before passing to such an advanced stage, we had to individually study the luminescent properties of the nanoparticles with many differing techniques; this has been done, as exposed in the first parts of the chapter by the use of far field and near field spectroscopic studies. After having confirmed that such nanoparticles are characterised by an important amount of signal (that could be easily detected with the SNOM system that we used), we show different tests on the performance of the near field microscope itself. Investigations about the resolution which we could reach, in addition to the genuineness of the SNOM images we obtained gave encouraging results. Finally, we will show by using two different excitation configurations: On gold plots or with guided mode, how we were able to prove possible the validation of a biosensor through the use of the near field optical microscope.

In the last chapter, we deal with the emission properties of silicon nanocrystals. A lot of controversial points of views exist until now concerning the emission mechanism of such nanoparticles. Our main aim in this work was to try to have a more precise idea about the different phenomena that take place when a silicon nanoparticle emits light after its excitation. More precisely, we were interested to know whether the dielectric constant of an embedding medium, by which the nanoparticle is surrounded, would play a role in its emission properties. In order to do so, we decided to place the silicon nanocrystals in diverse media, having different dielectric constants and to study the optical response in each case. From the comparison of what we obtained, we would draw the appropriate conclusions. In order to carry such a study, a confocal microscope was an appropriate tool since it permitted the detection of signal emanating from single nanocrystals.

Table of contents

Chapter I: Far and near field microscopy

Introduction:

From the time the first optical microscope was realized by Zacharias Jansen in the years 1590, technical progress has led to a considerable amelioration of the quality and optical contrast of the images. However, four centuries later, no noticeable change had taken place concerning the functioning principle of optical microscopes. In conventional optical microscopy the sample to be studied is illuminated either by reflection or transmission and the progressive components of the diffracted light by the details of the object are collected by one or more lenses (the objective), and interfere to form the image. A principal characteristic of a microscope is its resolving power. In this chapter we will present two microscopes which we have used during our measurements: Confocal and near field optical microscopes. We will have a general idea about the working principle of each one, see the difference between near and far field measurement, and will compare between the advantages and inconvenient usually encountered by the use of both types.

I-1 Confocal microscopy:

Confocal microscopy was first introduced by Marvin Minsky in 1955 while he was a junior fellow at Harvard University.[8] His invention permitted to create sharp and more contrasted images of a specimen that would otherwise appear blurred with a conventional microscope. It was based on the idea of excluding most of the light from the specimen that is not from the microscope's focal plane. This could be done by illuminating a single point of the sample to be studied at a time, thus avoiding most of the unwanted scattered light that obscures an image when the entire specimen is illuminated at the same time; additionally, the light returning from the specimen would pass through a second pinhole aperture that would reject rays that are not directed from the focal point. The remaining desirable light rays would then be directed to the photomultiplier and the image gradually reconstructed by scanning the entire sample. The scanning of the sample can be done in two ways, either by displacing the sample, or the optical components directing the light on the sample. In his case, Minsky scanned the specimen by moving the stage rather than the light rays, by using a 60Hz solenoid to move the platform vertically and a lower frequency solenoid to move it horizontally. Confocal microscopes can collect either reflected light or stimulated fluorescence from the studied

---

[8] Marvin Minsky, "Memoir on Inventing the Confocal Scanning Microscope," *Scanning* 10 (1988): 138, 128

specimen. In the present work, we are mostly interested in the second type of measurements.

I-1.1 Principle:

The main principle of a confocal microscope can be seen in Figure I- 1. It represents a pair of lenses that focuses light from the focal point of one lens, to the focal point of the other. This can be understood by looking at the green light rays in the figure.
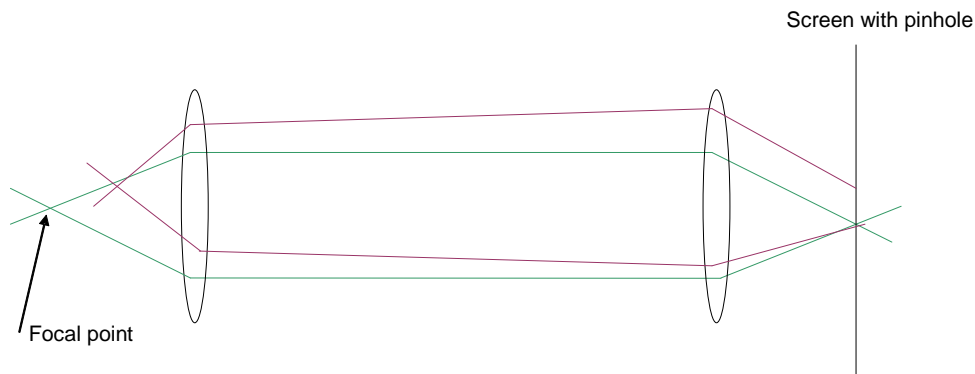
Figure I- 1 representation of two adjacent light source points in a confocal setup.

The violet lines represent light from another specimen, which is not at the focal point of the left hand side lens. The image of the violet point is not at the same position as that of the green one; in this configuration, the aim is to see only the image of the dark green point. Thus if a screen with a pinhole is placed at the other side of the lens system then all of the light from the dark point will pass through the pinhole, and the light from the violet one is out of focus. Also, most of the outside light will be blocked by the screen, resulting in an image of the violet point that will be much more attenuated compared to the green one.

Also, an additional procedure is to put a pinhole in front of the light source itself. In fact, in conventional microscopy, the whole region of the field of the view of the specimen fluoresces since it is entirely illuminated. Even thought in this configuration the highest intensity of the excitation light is at the focal point of the lens, other points of the sample get some part of this light and do fluoresce. In our case, light at a green point may include light which has been scattered from other violet points, leading to an obscuration of the samples fluorescence. To reduce this effect, the confocal microscope focuses a point of light at the in-focus green point by imaging a pinhole aperture placed in front of the light source.

11
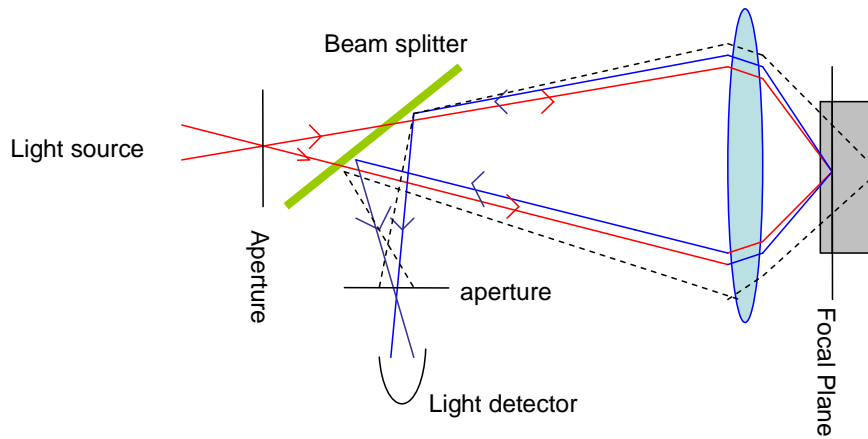
Figure I- 2 Confocal microscopy principle

Combining the two pinhole positions as in Figure I- 2 tremendously reduces the background haze that is typical of a conventional fluorescence image. These specific two points form 'conjugate points", where the focal point of the objective lens (or specimen point) forms an image where the pinhole/screen is. From such a concept stems the word 'confocal', where the pinhole is conjugate to the focal point of the lens.

II-1.2 Basic confocal setup:
A typical confocal setup is shown in Figure I-3
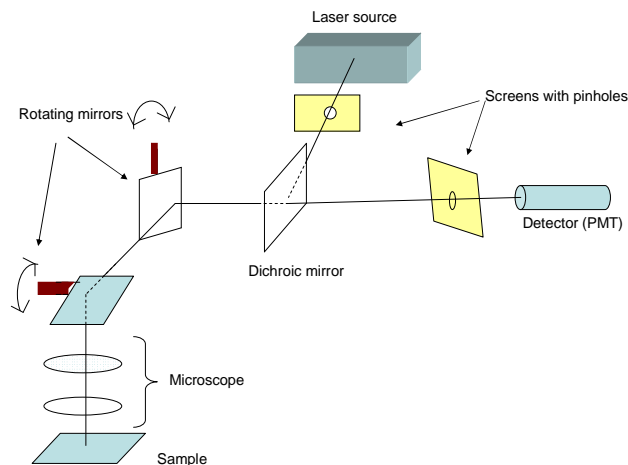
Figure I-3. Typical confocal setup

What happens is the following: first the laser provides the intense excitation light, which reflects off a dichroic mirror. Two cases of figure present themselves: The first is as presented in Figure I-3; the laser light is reflected to an assembly of motor driven scanning mirrors (horizontal and vertical). These scan the laser across the specimen and

the emitted light is descanned by the same mirrors that are used to scan the excitation light, to pass through the dichroic mirror. The light that reaches the pinhole is then detected by the sensing element, such as a photomultiplier tube. The second would function with the same principle, but instead of having moving optics that would scan the laser light over the sample, it would be the specimen itself which would be motor driven and moving under the laser excitation. The visualization of the image is finally done for both cases through the use of a computer which is connected to the detector, which builds up the image one pixel at a time.

II-1.3 Advantages and disadvantages of confocal microscopes:

Confocal microscopy offers several advantages over conventional microscopy, including the ability of controlling the depth of field, reduction of background information away from the focal plane (or degrading out of focus information), and the ability to collect serial optical sections from thick specimens; the last property permits the feasibility of an important and unique utility of the confocal microscope, which is the building of a 3-D optical rendition of the specimen. The laser scanning confocal microscope and much improved optical elements played an important role in the advancement of optical microscopy. This could be done with the use of a wider spectrum of laser light sources coupled to highly accurate accousto-optic tunable filter control and the combination of more advanced software packages with modern high performance computers. In the following we present separate elements and properties of the confocal microscope, which serve as essential evaluation points for its performances.

a- Incident light intensity:

A drawback in using light confining optical components in front of the detector significantly reduces the emission of the intensity that reaches the detector. In order to avoid such an inconvenient, special measures have to be considered: for example, a special attention must be paid for the sensitivity of the detector and its noise behavior, which are of vital importance.[9] Also, delicate measures must be taken in order to increase the number of photons arriving at the photo detector; this can be done by averaging data from many frames. But this has also the drawback of slowing the effective frame rate of the microscope.[10] In the case of fluorescence studies, another method would be to increase the number of studied fluorophores, or increase the intensity of excitation light; however the first could lead to quenching phenomena and the second to photo bleaching or even a damage of the studied specimen or a degradation of the used

---

[9] C. J. R. Sheppard, D. M. Hotton, et David Shotton, *Confocal Laser Scanning Microscopy*, 1er éd. (BIOS Scientific Publishers, 1997)

[10] Denis Semwogerere et Eric R. Weeks, "Confocal Microscopy," *Encyclopedia of Biomaterials and Biomedical Engineering* (2005): 1

fluorophore. Thus, in each of the measures to be taken, one must be careful to use the appropriate method in order to have a better signal to noise ratio concerning the signal reaching the detector.

b- Pinhole size:

Logically, decreasing the size of the pinholes in front of the detector and light source leads to an improvement of the quality of the obtained image. However, as the pinhole size is reduced, the number of photons that would arrive to the photo detector would be also much less. One would thus have to think of increasing the number of photons reaching the photo detector by employing one of the methods described in the previous section (incident light intensity). Also, previous studies have shown that optical sectioning does not improve considerably with the pinhole size below a certain limit.[11] This limit approximates the radius of the zero of the 'airy disk', which we will see in the following.

c- Resolution:

Another limitation concerning conventional microscopy is its optical resolution. In fact, as in conventional microscopy, confocal microscopy has also inherent resolution limitations due to diffraction. These depend on the wavelength of the light source and the numerical aperture of the objective lens.[12] Ideally the image of a point source is a single intense point having a radius R=0. However due to effects of diffraction, it appears in the focal plane as an 'Airy disk', whose dimensions depend on the diffraction effects (through wavelength a numerical aperture). The dimensions of these airy disks set the scale for which details can be resolved in a confocal image. The diffraction limit can be expressed by the Rayleigh criterion, a concepts which we will see in the following sections.

I-2 Rayleigh criterion and the passage from far to near field:

I-2.1 General view:

A principal characteristic of an optical microscope is its resolving power. The depth of field of a microscope permits an observation without the difficulty of the variations of height in the order of $\lambda/10$. Things become different when talking about the lateral resolution. In fact, information about lateral details of objects which are inferior to the wavelength used to illuminate the sample can be hardly picked up due to the fact that they are easily lost between the sample and the microscope's objective. It is the diffraction phenomenon which is at the origin of these effects: the fact that the image of a point is not punctual. In these conditions, the focalization of the ray of light which is originating from *a point* will be seen as *a spot* which is called Airy disk, whose dimensions are in the best of case of the order of the wavelength (Figure I- 4).

---

[11] James Pawley, *Handbook of Biological Confocal Microscopy*, 2 éd. (Springer, 1995)

[12] Shinya Inoué et Kenneth R. Spring, *Video Microscopy : The Fundamentals*, 2 éd. (Springer, 1997)
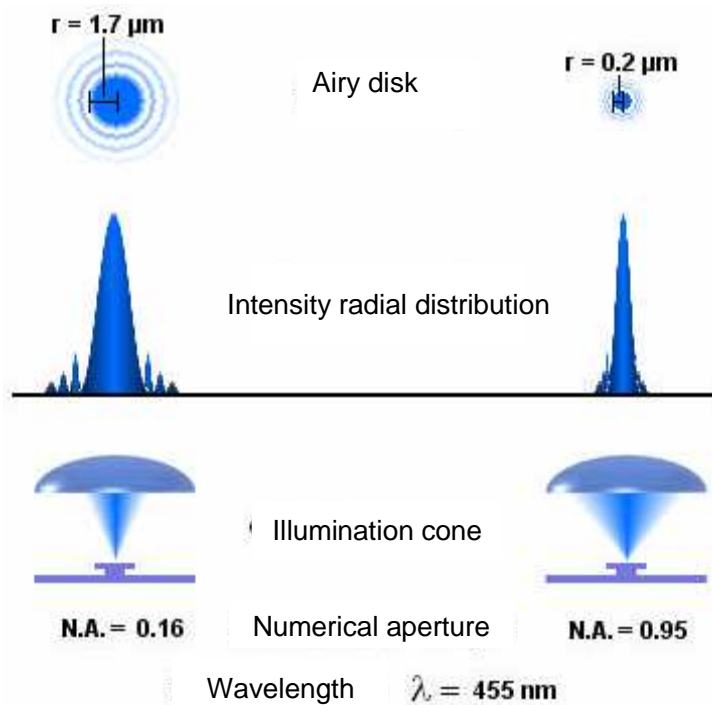
Figure I- 4 Profiles of Airy disks of one point with two microscopes having two different numerical apertures.

Even for the best optical microscope, the image of a point cannot be, but circular. In other words, if we try to observe with an optical classical microscope two points close one to another, the two airy disks will be superposed one on another, and it will not be possible to observe them directly. We can state that it is due to what we call limitation in resolution of all kinds of apparatuses which give images of objects through the use of the principle of conventional optical microscopy (Figure I- 5).
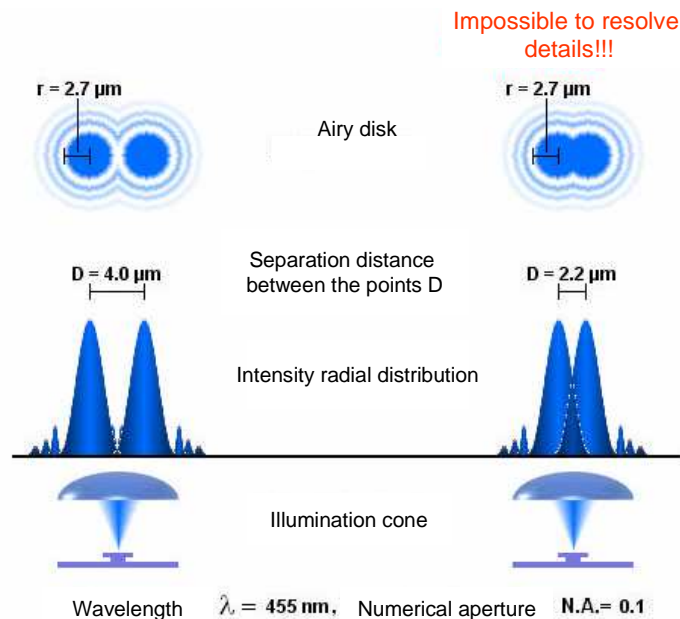
Figure I- 5 image of two points (Airy disks) through a classical microscope. The airy disks juxtapose one on the top of the other an it is impossible to distinguish them separately

In the XIXth century, the German Ernest Abbe (1873) and the English Lord Rayleight (1896) have introduced the concept known as the limit of the spatial lateral resolution due to the diffraction of light.[13] For an optical microscope which works in the visible domain for example, at 500nm the lateral resolution is approximately limited to 250 nm. This can be summarized in the following formula:

$$\Delta x = \frac{0.61\lambda}{n\sin(u)}$$

Where:

* λ is the wavelength of the exciting light

*n is the index of refraction of the media surrounding the optical system

*u is the opening at half angle of the objective, nsin(u) is called the numerical aperture (N; A) of the objective and characterizes the maximal half angle under which the object can be observed under the objective.

∗ Δx represents the minimal distance between two points which can still be seen as separated in the image space, this is the resolution of the microscope.

Thus, in far field optical imaging, the object is observed by an objective having a numerical aperture N.A. Consequently, only the components of the field whose wave vector $\vec{k}$ is inside the cone described by the N.A can reach the detector. In other words, the condition for the detection of a spatial frequency $\vec{k}$ can be expressed by the following relationship:

$$\sin(\vec{z},\vec{k}) \le NA$$

Such a relationship shows that the high spatial frequency waves whose direction of propagation falls outside the observation cone, and those with highest frequencies, which are evanescent across the observation direction z are not contained in the spectrum of spatial frequencies collected by the objective.

---

[13] Max Born et Emil Wolf, *Principles of Optics: Electromagnetic Theory of Propagation, Interference and Diffraction of Light*, 6 éd. (Cambridge University Press, 1997)

I-2.2 Mathematical approach to the limit of lateral resolution:

In this paragraph, we will show through the use of Fourier transforms that whatever the object we are observing under the microscope, we will never be able to observe details which are smaller than half the wavelength used to excite it with a classical far field microscope, and that there can be a loss of information concerning the specimen to be studied.

We will first consider that we are in the illumination case of the object by transmission, and that the medium by which the system is surrounded has a refractive index n=1. The plane which contains the object is the (x, y) plane and we will only consider objects which are homogeneous in the y direction. All objects have a transmittance which expresses the capacity to transmit light when they are illuminated. Such a transmittance function gives the repartition of light that is crossing the object under a uniform illumination of the considered spatial coordinate x. Also, for each spatial coordinate x of the object in the coordinate space, there can be associated a spatial frequency f_x in the frequency space, and by using the Fourier transform, it is possible to decompose the transmittance function of the object on the basis of spatial frequencies. Thus, the light collected by the microscopes objective during the formation of an image is nothing but a selection of spatial frequencies of the object, whose interval depends on the numerical aperture N.A of the microscopes objective. These spatial frequencies are converted to the spatial coordinate space by the inverse mathematical operation. These ideas can be summarized as in the following:

$$f(x) \xrightarrow{\;FT\;} \tilde{f}(k) \xrightarrow[filtration]{N.A} \tilde{g}(k) \xrightarrow{\;FT^{-1}\;} g(x)$$

Where:

$f(x)$ Is the transmittance function of the object, considered in the coordinate space.

$\tilde{f}(k)$ Is the transmittance function of the object, considered in the spatial frequency

   space.

$\tilde{g}(k)$ Is the transmittance function of the object, considered in the coordinate space after

   filtration by an objective having a numerical aperture N.A.

$g(x)$ Is the transmittance function of the object, visible through the microscope.

FT Fourrier transform operation.

FT^{-1} is the inverse Fourrier transform operation.

K=k$_x$=2πf$_x$ is the component of the wave vector according to the x direction.

We now consider an infinitely narrow luminous source along the x axis, described by the transmittance function $f(x) = \delta(x - x_0)$, which can be decomposed on the basis of spatial frequencies f_x as we indicate bellow[14]:

$$\widetilde{f}(k) = \int_{-\infty}^{+\infty} \delta(x - x_0)\exp(-ikx)dx = \exp(-ikx_0)$$

If this luminous source is observed with a classical microscope, whose objective has as opening angle $2u$, only the wave vectors $|k_x|$ which belong to the interval

$$\left[o; k_{max} = \frac{\omega}{c}\sin(u) \right]$$

are collected by the microscope, which corresponds to a spatial frequency interval $f_x \in \left[0; \frac{1}{\lambda} \right]$ (Figure I- 6)
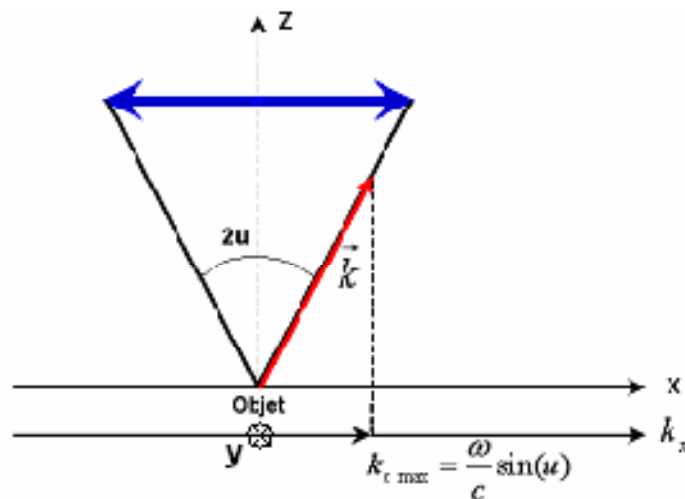
Figure I- 6: The microscope acts as a filter in the spatial frequencies which are not found in the cone of frequencies k$_{xmax}$

The constructed image by the microscope is given by:

---

[14] J. M. Vigoureux et D. Courjon, "Detection of nonradiative fields in light of the Heisenberg uncertainty principle and the Rayleigh criterion," *Applied Optics* 31, no. 16 (Juin 1, 1992): 3170-3177

$$g(x) = \int_{-k\max}^{+k\max} \exp(-ikx_0\omega)\exp(ikx)dk = \int_{-\infty}^{+\infty} C\left(k;-\frac{\omega}{c}\sin(u);+\frac{\omega}{c}\sin(u)\right)\exp(ikx)\exp(-ikx_0)dk =$$

$$\int_{-\infty}^{+\infty} \delta(x-x_0-x')\frac{2\sin\left(\frac{\omega}{c}x'\sin(u)\right)}{x'}dx' = 2\frac{\sin(\frac{\omega(x-x_0)\sin(u)}{c})}{x-x_0}$$

where $C\left(k;-\frac{\omega}{c}\sin(u);+\frac{\omega}{c}\sin(u)\right)$ is the unit rectangle function, meaning that k takes all

the values between $-\frac{\omega}{c}\sin(u)$ and $+\frac{\omega}{c}\sin(u)$ and that on this interval, C=1.

Now, even though the source of light is infinitely narrow, it would be seen with the microscope as a principal ray of light, whose width is given by the cardinal sinus function (Figure I- 7)

$$\Delta x = \frac{2\Pi c}{\omega \sin(u)} = \frac{\lambda}{\sin(u)}$$
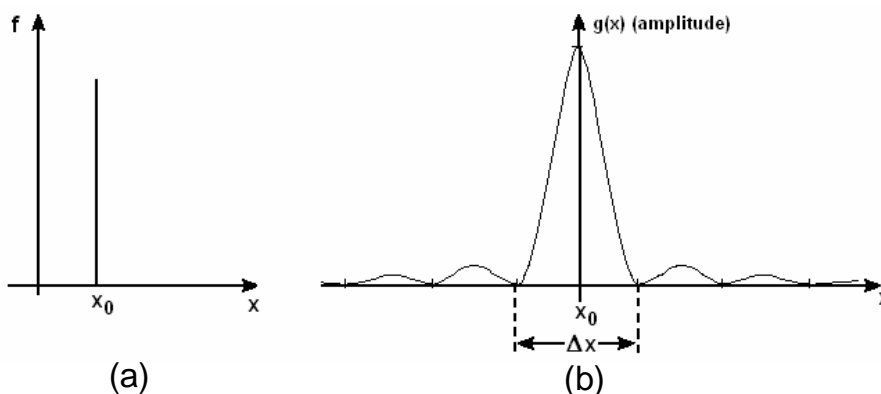
Figure I- 7 An infinitely narrow source : a) in the object space b) image of the source through the microscope

Thus, in order to distinguish two infinitely narrow sources with the optical microscope, they must be distant by at least $\lambda/2\sin(u)$ in such a way that the maximum of one would

coincide with the minimum of the other. This corresponds to Rayleigh criterion previously cited.

If we now consider an object of any shape, whose transmittance function is $f(x - x_0)$, we can obtain with the same method as the precedent one its image across the microscope:

$$g(x) = \int_{-k\max}^{+k\max} \exp(ikx) \tilde{f}(k)dk = \int_{-\infty}^{+\infty} C\left(k; \frac{-\omega}{c}\sin(u); \frac{+\omega}{c}\sin(u)\right) \exp(ikx) \tilde{f}(k)dk$$

$$= \int_{-\infty}^{+\infty} f(x - x') \frac{2\sin\left(\frac{\omega}{c}x'\sin(u)\right)}{x'} dx'$$

The last result is a convolution product, and one of its properties is that the width of the product can not be less than the width of each of its functions. In other words, if L is the width of the object, then the width of the image g of the object is:

$$\Delta x \geq \max\left(\frac{\lambda}{\sin(u)}, L\right)$$

Thus, the width of the image of the object can not be inferior to λ/sin(u). If however, the width L of the object is inferior to λ/sin(u), then this width is not restored by the image. We can now understand why there exists a limit in the lateral resolution that is intrinsic to each microscope, and that the sub-wavelength information of the object to be observed is lost in the propagation of light (filtered in function of its numerical aperture).

I-2.3 Diffraction of light across an aperture:

In order to understand where the loss of information is coming from while observing an object with classical imaging techniques, we propose to look at the evolution of the diffraction figure, on a screen, of a monochromatic plane wave with a normal incidence on an aperture, when we diminish the width L on this last(Figure I- 8). [15]

---

[15] J.M Vigoureux, "Optique et imagerie électronique: Microscopie optique à champ proche," Images de la physique (1993)
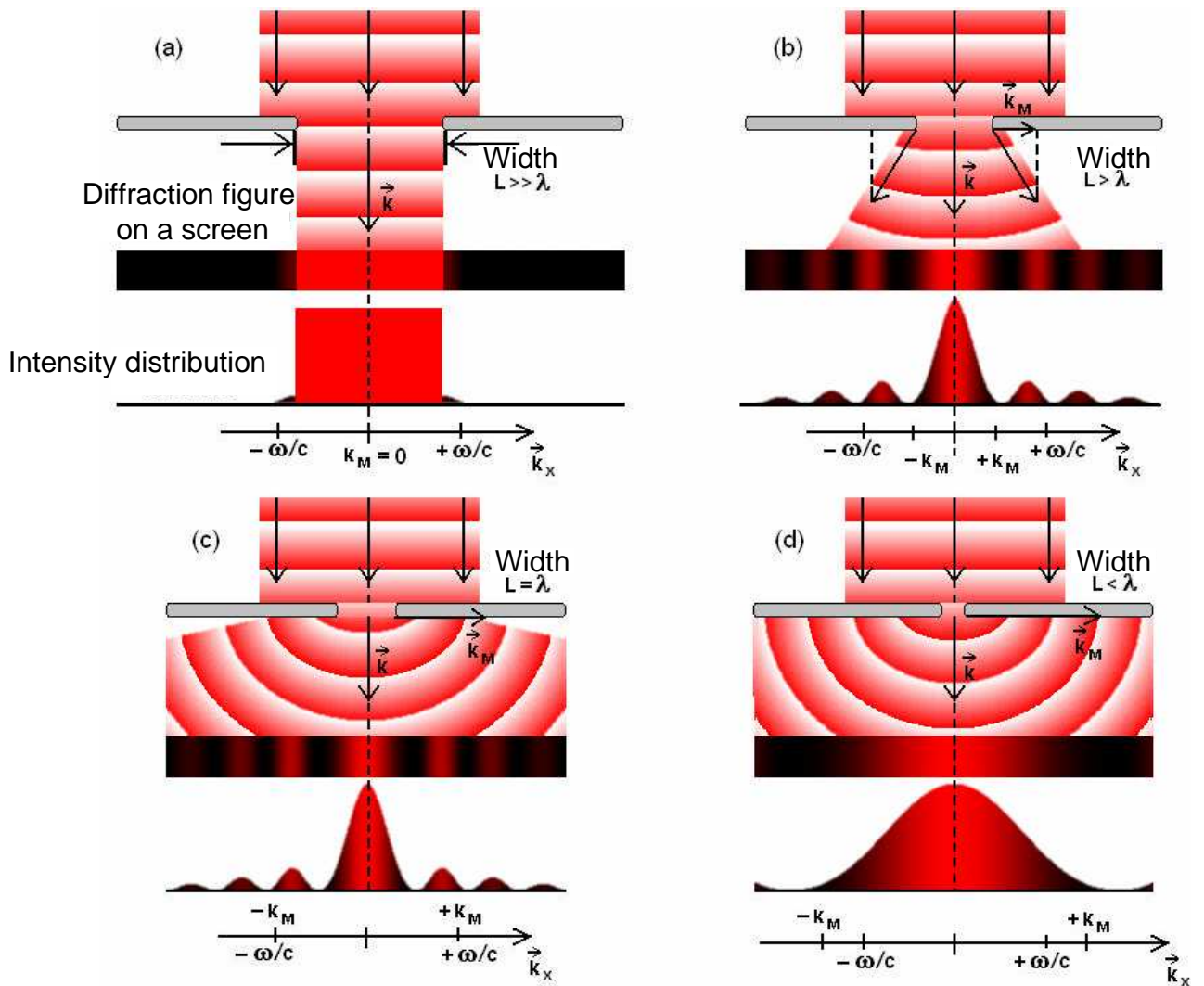
Figure I- 8 Evolution of the diffraction figure of light by a slot when the width L of the last diminishes

When the slot is wide open, light is practically not diffracted: the rays of light propagate across the slot without deviation. In the spatial frequencies space this means that the direction of the light wave vector is not modified through the passage across the slot. (Figure I- 8-a). As the width of the slot progressively diminishes, the rays of light that pass through it are more deviated (Figure I- 8 b-c). This corresponds to an augmentation of the value of the component k_x of the wave vector $\vec{k}$ of the light diffracted by the slit. Initially, when the slit is large, such a component is null; however as the width of the slot diminishes, the value of k_x increases until attaining the value of the modulous of the wave vector $k_x = |\vec{k}| = \omega/c$. Thus, there is an enlargement of the interval $[-k_M; +k_M]$ of the values of the k_x of the wave vector from $[0;0]$, for which the slit is wide open, until $[-\omega/c; +\omega/c]$ for which the width of the slit attains the value λ. Finally, if we continue to close the slits at a width which is less than the wavelength, the repartition of the light on the screen will spread in all the space; it becomes impossible to distinguish the

differences between the images for which the slit is smaller than the wavelength (Figure I-8 d). We thus understand that we lose part of the information concerning the dimensions of the slit when it is inferior to the wavelength. However, as the width of the slit diminishes less than the wavelength, the interval $[-k_M; +k_M]$ continues to grow bigger to values larger than $\left[-\omega/_c; +\omega/_c\right]$:

It has been shown through the use of Helmholtz equation[16] and the expression of an electric field $\vec{E}(x, y, z)$ characterising a monochromatic radiation of frequency ω from a light source at $z = 0$, that the field at all point at $z > 0$ can be seen as a superposition of plane waves whose wave vectors satisfy the following relationship

Equation 1

$$k^2 = k_p^2 + k_z^2 = \frac{\omega^2}{c^2}$$

Where $\vec{k}_p(k_x, k_y)$ are the coordinates of the wave vector belonging to the plane z=0, and $\vec{k}_z$ the component of the wave vector perpendicular to the (x, y) plane. Also, for a limited size object placed in an Oxy plane which can be described by a transmittance function $f(x, y, 0)$ (it can also be a reflectance, according to the chosen illumination mode), the electric field in the $z = Z > 0$ region can be proven equal to

Equation 2

$$\vec{E}(\vec{r}, Z) = \int_{-\infty}^{+\infty} \widetilde{f}(\vec{k}_p, 0) \exp(i\vec{k}_p . \vec{r} + k_z Z) d\vec{k}_p$$

Where $\widetilde{f}(\vec{k}_p, 0)$ is the bi-dimensional Fourier transform of the transmittance and $\vec{r}(x, y)$ the position vector in the z plane. From these two expressions we can see the following: At high spatial frequencies in the Oxy plane, meaning for large values of k_p, the Oz component of the wave vector can be pure imaginary $k_z = i(k_p^2 - k^2)^{1/2}$. In this case, the contribution to the electric field in the $z = Z$ plane manifests itself in a $\widetilde{f}(\vec{k}_p, 0) \exp(-i|k_z|Z)$ term which decreases exponentially along the Oz plane. Beyond a few wavelengths, the contributions of the waves to the field become negligible. These waves which propagate in the Oxy plane but decrease exponentially along the Oz axis are called the evanescent waves.

---

[16] Nathalie Landraud, *Nanostructuration optique de films sol-gel photochromiques par microscopie en champ proche*, Thèse en Doctorat de l'école polytechnique, 2002.

This is what we see in Figure I- 8-d, where as the width of the slit diminishes to attain values less than the wavelength, the interval $\left[-k_m;+k_m\right]$ will continue to grow beyond $\left[-\omega/c;+\omega/c\right]$ ($k_x > \omega/c$) thus k_z becomes imaginary, and the waves can not propagate to the screen. These waves stay confined in the neighborhood of the slit and are called the evanescent waves, which decay exponentially normally to the surface: We can not collect information concerning details which have dimensions less than the wavelength. The same kinds of waves also appear at the surface of separation between two dielectric media through the phenomena of total internal reflection. They contain all the information on the details of the slit, having dimensions inferior to λ, and constitute the near field diffracted by the slit.

As a summary, only the waves satisfying $k_p \le \dfrac{\omega}{c} = \dfrac{2\pi}{\lambda}$ can propagate. The maximal wave vector in the Oxy plane corresponding to a propagating wave is $k_p = \dfrac{\omega}{c} = \dfrac{2\pi}{\lambda}$ and the maximal frequency is $\dfrac{1}{\lambda}$. This has a fundamental consequence for teledetection imaging. Upon propagation, we lose all the information about high spatial frequencies. In other words, the fine details, or structures of $\vec{E}(x, y, 0)$ which are smaller than the wavelength of the radiation are lost during the propagation. More precisely, any optical image obtained from classical technique imaging (including confocal microscopy) cannot give details which are smaller than the wavelength (since the maximal frequency is $1/\lambda$.), since the information propagating at distances from the object are important compared with the wavelength; we say that we are collecting a 'far field'. Information about small details which are inferior to the wavelength are hidden in the evanescent waves localized in the neighborhood of the object; Thus in order to get through with such limits, one must reach for the information where it is. If we imagine a surface on which are engraved structures smaller than the wavelength, a detector placed at a small distance (from the surface) compared to the wavelength will be sensible to the evanescent waves. It will be thus sensitive to high spatial frequencies and would give images whose resolution is better than the detection wavelength. We talk in this case about near field detection.

I-3 Near field optical microscopy:

I-3.1 Breaking the diffraction limit through near field

Historically, the first ideas about near field optical microscopy techniques were proposed by the irish physicist E.H Synge, in 1928. He had proposed to use a method which consists of locally irradiating a sample with a light source, at a constant intensity, through a hole (whose dimensions are less than the light wavelength) through a perfectly opaque screen. The hole would then scan the surface of the specimen and the collection of point by point information on the properties of the sample would be done by the use of a photomultiplier tube collecting the transmitted light as we show in Figure I- 9.
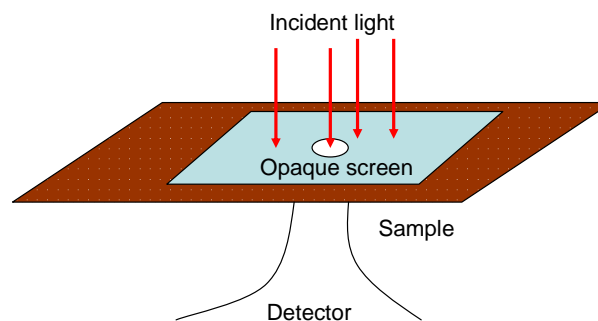
Figure I- 9 Scematic presentation of the nano source principle proposed by Synge

Such an idea has been based on the following concepts: Taking into consideration what we have discussed in the previous section, the first simple idea that would come into mind to make a near field measurement would be to place a detector so close to the surface of the sample that it would be able to collect the non propagating (evanescent) waves emitted by it. However, such a configuration cannot be easily done since it is very difficult to place a detector at such a close distance of a sample. On the other hand, we have seen in the previous section that objects having sub wavelength dimensions can transform through diffraction part of a propagating wave into an evanescent one. By applying the principle of inverse light path, sub-wavelength objects can transform an evanescent wave into a progressive one. More specifically, by placing a subwavelength hole in the near field of the sample, the evanescent waves present at its surface will be partially transformed into propagating ones, and the information which they contain will reach the detector which is placed in the far field. In this way, by getting rid of the spatial resolution limitations due to the diffraction of light, the criteria which were initially defined in conventional microscopy become obsolete. The new resolution defining the limitation parameters in this case are the dimensions of the probe and the sample-probe distance.

- In a first place it is the size (and form) of the hole, or of the subwavelength system (the probe) which will perturb the evanescent waves at the neighborhood of the object, knowing that the more the probe is small, better it will be able to 'see' the fine details of the structure present on the surface of the sample to be studied.
- The distance sample-probe plays an essential role, since as we get away from the surface of the sample, the amplitude of the evanescent waves decreases exponentially. The information that contains the finest details is most nearly confined to the surface.

The technical means which were present for Synge et Al.[17] could not allow him to put into application the ideas he developed concerning the near field. It is about 40 years later that Pohl et al.[18] proposed the first version of the near field optical microscope. Their setup consisted of a quartz tip as a nanoprobe, which was sliced, chemically attacked and metallized. The control of the distance between the sample and probe was assured by the measure of a tunneling current between the metallization and the surface of the sample. In such conditions, details reaching 25nm could be easily discerned with an illumination having 488nm as a wavelength, meaning a resolution of about $\lambda/20$, which confirmed well the Synge's theory. The improvements of such a technique took a tremendous advance from this date on, where in 1986 E.B.etzig *et al* proposed the use of a pulled and heated micropipette[19] and in 1987 that of an optical fiber[20] as a nanoprobe. With the last, we see the birth of the first optical microscope which uses an optical fiber based nanoprobe in order to collect the evanescent wave. . In the following we will present a preview of the most important configurations of aperture SNOM, in addition to their most inherent advantages and disadvantages.

I-3.2 Aperture SNOM experimental configurations

The concept of aperture SNOM materializes the idea of the nano-hole which was suggested by Synge. The role of such an optical aperture is, depending on the configuration of work, either to confine, or to collect the light on a much localized zone of the sample. Usually such an aperture is obtained by metalizing an optical fiber whose extremity has been elongated and opened, either by heating and pulling, chemical etching, or even by the combination of both methods. The final result would be a

[17] D. W. Pohl, W. Denk, et M. Lanz, "Optical stethoscopy: Image recording with resolution lambda/20," *Applied Physics Letters* 44, no. 7 (Avril 1, 1984): 651-653

[18] Ibid.

[19] E. Betzig et coll., "Near Field Scanning Optical Microscopy (NSOM): Development and Biophysical Applications," *Biophysical Journal* 49, no. 1 (Janvier 1986): 269–279

[20] E. Betzig, M. Isaacson, et A. Lewis, "Collection mode near-field scanning optical microscopy," *Applied Physics Letters* 51, no. 25 (Décembre 21, 1987): 2088-2090

homogeneously spread metallic thin film on the surface of a conically shaped optical probe, with a defect free circular aperture on the end of the fiber.

a)   b)
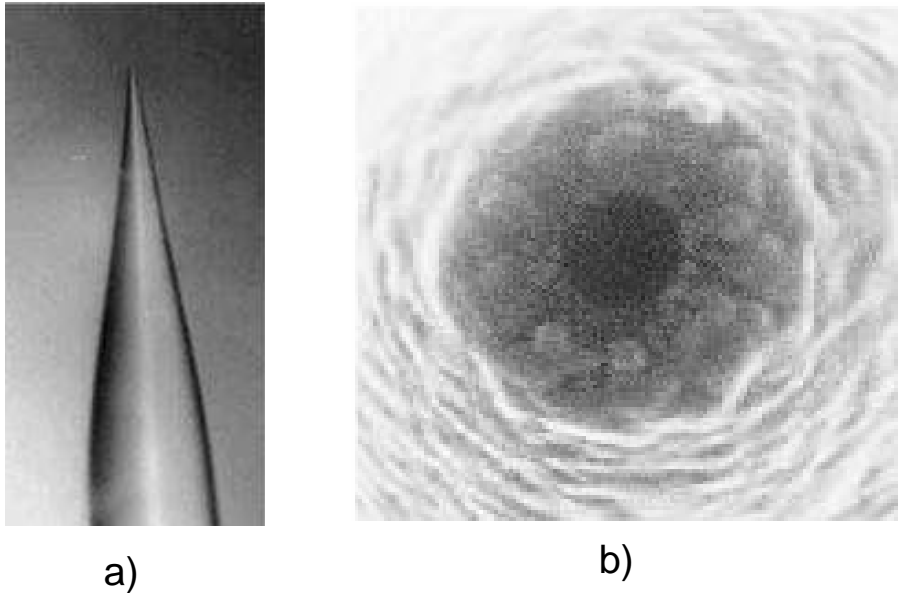
Figure I- 10Elongated metalized optical fiber : a)Fiber image b) Nano-aperture

Such a probe can be used with two different functions:

- To locally illuminate the sample and the resulting propagating wave of this interaction can be detected in the far field either in the transmission or reflection mode.
- To locally detect evanescent waves generated on the surface of the sample; the collected waves being transformed into propagating ones and sent to the other extremity of the fiber in order to be detected by a photo detector.

Thus according to these different functions, we can distinguish two types of SNOM configurations:

- The local illumination mode, where the optical fiber is used as a nanosource, and the detection of the signal containing the near field information is done either through transmission or through reflection.
- The local collection mode, where the fiber is used as a near field nanocollector, and in this case the sample is illuminated either by reflection, transmission, or total internal reflection.
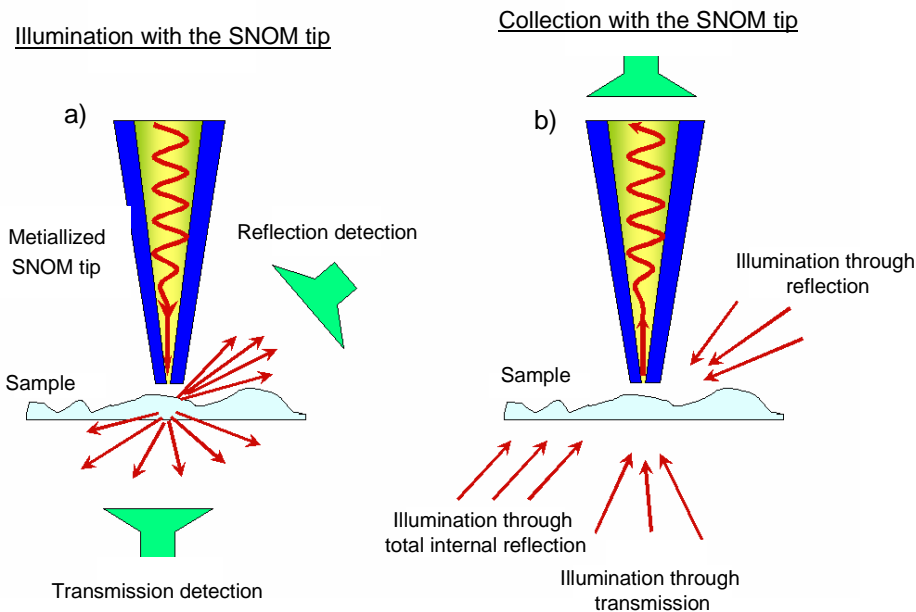
Figure I- 11 Illumination a) and collection b) mode SNOM

I-3.2 Advantages and disadvantages of SNOM measurements

As we see, near field optical microscopy reveals itself to be an essential tool for detecting near field waves, which can not be perceived with conventional microscopy. These bring much detailed information about the studied sample, with resolutions that can attain 30 to 50nm. Also, such setups have the advantage of confining either the illuminated or captured zone, thus minimizing the noise coming from diffusing light originating from adjacent zones to the studied regions. Also, the different available SNOM configurations permit to have an important diversity in the near field use, depending on the desired application, for example as in biological purposes,[21] medical applications[22] or simply fundamental research.[23]

However, as in all set ups, some inconvenient also prevail on the functioning of the apparatus. For example one must always have a special attention to the power of injected laser inside the SNOM tip. In fact, the optical power inside a metallized tip can be the cause of thermal effects which would be the reason for the breakage of the SNOM tip (by melting the metalized part), or a change of its shape and dimensions.[24] Also, due to the nature of the setup, near field methods are constrained to image surfacing. An

---

[21] T. Hartmann et coll., "A Scanning Near-field Optical Microscope (SNOM) for Biological Applications" (Kluwer Academic Publishers, 1993), ScientificCommons, http://edoc.mpg.de/318604

[22] Michael Hausmann et coll., "Imaging of human meiotic chromosomes by scanning near-field optical microscopy (SNOM)," *Micron* 34, no. 8 (Décembre 2003): 441-447

[23] H.-U. Danzebrink et coll., "Optical microscope with SNOM option for micro- and nanoanalytical investigations at low temperatures," *Applied Physics A: Materials Science & Processing* 76, no. 6 (Avril 15, 2003): 889-892

[24] B.I. Yakobson et M.A. Paesler, "Tip optics for illumination NSOM: extended-zone approach," *Ultramicroscopy* 57, no. 2-3 (Février 1995): 204-207

additional problem is that at these small distances to the sample, the interaction of the tip with the electromagnetic field can change the local field and the interpretation of the images may become difficult.[25] But most importantly, the factor that is not to be neglected at all is the difficulty in producing aperture SNOM tip which respond to reproducible geometrical characteristics, in addition to the high degree of precision which has to be always cared about in handling them. In fact, as we will see in the coming chapter, the production of a SNOM tip requires many tedious steps of fabrication and characterization, which in many of the cases do not show positive results. Also, breaking a SNOM tip can be done very easily, which gives the job a higher discouraging degree of difficulty.

I-4 Conclusion:

In this chapter, we have seen that depending on the type of application we need for optical imaging or investigation, different alternatives concerning the choice of a microscope can be considered. Confocal microscopy is a far field propagative wave type of microscopy, which eliminates any interfering background noise through the use of pinholes in front of the light source and photodetector. It is characterized by its ease of accessibility and use, in addition to a resolution which can reach the orders of about 200nm. Near field optical microscopy on the other hand is a surface based type of microscopy, whose main characteristic remains in its ability to break Rayleigh diffraction criteria and consequently resolve object which are much smaller than the wavelength of the light used to illuminate the sample. Its main disadvantage however consists of a very fragile and delicate instrumentation, which renders difficult the manipulation of such a technique. For our measurements, we decided to use confocal microscopy in order to study emission properties of silicon nanoparticles, since in this case we were more interested in the general spectroscopic behavior of nanocrystals than in their imaging. For the hybrid nanoparticles however, we used different kinds of near–field configurations, since in this case, our aim was to prove possible the use of the near field tool itself as an essential technique for biological detection and applications. Nonetheless observing the nanoparticles with both techniques appears surely of fundamental importance, since it opens the door for the discovery of new properties concerning both, hybrid nanoparticles and silicon nanocrystals.

---

[25] Ch. Lienau et coll., "Near-field scanning optical microscopy of polarization bistable laser diodes," *Applied Physics Letters* 69, no. 17 (Octobre 21, 1996): 2471-2473

Chapter II Experimental setups and configurations

Introduction

In the last decades, the studies of nanoscopic objects have been possible through the tremendous advancements achieved by technological revolutions, toward the fabrication of most concise and resolution enhancing instruments. With such innovations, many doors have been opened for investigations at small scales, like discovering the magnetic, topographic, and optical features of one and the same object. Our work mostly concerned the study of the optical properties of nanoscaled particles, placed in different sample configurations and having variable constitutions. In order to attain such a goal, and depending on the type of investigations we were undergoing, we referred to the use of two main instruments, which will be described in detail in this chapter: a commercial Omicron Twin SNOM and a home built single molecule confocal microscope.

The Omicron Twin SNOM microscope that we used helped us to have a better idea about the behaviour of the hybrid nanoparticles that we studied, and was an essential tool for confirming their important role as biosensors in the near field. Such kind of examinations have been performed at the 'nanoptec center' in Lyon, which is a common platform for nanoscale studies regrouping different equipments and groups emerging from different institutions in Lyon. As we will demonstrate it in the coming sections, the Twin SNOM has many configurations that helped us to acquire different kinds of information concerning the examined samples. We will also present detailed explanations about the fabrication and characterization of SNOM tips, which play an essential role in near field measurements.

We were able to study single silicon nanocrystals in different media, through the use of a homemade confocal microscope among the team of the OSMP (Optical spectroscopy and Molecular physics) group at Chemnitz Technical University (Germany). This microscope has been designed in such a way as to allow us to attain a resolution of about 300nm, which is suitable for the kind of samples that we fabricate for the nanoparticle studies we undergo. A detailed description of the set up will be given at the end of the chapter. However, before passing to the presentation of the microscopes, we will start by presenting the conventional far field spectrometers that we used for the preliminary studies which we performed on the hybrid nanoparticles.

II.1 Spectroscopy set up for the investigation of hybrid nanoparticles fluorescence emission

The set up used for acquiring emission spectra is as the following: An argon laser directed toward a cuvette containing the hybrid nanoparticles solution (Laser Coherent innova 300) emits (λ=488nm) at a power of few mW. A system of lenses leads the resulting fluorescence light toward the monochromator (Jobin-Yvon H25 monochromator), and the detector, a water cooled photomultiplier tube (C31034 Series Burle electron tube) to obtain the maximum collectable signal; finally, a lock in amplifier system (EG&G Princeton Applied Research (Model 5205) Lock-In Amplifier) with the accompanying chopper is used to get rid of any background signal that would interfere with the measurements. A notch filter at λ=488nm (Kaiser optical systems Hollographic Notch filter) cuts the laser light in front of the monochromator. Casually some attenuating filters are also used to prevent the photomultiplier tube from any damaging from intense light. A schematic view of the set up is presented in Figure II- 1
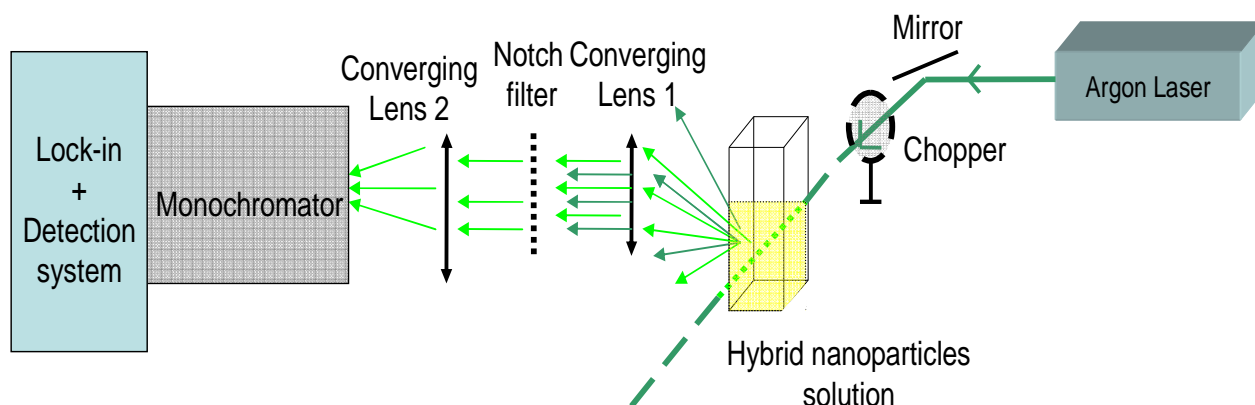
Figure II- 1Emission spectroscopy setup for nanoparticles in solution

To get more accurate results, the same setup will be used by getting rid of the solvent, with a glass plate replacing the container; more explanations will be given concerning the reasons of such a choice in the coming chapter. In order to achieve such a step, we simply replaced the cuvette by a drop of the colloidal solution that is left on a cleaned glass plate dry in the air. For a better comparison, we used the same setup as that utilized for the emission spectrum in solution; the parameter that varied however is the

geometrical shape and configuration of the sample to be studied; the following explains the reason for such change.

 In a conventional spectrophotometer setup, the detector used to collect the emitted signal from the sample is placed in front of the studied specimen, in a perpendicular direction with respect to that of the exciting laser (Figure II- 31). The laser crosses the container (which usually has a width of about 1 cm) and excites the nanoparticles. The amount of emitted fluorescence depends on the amount of absorbed light and so on the material through which the exciting laser is passing. This leads to take into consideration the Beer-Lambert law (illustrated in Figure II- 2) which is an empirical relationship that relates the absorption of light to the properties of the material through which the light is travelling, it is expressed with the following:

$A = \varepsilon \, l \, c$

 Where: ε is the molar absorptivity of the absorber.

       L is the distance that the light travels through the material (path length).

       C is the concentration of absorbing species in the material.

$A = \varepsilon \, l \, c$
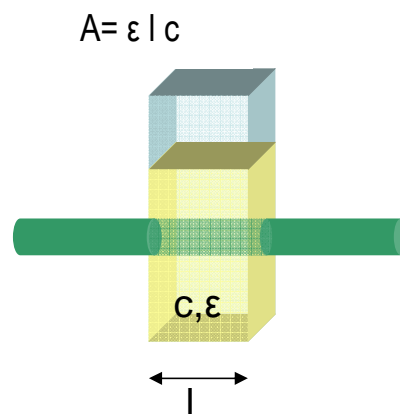
Figure II- 2   illustration for Beer-Lambert Law

In order to have a maximal signal emanating from the sample, it is of our benefit to provide the conditions for maximum absorbance. As it is not possible to have any control on the molar absorptivity of the nanoparticles, we can optimise the measurements by varying the remaining parameters i.e. the concentration of the absorbing species and the path length of the laser light.

In the case of nanoparticles dried on a glass plate, the concentration of the absorbing species (the hybrid nanoparticles) can be increased by applying several drops one over the other consecutively after their drying on the substrate. The variation of this parameter can be helpful to have a better signal, but not as essential as the remaining variable: the path length of light. In fact, many trials have been done in the beginning of the experiment to obtain fluorescence spectra, by placing several nanoparticles solution drops on the surface of the glass plate, with the substrate placed in a perpendicular position with respect to the incident beam (Figure II- 3-a); however the results weren't satisfying.

This can be explained as the following: The number of nanoparticles excited by using such a configuration is restricted in the area having the dimension of the laser spot covering the surface. Also, the path length through which the laser is in contact with the nanoparticles is infinitely small. This results into having a fluorescence signal that is too small and which cannot be used to acquire any emission spectra. We found that the solution for this problem would be to vary the position of the glass plate with respect to the incident laser beam, so that the distance travelled by the light passing through the nanoparticles would be much longer and the number of excited hybrids much more important. In order to do so, we placed the surface of the substrate (covered by the nanoparticles) parallel with respect to the direction of the incident beam (Figure II- 3-b).
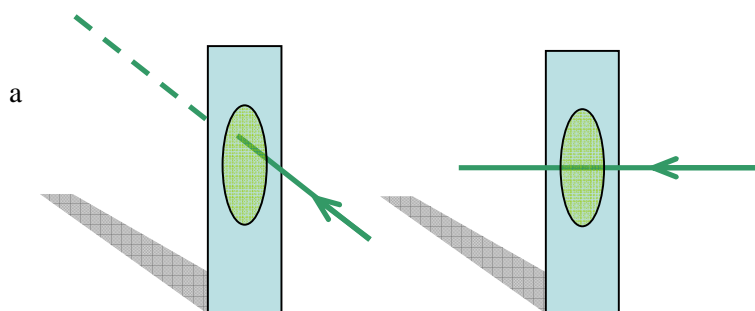
Figure II- 3 Different geometries of laser orientation with respect to a glass plate: a- perpendicular; b-Parallel

In such a configuration, the laser beam grazes the surface of the glass plate and excites the nanoparticles covering it, thus increasing the path length l by comparison with the previous geometrical situation. Such an amelioration in the system's geometry led to an increasing of the signal in such a manner that an emission spectrum of the nanoparticles on the substrate was now easily obtained; an illustration for the final setup in shown in Figure II- 4
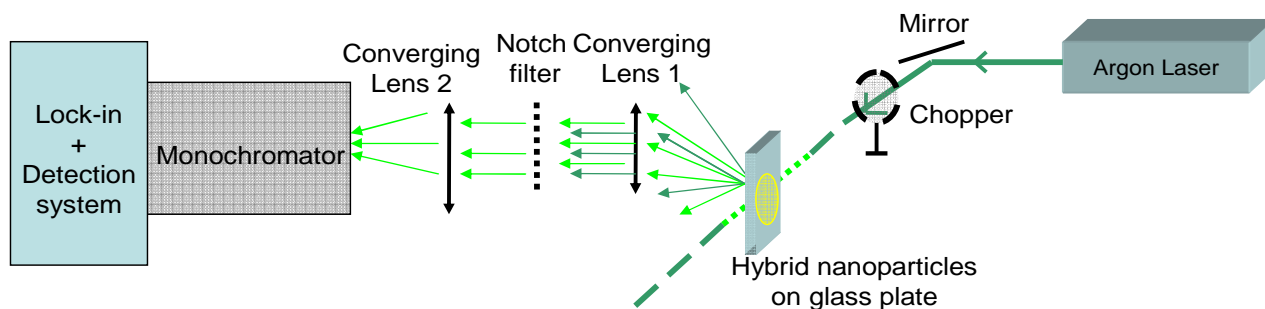
Figure II- 4Emission spectroscopy setup for nanoparticles on a glass plate

Now that we have a review about the different far field spectroscopic setups which we used, the next step would be to have a closer look on the different microscopes used in our studies, that is the confocal and near field optical microscopes.

II-2 The near filed optical microscope:

II-2.1Twin SNOM presentation:

The Near field optical microscope with which the near field studies have been pursued is a commercial Twin SNOM (Figure II- 5) conceived by the German society Omicron Vacuumphysik. It has been constructed on the platform of the classical optical microscope Zeiss Axiotech, which has been modified in order to place a rotating arm, a piezoelectric table a CCD camera and a special collection objective. In the following, we will present its basic elements and how it can be used for the study of nano-objects.
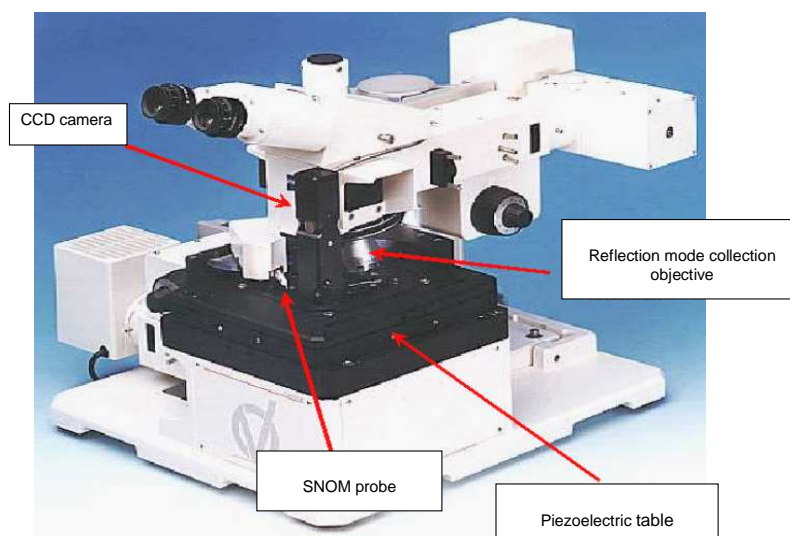
Figure II- 5 Omicron SNOM configurat

II-2.2 Basic elements of the Twin SNOM:

a) SNOM tip positioning and shear force system:

The rotating arm has been specially designed in order to fix and position the near the field probes above the sample. These probes are made either of pulled and heated or chemically etched optical fiber, having apertures at their end of the order of 150 nm
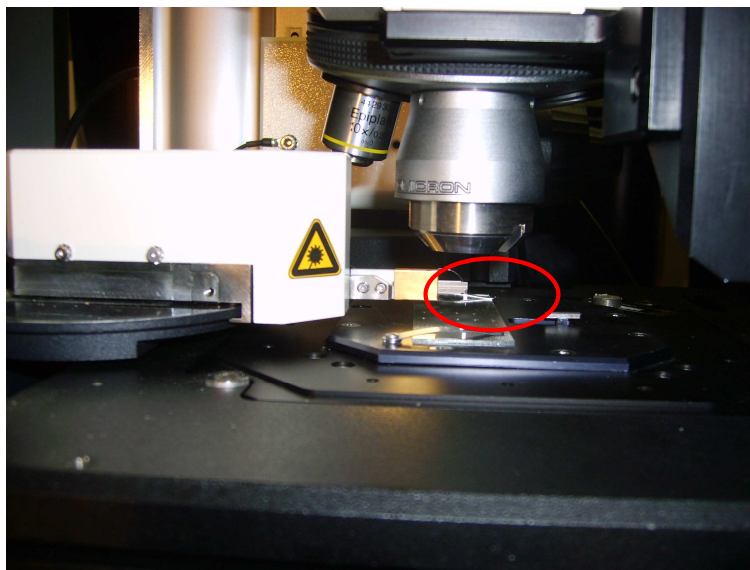
Figure II- 6SNOM tip on rotating arm

However, in NSOM, the resolution is primarily limited by the probe size and the probe to sample separation.[26] Thus, the fundamental ingredient for the imaging process is a suitable interaction between probe tip and sample to stabilize and control the tip-sample distance.[27,28] Many techniques have been studied in order to assure such a stabilized distance, ranging from the tapping mode SNOM which utilizes the attractive-mode

---

[26] E. Betzig, P. L. Finn, et J. S. Weiner, "Combined shear force and near-field scanning optical microscopy," *Applied Physics Letters* 60, no. 20 (Mai 18, 1992): 2484-2486

[27] Stefan Hoppe et coll., "Spectroscopy of the shear force interaction in scanning near-field optical microscopy," *Ultramicroscopy* 102, no. 3 (Février 2005): 221-226

[28] A. Harootunian et coll., "Super-resolution fluorescence near-field scanning optical microscopy," *Applied Physics Letters* 49, no. 11 (1986): 674-676

atomic-force microscopic (AFM) information to regulate the sample/tip distance,[29] till the shear force mode, which uses the distance-dependant shear force between a laterally oscillating optical fiber tip and the sample,[30,31] the last is what we used in our SNOM microscope. In this mode, we excite a fiber tip to vibrate laterally at its resonance frequency. Upon approaching the tip to the sample, this vibration is damped due to the shear force interaction between the tip and the surface.[32] There are many possible mechanisms for explaining such a behavior, where viscosity, Vander Waals forces, capillary forces and non-linear bending force mechanisms have been proposed.[33,34,6] Generally in such systems, changes in both the amplitude and the phase of the vibration can be measured and used as a feedback signal. Detecting this change can be done in two different ways: a first one is accomplished by focusing a laser beam on a modulated fiber-optic probe and measuring the laser spot diffracted by the probe with a split detector.[35] The signal obtained from the detector is then proportional to the vibration amplitude and can be used in a feedback loop to perform the distance control.[36] The second way is based on various non optical methods by using a standard tuning fork,[37] a piezo tube, and a piezo plate[38] etc... . However, non optical methods present obviously more advantages than the optical ones, such as preventing stray light from disturbing measurement. It is interesting to note that through this process, the movement of the tip can be also influenced by the substrate material.[39] We will present more information about the fabrication and use of the SNOM tips in the coming section of this chapter.

The coarse positioning of the tip is done through a piezoelectric system implemented within the rotating arm, which allows us to move it in x,y and z ($0.5x0.5x1cm^3$) directions, with a maximum amplitude of $0.1x0.1x1$ cm^3 .This movement is essential for the placement of the probe above the area which is desired to be scanned, just before a measurement.

[29] R. Toledo-Crow et coll., "Near-field differential scanning optical microscope with atomic force regulation," *Applied Physics Letters* 60, no. 24 (Juin 15, 1992): 2957-2959

[30] Hoppe et coll., "Spectroscopy of the shear force interaction in scanning near-field optical microscopy."

[31] Toledo-Crow et coll., "Near-field differential scanning optical microscope with atomic force regulation."

[32] A. Drabenstedt, J. Wrachtrup, et C. von Borczyskowski, "A distance regulation scheme for scanning near-field optical microscopy," *Applied Physics Letters* 68, no. 24 (Juin 10, 1996): 3497-3499

[33] Guangyi Shang et coll., "Detection of shear force with a piezoelectric bimorph cantilever for scanning near-field optical microscopy," *Surface and Interface Analysis* 32, no. 1 (2001): 289-292

[34] M. J. Gregor et coll., "Probe-surface interaction in near-field optical microscopy: The nonlinear bending force mechanism," *Applied Physics Letters* 68, no. 3 (Janvier 15, 1996): 307-309

[35] Shang et coll., "Detection of shear force with a piezoelectric bimorph cantilever for scanning near-field optical microscopy."

[36] Anatoly Shchemelinin et coll., "A simple lateral force sensing technique for near-field micropattern generation," *Review of Scientific Instruments* 64, no. 12 (Décembre 0, 1993): 3538-3541

[37] Khaled Karrai et Robert D. Grober, "Piezoelectric tip-sample distance control for near field optical microscopes," *Applied Physics Letters* 66, no. 14 (Avril 3, 1995): 1842-1844

[38] Hoppe et coll., "Spectroscopy of the shear force interaction in scanning near-field optical microscopy."

[39] Ibid.

b) The piezo electric table

The piezoelectric table (Figure II- 7) assures the control and sweeping of the samples, which are stabilized through a sample holder that is mechanically fixed on it. It is a translational table which assures a sweeping movement of about 100×100×10 µm^3 with a resolution of 1×1×1 nm^3.
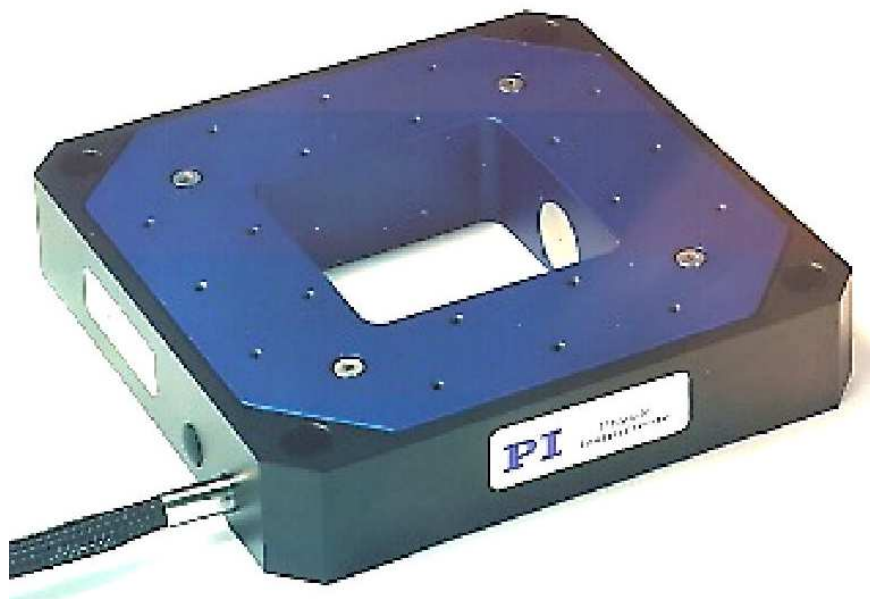
Figure II- 7 Omicron SNOM piezoelectric table

The principle on which the positioning movement of the table (and SNOM tips) takes place is the following:

The table is placed on piezoelectric plates, which are not fixed rigidly. By a smooth increase of the tension on the piezoelectric plates, the table can move in a lateral direction. The applied pulses have such a small release time (in the order of tens of microseconds), that the inertia of the table does not allow it to follow the retraction movement of the piezoelectric pates when the applied voltage is stopped. By repeating such a cycle, we obtain an important displacement in the desired direction, in a total interval of 5×5 cm^2 in the horizontal   plane.

c) The CCD camera:

The CCD camera (Figure II- 8) allows us to observe the sample and tip with a side view. This gives us the possibility to quickly approach the tip toward the sample, in the initial stage of a measurement, without running the risk of breaking it. This camera can also be used in order to optimize the quantity of light that we inject in the SNOM fiber when using it as a nanosource of light in the reflection mode SNOM configuration. It can also help us to estimate the cleanness of flat samples which we are studying, since it can reflect the image of small residues on their surface in, or verifying the injection of light through waveguides when using the implemented injection devices, while working with transparent waveguides.

Figure II- 8 A SNOM tip seen by the CCD camera

d) The collection objective:

Many collection schemes have been employed in order to gather the light emitted or reflected from samples in SNOM experiments, these can vary from detection by an objective lens, to the use of an optical fiber, or collection of the emitted light through the SNOM tip[40] (the same tip as that used for illumination[41],[42]). In our case, we referred to the use of a special ellipsoidal mirror and lenses as a collection objective, capable of

---

[40] A. Cricenti et coll., "Optical nanospectroscopy study of ion-implanted silicon and biological growth medium," *Journal of Alloys and Compounds* 362, no. 1-2 (Janvier 14, 2004): 21-25

[41] Akio Kaneta et coll., "Discrimination of local radiative and nonradiative recombination processes in an InGaN/GaN single-quantum-well structure by a time-resolved multimode scanning near-field optical microscopy," *Applied Physics Letters* 83, no. 17 (Octobre 27, 2003): 3462-3464

[42] C. Durkan et I. V. Shvets, "40 nm resolution in reflection-mode SNOM with [lambda] = 685 nm," *Ultramicroscopy* 61, no. 1-4 (Décembre 1995): 227-231

collecting the light scattered between 53° and 85°,[43] with respect to the probe axis. It is constructed in such a manner that it covers an important probe-sample area, assuring a collection of about 80% of the collected light; the tip, however should be centred at the focus point of the reflection objective in order to have such an efficient collection.
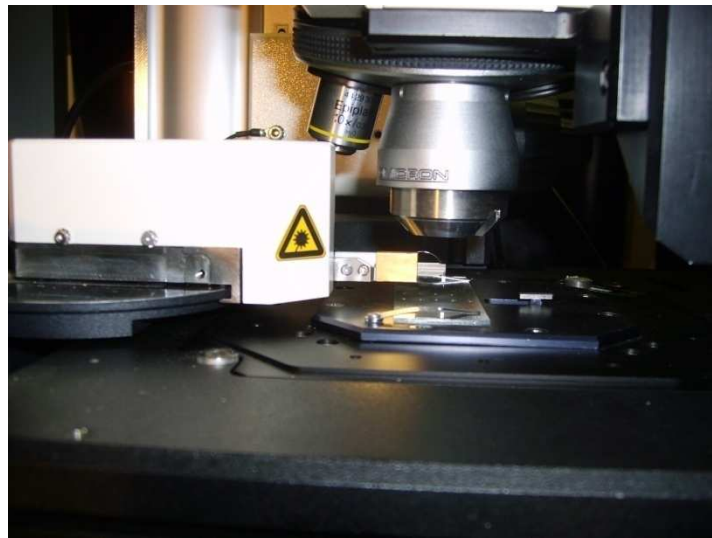
Figure II- 9 Collection objective above SNOM tip

Figure II- 10 Collection objective covering SNOM tip

---

[43] P. G. Gucciardi et M. Colocci, "Different contrast mechanisms induced by topography artifacts in near-field optical microscopy," *Applied Physics Letters* 79, no. 10 (2001): 1543-1545

II-2.3 Making a SNOM measurement:

Using these basic elements, we can start a measurement using the Twin SNOM by applying the following procedures:

After having glued a SNOM tip on the bimorphe, we place it on the rotating arm so that the SNOM system finds its resonance frequency. This is done by taking into consideration the phase shift between the detection and the excitation, and the amplitude picked up from the detection side of the piezo bimorph, with respect to the excitation frequency. This resonance frequency is used by the shear force module as a reference in order to maintain constant the distance tip-sample in a near field scan.

As a first step, the SNOM tip is approached manually from the sample (by using a special coarse position remote box, which lets us control the direction and velocity of the probe), until a very small gap is left between the end of the tip and the sample. The piezoelectric plates of the bimorph are responsible of this movement; their operation has been described in the previous section. This procedure can be monitored by looking at the CCD camera, which gives an overall view of the tip-sample situation, and is essential for preventing the tip from crashing down on the surface of the examined surface; the second step consists of placing the tip only at few nanometers away from the sample, through the use of the auto approach option of the Twin SNOM; in this case, what is happening is the following:

1) The sample is ramped toward the tip.

2) If no feedback signal is detected, the sample is retracted in one step (fine control piezo)

3) The coarse approach step motor drive moves a specified number of steps forward (1-10, selectable in the remote box settings menu). The tip moves toward the sample by this number of steps.

4) The sample is then again ramped toward the tip.

5) If no feedback signal is detected, this sequence will be repeated automatically.

6) If a feedback signal is detected, the ramp stops and the feedback loop becomes active, hence terminating the auto-approach.

Detection of the feedback means that the distance between the tip and sample surface is so small that shear force mechanism has started. We then proceed to the fine-adjusting of the vertical tip position (working with the same principle) until the gap distance is in the orders of few nanometers.

We can now proceed to a measurement, or in other words, to acquire a SNOM image, taken into account that all the optical optimizations have already been done and that the SNOM system has been well isolated from any optical or mechanical perturbation. The Twin SNOM Omicron system has been designed in such a way that during the scanning of a sample with a SNOM tip, it is not the probe that moves in the Z, X, Y-direction above the sample to collect the contained information in the near field. Indeed, the probe is kept fixed, and the piezoelectric table moves the sample under it, enabling in this way the collection of the info by the tip. Thus it is important at first to precise the area of the sample to be scanned and the velocity at which this scanning has to be done. We usually start with large frames to have a general view about the studied surface and then zoom into the desired area.

II-2.4 SNOM configurations:

Two different SNOM setups were used for the different measurements; for near field reflection mode and guided mode imaging, one SNOM was used, which we will call SNOM 1. For near field spectroscopic acquisition, a transmission mode microscope was employed which will be SNOM 2. The two used microscopes have the same working principle, but differ in some points in the optical geometry as will be seen in the following.

a) SNOM 1:

i) Reflection Mode

The imaging of nano objects has been possible to us through the use of SNOM 1, in the illumination-reflection mode. This has been applied for the visualization of nanoparticles (hybrids or Si nanocrystals) either on a glass plate, or on gold plots. Two main steps characterise such studies for each kind of nanoparticles, the first one consists of visualizing both the fluorescence and reflected light from the nanoparticles, while the second one is about collecting only the fluorescence itself. In all cases we also collected a topographical image of the sample under study. For visualizing the last, we used different notch filters depending on the wavelength of light used to excite the nanoobjects, and to cut any reflected laser reaching the detector. In all cases, topographic images accompanied the optical ones. The following figure gives a clear idea of the generally used configuration.
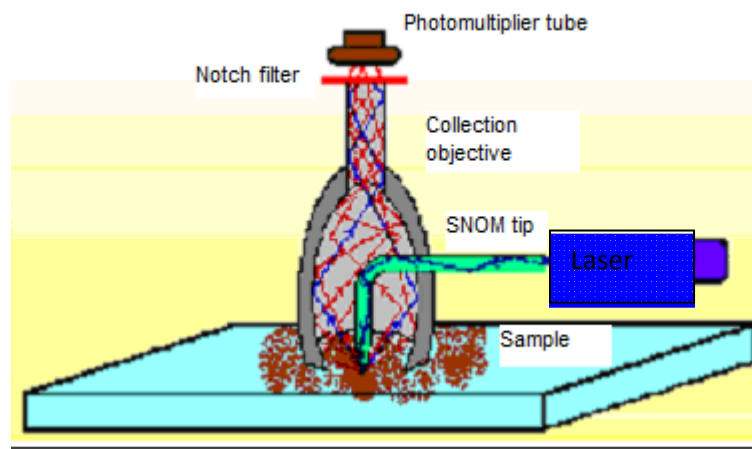
Figure II- 11 Reflection mode SNOM configuration

In Figure II- 11, the brown dots represent an ensemble of nanoparticles deposited by spin coating on a glass substrate (before deposition, the glass substrate has been thoroughly cleaned). These are excited by a laser injected in the tapered SNOM tip, which is placed just above the sample. The special collection objective previously mentioned covers the ensemble (tip-sample-nanoparticles) to gather all the light emanating from the system, and directs it through a system of lenses to the photomultiplier tube. When imaging the fluorescence of nanoparticles, special notch filters are placed in the trajectory of the collected light. The same system has been used for the excitation of the nanoparticles deposited on gold nanoplots instead of ones spread on a glass substrate. We referred to the excitation of the nanoobjects by the use of different continuous laser wavelengths. These were either at 488 nm or 514 nm and were provided by a coherent argon laser,[44] or at 633 nm whose source was a small He-Ne laser; (Melles- Griot). The injection of the laser in the optical fiber was done with a lens coupling system, where a special attention was given to keep the power of the penetrating light under a limit of about 1µW, so that the metallic layer covering the SNOM tip would not be harmed with an elevated laser power. Angular diagram measurements showed no melting effects with such a range of used power. Two types of photomultiplier tubes were used, either a small Hamamatsu Photosensor module (H7710-02 type) or a C31034 series burle type photomultiplier tube for an increased sensitivity.

---

[44] "argon laser on Coherent inc.," http://lasers.coherent.com/

ii) Guided Mode:

The setup used for the visualisation of the guided modes in near field optical microscopy has been previously implemented on SNOM 1 for the visualisation of passive waveguides, SBN photorefractive effects and LiF optical waveguides.[45],[46] The main tool consists of an added piezoelectric module (a fibre coupling system) on the piezoelectric table, capable of achieving nanometric movements in the X-Y-Z directions with a liberty of movement reaching 5x5x5 μm^2, with steps which can be varied between 40 and 400 nm. Such a coupling piece permits a perfect control of an optical fibre placed at the entry of a waveguide, thus allowing the injection and variation of injection conditions and position of a laser light inside the waveguide in question. The following Figure II- 12 gives a clearer description of the system:
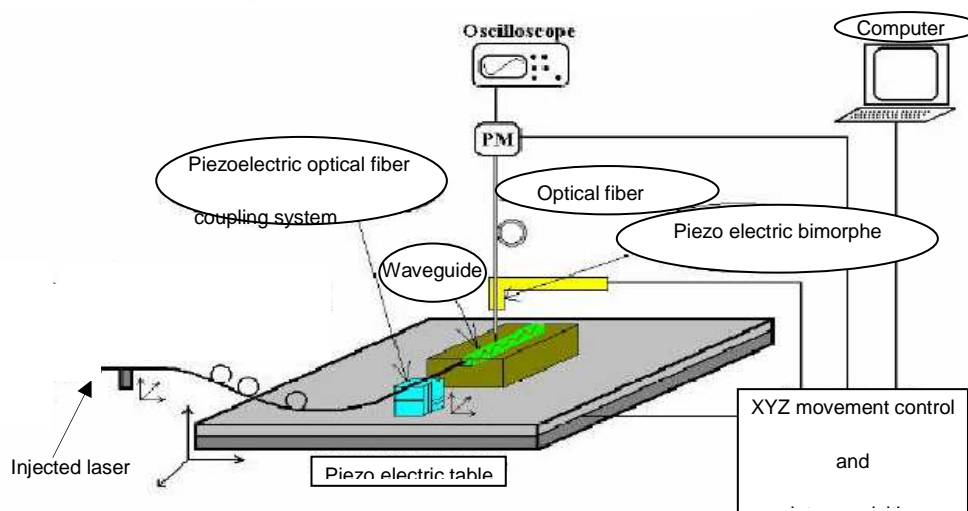
Figure II- 12 SNOM guided mode configuration

As we can see, the concept of the general functioning mode of the system is basically simple, where an injected laser light inside a fiber is coupled inside the studied waveguide through the added piezoelectric optical fiber coupling system. As the light passes through the waveguide, the evanescent field at the surface is collected with the SNOM tip (which can this time be untapered) and guided to the photomultiplier tube. The last is then connected to the SNOM data acquisition system which also is responsible of the movement control of both the SNOM tip and piezo electric table. An oscilloscope connected to the signal detector can be also used to monitor such an optical signal.

---

[45] Sergey M. Kostritskii et coll., "Leakage of a guided mode caused by static and light-induced inhomogeneities in channel HTPE-LiNbO[sub 3] waveguides," dans *Integrated Optical Devices: Fabrication and Testing*, vol. 4944 (présenté au Integrated Optical Devices: Fabrication and Testing, Brugge, Belgium: SPIE, 2003), 346-352, http://link.aip.org/link/?PSI/4944/346/1

[46] Azzedine Boudrioua et coll., "Linear and nonlinear optical properties of implanted Ca4GdO(BO3)3 planar waveguides," *Journal of the Optical Society of America B* 22, no. 10 (Octobre 1, 2005): 2192-2199

43

b) SNOM 2:

Transmission mode SNOM

We used the illumination-transmission mode SNOM for the measurement of hybrid nanoparticles emission spectra. The main setup with which this SNOM functioned is represented in the lower part of figure II-13. The functioning principle is very similar to that of the SNOM 1 reflection mode, where the same kind of metalized SNOM tip is kept at a nanometric distance from the sample to be studied with a shear force system, and illuminates it to excite the elements deposited on its surface. The collected light this time however is not reflected from the sample (gathered by using the special covering Omicron collection objective), but is instead the transmitted one. In fact, in such case the SNOM configuration has been designed in such a way that the sample is placed directly above transmission module optics (a system composed of an optical objective, cladded optical fibres, mirrors, etc...) leading the emitted light collected by these optical elements, to either the spectrometer or to the SNOM acquisition system entry. The imaging spectrometer is of Triax 180 Horiba Jobin Yvon type, while the detector is a water cooled R3310-02 Hamamatsu type photomultiplier tube. In our case, as we will explicitly show in the coming chapter, it is mostly the spectroscopic part which we will be using for our measurements. It is also of pure logic to use a substrate that is transparent for such a case of figure, in order to permit a good collection of light by the transmission module optics. This is why the substrate we used for such a configuration is a very thin cover glass on which we deposited the nanoparticles to be studied.
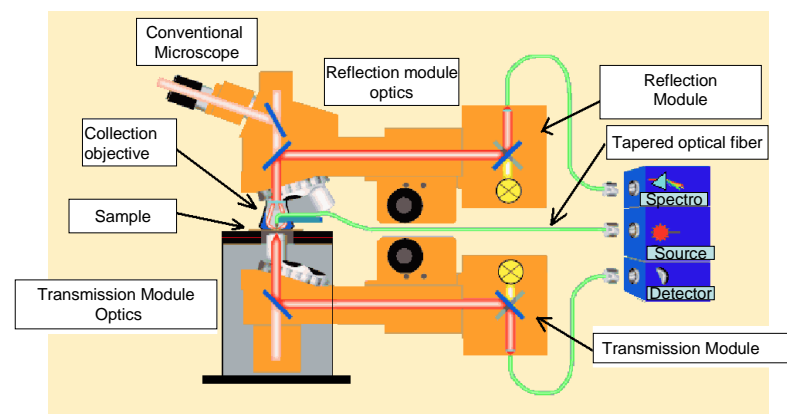
Figure II- 13 Transmission mode configuration

II-3 SNOM tip fabrication and characterisation: [1]

As already stated previously, an essential factor which plays a very important role in determining the quality and resolution of near field optical images is the influence of the tip shape, aperture and nature.[47],[48],[49] Thus, a fundamental stage of the experimental process consists in the fabrication and characterisation of the SNOM tips which would be used as probes during the near field measurements. The different processes concerning these SNOM tips can be resumed in Figure IV- 15
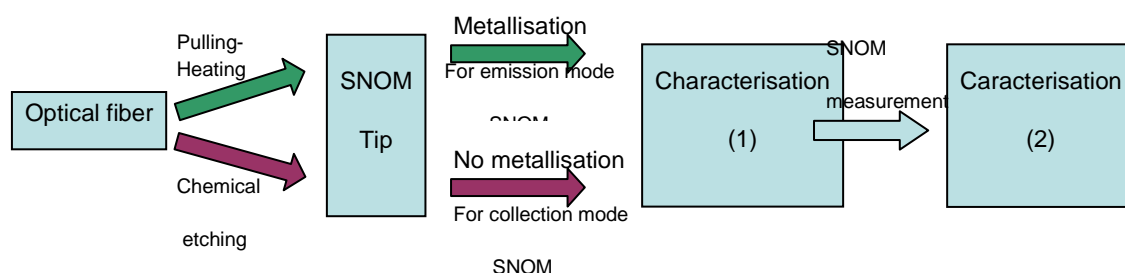
Figure II- 14 SNOM tip fabrication processes

All the SNOM images that we obtained have been collected by the use of tips which have been fabricated essentially with two different methods: The first one consists of heating and pulling standard monomode optical fibers of diameter 125 µm, and the second of using chemical etching. For SNOM measurement in the emission mode, a supplementary metallization step of the tips was found necessary in order to confine light in a very small aperture at its end; thus after fabrication of the conical end shaped tips, a second step consisted of covering them with a thin layer of aluminium (with a thickness in the order of about 80-100 nm) by using a metal evaporator. Finally, knowing that a SNOM image obtained with a truncatured probe (broken tip)[50],[51] can be subject to an important number of artefacts, we paid attention to keep track of the shape and transmission properties of each used tip, at the beginning and end of each SNOM measurement.

---

[47] O. Sqalli et coll., "Improved tip performance for scanning near-field optical microscopy by the attachment of a single gold nanoparticle," *Applied Physics Letters* 76, no. 15 (Avril 10, 2000): 2134-2136

[48] CDIV Shvets, "Reflection-mode scanning near-field optical microscopy: Influence of sample type, tip shape, and polarization of light," *Journal of Applied Physics* 83 (1998): 1171

[49] D. Barchiesi et D. Van Labeke, "A perturbative diffraction theory of a multilayer system: applications to near-field optical microscopy SNOM and STOM," *Ultramicroscopy* 57, no. 2-3 (1995): 196-203

[50] Gerd Kaupp et Andreas Herrmann, "Scanning near-field optical microscopy by near-field reflectance enhancement: a versatile and valid technique," *Journal of Physical Organic Chemistry* 12, no. 2 (1999): 141-143

[51] Gerd Kaupp, Andreas Herrmann, et Michael Haak, "Artifacts in scanning near-field optical microscopy (SNOM) due to deficient tips," *Journal of Physical Organic Chemistry* 12, no. 11 (1999): 797-807

II-3.1 Preparation techniques:

a) Heating- Pulling method:

The mechanical heating-pulling method is a tip fabrication process using a micropipette puller, the 'P-*2000 laser based micropipette puller*[52]' and an uncladded optical fiber. Such a method presents many advantages such as its being a fast and cheap technique, without any risk for the manipulator. As its name presumes, its functioning principle is thermal and mechanical: an uncladded optical fibre (of about 1cm) is held horizontally from the edges by two fixed trolleys, in front of the trajectory of a pulsed CO_2 laser beam (the laser beam is focalised on a very small point on the fibre with the help of a concave mirror). After having fixed heating-pulling parameters, such as the tension applied on the fibre, the pulling force and the power of the laser, the optical fibre is subjected to simultaneously a strong laser pulse (for about 0.1 sec) which causes its heating ,accompanied by a strong pulling at the sides due to the trolleys going apart in opposite directions. Figure II- 15 shows an illustration of the configuration used for such a process.
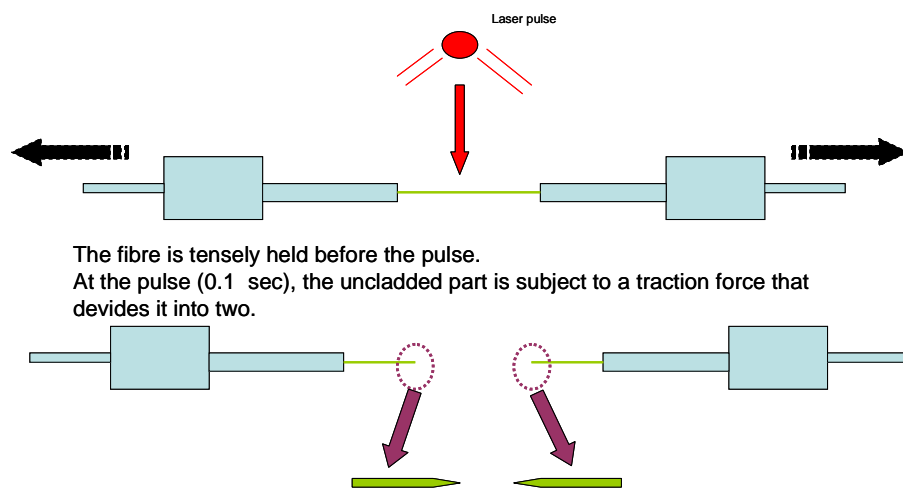
Figure II- 15 heating and pulling process illustration

The result is a sectioning of the fibre into two parts (without breaking it) where the extremities of the fiber in contact with the pulse take the form of a cone. We can also have a control on the shape and length of the SNOM tip by varying the heating and pulling parameters. In our case, the parameters we chose produced SNOM tips that had a length of about 800 μm and an aperture width of about 200 nm.

---

[52] "P-2000 | Quartz Micropipette Puller - Microelectrode Puller - Needle Puller - Fiber Puller," http://www.sutter.com/products/product_sheets/p2000.html

b) Chemical etching:

The aperture SNOM tips can also be obtained by a different mechanism than the heating and pulling which is the chemical etching.[53,54] In this case, we use the strong chemical reactivity of fluohydric acid (HF) in combination with a non-miscible solvent (oil etc..). The HF, generally concentrated between 40 % and 50 % is placed in a Teflon beaker, where we then add our solvent which will cover the whole surface of the already present liquid. An optical fibre (can be cladded or uncladded) is then vertically inserted in the beaker (Figure II- 17). At this stage of the process, we naturally see the formation of a meniscus along the dipped fibre, between the HF and the solvent. It is the physical properties of the meniscus which will 'draw' the form of the tip. The reduction of the length of the fibre, linked to its being attacked by the HF, will lead to the continuous diminution of the meniscus and so will shape the form of the fiber into a regular tip. Such a fabrication method is simple, inexpensive, but can be dangerous for the manipulator due to the use of HF. The principal experimental factors playing a role with the shape of the tip are the HF concentration, the temperature of the bath in which the system is placed, and the time in which we leave the fibres in contact with the HF acid. The principal inconvenience of such a technique lies in the fact that tips fabricated in this way usually present a rough surface due to the HF acid effect and are thus not suitable for a good metallization.
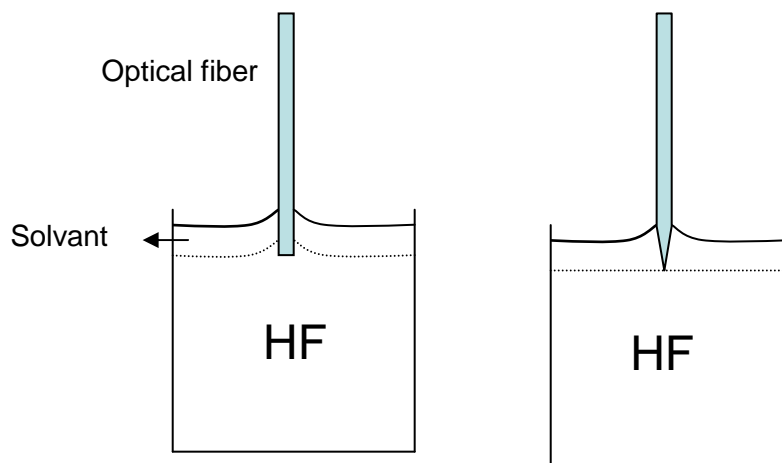
Figure II- 16 SNOM tip fabrication through chemical etching process illustration

I

[53] Yung-Hui Chuang et coll., "A simple chemical etching technique for reproducible fabrication of robust scanning near-field fiber probes," *Review of Scientific Instruments* 69, no. 2 (Février 0, 1998): 437-439
[54] Y. D. Suh et R. Zenobi, "Improved Probes for Scanning Near-Field Optical Microscopy," *Advanced Materials* 12, no. 15 (2000): 1139-1142

Figure II- 17 Chemical etching process setup. The white peaces are used as tip holder. The left handed knob is used to dip the tips down to the HF bath.

II-3.2 Metallization:

Metallization is an optional stage of the fabrication process, depending on the way of measurement that is desired to be done. In fact, moralized SNOM tips are in principle used for SNOM experiments in the emission mode; however, they also present ameliorations for SNOM imaging that can also be useful for collection mode near field optical measurements. Metallizing a SNOM tip consists of depositing a very thin layer of metal (in our case it is aluminium that is held by a layer of chrome) all over its surface.

Such a process will permit to improve the characteristics of the SNOM tip, meaning we would be having:

1) Less signal losses due to the 'covering' aluminium layer: Meaning that if used in a collection mode, such a tip would permit a better signal collection.
2) A smaller aperture, which would be leading of course to a better reached resolution.

In order to apply such a process, we referred to the use an evaporator, which is a system usually used for the formation of thin films by evaporating a substance on a flat surface. In our case, the evaporated substance was a thin aluminium film (preceded by a

chromium one) repartitioned on the whole surface of the SNOM tip. The evaporator working mechanism can be described as follows:

First an ensemble of six probes are placed in a special rotating system such that the tips would be making an inclination angle α=10° with respect to a horizontal plane as shown in Figure II-18 and Figure II-19.
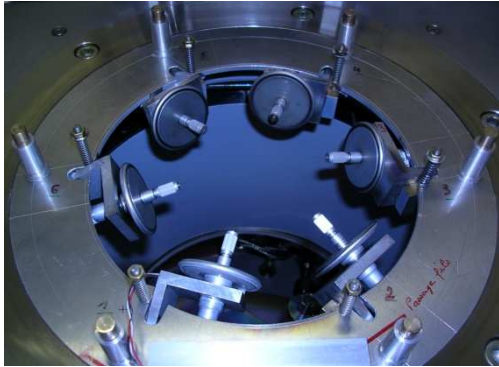
Figure II- 18 SNOM tip holders inside metalizing machine, showing a 10° inclination with respect to a horizontal line

The rotating system is then placed in the evaporator where a flux of aluminium particulates (produced with the use of heating filament acting on an aluminium pellet) covers the SNOM tips which are turning along their axis of rotation, defined by the axis of the SNOM tip itself, as see in the following figure:
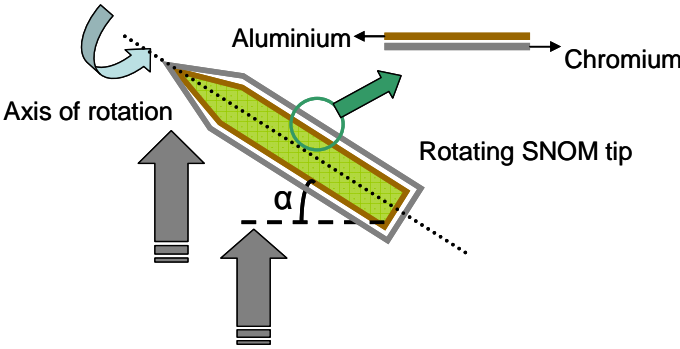
Figure II- 19 SNOM tip Metallization principle

Due to shadowing effect between the trajectory of the evaporated metal and the probe, the inclination angle α and the thickness of deposited metal define the aperture size of the SNOM tip. In general, the thickness of the chromium layer is about 8-10 nm, and that of Aluminium 80-100 nm.[55,56] These parameters are important in order to produce a good compromise between having a SNOM tip with a suitable aperture size (too much deposited metal can be the cause of an obstructed aperture) and a film thickness which would not risk any melting or damaging from laser injection (an over thin layer risks such a harm). The apertures we obtained for metalized tips after such a process have dimensions in the order of 100-150 nm, meaning that the geometry of the system helped into creating SNOM tips having apertures smaller than unmetalized ones. It is important to note however the reproducibility of such a process is not always feasible, where the percentage of success for metallization is about 30-40%.

II-3.3 Characterisation Methods:

As we previously explained, a leaking or truncated SNOM tip can be the cause of many SNOM artefacts; thus it was essential to be sure of the quality and form of the tips we used before and after our measurements, in order to have genuine image and be certain of the fact that the tip did not brake during the acquisition. To do such quality controls, we used many characterization processes depending on the stage of fabrication and experiments. These can be summarized in the following chart:
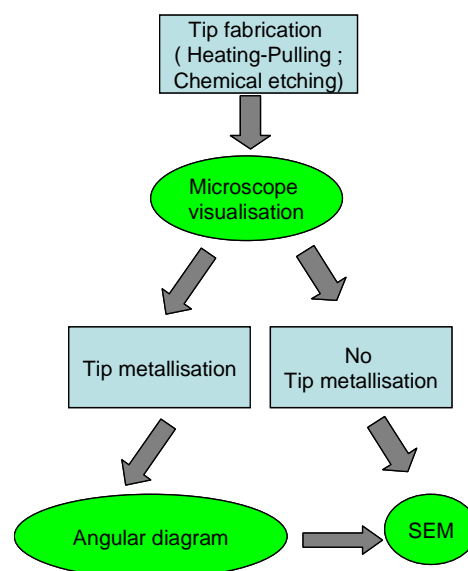
Figure II- 20 Different SNOM tip characterisation methods

[55] N. Chevalier et coll., "Aperture-size-controlled optical fiber tips for high-resolution optical microscopy," *Review of Scientific Instruments* 77, no. 6 (Juin 0, 2006): 063704-5
[56] T. Held et coll., "Method to produce high-resolution scanning near-field optical microscope probes by beveling optical fibers," *Review of Scientific Instruments* 71, no. 8 (2000): 3118-3122

A first test is done right after the fabrication of the SNOM tip (by pulling-heating method or chemical etching) simply by checking it under binoculars. If these have the right shape, they can be either metallized (mostly applied for pulled-heated SNOM tips). After metallization, we can verify pulling the spatial distribution of the light emitted by the SNOM tip by testing it with the angular diagram apparatus. If not moralized, the tip is usually directly used after looking at its shape under microscope. We finally complete our information with the SEM, however after which no SNOM measurements are possible due to the configuration of the used SEM.

a- Optical Microscope:

This optical tool which is simple by its principle and manipulation is used as a first stage in the quality control process. After having undergone a heating-pulling process, the tip is directly seen observed under the microscope. With a (X4) enhancement, we can distinguish the shape of the tip and the form of the obtained cone. The most important conditions that must be fulfilled for a good transmission and successful metallization are a continuous, regular, symmetric aspect, and a length which is about 800µm. Such criteria also play a role in the resonance frequency of the SNOM tip, which is essential for a good shear force regulation of the probe during an acquisition.
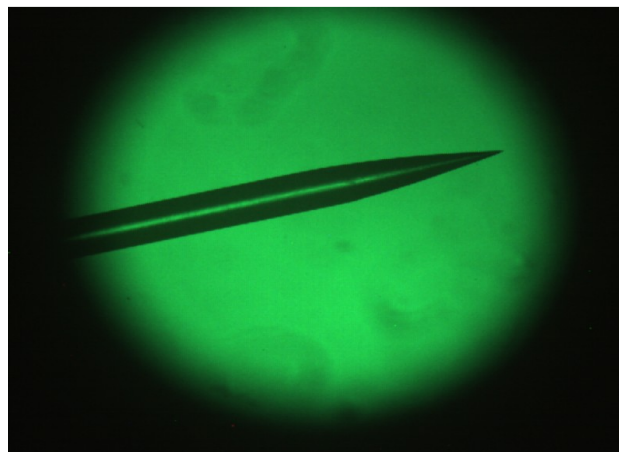
Figure II- 21 SNOM tip image under a microscope

b- Angular diagram:

By this designation, we mean to measure the spatial angular distribution of the emitted rays of light from the probe's aperture when it is penetrated by a laser. The data collected with such a kind of acquisition permit us to deduce information (which can not be obtained with a simple microscope) about the shape and morphology of the tip, in addition to an average value of the aperture's dimensions. Thus with this procedure we can know if the considered probe has a narrow aperture that could help us to attain high resolutions or if on the contrary, it has leaking along its cone that would disturb the measurements. The main setting consists of a photomultiplier tube which is fixed to a rotating arm that makes a half circle trajectory in the XY plane around a light emitted by SNOM tip that has been injected by a laser. The intensity of emitted light is then recorded as a function of the rotating angle starting from -90° till 90°. The same step is repeated after rotating the SNOM tip on itself at the angles φ of 60° and 120°.
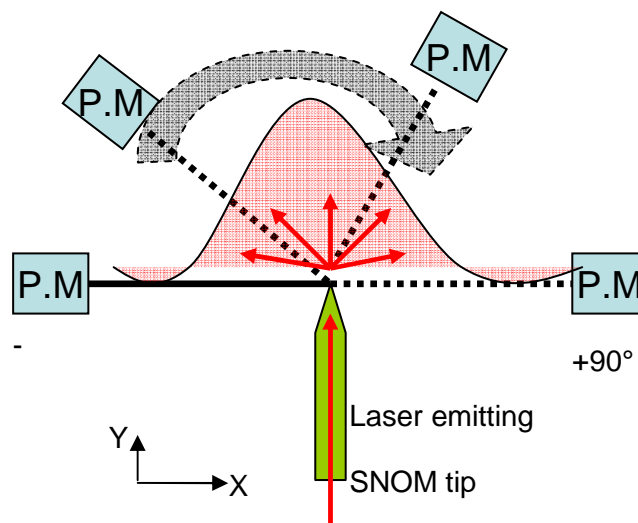
Figure II- 22 Angular diagram principle

Such a system is based on a proposition done by Karrai et al whose setting follows the same principle, but only differs in some points with the geometry[57]. Karrai had in fact found by measuring the far field angular intensity distribution L(θ) of a λ=633nm radiation transmitted through circular apertures with diameters ranging between 60 and 500 nm, that L(θ) depends sensitively on the aperture diameters down to diameter values of λ/6.

---

[57] Christian Obermuller et Khaled Karrai, "Far field characterization of diffracting circular apertures," *Applied Physics Letters* 67, no. 23 (Décembre 4, 1995): 3408-3410

Such a property was thus used to determine the optical aperture size of metal coated tapered optical fiber tips for SNOM measurements. Thus, as we see in figure Figure II- 23 the far field angular distribution of the light intensity going out from a leaking free, homogeneously circular aperture SNOM tip follows the shape of a Gaussian at the three angles of rotation φ.
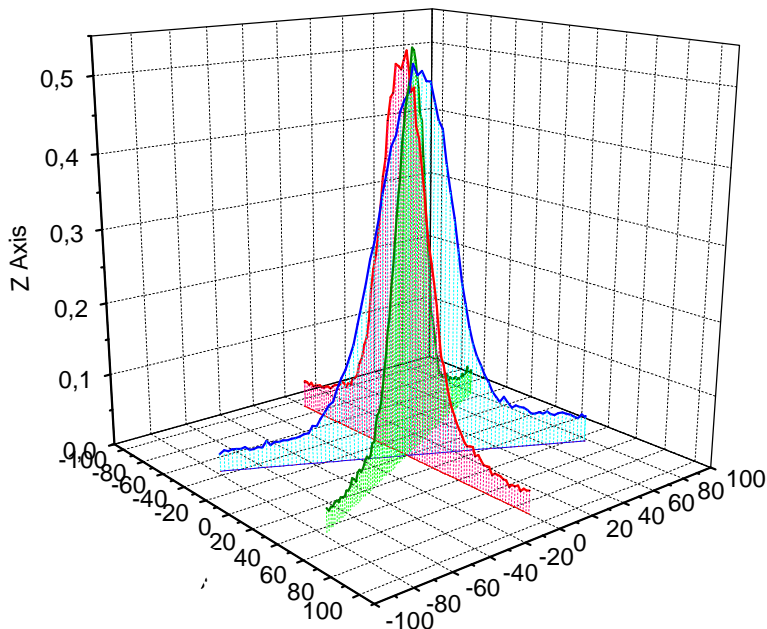
Figure II- 23 Angular diagram of a good SNOM tip

A SNOM tip having a small homogeneous circular aperture will tend to give an angular diagram in the form of a large Gaussian (having a large FWHM). By successively making SEM and angular diagram measurements and relating the results, we established an approximate correspondence between SNOM tip aperture and Gaussian FWHM obtained with our system. Thus it was possible later on to have an idea about the aperture diameter of a SNOM tip by only looking at the FWHM of the angular spectrum it gave. In the following we show a picture of the angular diagram measurements setup and its different constituting elements.
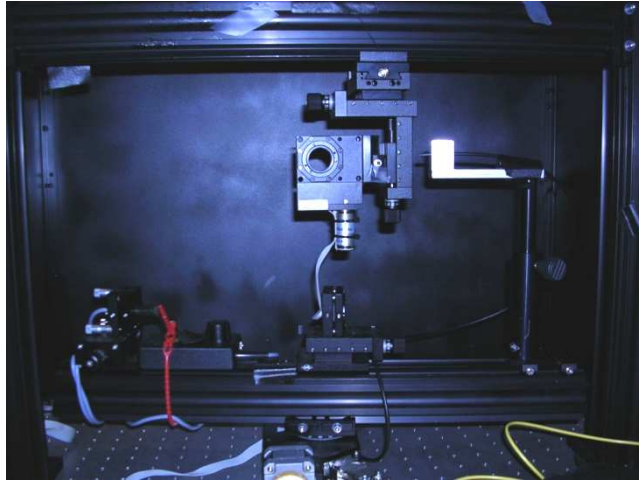
Figure II- 24 Picture of angular diagram set up

b- SEM (Scanning Electron microscope):

Scanning electron microscopy is a non optical method with which we can also control the quality and aperture diameter of the SNOM tip. In such a case, a beam of electrons scan the surface of the probe tip to be analysed, which, in response emits primary and secondary electrons. Detectors are then used to analyse these emitted electrons and to reconstruct an image of the surface. In our case, SEM measurements permits us to complete the information that we obtained by analysing the angular diagrams. In fact, through such a technique, we can have images that tell us if the SNOM tip metallization is of good quality (homogeneity, obstruction of the SNOM tip aperture,..) and if the fabrication process of the tip itself (heating-pulling or chemical etching) has been successful (state of the surface of the tip, its roughness, the shape of the end of the tip, the length, and opening angle). In the following we present an image of a SNOM tip obtained by SEM, where a diameter of about 130 nm can be clearly discerned.
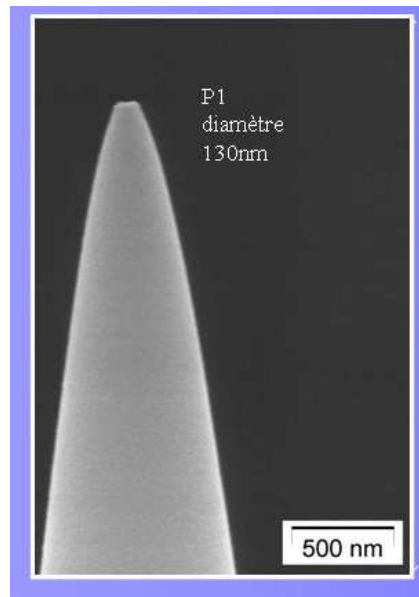
Figure II- 25SEM image of a SNOM tip

Unfortunately, due to the configuration of the S.E.M setup, the studied probe can not be used after its observation with SEM; for SNOM acquisition. However the knowledge obtained with this type of microscopy is essential for finding a correlation between angular diagram FWHM and SNOM aperture, in addition to the development and amelioration of all the necessary processes used for tip fabrication.

II-4 The confocal microscope

II-4.1 Experimental setup and technique:

The single silicon nanocrystals have been performed in a home built scanning confocal microscope in the Optical Spectroscopy and Molecular Physics group at T.U Chemnitz (Germany)[58]. All measurements took place at room temperature, and the main scheme of the set up is shown in Figure II- 26

---

[58] " Under the Supervision of Prof.Dr. C.von Borczyskowski
web site: http://www.tu-chemnitz.de/physik/OSMP/."
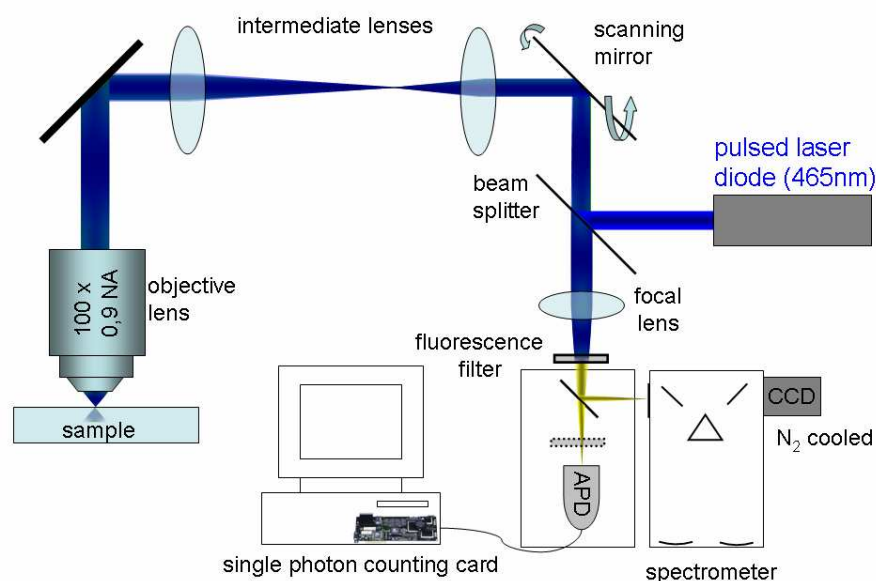
Figure II- 26 Single molecule detection confocal microscope setup scheme. (courtesy of Danny Kowerko OSMP group- TU Chemnitz)

The processes taking place during a measurement are the following:

First, a 465 nm laser beam having a power of a few micrometers (6-8 µW).is emitted from a pulsed laser diode at high frequency (about 80 MHz), A beam splitter placed in front of the laser diode directs the laser towards a scanning mirror. The role of such a mirror is to direct the beam at specific area of the studied sample and to assure its scanning while acquiring a confocal image, during a measurement. Afterwards, an intermediate system of lenses and optical elements (Beam extender, electro-optic modulator etc...) improves and focuses the light towards a 100× objective lens (Zeiss 'EC. Epiplan Neofluar) with a numerical aperture of NA ¼ 0.9.which is directly placed above the sample to be studied. After its excitation, the light emitted from the sample is collected by the same objective and is directed through the same path of the exciting laser toward the beam splitter. The transmitted signal of the beam splitter reaches the detecting system after having passed through a long pass filter '500 nm-ALP', which serves to block the laser excitation light, and a 3:1 beam splitter, which couples one part of the light into a spectrometer (Acton Research Corp. Acton-Spectra Pro-27 5') equipped with a liquid nitrogen cooled CCD camera (Princeton instruments).The other part is directed to a very low dark count rate avalanche photodiode(Perkin Elmer, SPCM-AQR-16') related to a single photon counting card, which served as a photodetector. As we will see it in the coming sections, these two types of detectors will

help us obtain two kinds of specific information about the emission of silicon nanocrystals: both the temporal and spectral behaviour.

II-4.2 Making a measurement:

Before any measurement, a perfect allignement of the optical signal must be provided. This can be done by using a calibrating sample, whose optical properties (number of photons emitted for a certain concentration of nanoparticles) are already known with such a system. Then, during a measurement, a first scan of a large area of the sample is done (the maximum full range area that can be attained is about 150 µm), however in most of the cases such important dimensions are not of an essential need, and an image of tens or few tens of micrometers can be enough (supposing of course that we are using a sample having a standard nanoparticle concentration). . An image of the scanned are is then obtained as in the following figure:

10µm

10µm
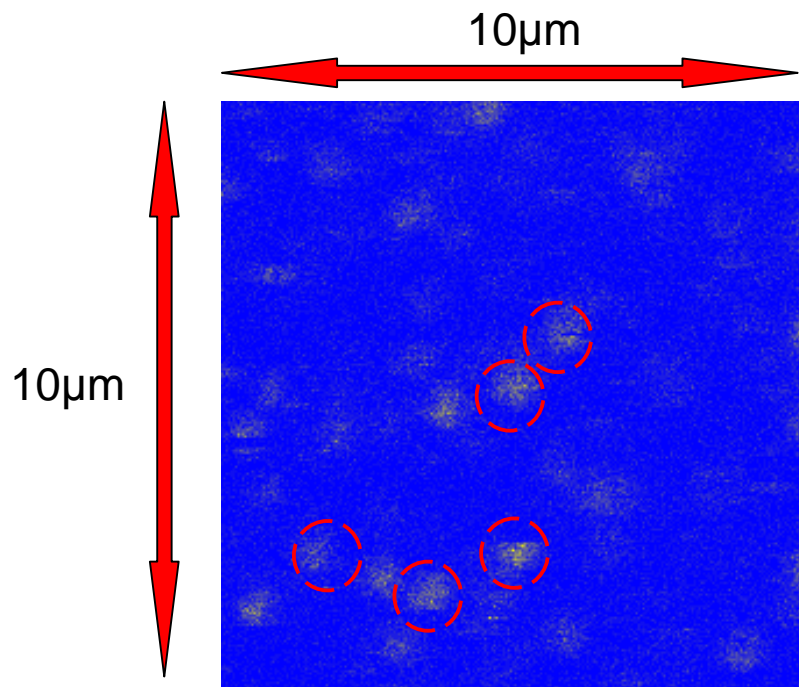
Figure II- 27 : Confocal image of a set of Silicon nanoparticles (yellow spots in red circles)

We see in Figure II- 27 a set of silicon nanocrystals (represented by the yellow spots) dispersed on the substrate. These must be well dispersed in order to be in the conditions of single nanocrystal studies (a few micrometers is on average a good separation distance). Many experimental parameters must be verified before making an acquisition measurement, such as the power of the excitation light, a good alignment of the optical system, a well focused laser light etc… The single photon counting card also can help knowing if the conditions in which we are working are optimum.We then zoom on a small

area containing the dispersed nanocrystals. A computerized control system enables (through the rotation or tilting of the scanning mirror) to direct the laser beam on one of the spotted nanoparticles (in red circles in Figure II- 27). At the time of measurement, the laser beam is focused and both a time trace and a corresponding emission spectrum of the optical response of the nanocrystal can be taken simultaneously from respectively the avalanche photodiode, and the N_2 cooled spectrometer. This can be done for a period of time which is precised by the user. Finally, both the spectrum and time trace can be recorded and analysed by using simple analysing programs such as Origin.

CHAPTER III : NEAR FIELD OPTICAL INVESTIGATION OF HYBRID NANOPARTICLES

Chapter III- Near-field optical investigation of hybrid nanoparticles

Introduction

The main subject of this chapter is a near field optical study of chemically synthesised hybrid nanoparticles, which can be, as we will prove it, perfect candidates for the confection of biological devices such as biosensors. The use of a near field optical microscope in such a situation is of essential importance, since it allows us to reach resolutions which can permit us the study of local phenomena that can not be usually attained with conventional microscopy. However, to attain such a goal, not only will we be subject to a detailed study of the nanohybrids themselves, and a search of the most appropriate steps to follow in order to have the most concise measurements; but we will also verify the eligibility of the conditions in which we are working, including the resolution we can attain with the SNOM tip and we are using, and the genuineness of the images we obtain.

The general scheme of our investigations is presented in Figure III- 1. Many characterizing preliminary studies had to be taken into account in order to assure best working conditions and an accurate analysis of the obtained final results. The sequence of acts has been taken by considering several factors at each step, including the scale in which we are working (from macroscopic to microscopic), the different characterising methods concerning the different properties of one object (optical, topographic, etc…), and of course the experimental obstacles which may present themselves during the experiment under study (an exceedingly rough surface to be studied with a fragile SNOM tip, a too low optical signal, and inappropriate excitation wavelengths).

We have chosen to start with a far field spectroscopic characterisation study of the nanoparticles presented in the form of a solution. We have begun with emission and absorption spectra of the nanoparticles in solutions, and then on a glass plate. Such experiments would permit us to have a deeper idea about the most appropriate excitation wavelength and emission spectra shape for near field investigations.

The next step is a preliminary near field study which consists mostly of the optical spectroscopic studies of the hybrids through a near field spectral examination of their emission, and a surface study of the best substrate and the best deposition method to use for optimised near field measurements (whether they are of optical or topographic nature). Finally, the last stage covers the near field measurements themselves, which were divided into three different steps. At first a near field simple visualisation of the nanoparticles dispersed on a glass substrate would permit an appropriate analysis of the conditions in which we are working: Tip resolution, near field artefacts, influence of the substrate etc… Then we will present a thorough look on use of the nanohybrids as biosensors. The different SNOM techniques enable us to detect the presence of certain composites of a medium through the use of two different biosensor configurations: a gold nanoplots biosensor and a waveguide biosensor.

Figure III- 1 General work plan
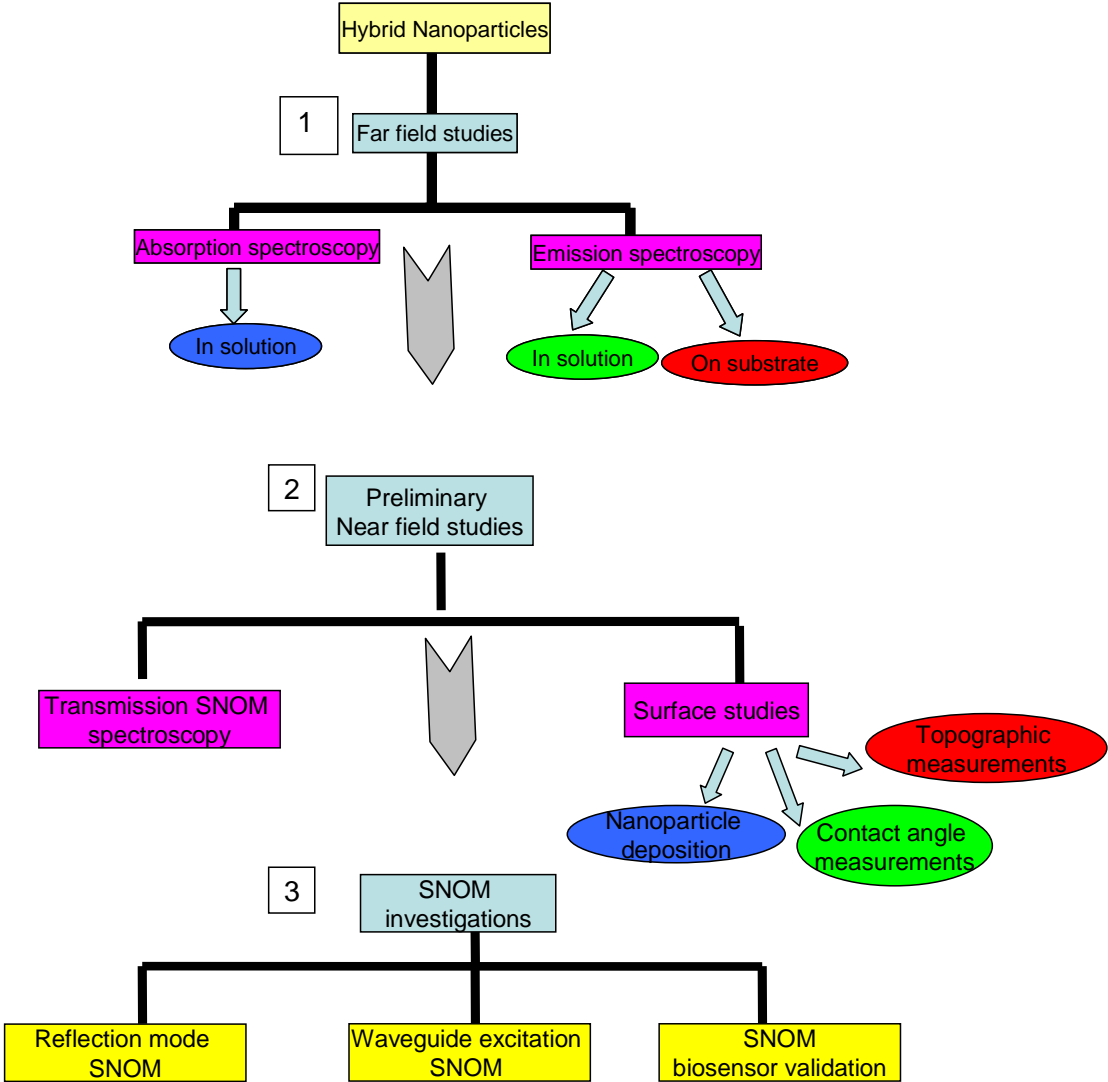
III-1 Hybrid Nanoparticles

III-1.1 Presentation:

Nanohybrid materials are a new class of size controllable mineral nanoparticles. They can be single phased or associated (core/shell) and functionalised on the surface with the help of stable chemical bonds linking between the particle and organic elements, which themselves   can made of either luminescent compounds (Rhodamin, Fluorescein..) or biological molecules. Their major interest lies in the fact that they can combine both the properties of the inorganic matrix (optic, magnetic...) with those of the organic molecules, and surface grafting (fluorescence, biological activation etc...). Such an association should permit a control and modification of the optical properties and chemical reactivity of the material, accompanied with a generation of specific characteristics which correspond to those of biological nanoprobes. The two most important characteristics for such an application are:

1) A mineral core having a size inferior to a few manometers diameters so that an eased dispersion in biological media can be assured, since such dimensions are close to those of an important number of biochemical molecules, thus permitting a better fusion.
2) A covering layer on the surface of the particle which permits thought hybrid bonding, to link a mineral particulate presenting functional and structural characteristics with organic molecules presenting complementary functional and biological properties.

III-1.2 Gd_2O_3: Tb^{+3}/ Polysiloxane -FITC nanohybrids: motivations of use

In our case, the nanoparticles we studied were synthesised chemically by Nano-H[59] society. They have a diameter of about 20 nm and are composed of a gadolinium oxide core, covered with a polysiloxane shell, containing fluorescein molecules. These nanoparticles are presented in a water solution at a concentration of about 0.5 mg/l. Their synthesis has been at the origin of a patent and articles whose main contents will be summarized in the following,[60],[61]. Our interest in such nano-objects relies mostly in

---

[59] "http://www.nano-h.com/."
[60] Cedric Louis et coll., "Nanosized Hybrid Particles with Double Luminescence for Biological Labeling," *Chemistry of Materials* 17, no. 7 (Avril 1, 2005): 1673-1682.
[61] ""Nanoparticules hybrides comprenant un coeur de Ln2O3 porteuses de ligands biologiques et leur procédé de fabrication"
C. Louis, S. Roux, C. Marquette, P. Perriat, R. Bazzi, G. Ledoux, O. Tillement
French Patent, N° 04.02115, 2004."

their being excellent candidates for biological applications, and most precisely in bio-functioning as will show the characteristics of each of its constituting elements.Figure III- 2 shows an illustration and main characteristic of a nanoparticle
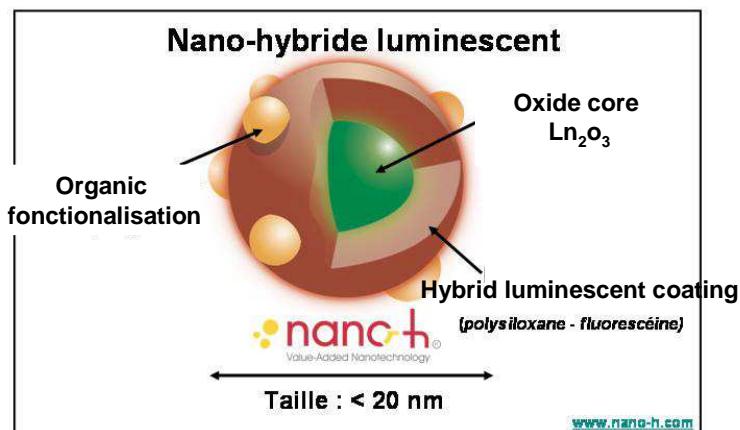
Figure III- 2 Main constitution of a studied hybrid nanoparticle

The gadolinium oxide core is known to its different advantages, all beneficial for biological applications, weather optical, magnetic, or therapeutic. For example, such matrix can be luminescent when incorporated with impurities (such as EU^{+3}, Tb^{+3}, Nd^{+3}). In fact, such ions have emission spectra with fine lines, with de-excitation times much longer than classical organic molecules or semi-conductors, when excited under UV or higher energies.   These can therefore be used as for multi-labelling tools. Also, gadolinium complexes materials constitute a very suitable IRM contrasting agent, due to[62] their high magnetic moment reaching $7\mu_B$. Finally, it has a neutrophage behaviour which can be very useful for therapeutic applications.

The role of the polysiloxane shell is basically to protect the nanoparticles against their dissolution or transition into the hydroxide stage in the different solvents and buffers in which they could be used; they also assure a good dispersion of the particulates in such media. However, such a covering permits also the addition of complementary organic fluorophores (such as FITC in our case) to the nanoparticle, through their incorporation in the polysiloxane shell.

The inclusion of an important *modulable quantity* of FITC in the polysiloxane network is particularly interesting since it leads to the synthesis of highly luminescent markers, which will permit an amplification of the final fluorescence of the nanocomposite. In fact,

---

[62] Futoshi Shikata et coll., "In vitro cellular accumulation of gadolinium incorporated into chitosan nanoparticles designed for neutron-capture therapy of cancer," *European Journal of Pharmaceutics and Biopharmaceutics* 53, no. 1 (Janvier 2002): 57-63.

such an insertion will help surpassing the convenience of a low absorption and luminescence of gadolinium oxide. These luminescent object thus seem to be perfectly suitable for bio molecular marking, where the functionalisation of a biological entity by this type of hybrid nanoparticles will be equivalent to its marking by many tens, even hundreds of fluorescent molecules, while a direct marking of these fluorophores to the biological specie is usually limited to only a few molecules due to the low number of available sites.

It is this essential property, accompanied by a feasible biological surface activation of the nanoparticles, which we will be using for the study of our hybrid nanoparticles through SNOM investigation. In fact, we will see that with their use and that of SNOM, we can constitute different biosensors with different configurations, capable of detecting the presence of specific analytes. In the following we will present a brief overview of the nanoparticle's synthesis method, followed by a presentation of their principal characteristics.

III-1.3 Chemical synthesis and characteristics

The first stage for the preparation of the nanoparticles consists of the production of the gadolinium oxide core itself, which will then be followed by the coating of the external surface with the FITC incorporated polysiloxane layer.

The preparation technique of the hybrid nanoparticles core is based on the 'polyol' method, which consists of a direct precipitation of a solid in a polyalcohol at a temperature that is generally between 150 °C and 250°C. The originality of such a procedure resides in the fact that the polyalcol plays at the same time the role of solvent and complexing agent. The chosen Polyalcohol in this case is the Diethylene glycol (DEG) Kept at about 70°C, in which gadolinium and terbium chloride salts are dispersed at a concentration of 0.2mol/l at ambient temperature . The solution is held at warmth of 120 °C under agitation. When the hotness reaches 100°C, 1 ml of an aqueous NaOH solution at a concentration of 3mol/l is added. After about an hour of heating, the system is bought to about 180°C and agitated for about 4 hours. The final solution is transparent and stable for weeks. Supplementary dialysis and purification steps of the obtained solution are necessary in order to get rid of residual ions (the yield of the reaction is about 30 %). Thus, with such a procedure, gadolinium nanoxides (doped by Tb^{+3} can be obtained by precipitation at a temperature less than 200 °C in the DEG. The particles

have a size of about 3nm, with a spherical morphology, and are highly dispersed. The size of the nanoparticles can be adapted and poly-doped from 3nm to 20nm[63].

The next step consists of covering the surface of the gadolinium nanoxides, where two principal polysiloxane precursors are used: (3-aminopropyl) triethoxysilane (APTS) and tetraethylorthosilicate (TEOS). The used procedure for such a goal is an adaptation of the work of Stöber et al[64] and de Van Blaaderen et al[65] in DEG, a polyalcoholic medium. In a first stage, the particulates are pre-grafted with fluorescein coupled (APTS) through addition of the last to the aqueous solution at 40°, under agitation for 20 minutes. After addition of an adequate quantity of water (aqueous solution of triethylamine), and agitation at 40°, the rest of the precursors are added: (APTS) and (THEOS). The APTS permits the grafting through the active grouping of (-NH$_2$) elements on the surface, while the (TEOS) permits the linking of the polymer bonds of the protecting layer, rendering much more compact. The solution is thus left for about an hour under agitation at the same temperature. Finally, a second water volume is added and the solution is left agitating within the same conditions for 48 hours. We are thus left with a solution of hybrid gadolinium oxide cored nanoparticles covered with a layer of FITC containing polysiloxane.

It is important to note that the thickness and composition of the formed polysiloxane layer is controllable since it's in direct relationship with the quantity of precursors introduced in the colloidal solution, and the size of the nanoparticles. Also, one can change the solvent in which the nanoparticles are initially synthesized, thanks to the protecting external polysiloxane layer. Finally, the last stage consists of the activation of the nanohybrids with bio molecules through the use of amine functions at its surface. For example in our case, we were especially interested in the grafting of biotin molecules, which would then play the role of anchoring sites to streptavidin proteins .In order to do so, a biotinised solution was added to the colloid solution containing the nanocomposites to be grafted. The solution is then agitated for three hours at ambient temperature and is thus dialysed in a mixture of DEG / DMSO (demthylsulfoxide), twice 8 hours, with a volumic ratio 1:80.

---

[63] R. Bazzi et coll., "Synthesis and properties of europium-based phosphors on the nanometer scale: Eu2O3, Gd2O3:Eu, and Y2O3:Eu," *Journal of Colloid and Interface Science* 273, no. 1 (Mai 2004): 191-197.

[64] Werner Stöber, Arthur Fink, et Ernst Bohn, "Controlled growth of monodisperse silica spheres in the micron size range*1," *Journal of Colloid and Interface Science* 26, no. 1 (Janvier 1968): 62-69.

[65] A. Van Blaaderen, J. Van Geest, et A. Vrij, "Monodisperse colloidal silica spheres from tetraalkoxysilanes: Particle formation and growth mechanism," *Journal of Colloid and Interface Science* 154, no. 2 (Décembre 1992): 481-501.

The specific binding method between streptavidin and biotin molecules will be explained in more detail later on in this chapter.

III-1.4 Optical properties:

When excited in the U-V region, the emission spectra of uncovered nanoxide particles doped with Tb^{+3} are characterised by four principle peaks, where the most intense one is centred about λ_{em} =545 nm[66] (see Figure III- 3)
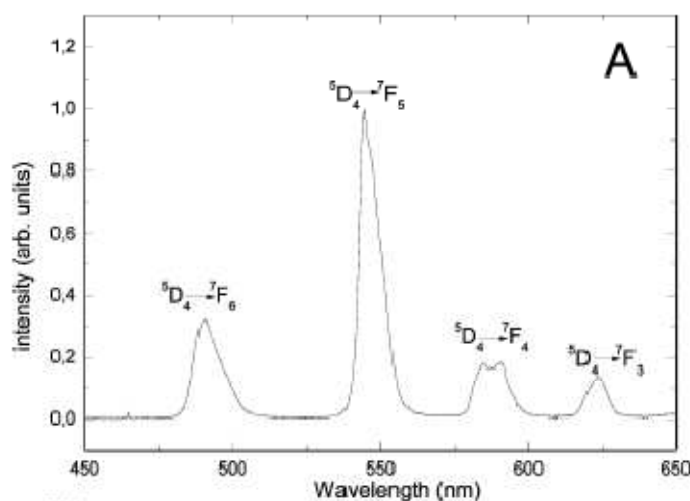
Figure III- 3 Emission spectrum of **Gd₂O₃ colloid excited at 230nm from reference** ([67])

For polysiloxane embedded nanoparticles, such a wavelength is in a spectral region where polysiloxane does not absorb light. However, when exciting the same kind of nanoparticles (polysiloxane labelled without fluorescein) at λ_{exc} =230nm, the luminescence characteristic of the terbium ion doping the oxide matrix is conserved, with, however an exaltation of the emitted light. Supplementary experiments showed an augmentation of the light intensity in function of the size of the core of the luminescent gadolinium oxide. It was noticed that the more the surface of contact between the core and polysiloxane is important (for smaller nanoparticles), the more the luminescence is increased with an important factor. Such behaviour has been assigned to an energy transfer between the polysiloxane and the oxide core. This phenomenon is responsible of the amplification of luminescence with the thickness of the covering layer. Nevertheless, when the polysiloxane layer contains FITC molecules, the imposed emission spectrum is that of the fluorescein itself, and not the Tb^{+3} doped gadolinium oxides. This is due to the

---

[66] Cedric Louis et coll., "Nanosized Hybrid Particles with Double Luminescence for Biological Labeling,"
Chemistry of Materials 17, no. 7 (Avril 1, 2005): 1673-1682
[67] Louis et coll., "Nanosized Hybrid Particles with Double Luminescence for Biological Labeling."

fact that the efficiency of luminescence of such doped elements is much less than that of the fluorescein, where the luminescence of the first is found to be 200 times less than the second. This second property interests us the most in the nanoparticles and their biological applications, since our goal would be the collection of the luminescence provided by the FITC, due to its high quantum efficiency, which would be the most important to the kind of SNOM setup that we are using.

III.2 far field studies:

The basic scheme to the study of the considered nanoparticles starts with a macroscopic point of view and then passes to the microscopic one. Thus, a first step consists of studying their optical properties in the far field. Absorption and emission spectra were the perfect candidates for such a characterisation since they give us an idea about respectively, the most appropriate wavelength to use for exciting the nanohybrids and thus have a maximum response, and the emitted light wavelength under such an excitation. In part 1 of (Figure III- 1), we present a small scheme of the different studies which have been done in the far field. Each step will be explained with more details in the coming paragraphs.

II-2.1 Absorption spectrum:

 An absorption spectrum fort the solution in question has been measured by using a Perkin Elmer Instruments Lambda 900 spectrometer. The principle of measurement is simple: we illuminate the colloidal solution we want to investigate with a spectral light range of light wavelength (in the visible one in our case) at a defined intensity and collect the transmitted light at each wavelength. By comparing the incident and transmitted light intensity, we are able to plot in absolute unit the amount of light absorbed by the sample for each wavelength used to illuminate the sample. . The obtained spectrum is given in Figure III- 4.
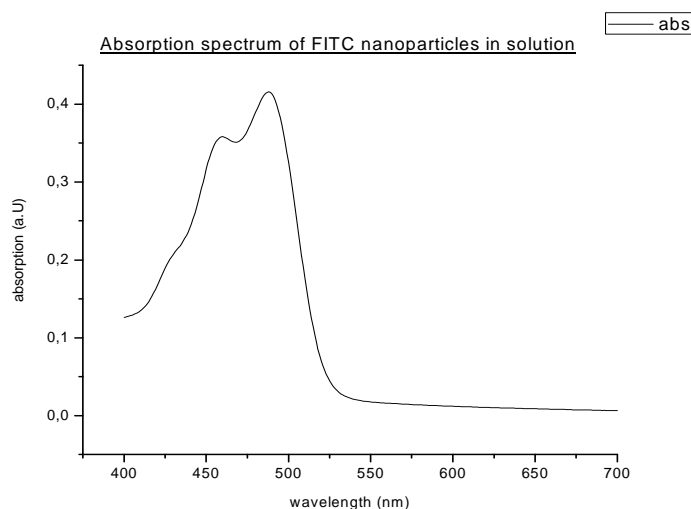
Figure III- 4: Hybrid nanoparticles absorption spectrum in solution

This spectrum strongly resembles one of those previously obtained for FITC molecules.[68] We can clearly distinguish a peak at about 490nm, meaning the nanoparticles absorb the most if we excite them with a laser light having close wavelength values. This led us to conclude that for our studies, it would be most appropriate to use an excitation light which is provided by an argon laser, since it can reach a wavelength of 488nm. In fact, we have considered such an excitation source all through our experiments concerning hybrid nanoparticles, in near and far field, in order to have a maximal absorption and consequently, a corresponding maximal emission of light emanating from the fluorophores for each kind of investigation. The wavelength of the emitted light itself can be studied by performing emission spectra, which will be talking about in the next step.

II-2.2 Emission spectrum:

a) Nanoparticles in solution:

 Knowing the emission wavelength at which the nanoparticles fluoresce is essential in order to place ourselves in the best conditions of light detection in near field. In fact, the most perturbing aspect of a near field configuration is the important difficulty in collecting the optical signal. Thus beginning by studying and getting more information about the kind of emitted light in the far field presents itself as being a basic and essential step to start with, in order to have a direct control over the fluorescence, and thus know how to optimize the experimental conditions for a maximal light collection. A first step has been to make emission spectra for the nanoparticles in solution; the experimental setup has been described in chapter III. Figure III- 5 shows the corresponding emission spectrum.

[68] Monique M. Martin, "Hydrogen bond effects on radiationless electronic transitions in xanthene dyes," *Chemical Physics Letters* 35, no. 1 (Août 15, 1975): 105-111, doi:10.1016/0009-2614(75)85598-9

FITC covered nanoparticles (in solution) emission spectrum with an excitation laser at 488nm
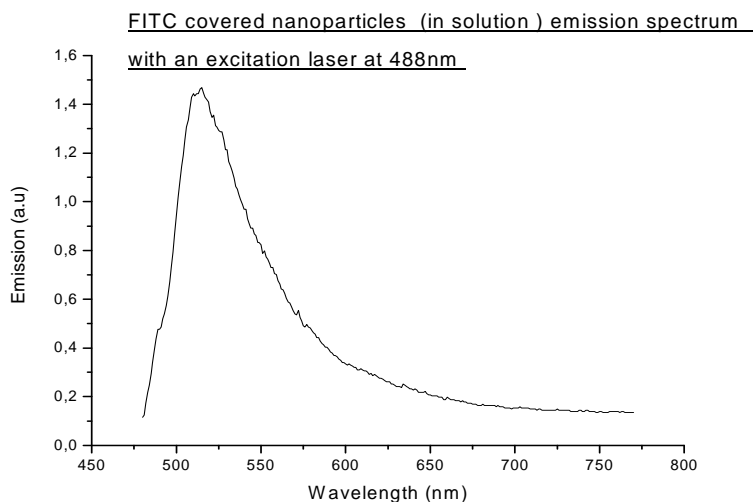
Figure III- 5 Hybrid nanoparticles in solution emission spectrum.

The typical FITC spectrum (where we can clearly distinguish a single band peaked at about 525nm) obtained in the present work is in agreement with that given in a previous study.[9] However, in this configuration, what we are considering does not only include the response of the nanoparticles to the excitation, but is actually an averaging of the whole system solvent + nanoparticles. Also, one should not forget the important effect of the solvent itself on the FITC molecules emission. In fact, hydrogen bonding between solute and solvent may lead to shifts in the spectrum: the fluorescence spectra shift to the blue when the hydrogen bonding power of the solvent increases, and there is a slight loss in the structure of the absorption and emission spectra.[69] The situation will be different when passing to near field optical studies, since in this case the configuration of the SNOM itself does not permit us to make studies of nanoparticles which are present in solution. Thus, in order to see in details if this factor plays a major role in the emission spectrum shape, the adopted solution to this problem consists of taking emission spectra of the nanoparticles only, without the solvent, which will be discussed in the next section.

b) Dried Nanohybrids:

In order to get rid of the solvent, we simply placed a drop of the colloidal solution on a cleaned cover glass and left it dry in the air. We have chosen a cover glass as a substrate since it has a very thin thickness, and would thus avoid any refraction effects which could hinder the measurements. For a better comparison, we used the same setup as that of the emission spectrum in solution; critical details about the experimental conditions in such a configuration have been previously described in the experimental

---

[69] Martin, "Hydrogen bond effects on radiationless electronic transitions in xanthene dyes."

section (chapter III). The spectrum obtained also shows one which is characteristic to fluorescein molecules, with a peak also about 520nm (Figure III- 6).

FITC covered nanoparticles (on cover glass) emission spectrum
with an excitation laser at 488nm
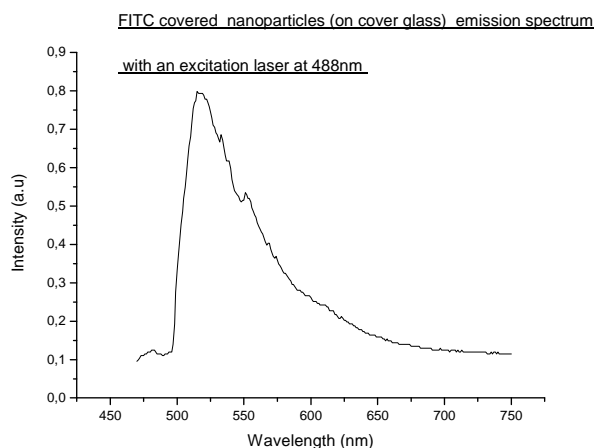
Figure III- 6: Hybrid nanoparticles on cover glass emission spectrum.

Taking into consideration the scales in which we are working, no important difference can be noticed with respect to the emission spectrum obtained in solution. However, we have now a clear idea about the shape of the emission spectra, whether in solution, or on a substrate.

We can see bellow a summarizing graph of the preliminary experiments done: the absorption spectrum and emission in solution and on a cover glass.

Absorption and emission spectra of FITC nanoparticles in solution and on glass plate
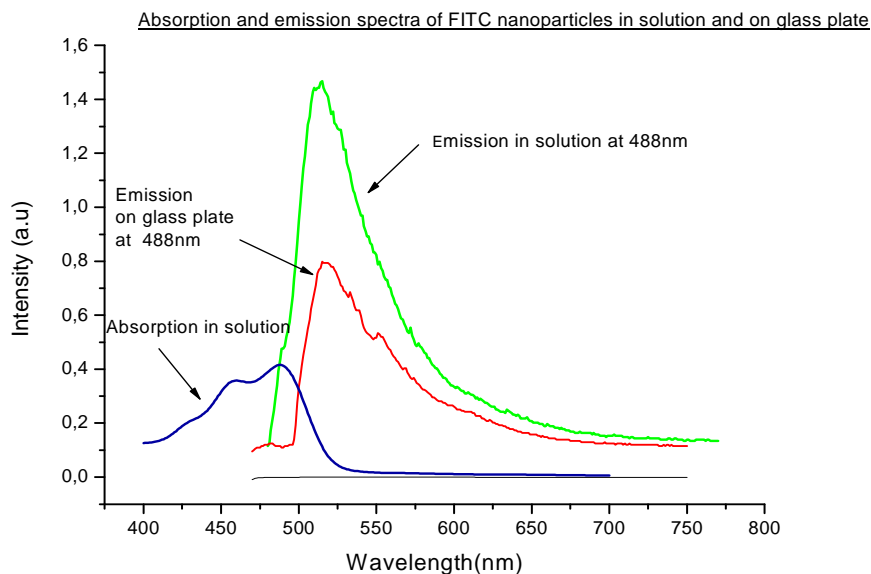
Figure III- 7: Summarization of emission and absorption spectra.

III-3 Preliminary near field optical studies;

Now that we have had a general idea about the spectral features of the nanoparticles in the far field, a second step would be to do a characterization in the near field. We first thought about SNOM spectroscopy and imaging by using respectively for each cases the two different configurations of the near field illumination mode: transmission and reflection. However, in this case, we are dealing with an additional element (the SNOM tip) which should be also considered. Moreover, as the nanoparticles are originally presented in a colloidal solution, one would thus have to find an easily exploitable way in order prepare nanoparticles samples that would be suitable for such kind of configurations. This led us to considering a number of trial and error attempts of many surface linked studies. In the following, we will present the different steps that we tried, and the corresponding results obtained in each case.

III-3.1 Transmission mode near field optical microscopy:

Trying to characterize the nanoparticles with near field optical spectroscopy has been one of the methods that we adopted in order to know more about the spectral shape of the fluorescence signal emanating from them in the near field. In fact, contrarily to far field spectroscopy which offers information only on ensemble-average quantities, SNOM spectroscopy has been used as an essential tool to study the behavior of single particles, due to its ability to reach very high resolutions. For example, systems such as single

quantum dots (InGaAs/AlGaAs,[70] InGaAS/GaAs,[71] GaAs/AlGaAs,[72] or island grown CdSe) or, GaAs/ AlGaAs quantum wires and wells[73] have been studied with such a tool. In most cases, this led to obtain a very highly resolved sharp spectra, which were then associated in most cases to emissions emanating from the excitons within the dots. This kind of information could not have been obtained by using far field spectroscopy, since far field spectra have much poorer resolution due to inhomogeneous spatial broadening. Very highly resolved sharp spectra can be obtained within special conditions such as very low temperature and well separated quantum dots which can be singled out separately, in order to exclude any possibility for thermal or inhomogeneous broadening effects. In the case of single quantum dots for example, an increase of temperature leads to broader peaks due to thermal activation of the excitons out of the quantum dot region.[74]In our case however, we studied nanoparticles having constitutions and physical properties much different from those of quantum dots, and have done our experiments at room temperature by using the transmission SNOM described previously. The studied sample was prepared by placing a drop of the nanoparticles solution on a glass plate, and leaving it to dry in air until the solvent would have evaporated as we show in the following figure.

[70] A. Chavez-Pirson et coll., "Near-field optical spectroscopy and imaging of single InGaAs/AlGaAs quantum dots," *Applied Physics Letters* 72, no. 26 (Juin 29, 1998): 3494-3496, doi:10.1063/1.121638

[71] D. Pahlke et coll., "Photoluminescence of buried InGaAs/GaAs quantum dots spectrally imaged by scanning near-field optical microscopy," *Applied Surface Science* 123-124 (Janvier 1, 1998): 400-404, doi:10.1016/S0169-4332(97)00489-3

[72] H. F. Hess et coll., "Near-Field Spectroscopy of the Quantum Constituents of a Luminescent System," *Science* 264, no. 5166 (Juin 17, 1994): 1740-1745, doi:10.1126/science.264.5166.1740

[73] H. Zhou et coll., "Scanning near-field optical spectroscopy and imaging using nanofabricated probes," *Applied Physics Letters* 75, no. 13 (1999): 1824-1826, doi:10.1063/1.124840

[74] F. Flack et coll., "Near-field optical spectroscopy of localized excitons in strained CdSe quantum dots," *Physical Review B* 54, no. 24 (Décembre 15, 1996): R17312, doi:10.1103/PhysRevB.54.R17312.
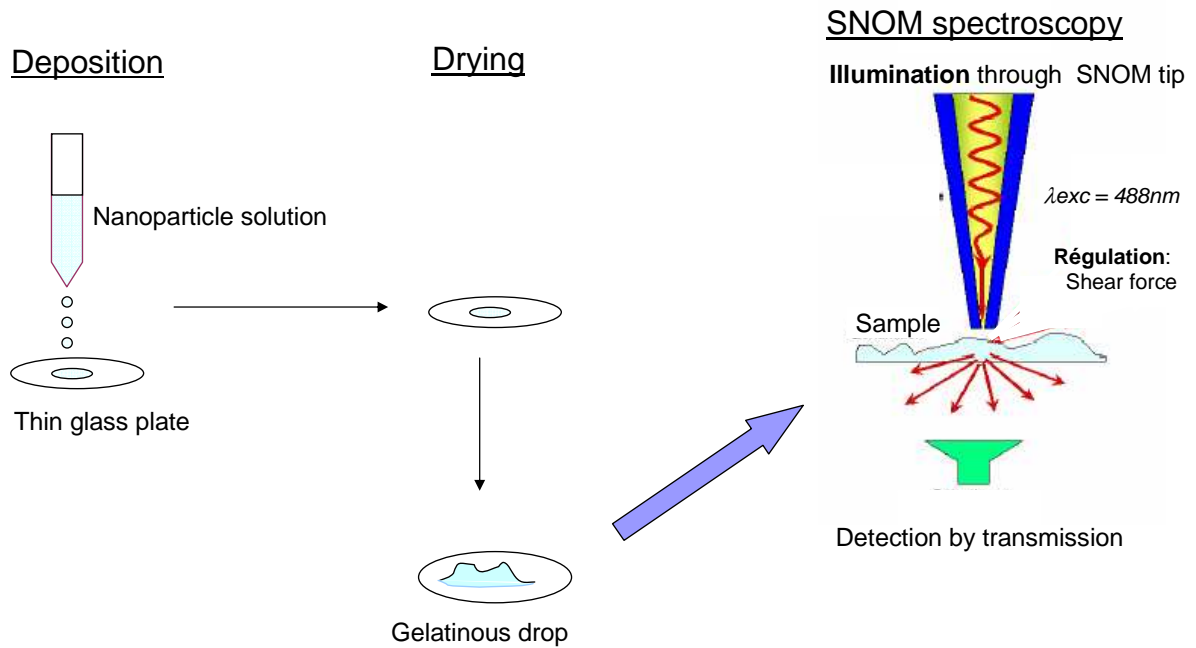
Figure III- 8 Sample preparation steps for transmission SNOM spectroscopy

We then placed the sample under the SNOM tip, which was approached until the distance between them reached a value of a few nanometers; we could then consider that we are working within the conditions of near field optical microscopy, the obtained near field optical spectrum is shown in Figure III- 9 :
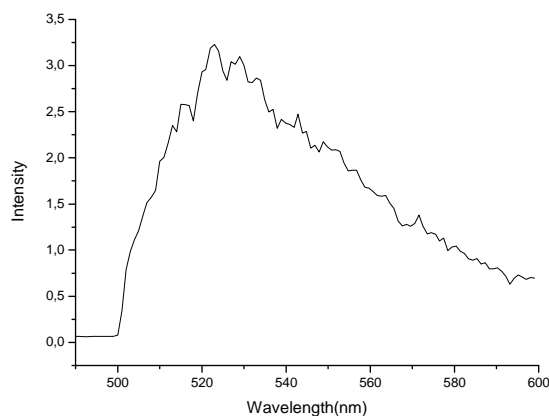
Figure III- 9 Hybrid nanoparticles SNOM transmission emission spectrum.

As we can clearly see, the peak of the obtained spectrum is about 520nm, which corresponds to that obtained in our far field studies on the hybrid FITC nanoparticles.

The signal to noise ratio is fairly good except for the range covering the (520-540 nm scale) which is most probably due to external noise or perturbing factors. A more detailed discussion about the conditions in which the spectra where studied will be presented in the coming paragraphs.

Now, in order to get a better comparison between the near and far field spectra, we superposed both of them on top of each other to have the following (Figure III- 10):
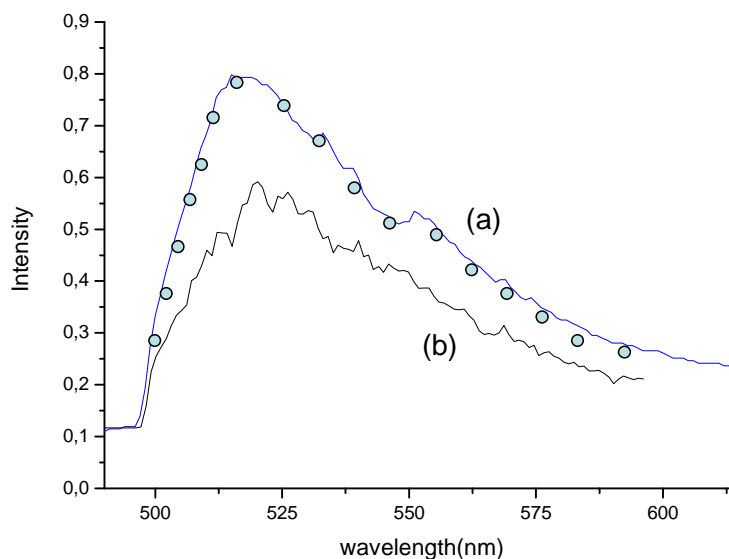
Figure III- 10 : Far- field (a) and Near-field (b) emission spectra.

We should precise however that the scales have been modified in order to be able to compare both spectral shapes at the same time. As we can see at a first glance, the near and far field spectra have a very similar shape. Such a case has been also already obtained previously with different studied systems such as gold arrays,[75] Si nanocrystals,[76] or layered growth CdSe quantum dots samples;[77] this behaviour has been assigned in each case for different reasons such as spatial inhomogeneities, the dimensions of the studied objects or the nanoparticle's preparation conditions. In our case, we observed the nanoparticles with the following conditions:

[75] L. Aigouy et coll., "Near-field optical spectroscopy using an incoherent light source," *Applied Physics Letters* 76, no. 4 (Janvier 24, 2000): 397-399, doi:10.1063/1.125766

[76] J. K. Trautman et J. J. Macklin, "Time-resolved spectroscopy of single molecules using near-field and far-field optics," *Chemical Physics* 205, no. 1-2 (Avril 15, 1996): 221-229, doi:10.1016/0301-0104(95)00391-6

[77] Flack et coll., "Near-field optical spectroscopy of localized excitons in strained CdSe quantum dots."

1) We were working at room temperature (so thermally activated processes were still taking place).

2) About a hundred of FITC molecules are attached to one nanoparticle; meaning that we were already taking into consideration the spectrum of an ensemble of FITC molecules by observing one nanoparticle, thus leading to a distribution of molecular nano environement.

3) The effective sample area probed being at least of the orders of the excitation region (of the orders of the probe aperture), that is, about 150 nm, we were most probably observing agglomeration of nanocrystals containing a very important number of nanoparticles under the area covered by the SNOM tip. We will later see that the preparation method (cited in the beginning of the paragraph) of such samples leads to the formation of enormous agglomerations under the SNOM tip.

Even if we suppose that the spectrum we obtained corresponds to the emission of single nanoparticles, it would still have been likely to obtain spectra resembling the far field one. In fact, Buratto *et al.* have studied room-temperature characteristics of single dye molecules,[78] and have observed that for 85% of the studied cases, spectral shapes were found to be identical to the ensemble spectrum. The broadening of the single molecule spectrum was thus attributed to unresolved vibronic coupling, which can be the same case with FITC. While broadening in the ensemble spectrum occurred due to the distribution of nano-environements.

Now, a small discussion is worth to be mentioned, concerning the tip shape and effect in near field spectroscopy:

It has been established that in the case of aperture less SNOM tips, the coupling efficiency between the tip apex and the light depended on the exciting wavelength. The sharper the cone, the stronger the variations are,[79] and thus the more the impact is seen on an acquired spectrum. In other words, two different tips having different shapes would give two different emission spectra for the same optical signal. Up to our knowledge, no similar assumptions have been cited for open aperture SNOM tip

---

[78] Kenneth D. Weston et coll., "Room-temperature fluorescence characteristics of single dye molecules adsorbed on a glass surface," *The Journal of Chemical Physics* 109, no. 17 (Novembre 1, 1998): 7474-7485, doi:10.1063/1.477370

[79] Aigouy et coll., "Near-field optical spectroscopy using an incoherent light source."

spectroscopy; however it has been already implied that a tip having a narrower opening would presumably permit us to have higher resolution spectra[80], and that the tip shape and position above the sample may affect the emission life time (a nearby tip to the sample means a smaller life time) of the studied object. However, an important point which should be taken into consideration is the flux density emitted by the probe tip. In fact, as we already mentioned in chapter II, the SNOM tips we are using are metallized by a thin layer of aluminium. This process is essential in order to be able to confine the excitation light in a small area of the sample, but also constitutes some inconvenience: an over small aperture can reach very high temperatures and thus lead to the bleaching of the studied nanoparticles. In fact, as the light passes through the probe, a small amount is absorbed by the metal, which heats it. If the sample is temperature sensitive, then it runs a danger of photo-bleaching. In order to keep it in ambient temperature, it is essential to use probes having apertures whose diameter is not smaller than the fifth of the exciting wavelength.[81] In our case, we paid attention into fulfilling this condition in all of our SNOM experiments, where the average aperture we used is about 150nm and the excitation wavelength 488nm.

As these results were just intended to give us an overall idea about the emission properties of the nanoparticles, we must admit that two supplementary points must have been taken into account in order to have a precise comparison between near and far field spectra:

1) The photon flux reaching the nanoparticles in question must have been chosen to be the same in the two kinds of measurements, in order to be in the same experimental conditions, and have a clearer idea about the difference between the optical responses of the nanoparticles in the two different configurations. However, we only have an average idea about the shape and aperture size of the SNOM tip, so that a precise calculation could not have been done.

2) A normalisation for the transmission near field spectra is necessary in order to take into account:
   - Excitation light intensity variations

   -The absorption of the optical elements of the microscope

---

[80] Flack et coll., "Near-field optical spectroscopy of localized excitons in strained CdSe quantum dots."
[81] Trautman et Macklin, "Time-resolved spectroscopy of single molecules using near-field and far-field optics."

- The optical response of the tip[82]

Now that we were sure of our ability to collect the fluorescence signal of the hybrid nanoparticles we are using, the next step was to have a near field optical image of what we obtained spectrally. However, this could not be done, since we were stopped by topographical constraints which will be explained in the next section.

III-3.2 Reflection mode near field optical microscopy: A first trial

Having had a general idea about the spectral features of the hybrid nanoparticles within near and far field, the next step consisted of trying to image them optically and topographically. However, as already mentioned, we are dealing in this case of figure with an additional element which is the SNOM tip. This factor will lead us into trying different surface related studies as will be seen in the following.

A first idea for the preparation of a sample for near field studies has been to place a drop of the nanoparticle solution on the substrate and let it dry in air, the sample would then be examined with the SNOM in reflection mode; such a process is represented in the following figure.

Deposition

Nanoparticle solution

Drying

Thin glass plate

Gelatinous drop

Illumination through SNOM tip

Detection by reflection
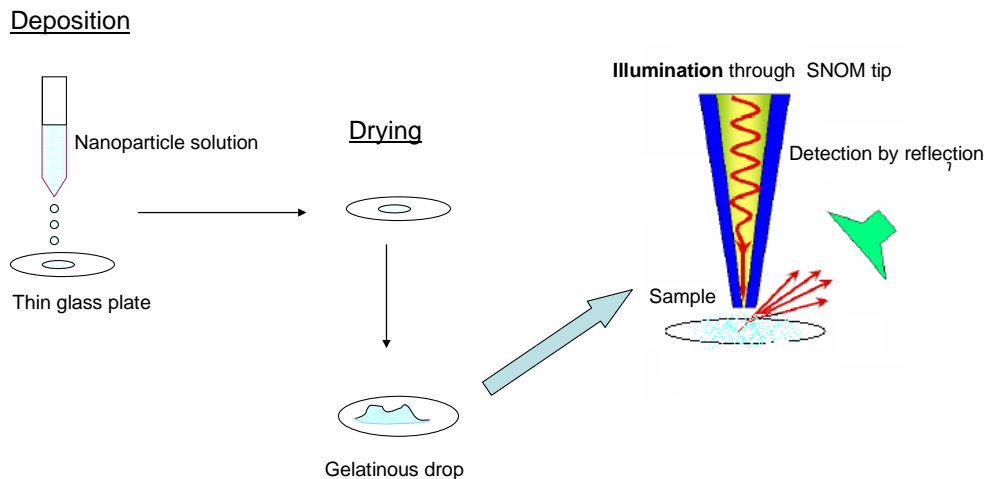
Sample

Figure III- 11 First sample preparation process for reflection mode SNOM imaging

However, such a process leads to the formation of big agglomerates that would constitute an obstacle to the small and concise displacement of the SNOM tip during the image acquisition. In fact, small solid particles dispersed in an evaporating drop will

[82] Aigouy et coll., "Near-field optical spectroscopy using an incoherent light source."

migrate to the edge of the drop and will form a solid ring, (this migration is due to an external current in the drop, which is driven by the loss of the solvent by evaporation and geometrical constraints so that the drop would maintain an equilibrium shape with a fixed barrier.[83] This results in very blurry and unclear SNOM images as seen in the following figure (Figure III- 12)
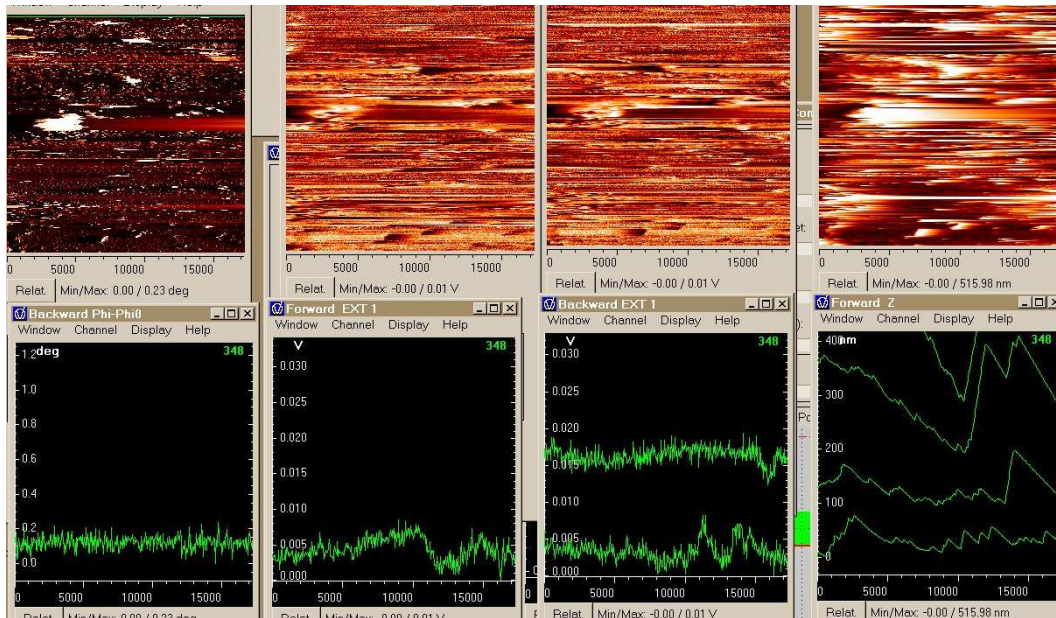
Figure III- 12: Shear force SNOM topographic and optical image of a dried droplet of nanoparticles solution

In this figure, the border images correspond to topographic ones, obtained by recording either the displacement of the tip during a scan (right handed image, called z –motion topographic image), or the phase difference of the oscillations of the SNOM tip as it follows the changing topography of the sample surface(called phase topographic image).The central ones correspond to optical images, simultaneously recorded by gathering the optical information reaching the collection objective during the scan.

We can clearly discern horizontal stripes on all of the figures and on all the scanning area , meaning that in the course of a scan line, the tip had been subject to such sudden elevations (up to 200nm) that it was unable to compensate in height during the rest of the scan. There are also some spots where a correlation between optical signal and topographic image (bottom of the figure) can be clearly seen showing the presence of diffusing (or light emitting) bodies. These two observations lead us to conclude that the scanned area consists of dispersed large aggregations of the hybrid nanoparticles. Their important dimensions seem to hinder the study of their optical properties in the near field and eventually constitute an important risk for the breakage of the tip. In fact, angular

---

[83] Robert D. Deegan et coll., "Contact line deposits in an evaporating drop," *Physical Review E* 62, no. 1 (Juillet 1, 2000): 756

diagrams taken before and after such an acquisition were completely different. Also, no optical signal could be detected again with the same tip, even when it was placed within the same initial conditions. The hypothesis of a damaged tip was thus proposed. This is shown in the following figure, where a second scan on a zoomed small area of figure 1 (dimension of 1μm*1μm), showed a defined topographic image (Figure III- 13:), but no corresponding optical one.
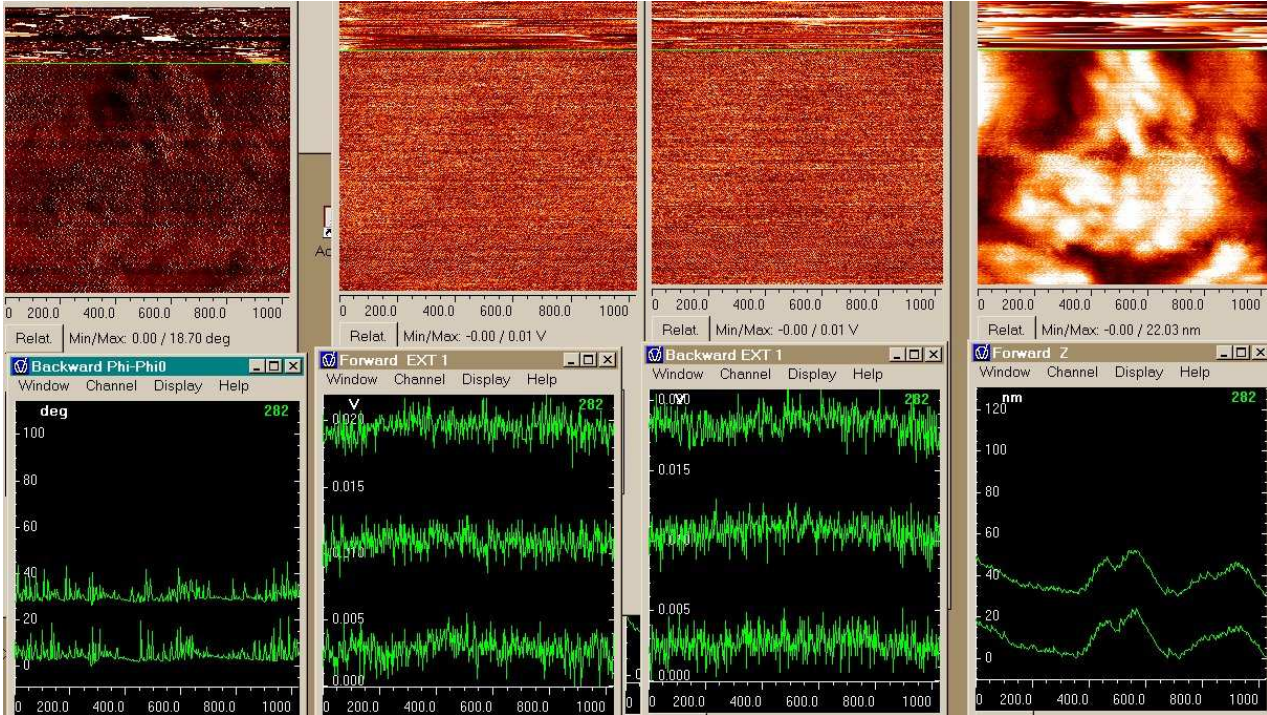
Figure III- 13: Zoom of a smaller region of Figure III- 12: Shear force SNOM topographic and optical image of a dried droplet

The next step would therefore consist of trying to find a way in order to prepare samples that would be more suitable for such kind of measurements. A large number of processes exists for the deposition of small bodies such as nanoparticles on the surface of a substrate.[84],[85] These depend however on the desired kind of sample obtained and the ends it will be used for. In our case, two methods attracted our attention: SVD (Surface Vertical Deposition) (also referred to as EVCD (Evaporation Driven Colloidal Deposition) and Spin Coating. They have advantages such as providing us with a single layered nanoparticle sample, a control of their spacing, and a short time consuming preparation.

III-3.3 Deposition of nanoparticles on the surface:

a) Surface Vertical Deposition Method overview:

The surface vertical deposition (SVD) method, is primarely used to synthesize nanoparticle films. It has been used for the deposition of gold nanoparticles[86] and self assembled nanoparticles wires on various substrates. In this process, the substrate is placed vertically in a nanoparticle suspension and is gradually exposed by evaporation or other slow solvent removal. During the film's formation, we observe that the colloidal particles are deposited only at the solid-liquid-gas interface. But evaporation is not a necessary condition, but only provides a mean for slowly dropping the liquid level. In this method, the areal density of nanoparticles in a sub monolayer nanoparticle thin film made by SVD depends on factors such as the descending velocity of the suspension surface, the concentration of the gold nanoparticle suspension, the contact angle between the suspension and substrate, the suspension viscosity and the average radius of nanoparticles. The main factor responsible for such a process being the interface force between the solid substrate and the liquid suspension surface at the solid-liquid-gaz junction[3], the deposition of the nanoparticles should also take place not only by letting the liquid level drop, but inversely by pulling up the substrate from the nanoparticle solution itself. This is exactly what we have done (see Figure III- 14), where we have used a dip coating machine with which the solute was immersed rapidly in a nanoparticle solution,

[84] S. J. Kim et coll., "Effects of nanoparticle deposition on surface wettability influencing boiling heat transfer in nanofluids," *Applied Physics Letters* 89 (2006): 153107

[85] D. M. Tanenbaum, A. L. Laracuente, et A. Gallagher, "Nanoparticle deposition in hydrogenated amorphous silicon films during rf plasma deposition," *Applied Physics Letters* 68 (1996): 1705

[86] J. J. Diao et coll., "Surface vertical deposition for gold nanoparticle film," *JOURNAL OF PHYSICS-LONDON-D APPLIED PHYSICS* 36, no. 3 (2003): 25-28

and very slowly removed from it, simulating the slow decrease of the solution due to evaporation in a regular SVD experiment.

Surface Vertical Deposition principle

Substrate pulled upward

Water level going down by evaporation
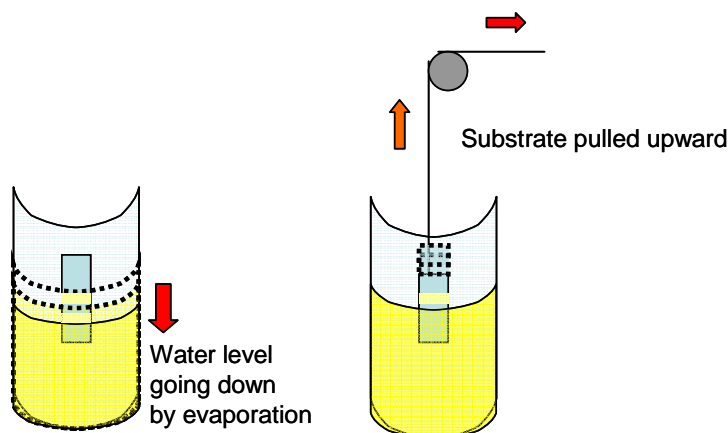
Figure III- 14: Illustration of SVD used for nanoparticle deposition

b) Spin coating method overview:

This method is used for homogeneously dispersing nanoparticles on the surface of a substrate (see Figure III- 15). It consists of putting a small drop of a colloidal nanoparticle solution on a substrate and let it spin at high velocity for a few minutes. The dispersion of the nanoparticles will essentially take place in two different stages: First the centrifugal force created due to the spinning will eject an important amount of the solution off the substrate and a thin uniform liquid film will subside. The solvent will then evaporate and the solute will be deposited homogeneously on the support.[87] The spacing and the distribution of the deposited nanoparticles depends on parameters such as the concentration of the solution, the frequency of rotation, the viscosity of the solvent and its wetting of the substrate, and finally it evaporation rate[88],[89].

---

[87] R. M. van Hardeveld et coll., "Deposition of inorganic salts from solution on flat substrates by spin-coating: theory, quantification and application to model catalysts," *Applied Surface Science* 84, no. 4 (Avril 1995): 339-346, doi:10.1016/0169-4332(95)00010-0

[88] A. Partridge, S. L. G. Toussaint, et C. F. J. Flipse, "An AFM investigation of the deposition of nanometer-sized rhodium and copper clusters by spin coating," *Applied Surface Science* 103, no. 2 (Octobre 1, 1996): 127-140, doi:10.1016/0169-4332(96)00520-X

[89] Y. K. Hong et coll., "Controlled two-dimensional distribution of nanoparticles by spin-coating method," *Applied Physics Letters* 80 (2002): 844

Spin coating principle:

3) Action of evaporation

1) Drop of nanoparticles

solution on substrate

2) Action of centrifugal force

4) Dispersed nanoparticles
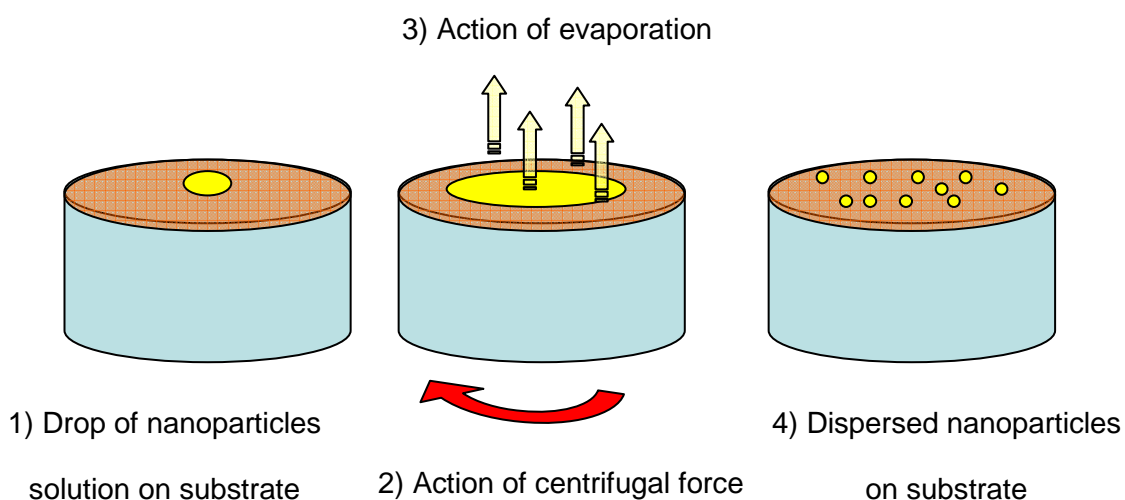
on substrate

Figure III- 15: Illustration of spin coating method used for nanoparticles deposition

If we take a closer look for both methods, we can see that there are some common criteria for having a good nanoparticle deposition on the substrate in question. They include the nanoparticles colloidal solution concentration, the viscosity of the solvent and the wetting of the substrate. Thus for making the suitable choice of a substrate, we had to make supplementary wetting tests in order to choose one which would be having a small contact angle with the solvent we are using (a substrate that would mostly be wet by the solvent).

III-3.4: Contact angle measurements:

Intermolecular interactions between a liquid and a solid surface (when the two are brought together) lead to the specification of the amount of wetting between these two elements. The degree of wetting is described by the contact angle, the angle at which the liquid-vapor interface meets the solid-liquid interface.[90] If the wetting is very favorable, the contact angle will be low (< 90°), and the fluid will spread to cover a larger area of the surface, otherwise, the wetting is unfavorable.

---

[90] J. N. Israelachvili, "Intermolecular and surface forces" (1992)

We have performed contact angle measurements between the solvent used in our nanoparticle colloidal solution (water in our case) and a number of substrates, by using a contact angle goniometer.
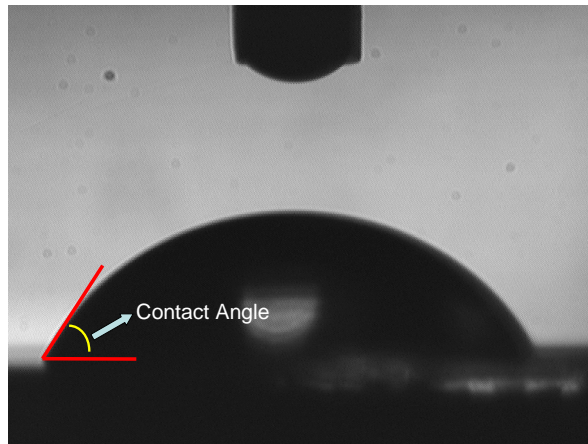
Figure III- 16: Representative image of contact angle measurements

It is important to note that before making any measurements with the goniometer, the substrates were cleaned in a similar way as that employed just before the deposition of the nanoparticles for near field measurements. This has been done in order to provide us with a concise idea about the interaction of the solvent and substrate within the same conditions used for the SNOM experiment; in other words, the use of a different solvent for the cleaning of the substrate may alter its surface and hence affect the contact angle measurements.

We studied the contact angles between water and four different substrates made of different materials: Glass, Silicium, lithium Niobate and Saphire.

The choice was based on the fact that these materials constitute perfect candidates for the fabrication of waveguides,[91,92,93] and thus would be useful to use for the excitation of nanoparticle and near field measurements.Table III- 1 bellow shows the different contact angles measured for each case:

[91] Jaeyoun Kim, Guangyu Li, et Kim A. Winick, "Design and Fabrication of a Glass Waveguide Optical Add?Drop Multiplexer by Use of an Amorphous-Silicon Overlay Distributed Bragg Reflector," *Applied Optics* 43, no. 3 (Janvier 20, 2004): 671-677

[92] Rebecca Kozodoy et coll., "A hollow sapphire waveguide for stereotactic intraventricular CO2 laser neurosurgery: a rat model," *Lasers in Medical Science* 9, no. 4 (Décembre 29, 1994): 273-281

[93] K. Peithmann et coll., "Fabrication of embedded waveguides in lithium-niobate crystals by radiation damage," *Applied Physics B: Lasers and Optics* 82, no. 3 (Mars 1, 2006): 419-422

studied Material	Contact angle (°)
Glass	22
Silicium	42
Niobate	54
Saphire	73

Table III- 1: Measured Contact angles

Thus, it was clear for us that in this case, the glass substrate, giving the smallest angle, seemed to be the most suitable one for both the deposition techniques described in the previous section and the expected SNOM experiments.

III-3.5 Glass substrate topographic measurements:

As the glass substrate was found to be constitutionally suitable for nanoparticle deposition, a last control had to be done about its smoothness. This is necessary in order to see weather we would be able to distinguish the substrate's corrugations from the deposited nanoparticles on its surface. This led us to make SNOM images of a well cleaned cover glass, giving the following results:
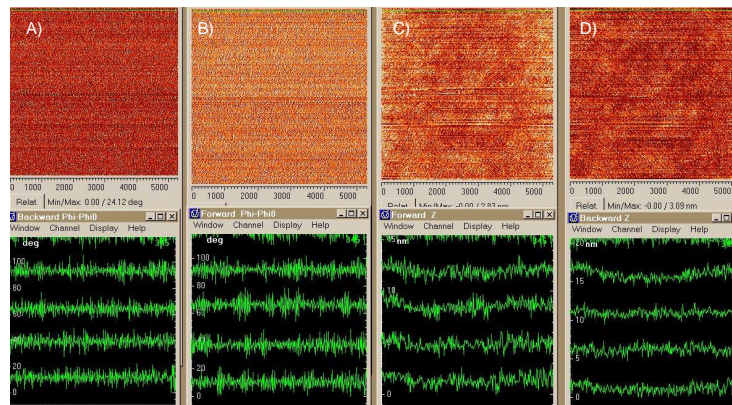
Figure III- 17 : Phase: A (backward) –B (Forward) and Z-height: C (Forward)-D (Backward) topography images of the substrate

The first two images are the recorded phase images in a backward and forward movement of the tip in a 5 µm^2 area of the glass sample, and the remaining ones are topographical z-height images of the same area with the tip also moving in the same directions. This procedure has been repeated on many regions of the sample, and with the use of different tips, in order to have a statistical idea about the surface's shape. We globally obtained the same kind of images. As we can see, in all images, some very small corrugations (in the order of a few nanometers) could be distinguished on the surface of the cover glass. The dimensions of the hybrid nanoparticles being in the order

84

of about 20 nm, the topographic images would then show a clear profile of their shape if this substrate was used. We should note however that an AFM measurement would have been more concise than a topographic SNOM one due to the very high resolution that an AFM system can attain laterally (less than few nanometers), and thus would help us to have a clearer idea about the surface state; However, in this situation, the SNOM omicron shear force system would be enough for this kind of substrate study, since the *vertical resolution* that could be attained with such a system could easily reach the order of a few nanometers and give us as a clear idea about the height of the corrugations on the glass cover.

We tested both the SVD and spin coating methods in order to see which one is more suitable for the kind of studies that we wanted to do. Unfortunately the SVD method showed no clear evidence of nanoparticle surface deposition; we may relate this fact to a too high velocity of retraction or an over dissolved solution. Future plans have been made in order to repeat the same experiment but by varying parameters such as the velocity of the retraction or the concentration of the solution. The spin coating method however showed much better results than SVD, and the results they showed will be discussed in the following section.

III.4 Near field fluorescence imaging of nanohybrids on a glass substrate:

After having deposited the nanoparticles on the surface of the glass substrate by spin-coating, we directly imaged them with the SNOM in order to see if it is possible to detect their photoluminescence in an illumination-reflection mode. This technique is described in Chapter II, but we show the reflection configuration as a reminder in the following figure.
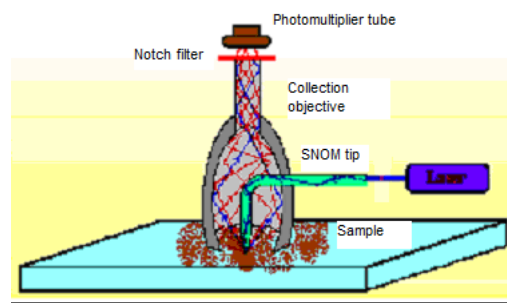
Figure III- 18 SNOM Reflection configuration scheme

We obtained the following images (Figure III- 19):
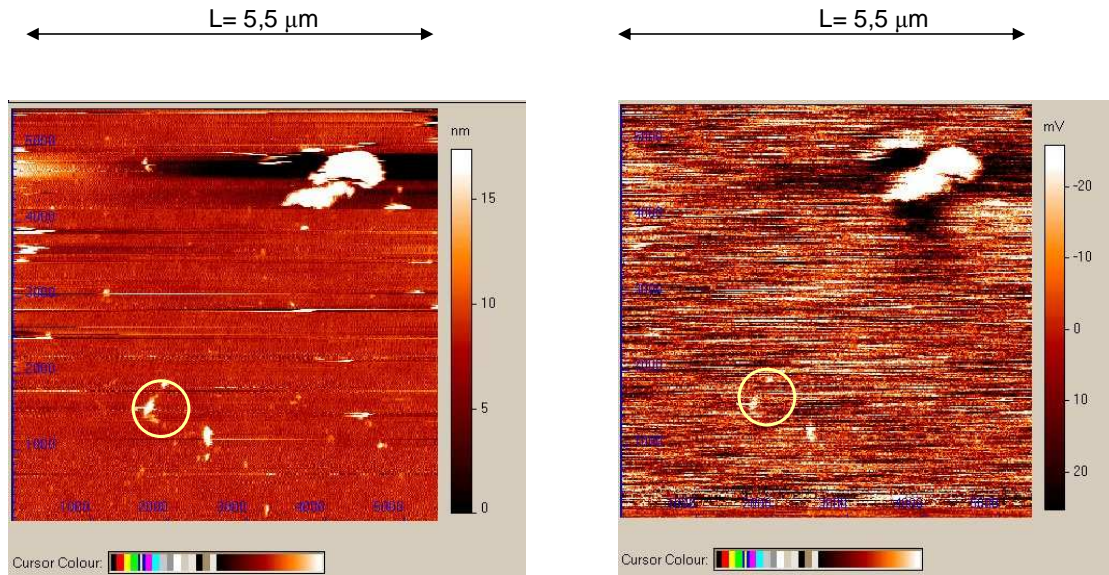
Figure III- 19: SNOM images of hybrid nanoparticles a) Topographic b) Optical

These images were obtained in a first scan, where their dimensions are in the orders of $5,5\mu m \times 5,5\mu m$. The left image corresponds to a topographic one, while the right one corresponds to the optical image recorded by gathering the optical information reaching the collection objective, at the same moment. The right handed legend shows for the topographical image the variation of the height with the respective color while for the optical one, it is the variation of the collected signal that is taken into account. The white dots represents aggregations of the deposited nanoparticles on the glass substrate; what attracts our attention is that the height of the dots corresponds to the expected diameter of one nanoparticle (from the legend, about 20 nm), implying that only one single layer of the nanoparticles has been deposited. We can also distinguish on the optical part of the image a resemblance with the topographical one. We should remember here that the optical part does not represent the reflected laser light (since it has been presumably cut out by the notch filter), but basically the fluorescence light emitted from the fluorescein molecules that have been attached chemically on the nanoparticles.

As the SNOM method is one usually used to attain resolutions which are higher than half the wavelength used to illuminate the sample, we tried zooming into smaller regions of the 'lowest part 'aggregations of Figure III- 19 in order to see if we could still distinguish them optically and topographically with the Twin-SNOM and to know what resolution we could attain with our system. We will show in the following figure a comparison between the obtained phase and optical images, which is a scan of the region inside the circle on the upper image. The dimensions of each SNOM image are about 1.3 µm ×1.3 µm.

L= 1.3µm   L= 1.3 µm

Phase-topographic image   Optical image
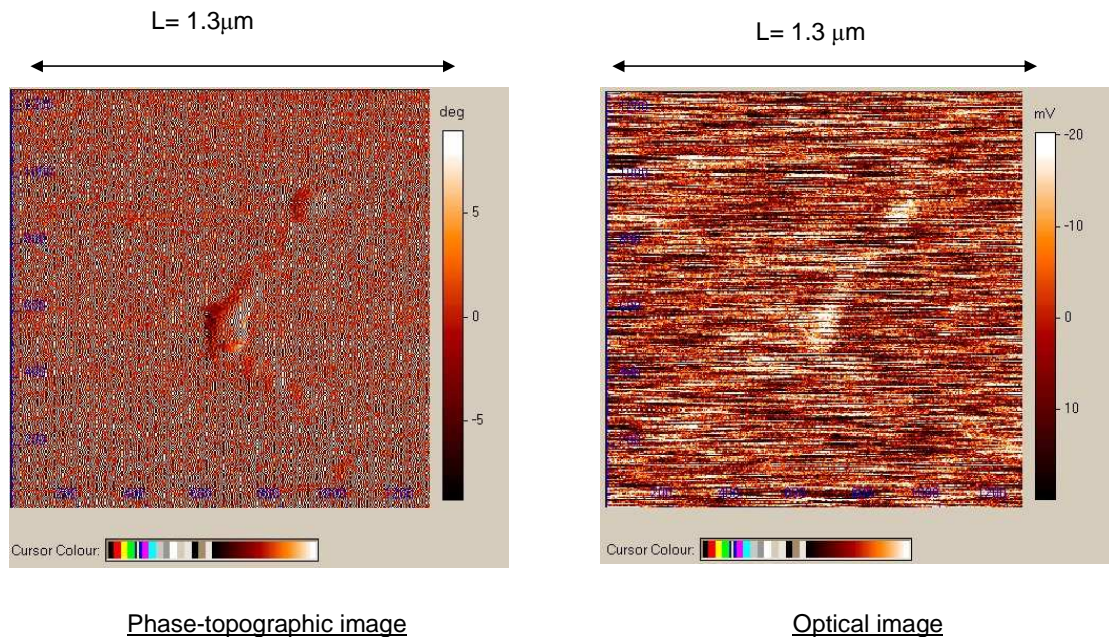
Figure III- 20: Phase- topographic and optical image of zoomed part in Figure III- 19

As we can see, we still have a resemblance between optical and topographic images; the optical image presents however a background that is considerable with respect to the signal emitted by the nanoparticles. Other publications have shown such a background for SNOM images of similarly fabricated samples, but with SNOM microscopes having different geometries compared to the one we used.

They were explained either as due to a superposition of coherent scattering phenomena in an A-SNOM[94] or were considered as coming from structures on the surface of the cover glass[95]. We have tried to find the explanation for such an image and we thought of many options:

1) The notch filter is a little bit titled with respect to the direction of the incoming signal and so some diffused laser signal (by the surface of the cover glass) has reached the detector in addition to the fluorescence. So what we would be seeing are interference patterns between light emitted from the tip and light reflected from the sample.

---

[94] S. Diziain et coll., "Coherent scattering phenomena in apertureless scanning near-field fluorescence microscopy," *Optics Communications* 276, no. 1 (Août 1, 2007): 180-185, doi:10.1016/j.optcom.2007.03.078
[95] T Sugiura et coll., "Gold-bead scanning near-field optical microscope with laser-force position control," *Optics Letters* 22 (1997): 1665, 1663

2) There are some interference effect coming from the interaction between the emitted fluorescence light and the laser light that lead to such observations.

3) The cover class that we used has some traces of impurities, thus implying substrate auto fluorescence. This phenomenon has been noticed in many fluorescence experiments of biological nature (with laser excitation at wavelengths reaching the visible range 400-600 nm) and in which cover glasses or glass microarrays were used as substrates.[96] The traces of impurities causing such a background may be generated through oxidation during manufacture or storage, and most probably have a single or conjugated π bonding. Adsorption of organic molecules from the environment during storage can also result in significant autofluorescence.[97]

Now that we have an idea about the different elements constituting (Figure III- 20), an interesting point would be to have a closer look on its resolution. We will first start by a small reminder of resolution notion in a SNOM measurement, and will then try to analyse the same figure in terms of such a definition.

III-4.1 Resolution discussion

The term 'resolution' in near field optical microscopy is still not fully defined, and may even seem as an intriguing concept[98]. In fact, resolving power in this case is not a property exclusively inherent in the microscope as in conventional optics, but also depends on the probe-sample interaction, topography, scanning mode, and polarisation of the incident light, making such a definition a much more complicated one than in far field microscopy.[99,100,101,102] The lateral resolution of an aperture SNOM was also considered as being limited by the effective size of the aperture. Being in the obligation to find a way to describe the discrimination between different elements in a SNOM image, different groups in the scientific society employed varying definitions for such a concept. Some talked about spatial resolution, defined as the width of the smallest discernible

[96] K. Bacia, S. A. Kim, et P. Schwille, "Fluorescence cross-correlation spectroscopy in living cells," *Nature Methods* 3 (2006): 83-89

[97] N. Raghavachari et coll., "Reduction of autofluorescence on DNA microarrays and slide surfaces by treatment with sodium borohydride," *Analytical Biochemistry* 312, no. 2 (2003): 101-105

[98] M. Labardi et coll., "Assessment of NSOM resolution on III-V semiconductor thin films," *Applied Physics A: Materials Science & Processing* 66 (1998): 397-402

[99] J. Schöfer et coll., "Influence of aperture diameter on image contrast and resolution in scanning near-field optical microscopy," *Journal of Applied Physics* 81 (1997): 5871

[100] S. I. Bozhevolnyi, "Topographical artifacts and optical resolution in near-field optical microscopy," *Journal of the Optical Society of America B* 14, no. 9 (1997): 2254-2259

[101] J. Schöfer et coll., "Influence of aperture diameter on image contrast and resolution in scanning near-field optical microscopy," *Journal of Applied Physics* 81 (1997): 5871

[102] S. I. Bozhevolnyi, "Topographical artifacts and optical resolution in near-field optical microscopy," *Journal of the Optical Society of America B* 14, no. 9 (1997): 2254-2259

feature.[103,104]Other considered a line cross section of a region in the SNOM images and studied the respective optical and topographic line profiles; the resolution was thus considered as being the Full Width at Half Maximum (FWHM) of a peak shaped feature.[105, 106,107] However not all the studied specimens in SNOM had a shape which could be fit. An appropriate solution to this problem was the calculation of an "edge " or " rate resolution'", defined as the width over which the signal drops from its 90 % value to its 10% its 10% [108,109,110,111,112].

These three different definitions were used for the calculation of the resolution of the fluorescence[113,114,115,116,117] and scattering images[118,119,120,121,122] .Thus, we found it appropriate to try to analyse the different images we obtained by comparing between the methods of the previously defined terms for " resolution" and to compare them with the

[103] Drabenstedt, Wrachtrup, et von Borczyskowski, "A distance regulation scheme for scanning near-field optical microscopy."

[104] B. Hecht et coll., "Scanning near-field optical microscopy with aperture probes: Fundamentals and applications," *The Journal of Chemical Physics* 112 (2000): 7761

[105] R. Eckert et coll., "Near-field fluorescence imaging with 32 nm resolution based on microfabricated cantilevered probes," *Applied Physics Letters* 77 (2000): 3695

[106] P. G. Gucciardi et M. Colocci, "Different contrast mechanisms induced by topography artifacts in near-field optical microscopy," *Applied Physics Letters* 79 (2001): 1543

[107] J. M. Kim, T. Ohtani, et H. Muramatsu, "25 nm resolution single molecular fluorescence imaging by scanning near-field optical/atomic force microscopy," *Surface Science* 549, no. 3 (Février 2004): 273-280

[108] Labardi et coll., "Assessment of NSOM resolution on III-V semiconductor thin films."

[109] V. Sandoghdar et coll., "Reflection scanning near-field optical microscopy with uncoated fiber tips: How good is the resolution really?," *Journal of Applied Physics* 81, no. 6 (Mars 15, 1997): 2499-2503

[110] J. Koglin, U. C. Fischer, et H. Fuchs, "Material contrast in scanning near-field optical microscopy at 1–10 nm resolution ," *Physical Review B* 55, no. 12 (Mars 15, 1997): 7977

[111] G Y Shang et coll., "Development of a shear force scanning near-field fluorescence microscope for biological applications," *Ultramicroscopy* 105, no. 1-4 (Novembre 2005): 324-329

[112] L. T. Nieman, G. M. Krampert, et R. E. Martinez, "An apertureless near-field scanning optical microscope and its application to surface-enhanced Raman spectroscopy and multiphoton fluorescence imaging," *Review of Scientific Instruments* 72 (2001): 1691

[113] Drabenstedt, Wrachtrup, et von Borczyskowski, "A distance regulation scheme for scanning near-field optical microscopy."

[114] Rolf Eckert et coll., "Near-field fluorescence imaging with 32 nm resolution based on microfabricated cantilevered probes," *Applied Physics Letters* 77, no. 23 (Décembre 4, 2000): 3695-3697.

[115] Shang et coll., "Development of a shear force scanning near-field fluorescence microscope for biological applications."

[116] Kim, Ohtani, et Muramatsu, "25 nm resolution single molecular fluorescence imaging by scanning near-field optical/atomic force microscopy."

[117] Linda T. Nieman, Gerhard M. Krampert, et Robert E. Martinez, "An apertureless near-field scanning optical microscope and its application to surface-enhanced Raman spectroscopy and multiphoton fluorescence imaging," *Review of Scientific Instruments* 72, no. 3 (Mars 0, 2001): 1691-1699.

[118] M. Labardi et coll., "Assessment of NSOM resolution on III-V semiconductor thin films," *Applied Physics A: Materials Science & Processing* 66, no. 0 (Mars 1, 1998): S397-S402.

[119] Bert Hecht et coll., "Scanning near-field optical microscopy with aperture probes: Fundamentals and applications," *The Journal of Chemical Physics* 112, no. 18 (Mai 8, 2000): 7761-7774.

[120] P. G. Gucciardi et M. Colocci, "Different contrast mechanisms induced by topography artifacts in near-field optical microscopy," *Applied Physics Letters* 79, no. 10 (2001): 1543-1545.

[121] Koglin, Fischer, et Fuchs, "Material contrast in scanning near-field optical microscopy at 1–10 nm resolution ."

[122] Sandoghdar et coll., "Reflection scanning near-field optical microscopy with uncoated fiber tips."

approximated width of the SNOM probe aperture that we used for this experiment. This would help us also to see whether or not a resolution smaller than the aperture can be obtained and try to explain the results. In order to calculate concisely the above parameters, we thought about applying a fitting to the obtained cross sectional line and determine them after trying to obtain the most suitable fitting. Let us consider Figure III-20and see how we can determine the attained resolution. We thus take a cross section of an area of the figure, in which we can clearly distinguish optical and topographic signals.

| Topographic image | Optical image |
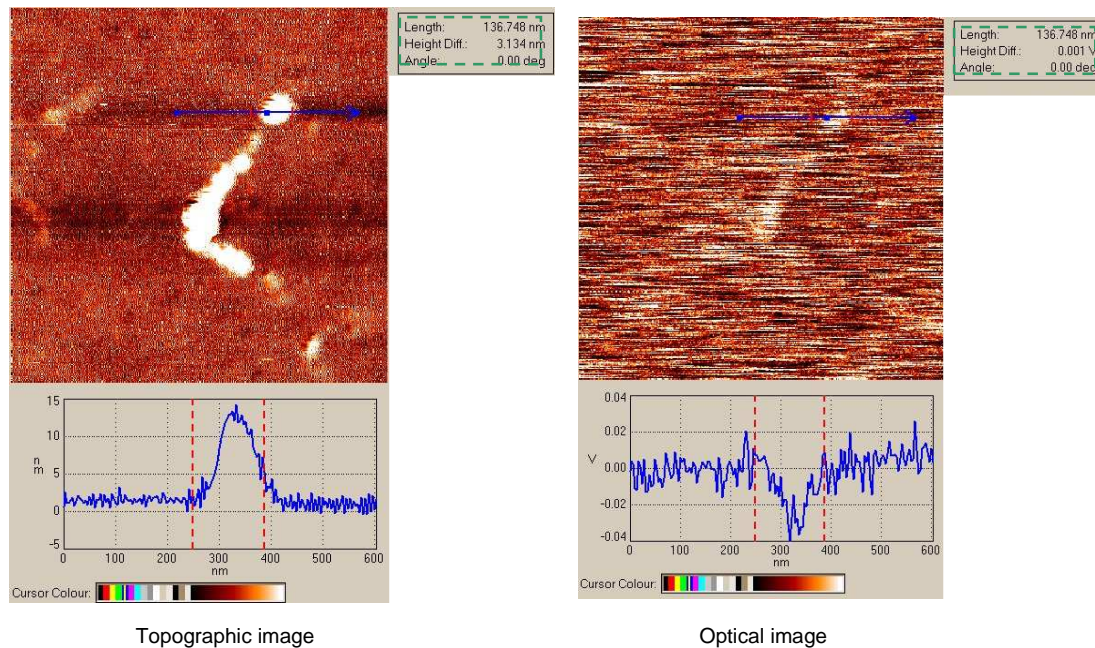
Figure III- 21: SNOM topographic and optical images of hybrid nanoparticles with respective line profiles.

The lower graphical parts of the topographic and optical images show respectively the Z variation of the tip and the change in the optical signal under the region represented by the blue arrows on the images. The red dotted lines however delimitate the region between the two red marks on the blue arrow. The upper right readings (in the green square) give the distance between the two red marks and their height difference.

The graphical parts were analyzed and fit to give the plots in Figure III- 22The FWHM values written on the figures have been determined using the 'Origin' program after applying the fittings; the blue lines mark the points at which the fittings of the graphs increase from 10% to 90% of their value. Their intersection with the fitting curves are denoted A, B and A', B' for respectively the topographic and optical graphs. The edge resolution has been calculated by determining the distance that separates A from B and A' from B'.

 As it is seen on Figure III- 22, both of the resolutions calculated for the optical signal are better than that of the topographic one. In fact, for the first we have a FWHM of about 64

nm and an edge resolution equal to 48nm, while the second has 51nm and 41 nm for the same parameters. Attaining a different resolution in optical than in topographic signal is the sign of a genuine purely optical SNOM image free from z induced artefacts[123],[124],[125] However, concerning the question of whether the optical resolution is better or worse than the topographical one is a point of debate. Some authors consider that a better resolution can be attained with shear force mechanisms since feedback techniques based on atomic forces can, at least in principle, exhibit a spatial resolution on an atomic level;[126] others on the contrary predict a better optical resolution than a shear force one relying their argumentation on a comparison between Atomic Force Microscope (AFM) and SNOM topographic images, showing a much more resolved AFM image for the same object, having also a better optical resolution;[127] It is interesting to note that in the case of a metallized tip, the shear force sensor is typically considered to be a protrusion in the metal coating forming the rim surrounding the aperture.[128] The lack of resolution in SNOM topographic image is thus mostly being reported as due to tip convolution at the steep edges of the studied structure.

The comparison between an AFM and optical near field image using other configurations on the other side shows an equal resolution for both cases,[129] supporting the assumption of a better optical resolution than a shear force one. It has been also reported that in some cases, the shear force mechanism may even play a role in masking a much better optical than topographic resolution through the z-motion of the Near Field Optical (NFO) probe.[130] In summary, this issue depends on the shear force mechanism used and the SNOM tip shape and structure we are using; Definite criterions have to be considered when implying a better topographic resolution than an optical one while using a probe having a sub wavelength aperture, and these would refer to a very concise and sensitive shear force system which would follow the detailed shapes of the sample, in addition to a very sharp tip which would lead otherwise to enlarged and unresolved structures.

---

[123] B. Hecht et coll., "Facts and artifacts in near-field optical microscopy," *Journal of Applied Physics* 81 (1997): 2492

[124] Labardi et coll., "Assessment of NSOM resolution on III-V semiconductor thin films."

[125] Kim, Ohtani, et Muramatsu, "25 nm resolution single molecular fluorescence imaging by scanning near-field optical/atomic force microscopy."

[126] Bozhevolnyi, "Topographical artifacts and optical resolution in near-field optical microscopy."

[127] Labardi et coll., "Assessment of NSOM resolution on III-V semiconductor thin films."

[128] CDIV Shvets, "Reflection-mode scanning near-field optical microscopy: Influence of sample type, tip shape, and polarization of light," *Journal of Applied Physics* 83 (1998): 1171

[129] Nieman, Krampert, et Martinez, "An apertureless near-field scanning optical microscope and its application to surface-enhanced Raman spectroscopy and multiphoton fluorescence imaging."

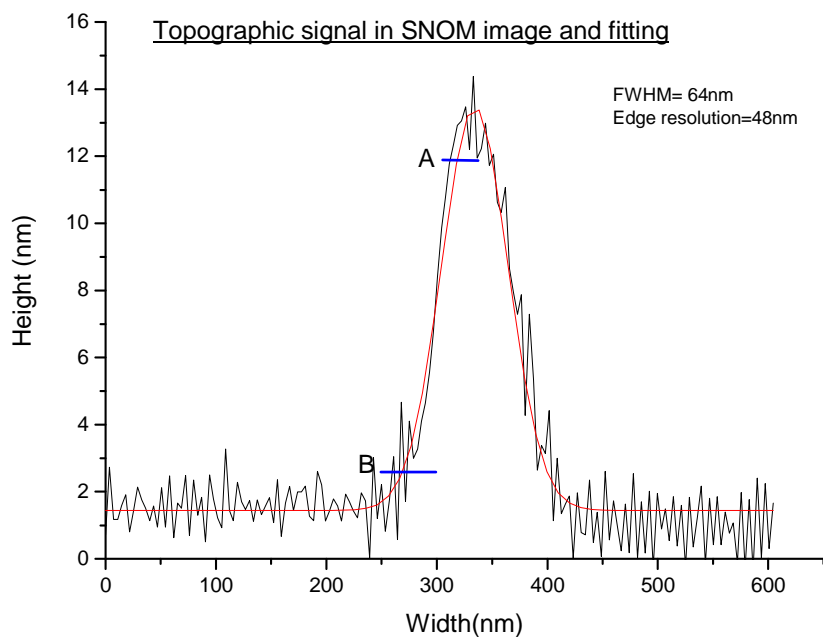[130] Hecht et coll., "Facts and artifacts in near-field optical microscopy."
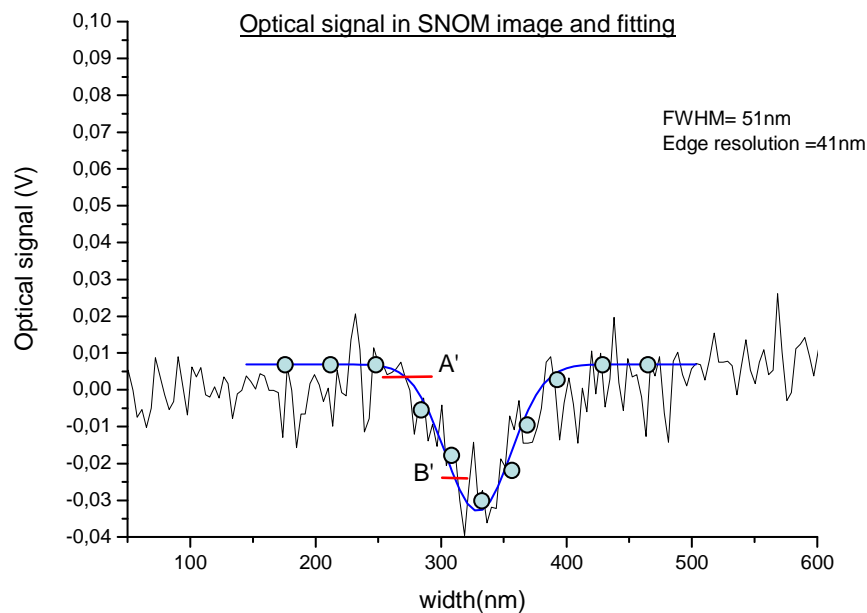
Figure III- 22: Profile lines of topographic and optical cross section of images in, showing respective fittings in each. The dotted line (upper part) represents fitting of the optical image while the straight red t line (lowest part) represents the topographic one.

Another point that should be discussed is how we obtained images having resolutions reaching values near 50 nm while the probe we used had a diameter of about 100 nm. If we consider the point of view of Pohl. *et al.,* this resolution is normally attainable since in aperture SNOM, the finest resolvable structures are approximately equal to the aperture *radius.*[131] Such a case has also already been studied by M.Labardi et al. where they had obtained a resolution about 20nm, even thought the metallized tips they used had apertures of 50 nm.[132] After a clear verification of their obtaining genuinely pure optical SNOM images, they concluded that such an enhanced resolution with respect to the aperture diameter can be explained by a near-field scatterer present in the vicinity of the aperture. Such small particles or minitips are formed on the aperture within the light pathway, acting as highly near-field scattering centers. Then it is the particle size, which is responsible of the higher resolution and not the aperture diameter; in summary, it is as if the microscope would behave like an apertureless one. This assumption leads us to wonder whether this same 'minitip' Pohl. *et al* are talking about is not exactly the same one referred to as a protrusion in the metallic rim, and which would be responsible of the shear force mechanism, having thus a double role.

III-4.2 Artefacts in near field optics

One important issue that has been the cause of several debates concerning near field optics is SNOM artifacts. Now if we look up the word "artifact" in the dictionary, we will find the following definition:

Artifact: A product of artificial character (as in a scientific test) due usually to extraneous agency.

In the near field case, and especially with near field optical microscopes with an auxiliary gap width regulation (shear force, tunneling), the artifact relies in the fact that the produced images can represent the path of the probe rather than optical properties of the sample. The possible existence of severe artifacts in near field optical imaging was suspected when noticing that a one-to-one existence frequently existed in structures recorded in near field optics and in topographic images. In particular, the same resolution was seen in both images. This would lead to some questioning since it is of little probability that two imaging processes resulting from different physical origins would have identical resolving power.[133,134] Thus SNOM operation in this mode brings up a serious problem of coupling which severely hinders access to pure optical information (which is essentially important since variations in the optical properties can be a

---

[131] Ibid.

[132] Labardi et coll., "Assessment of NSOM resolution on III-V semiconductor thin films."

[133] Hecht et coll., "Facts and artifacts in near-field optical microscopy."

[134] B. Hecht et coll., "Facts and artifacts in near-field optical microscopy," *Journal of Applied Physics* 81, no. 6 (Mars 15, 1997): 2492-2498

fingerprint of structural changes of the sample surfaces inspected) and consequently complicates the determination of optical resolution achieved.[135] Many theoretical models have been established in order to describe such tip-sample interaction and artifact formation.[136,137] The main solution to this problem had been to adopt a constant height mode (CH)of the tip in order to avoid any changes in the collected signal related to the topography of the sample. This can be done by starting with a constant gap mode (CG) imaging, determining the highest element of the scanned area, and shifting to the (CH) mode with a height corresponding to the defined one in the constant gap mode (in order to avoid any tip-sample contact). This should be done in addition to a prior knowledge of the studied object so that a good interpretation of the images could be made. For our system and the kind of sample we studied, such a procedure was found to be difficult since the tip deviated while passing from (CG) to (CH), as we realized we were unable to find the same elements of the same scanned area if we tried passing from (CH) to (CG) again. However, others ways that would help identify optical artifacts in (CG) mode were also suggested. At least one of the following requirements has to be satisfied by a near field image to be credible.[31]

1) The near field image is obtained in CH mode (already discussed)

2) The near field image is obtained in CG mode, but:

   a) Topographic and near field optical images are highly uncorrelated.

   b) Correlated structures are displaced by a constant amount. This indicates that optical and non optical zones do not coincide; meaning that such a displacement would be caused due to a misplacement of the aperture with respect to the most protruding part of the tip, which is subject to shear forces.[138,139]

c) The resolution of near field optics and shear force images are clearly different.

Let us try to verify the three points mentioned in the second case for the figure previously shown (Figure III- 21). We find a resemblance between the optic and topographic images, however, with a more or less important correlated with each other.

   1) Let us take a closer look to the delimitated areas in the previous figures and name the left handed dashed line a and the right handed one b concerning the optical image.

---

[135] K. D. Weston, J. A. DeAro, et S. K. Buratto, "Near-field scanning optical microscopy in reflection: A study of far-field collection geometry effects," *Review of Scientific Instruments* 67, no. 8 (1996): 2924

[136] Gucciardi et Colocci, "Different contrast mechanisms induced by topography artifacts in near-field optical microscopy."

[137] Hecht et coll., "Scanning near-field optical microscopy with aperture probes."

[138] P. G. Gucciardi et coll., "Versatile scanning near-field optical microscope for material science applications," *Review of Scientific Instruments* 68 (1997): 3088

[139] Hecht et coll., "Facts and artifacts in near-field optical microscopy."
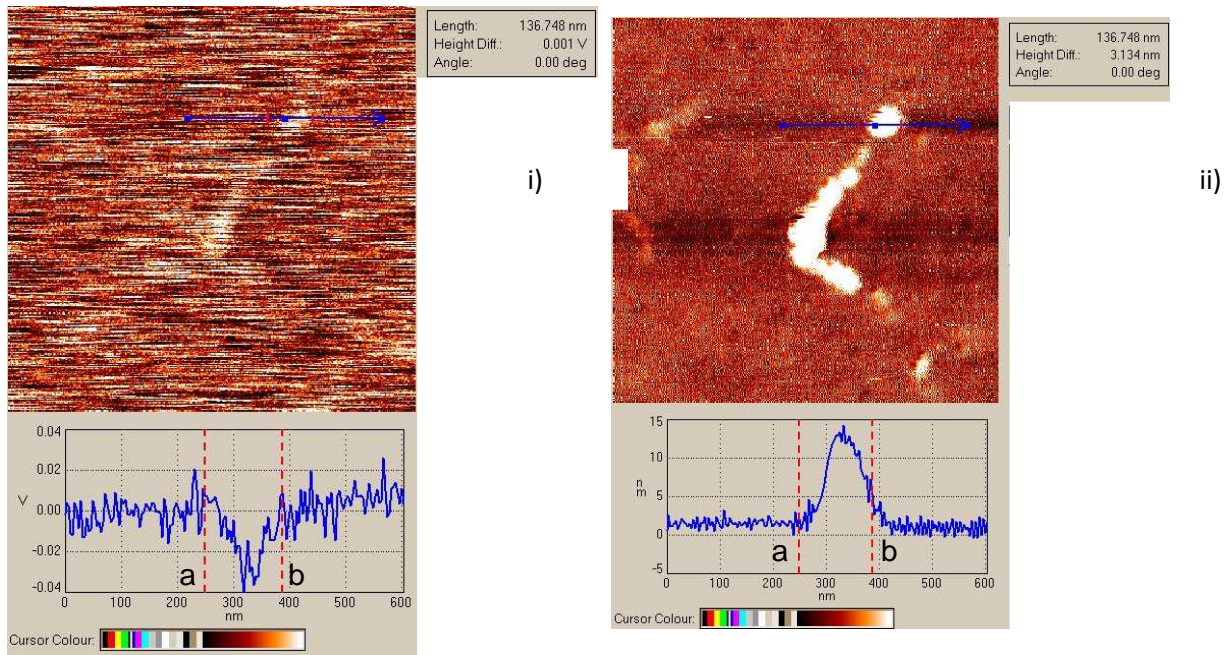
Figure III- 23: (i) Hybrid nanoparticles SNOM optical image and corresponding line profile for the region delimited under blue arrow, by point (a) and (b), (ii) , and corresponding topographic image and line profile, with the same points a and b.

In the Figure III- 23 -i, we delimitated the region in which we had a clear optical signal under the blue arrow (by also referring to the image) with the two border lines (a) and (b). Figure III- 23 ii- represents the topographical image of the same area with the corresponding topographic profile line. The border lines (a) and (b) of the optical image have been copied on the topographic one in order to compare between optical and topographic signal. As we can see on Figure III- 23, the optical signal (delimited by lines a-b) is shifted to the left with respect to the topographic one.
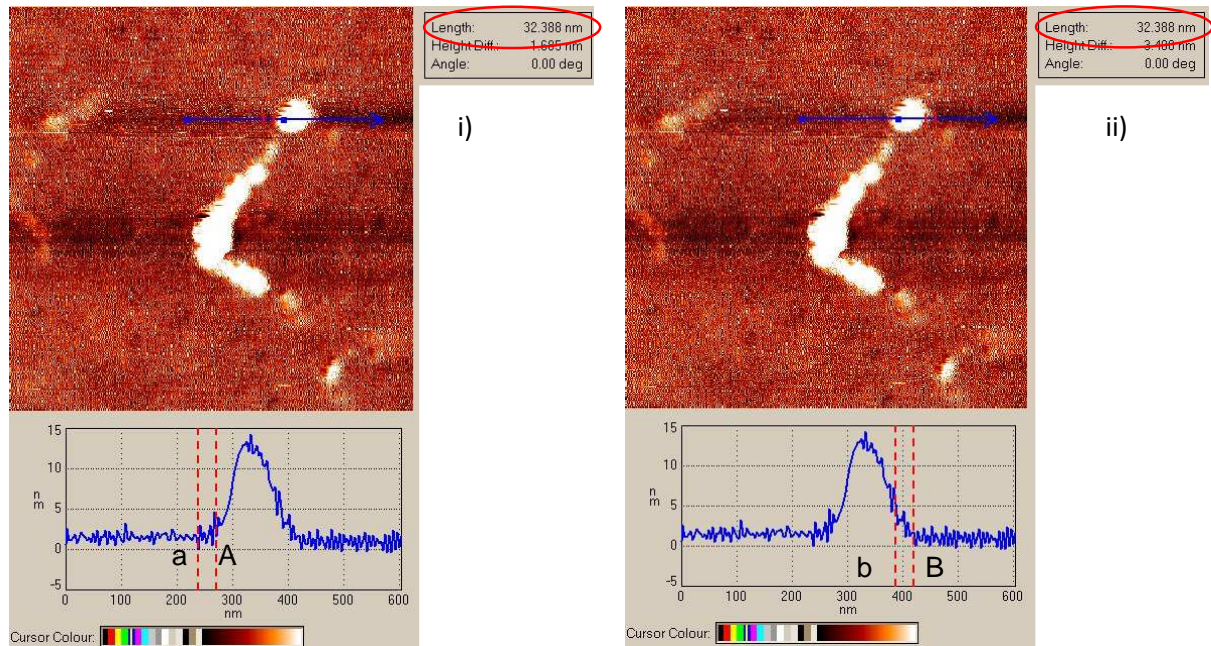
Figure III- 24: Comparison between topographic (AB) and optical (ab) profile line delimitations

This Shift is determined by looking at the Figure III- 24, where the same shift of about 32 nm is found on the left and right part of the image. A and B are the delimitating lines for the topographic profile. This implies that a protrusion responsible for the shear force mechanism is distanced by the same amount from the aperture (32 nm), which is a reasonable value, taking into account that the SNOM tip we used had an average diameter of 100nm.

2) As calculated in the previous section, and by the use of two different methods (FWHM and edge resolution), the optical resolution is different from the topographic one.

These points let us conclude that the criterions for an optically genuine near field optical image, free of topographic artifact have been fulfilled in our case and that what we are seeing is the optical signature of the hybrid nanoparticles.

III-4.3 Comparison between scattering and fluorescence imaging:

Knowing that the nanoparticles we used were of scattering nature, we thought it would be interesting to compare between SNOM scattering and fluorescence images, meaning respectively without and with a Notch filter. We used the same sample preparation method and SNOM configuration as that described previously, except for removing the notch filter in the case of non fluorescent imaging. The scanning area was about 1.6μm ×1.6μm and the features we studied were also aggregates of nanoparticles. The following figure (Figure III- 25) shows the topographic and optical images in the case of diffusion, accompanied by the profile lines of the region under the blue arrow. The choice for such a region at the border of the nanoparticle

agglomeration and not its center is justified by the fact that, being in a case where we are dealing with scattering and not fluorescence, the collected laser light interfered within the measurement and so the selected region was chosen in such a way as to be less affected by this factor.
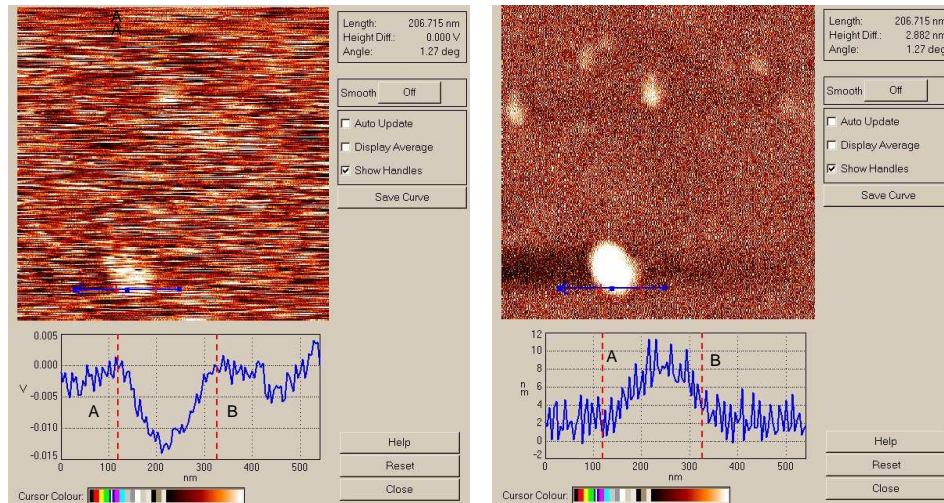
Figure III- 25: Optical (diffusion) and topographic SNOM images and profiles of nanohybrids

By following the same procedure as that used in the previous section, we clearly see that in this case also there is a clear shift between optical and topographic images. This shift is about 46 nm, as recorded in Figure III- 27 and Figure III- 26:
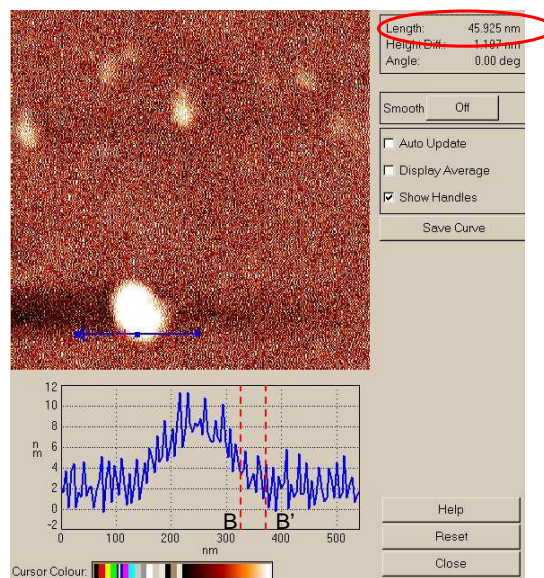
Figure III- 26 Shift between optical and topographic images of Figure III- 25 considering the apex at B

:
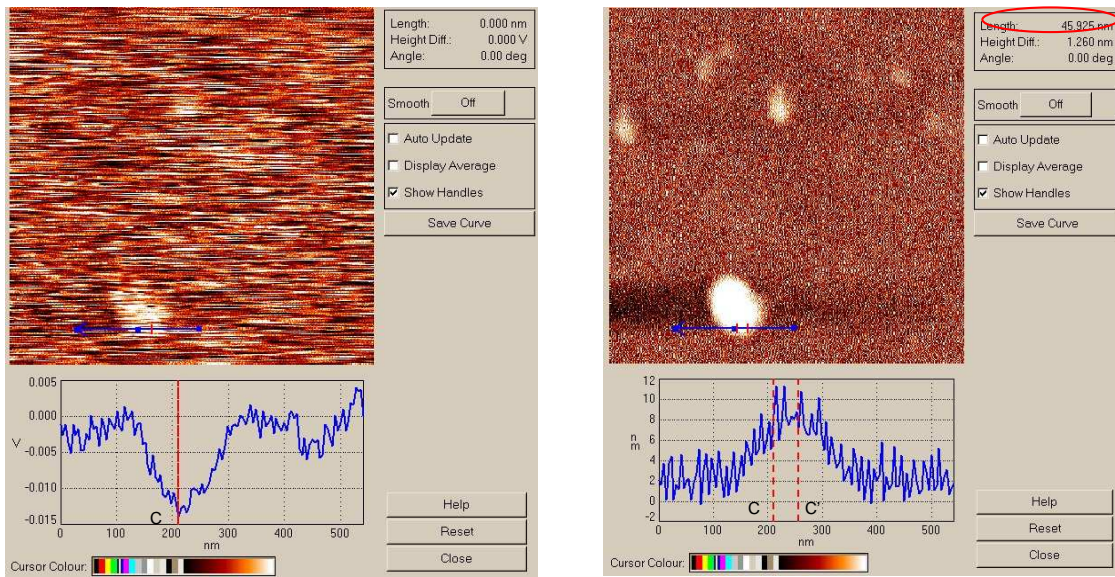
Figure III- 27 : Shift between optical and topographic images of Figure III- 25considering the apex at C.

Now after placing a notch filter on the pathway of the collected light signal, and scanning the same region, we obtain the following fluorescence and topographic images
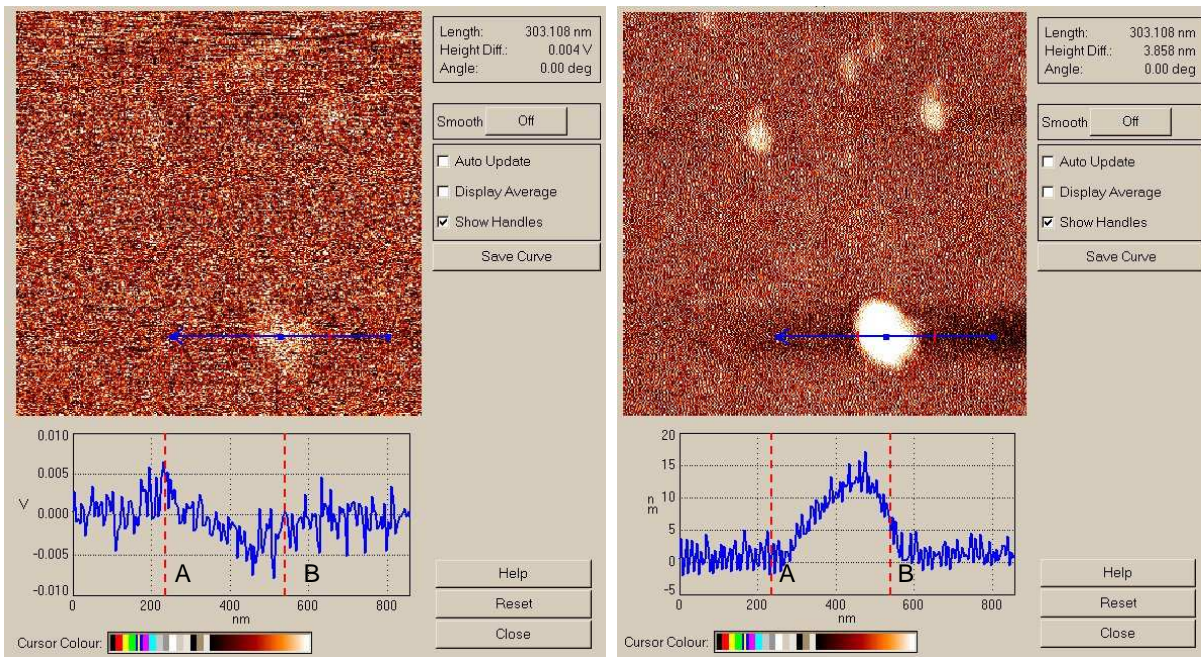
Figure III- 28: Optical (left) and topographic(right) images of nanohybrids after placing a Notch Filter

As in the previous cases, we still notice the same shift between topographic and optical images, by taking into account the left and right border A, B shifted by 46nm
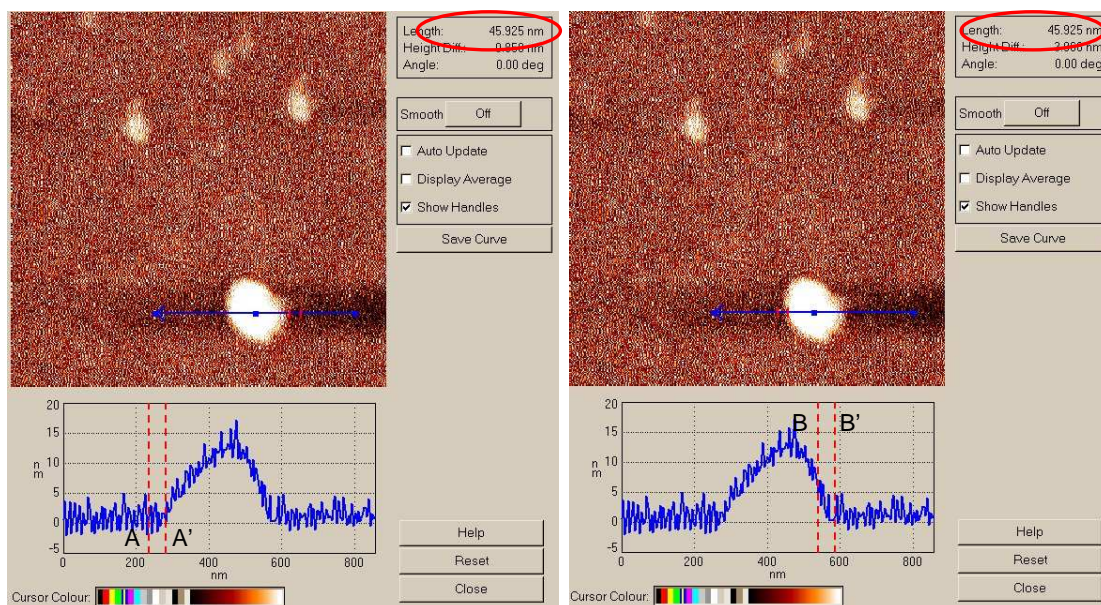
Figure III- 29 Shift between optical and topographic images of Figure III- 28considering A and B

Thus it appears that it is the same protrusion that has been responsible for the tip shear force mechanism while recording images Figure III- 25 till Figure III- 27, that was also responsible for the distance regulation process giving Figure III- 28 Figure III- 29, since in both cases we find the same shift between optical and topographic image, which is about 46 nm.

Regarding the second criterion of a genuine optical image, and which concerns the condition of a difference in resolution between topographic and optical images: If we try to do the same calculations as we did for the previous section, we find for the scattered light optical images an edge resolution of 80nm and a FWHM=90nm; The corresponding topographic images have edge resolution of 90nm and a FWHM equal to 112nm. Thus in both cases we are still encountering the situation where the optical resolution is better than the topographic one. A little discussion has to be made however concerning the similarities and differences between the fluorescence image(Figure III- 28) and a scattering one (Figure III- 25): Topographic images of both cases display the same elements constituted of four sets of aggregates, even thought shifted by a certain distance of few hundreds of nanometers; this shift must be due to a small displacement of the sample while trying to take off the Notch filter. The first impression that we have when comparing between the two optical images is that the fluorescence image is almost free of any background signal, contrarily to the diffusion one. This is logical if we consider that all the light that is scattered from the glass substrate is now being collected by the detector, including all kinds of light that may be emitted from the glass itself, and creating such a background. The signal level above the considered aggregate is also stronger in the scattering image (about 0.013 V compared to 0.006 V in fluorescence), since in the first one we are adding both fluorescence and scattering light, while in the second it is only the fluorescence we are collecting.

Also, if we come to compare the background between the fluorescence image obtained in the case of Figure III- 28 and the one we talked about in the previous section Figure III- 20, we find that the first has a much better S/N ratio. This may be caused by two reasons, the first is an assumption that has already been done, and which is that the notch filter was tilted with respect to the direction of incident light, and that by consequence some scattered light leaked into the detector. The second concerns the tip vibration: we can see from the topographic images that the oscillation amplitudes are larger in Figure III- 27 then in Figure III- 20 , It has been found however that even thought big oscillations may be responsible of a loss in lateral resolution, they also lead to a signal -to-noise ratio increase.[140] This may be the reason of such an improvement in our case, where the larger oscillations in the last figure are responsible for a better signal to noise ratio and thus a much clearer background.

One final point which we could address is the height of the nanoparticles in the topographic image: For a region in which we are taking the center (highest point) of the aggregate in consideration, we have a height of about 15nm, however the nanoparticles we are studying are known to be closer in height to 20nm; the reason of such a difference in size can be understood by looking at what appears on the right part of Figure III- 29 as a gap (black region). First we have to remember that the substrate is a pure flat cover glass whose topographic features have been already studied Figure III- 17 and have shown nothing but small corrugations of few nanometers height: this lets us conclude that the black region in Figure III- 29 is nothing in reality but a signature that the tip was subject to a displacement in the upper z direction while scanning the region at the left of the aggregate, and above it , and thus would be shifting the zero point level by a few nanometers, making the nanoparticle aggregate appear smaller of few nanometers in z direction than they actually are in reality.

In conclusion, we were able to prove in this section that the visualization of hybrid nanoparticles at small resolutions whether topographically (Z and phase topography), or optically (Scattering or Luminescence) is feasible by the use of near field optical microscopy. As evidenced by the different exposed methods, the criteria for artifact free images have been found to be fulfilled in all the types of recorded images. Finally, the resolution which could be attained with our setup and the SNOM tips we used, was found to attain values as small as 50 nm. The next step would be to combine both SNOM measurements and hybrid nanoparticles for their use in biological applications as in the following.

---

[140] Gucciardi et coll., "Versatile scanning near-field optical microscope for material science applications."

Chapter IV: Single silicon nanocrystals investigation with a confocal microscope[141]

Introduction

Silicon is known to be until now the most technologically important material to mankind, dominating the microelectronics revolution that influences our everyday life. This is due to the fact that it has many advantageous properties for advanced material processing, such as an electrical conductivity that can be controlled over a wide range (dynamically or permanently), superior chemical and mechanical characteristics, an SiO_2 oxidized state that is one of the best and most stable electrical insulator etc... . Even thought bulk silicon has always been known for its being spectacularly inefficient at emitting light, even at cryogenic temperature, in the 1990's first reports for light emitting porous silicon nanostructures were published.[142] Thus, a better knowledge of their optical properties has attracted considerable attention with the motivation of the development of light emitting Si devices (such as light- emitting diodes) that could eventually result in a new generation of Si chips and extend the functionality from microelectronics into optoelectronics.[143]

 A unique way to have a clear and concise idea about the emission properties of such Si nanostructures has been done through the use of Single nanocrystal spectroscopy (SNS).[144,145,146] In fact, such a technique consists of the study of only one and unique nanocrystal, buy looking at its spectral response (absorbed and emitted light when excited at a certain wavelength), it permits us to obtain information that would normally disappear in the ensemble average, thus eliminating for the effects of inhomogeneous broadening. It has revealed many unexpected physical phenomena such as ultra narrow emission line shapes, blinking phenomena, spectral diffusion and polarisation etc...[147].

---

[141] "This part of the thesis was made possible through the precious help and collaboration of Prof.Dr. Christian Von-Borczyskowski and his team at institute of physics and nanoMA, Chemnitz University of Technology and Prof.Dr. Friedrich Huisken and his team at Institute of solid state physics ,University of Jena (Germanyy) , in addition to the financial support provided by Max Plak Institute (Germany) through the Nanolum European Rsearch Group."

[142] L. T. Canham et al., "Luminescent anodized silicon aerocrystal networks prepared by supercritical drying," *Nature* 368, no. 6467 (Mars 10, 1994): 133-135.

[143] A. G. Cullis, L. T. Canham, et P. D. J. Calcott, "The structural and luminescence properties of porous silicon," *Journal of Applied Physics* 82, no. 3 (1997): 909-965.

[144] S. A. Empedocles et coll., "Photoluminescence from Single Semiconductor Nanostructures," *Advanced Materials* 11, no. 15 (1999): 1243-1256.

[145] Ilya Sychugov et coll., "Luminescence blinking of a Si quantum dot in a Si O2 shell," *Physical Review B* 71, no. 11 (Mars 29, 2005): 115331.

[146] J. Martin, F. Cichos, et C. von Borczyskowski, "Spectroscopy of single silicon nanoparticles," *Journal of Luminescence* 108, no. 1-4 (Juin 2004): 347-350.

[147] Todd D. Krauss et Louis E. Brus, "Electronic properties of single semiconductor nanocrystals: optical and electrostatic force microscopy measurements," *Materials Science and Engineering B* (Janvier 2000): 289-294.

Such kind of studies can be done through the use of different tools such as SNOM (Near field optical microscopy) or confocal microscopy.

In this chapter, we will present results that we obtained concerning the optical properties of small size Si nanocrystals by confocal single nanocrystal spectroscopy, and try to have a deeper understanding of their emission properties with respect to their sizes and dielectric environments. This will be done by placing size differing nanocrystals in different polymeric media which have unlike dielectric constants and trying to characterise the different varying parameters concerning their emission spectra in each case. The three kinds of dielectric we have chosen are PMMA, PVA and air. This choice has been based on the fact that there is a noticeable difference between one material's dielectric constant and the other (especially between PMMA and PVA). Such a contrast would allow us to have a better distinction between each matrices influence on the nanocrystal's emission. We will first begin by a general reminder about bulk silicon optical mechanisms, and then will try to understand what happens when the size shrinks until reaching nanometric dimension, to finally reach a size of about less than 3 nm.

IV-1 Silicon material overview general Properties:

IV-1.1 Bulk Silicon

As previously mentioned, bulk silicon is not a good candidate as a light emitting material; this is due to its band gap characteristic. In fact, looking at Figure IV- 1, we see that silicon is an indirect energy band gap material, whose conduction band energy minimum and valence band do not fall at the same wave vector.
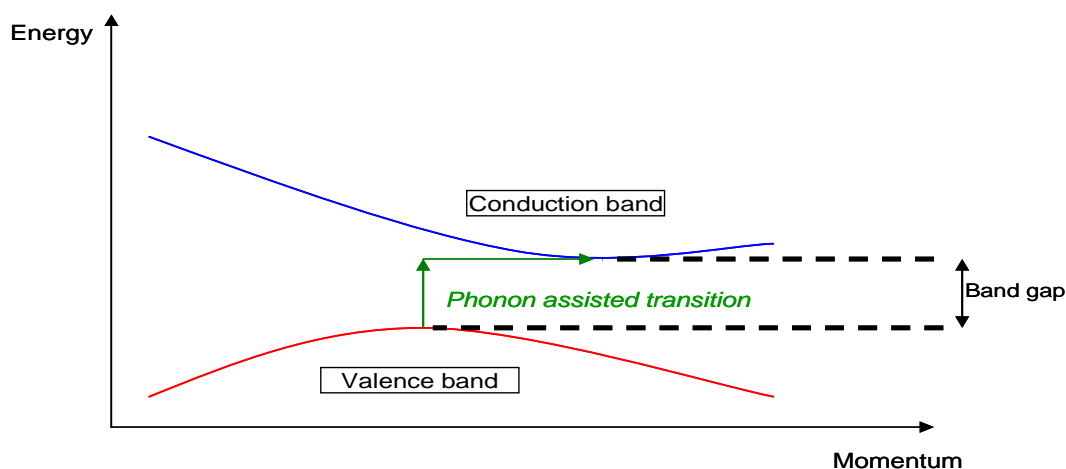
Figure IV- 1: Energy versus crystal momentum for a semiconductor with an indirect band gap

We talk about radiative recombination when an electron occupying the lowest energy state of a conduction band drops down to empty states of holes, which themselves occupy the upper states of the valence band, releasing its energy to photons of energy $\hbar\omega = E_c - E_v \approx E_g$, where E_g is the band gap energy of the semi conductor and $\hbar\omega$ is the photon energy. Besides this conservation of energy, momentum should be also conserved in such a process; three elements are entering in action is this case of figure, the photon, the electron and the hole. The photon wavelength ($\lambda = 1\mu m$ for silicon) is about three order of magnitudes larger than the Debroglie wavelength of the electrons (it is of the orders of the lattice constant of semiconductors $\approx 5\text{Å}$), thus the photon momentum can be neglected with respect to that of the hole and electron. We now come to deal with the remaining two elements, meaning the electron and hole. When both the electron and hole have the same momentum at the centre of the Brillouin zone the rule of momentum conservation is satisfied, and direct radiative recombination can normally take place. We say that in this case, we are in the situation of a direct band gap semi-conductor (like Ga As for example).

However, when there is a large momentum mismatch between electrons and holes, the momentum conservation rule can not be fulfilled, and the recombination process can not take place unless a third entity enters in action, like a phonon for example. This is what happens in indirect band semiconductors, such silicon. Thus, bulk silicon is considered as a poor emitter of light that cannot be used for applications where active light sources are required.

IV-1.2 Si nanocrystals S band and F-Band emission properties:

Contrarily to the bulk material, silicon nanocrystals have been surprisingly discovered as highly emitting agents. During their emission, two types of bands can be found:

The first one is a strong band who's emission spectrum extends from the 400 till 550 nm range of the visible spectrum, and is called the F- band (for Fast band) since it has a fast PL decay time of several nanoseconds. Such a band has been observed (even thought infrequently) as emanating from fully oxidized porous silicon,[148] and from most silicon nanostructures embedded in SiO_2 matrices, or silicon nanowires[149] with fairly large

---

[148] A. G. Cullis, L. T. Canham, et P. D. J. Calcott, "The structural and luminescence properties of porous silicon," *Journal of Applied Physics* 82, no. 3 (1997): 909-965.

[149] M. Dovrat et coll., "Optical properties of silicon nanowires from cathodoluminescence imaging and time-resolved photoluminescence spectroscopy," *Physical Review B (Condensed Matter and Materials Physics)* 75, no. 20 (Mai 15, 2007): 205343-5.

diameters.[150,151] Such a band has been interpreted as being due to either an intrinsic optical recombination in ultra small Si nanoparticles[152,153] (with a strong quantum confinement effect and a large band gap opening), to structure distortions that take place in small silicon nanocrystals (around 2 nm in diameter)[154] or to recombination in silicon oxide and interface defects,[155] the third case being unassimilated with the structures themselves, and so, nanocrystal size independent.

The second band on the other hand has an emission spectrum which extends from 500 till 900 nm, and is called the S band (S this time refers to 'slow') since it has a significantly slower PL decay times (compared to the F-Band) in the range of few microseconds. Such a band is a size dependant luminescence band, which shows a clear correlation with quantum size effects in silicon nanostructures. It has been the subject of many studies, but still holds a lot of controversial opinions concerning its origin. In fact, a major source of controversy and disagreement among researchers is the underlying mechanism behind the S band photoluminescence; the two models that are most noticeable are: first the quantum confinement model that assigns the PL to quantum size effects in the nanocrystalline silicon core of the nanostructure[156,157,158] and the surface chemistry model that assigns the photoluminescence to surface phenomena at the interface between the crystalline core and the host matrix that wrap the nanostructures,[159,160] or for example luminescent defect states[161] and oxygen vacancy states at the Si/ SiO$_2$ interface[162] etc... . In other words, the two mechanisms of radiative recombination in Si nanocrystal systems that dominate in photoluminescence, after the

[150] Shuji Komuro et coll., "Carrier dynamics in oxidized porous silicon," *Journal of Applied Physics* 80, no. 3 (1996): 1749-1756.

[151] P. M. Fauchet, "Ultrafast Carrier Dynamics in Porous Silicon," *physica status solidi (b)* 190, no. 1 (1995): 53-62.

[152] Gennadiy Belomoin, Joel Therrien, et Munir Nayfeh, "Oxide and hydrogen capped ultrasmall blue luminescent Si nanoparticles," *Applied Physics Letters* 77, no. 6 (2000): 779-781.

[153] Vladimir Svrcek et coll., "Blue luminescent silicon nanocrystals prepared by ns pulsed laser ablation in water," *Applied Physics Letters* 89, no. 21 (Novembre 20, 2006): 213113-3.

[154] J. Valenta et coll., "On the origin of the fast photoluminescence band in small silicon nanoparticles," *New Journal of Physics* 10, no. 7 (2008): 073022.

[155] Komuro et coll., "Carrier dynamics in oxidized porous silicon."

[156] L. T. Canham, "Silicon quantum wire array fabrication by electrochemical and chemical dissolution of wafers," *Applied Physics Letters* 57, no. 10 (1990): 1046-1048.

[157] A. G. Cullis et L. T. Canham, "Visible light emission due to quantum size effects in highly porous crystalline silicon," *Nature* 353, no. 6342 (1991): 335-338.

[158] D. Kovalev et coll., "Optical Properties of Si Nanocrystals," *physica status solidi (b)* 215, no. 2 (1999): 871-932.

[159] Cullis, Canham, et Calcott, "The structural and luminescence properties of porous silicon."

[160] Volker Lehmann et Ulrich G sele, "Porous silicon: Quantum sponge structures grown via a self-adjusting etching process," *Advanced Materials* 4, no. 2 (1992): 114-116.

[161] Yoshihiko Kanemitsu, Yunosuke Fukunishi, et Takashi Kushida, "Decay dynamics of visible luminescence in amorphous silicon nanoparticles," *Applied Physics Letters* 77, no. 2 (Juillet 10, 2000): 211-213.

[162] Vincenzo Vinciguerra et coll., "Quantum confinement and recombination dynamics in silicon nanocrystals embedded in Si/SiO[sub 2] superlattices," *Journal of Applied Physics* 87, no. 11 (Juin 1, 2000): 8165-8173.

creation of an exciton inside the nanocrystal, can take place either inside the nanocrystal (and this is when we talk about quantum confinement) or at the interface state. Studies showed that it is both effects that can enter into play through a model called the 'vibron' model[163] which we will explain more in detail in coming sections.

IV-2 Si nanocrystal elaboration, characterisation, and sample preparation.

IV-2.1 Nanometric size Si nanocrystals: fabrication techniques

With the advance of technology and available scientific means, synthesis and investigations of silicon on the nanometric scale has become possible. Different fabrication techniques exist for the production of luminescent silicon nanostructures, the simplest one is based on porous silicon, which can be obtained by electrochemical etching of crystalline substrates by using hydrofluoric acid (HF) based solutions,[164,165] others consist of producing Si Nc's embedded in SiO_2 with RF magnetron sputtering,[166] reactive evaporation,[167] chemical vapour deposition techniques (CVD)[168] etc.... The last technique can itself be applied with different preparation methods, including laser pyrolisis; such a process will be the subject of discussion of the following section.

The nanocrystals we studied were prepared via a special kind of CVD technique consisting of producing Si nanocrystals by using CO_2 laser induced decomposition of SiH_4 in a flow reactor and depositing a fine layer of the produced powder on a quartz or substrate after its expansion through a conical nozzle into a high vacuum.[169,170] These have been provided to us by Prof. F. Huisken et al. (private contact) and were synthesised at the Friedrich-Schiller-Universitat, institute fur Festkorperphysik, (Jena

[163] Amir Saar, "Photoluminescence from silicon nanostructures: The mutual role of quantum confinement and surface chemistry," *Journal of Nanophotonics* 3, no. 1 (Mars 12, 2009): 032501-42.

[164] F. Fonthal et coll., "Fabrication and Characterization of Porous Silicon on crystalline Silicon based devices," dans *Proceedings of the Electronics, Robotics and Automotive Mechanics Conference* (IEEE Computer Society, 2007), 170-174, http://portal.acm.org/citation.cfm?id=1299556.

[165] A. Givant, J. Shappir, et A. Sa'ar, "Photoluminescence anisotropy from laterally anodized porous silicon," *Applied Physics Letters* 73, no. 21 (Novembre 23, 1998): 3150-3152.

[166] S. Charvet et coll., "Substrate temperature dependence of the photoluminescence efficiency of co-sputtered Si/SiO2 layers," *Journal of Luminescence* 80, no. 1-4 (Décembre 1998): 241-245.

[167] U. Kahler et H. Hofmeister, "Visible light emission from Si nanocrystalline composites via reactive evaporation of SiO," *Optical Materials* 17, no. 1-2 (Juillet 2001): 83-86.

[168] Woo S. Cheong, Nong M. Hwang, et Duk Y. Yoon, "Observation of nanometer silicon clusters in the hot-filament CVD process," *Journal of Crystal Growth* 204, no. 1-2 (Juillet 1999): 52-61.

[169] G. Ledoux et coll., "Photoluminescence of size-separated silicon nanocrystals: Confirmation of quantum confinement," *Applied Physics Letters* 80, no. 25 (Juin 24, 2002): 4834-4836.

[170] Friedrich Huisken, Bernhard Kohn, et Vincent Paillard, "Structured films of light-emitting silicon nanoparticles produced by cluster beam deposition," *Applied Physics Letters* 74, no. 25 (Juin 21, 1999): 3776-3778.

Germany), in direct relation with the Max-Plank Institut fur Astronomie, (Gottingen-germany). The setup used to their synthesis is presented as the following[171] (Figure IV- 2)
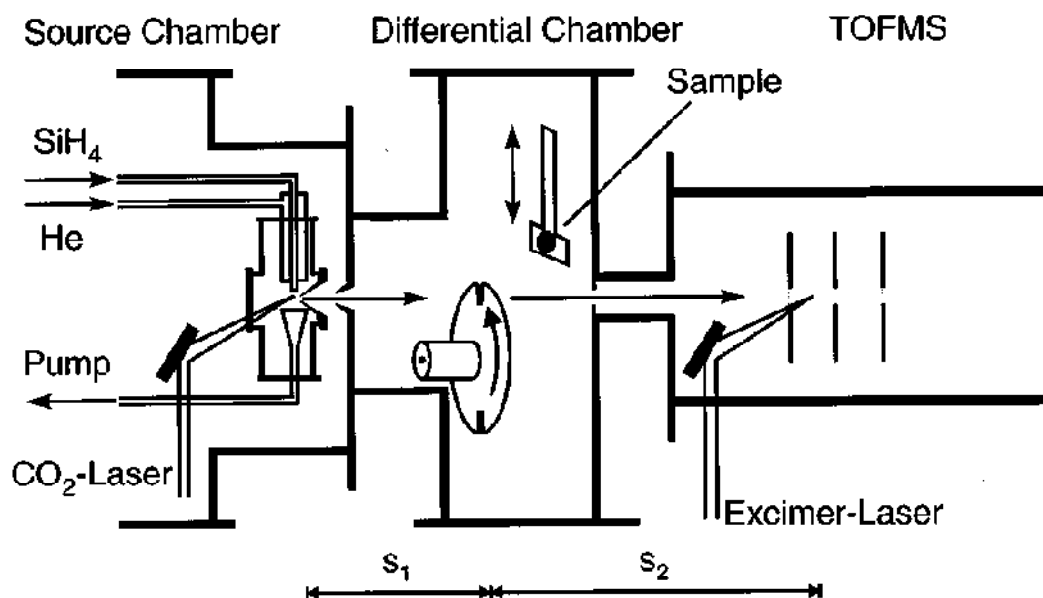
Figure IV- 2: Si Nanocrystal synthesis set up by laser pyrolisis taken from reference 221

The SiH_4 reactant gas is admitted to the centre of the flow reactor through a stainless steel tube having 3mm diameter. A focused radiation of a pulsed CO_2 laser, initiates the silane's decomposition. In this way, a saturated vapour of silicon atoms at elevated temperature ($\geq$1300K) is produced giving rise to condensation and subsequent growth of silicon clusters and nanoparticles. A major part of the nanoparticles produced during the CO_2 laser pulse are pumped away through a funnel and collected in a filter outside of the apparatus. The rest of the reaction products are then confined to the flow axis by a flushing helium flow through a coaxial outer tube with 12 mm diameter. All of these processes take place in a source chamber pumped by a 6000 l/s oil diffusion pump, a 350 m^3/h root blower, and a 65 m^3/h rotary pump. The reaction products are then extracted perpendicularly to both the gas flow and the CO_2 laser beam through the conical nozzle having a 0.3 mm diameter opening. After skimming, the clusters pass through a pressure-reducing differential chamber of 370 mm length to finally reach a time of flight mass spectrometer (TOFMS) in which the nanoparticles can be ionized by their radiation with an ArF excimer laser. The time-of-flight mass spectra are then measured by storing the detected ion signals as a function of their arrival time.

---

[171] M. Ehbrecht et coll., "Photoluminescence and resonant Raman spectra of silicon films produced by size-selected cluster beam deposition," *Physical Review B* 56, no. 11 (1997): 6958

An important item of the setup is the rotating chopper illustrated in the differential chamber (Figure IV- 3).It is a 123 mm diameter and 1mm thick disk having two diametrically opposed 1mm wide slits. Such disk permits a reduction of the size distribution of the extracted particles. In fact, the CO_2 laser being a pulsed one, the silicon clusters are generated in a pulsed mode. Due to the size-dependent velocity of the extracted particles, the cluster pulse becomes broadened and the clusters are separated according to their size. Using a light barrier, a frequency divider, and a variable delay generator, the CO_2 laser can be synchronised with the chopper. Knowing the distances S_1 between the nozzle and the chopper, and the appropriate time Δt_1 between the firing of the CO_2 laser and the moment when the particles pass through the chopper, it is possible to select from the entire cluster pulse the portion with the desired mean size and depose it on the substrate. This last deposition is done by placing a sample holder (located in the differential chamber) into the cluster beam.
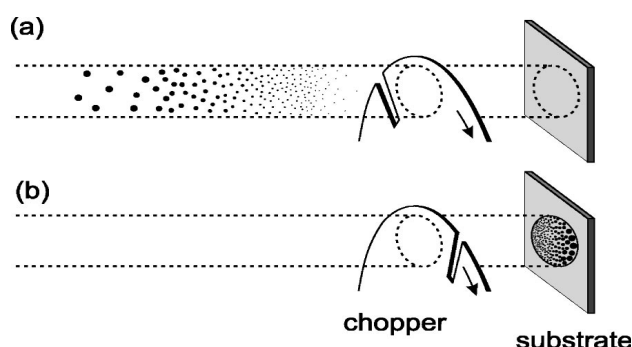
Figure IV- 3   Chopper nanoparticle size distribution, from reference 12 . a) Is an illustration of the separation of particles with different velocities in the pulsed beam. b) illustrates the situation when the particles have already passed the chopper slit. Due to the revolving chopper slit, Si particles of different sizes have been deposited at different positions on the substrate.

Thus such a setup permits us to obtain different samples depending on the desired application: a filter on which the produced nanoparticles are produced and directly directed, a substrate on which we can make thin films composed of size distributed nanocrystals, and finally ionized nanoparticles in the TOFMS system. The main differences between the first two cases are larger nanoparticles deposited on the filter, having a broader size distribution; however it is possible to collect much more particles in the filter than those deposited in the beam. In our case, we used a filter as our source of silicon nanocrystals.

IV-2.2 Characterisation:.

a) SNOM topographic characterisation

We will now present the results that we obtained with different characterization methods, which are important for having a deeper idea about the dimensions and structures of the Si Nc we are studying. We essentially referred to the use of two specific techniques: Topographic SNOM images and High Resolution Transmission Electron Microscopy (HRTEM). The first would inform us about the dimensions of the silicon nanostructures, while the second would certify to us their crystalline nature and give us an idea about the core size. Right after their preparation, when left outside the vacuum, a small SiO_2 shell covers the silicon nanoparticles due to their oxidation in air, enabling (unlike bulk silicon) a luminescence process to take place upon their excitation. Previous photoluminescence studies were performed on such particles, having diameters varying between 2.5 and 8 nm.[172] It was shown that a photoluminescence emanating from them could be detected, and had a maximum yield that could reach 100 % for sizes between 3 and 4 nm. A deeper discussion will be presented later concerning the processes taking place that could explain such a luminescence;

The size of the nanoparticles that we used is about 6nm, including the inside Si core and the outer SiO_2 shell. Such dimensions can be seen by taking a look at the SNOM topographic images (Figure IV- 2.) These have been obtained by dispersing the Si nanocrystals on a glass substrate by spin coating a drop of a dilute solution (composed of the Si nanoparticles dispersed in a solvent water or ethanol) on its surface, and visualizing the obtained sample using illumination-reflection mode SNOM (already described in chapter II). We should note that the optical image is of scattering SNOM type and not fluorescence one. Meaning that what is collected by the detector is both the exciting laser and emitted light from the Si nanoparticles.

Now, what we see inside the light coloured circles, are simply aggregates of Si nanocrystals. The optical and topographic images resemble well each other, but not totally identical however, excluding the hypothesis of topographic artefacts.

If we look closer at the topographic line profile, representing the Z height profile under the blue arrow, we see a typical height for two aggregates (in the white and yellow circle) of about 6 nm, which corresponds well to the diameter of the produced Si nanoparticles. This is due to the fact that, as we mentioned previously for hybrid nanoparticles, the spin coating process produces a single coating of aggregated nanoparticle's on the surface of

---

[172] G. Ledoux et al., "Photoluminescence properties of silicon nanocrystals as a function of their size," *Physical Review B* 62, no. 23 (Décembre 15, 2000): 15942.

the substrate, composed of one and only layer of nanocrystals. Thus, the height of the aggregate corresponds to the diameter of the nanocrystals, is about 6nm. Concerning the lateral resolution, we already mentioned in chapter III how it depends on the used SNOM tip; the opening of the SNOM tip we used being of the order of 150 -200 nm. Considering a large scan of about 5 micrometers, we could deduce that the agglomerate we see on Figure IV- 4 have an average width of about 200 nm, which represents an important number of Si nanoparticles monolayered as small bundles on the substrate .
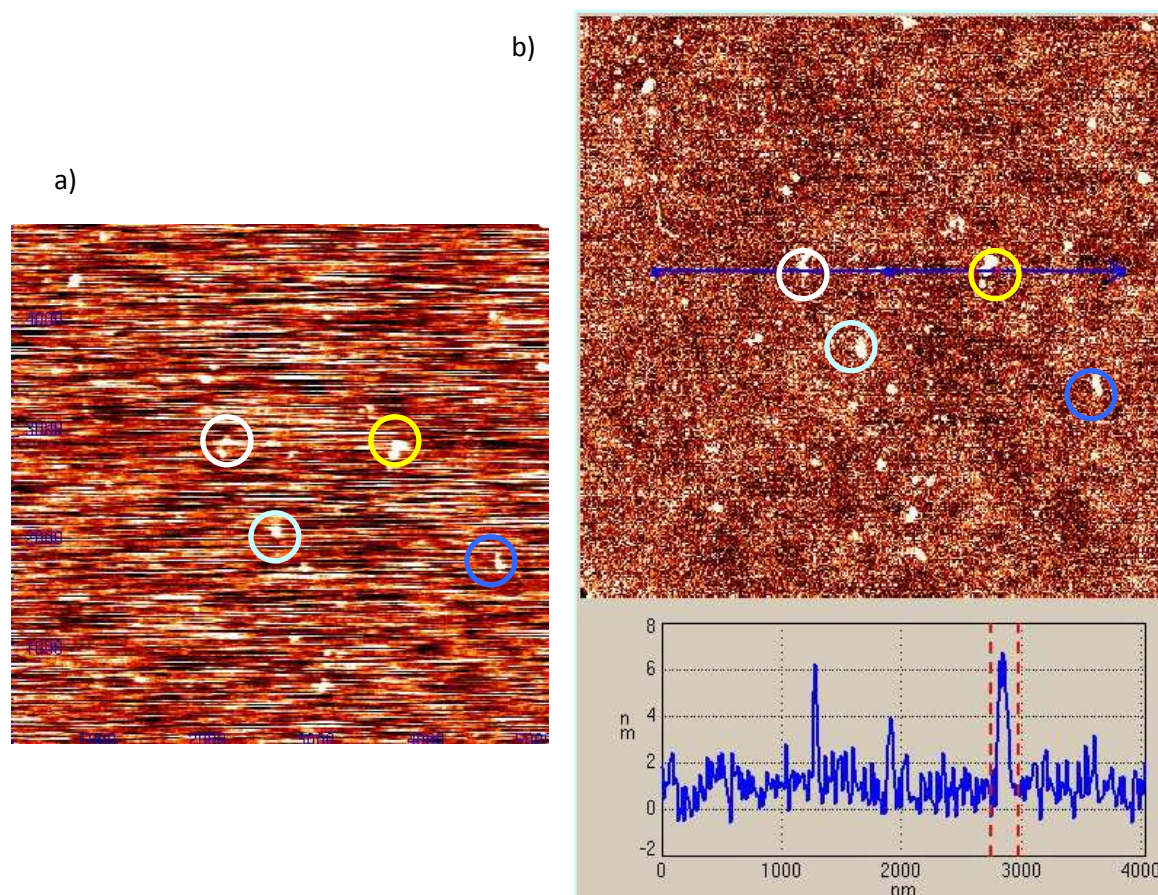
Figure IV- 4 Optical a) and topographic b) images of Si nanocrystals dispersed on a glass substrate. We see a correspondence between both images for different aggregates (inside coloured circles).

b) HRTEM images

Another way to characterise the Si nanoparticles is to look at their morphology and structure investigation, in particular of crystallographic nature. This is what we have done through the use of the High Resolution Transmission Electron Microscopy (HRTEM) and electron diffraction technique. We present in the following a HRTEM image of the

pyrolised Si nanocrystals (Figure IV- 5). This image is obtained by leaving a drop of water solution containing Si nanoparticles on a carbon film and letting it to dry in air, before placing it under the microscope. On the amorphous carbon, the nanoparticles appear of circular shape, well crystallized, and more or less aggregated.
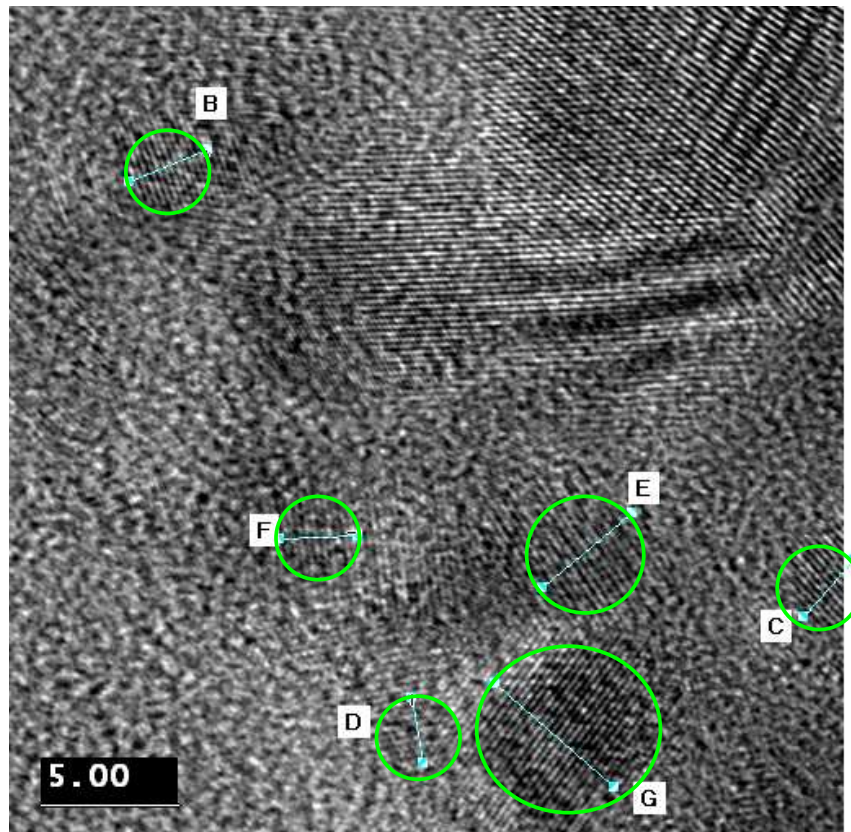
Figure IV- 5: HRTEM image of Si nanocrystals. The green circles represent separate nanoparticles.

Crystallographic studies have been previously performed on pyrolised silicon nanocrystals[173] and these were found to have a structure corresponding to the typical diamond cubic lattice structure of silicon. In our case, what we see in Figure IV- 5 are many interplanar fringes, each one directed at a certain angle. Each one of these spots represents the fringes of a single Si nanocrystal, where in each case a plane direction of the Face Centred Cubic (FCC) lattice is reflected. The corresponding diffraction rings were found to match well with those of typical Si particles. The outer silicon oxide shell could not be easily captured in Figure IV- 5 because the nanoparticles were deposited on an amorphous carbon film which could not provide a highly contrasted background.

---

[173] H. Hofmeister, F. Huisken, et B. Kohn, "Lattice contraction in nanosized silicon particles produced by laser pyrolysis of silane," *The European Physical Journal D - Atomic, Molecular, Optical and Plasma Physics* 9, no. 1 (Décembre 1, 1999): 137-140

Even though not all of the nanoparticles could be easily distinguished due to the agglomeration of some of them over the others (in here we treat with a case where most of the Si nanoparticles have been stuck in an evaporating drop of water), we could recognize some dispersed nano-sized particles, which we encircled with green rings that we called B, C, D, E, F, G. To have a precise idea of the dimensions of these nanoparticles, we present in the following figure the profile lines under the blue arrow inside the rings.
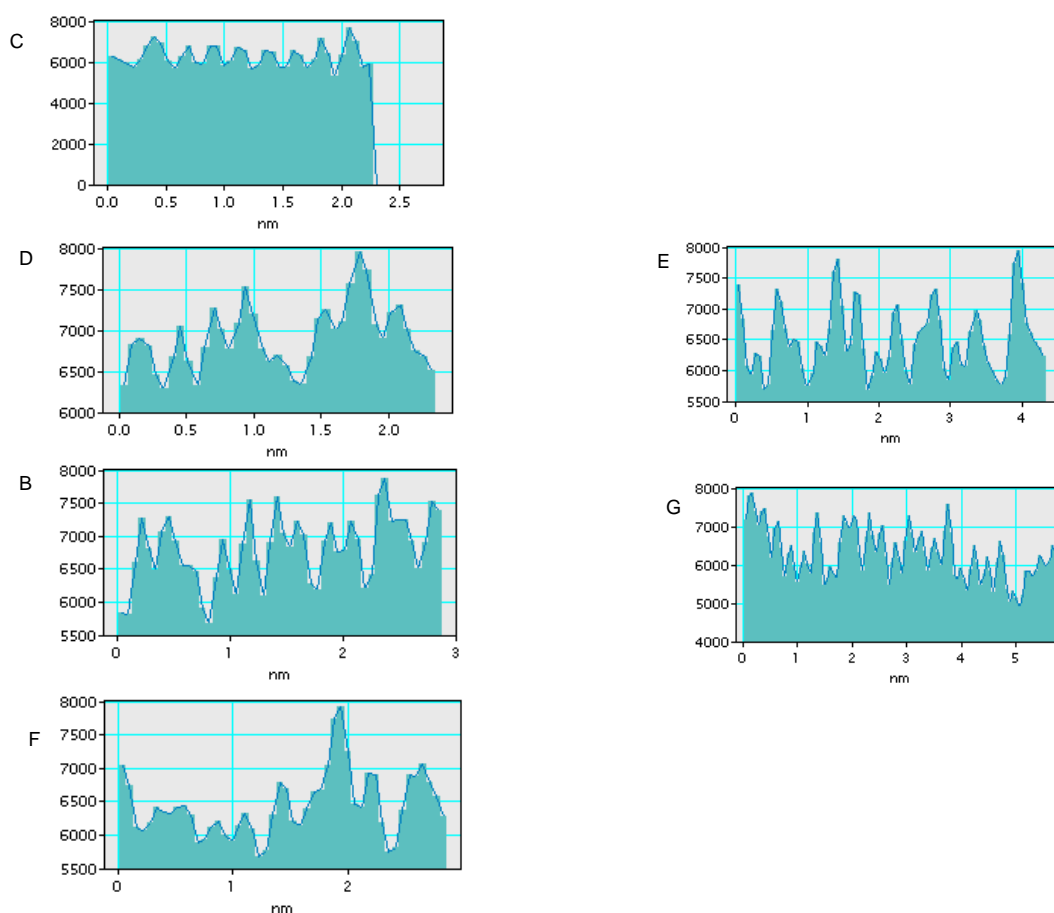
Figure IV- 6 Silicon nanoparticles interplanar fringes under the blue arrows of Figure IV- 4

Each profile line in Figure VI-6 is named after the circled nanocrystal which it represents. We see in the left handed figures that the dispersed nanocrystals have in average a Si core that is less than about 2.8 nm wide in diameter, while the right handed ones represent larger nanocrystals or agglomerations (4-6 nm). This means that the nanoparticles we are dealing with have a core width that is considerably small (about 2.5 nm), however some larger nanoparticles can be also present either due to an agglomeration of the nanoparticles originating from the sample preparation method

(evaporating drop of water), or to the fact that we are using Si nanocrystals coming from the filter used in the silicon nanoparticles preparation process, and which as we already mentioned, presents a large nanoparticles size distribution. However, as we will see later, the samples we used for Single Molecule Confocal Microscopy will be exposed to a spin coating process before any optical study, which would help to dissociate the aggregates and leave with us a majority of small nanocrystals having a diameter which is less than 3nm.

Thus we can conclude from the previous measurements that through the use of two different characterising methods: SNOM topographical imaging and HRTEM, we were able to have a clear idea about the dimensions of the nanoparticles: an Si nanocrystal would be having a core whose diameter is about 2.5nm, and would be surrounded by an SiO_2 shell of few nanometer (about 1.5nm) in thickness in order to form a total entity having a diameter reaching 5-6 nm.

IV-2.3 Sample preparation

In the goal of studying our Si nanocrystals in different conditions, one important step of our work consisted of adopting diverse sample preparation methods. As we will explain later with more details, one important aim was to be able to place the nanoparticles in different dielectric environments, and study their varying optical properties. An important condition was also to be able to make such studies on individual nanocrystals, meaning it was important to separate them from each other, and use a transparent media whose own optical properties would not affect the measurements. A very simple and practical method which would help us to produce such kinds of samples is the thin film polymer processing technique.

Such a procedure consists of dispersing the studied nanoparticles in a polymer solution, which, after application of a coating technique on a substrate, would result in the formation of a solid thin film, containing the Si nanocrystals in question. The two polymers we have used are PVA (Poly vinyl alcohol, repetition unit C_2H_4O), PMMA (poly methyl methacrylate, repetition unit $C_5H_8O_2$) for their differing dielectric constants (14 and 3.4 respectively). The mechanism on which such a procedure relies upon is the imbrications of the polymer chains one with each other when evaporation of the solvent takes place, thus causing the solidification of the ensemble. It is mostly probable that the cohesion of the system is due to hydrogen and Van der Vall bonds, without however the creation of new carbon-carbon bonds. The substrate we used was a small (1cmx1cm) Si wafer covered by a thin layer (few nm) of SiO_2, the coating technique used for covering it is spin coating, which assures a homogeneous repartition of the solution on the substrate and an evaporation of the solvent after rotation at a high speed. Before each

measurement we were very careful to provide a deep cleansing of the substrate. Such cleansing was done in different steps, including a deep rinsing with ethanol and alcohol, and a soaking bath of Pirahna solution (a mixture of sulphuric acid (H_2SO_4) and hydrogen peroxide (H_2O_2), in an ultrasound bath. Afterwards, we verified the cleanliness of the substrate on the wide field microscope and passed to the sample fabrication. A second check up with the wide field microscope was also done before each single nanoparticle confocal measurement, in order to make sure that no dust or contaminating agents covered the surface and that the nanoparticles were well distributed on the polymer film. We present the different steps we followed for the preparation of our samples in the following schemes.

a) For PVA:
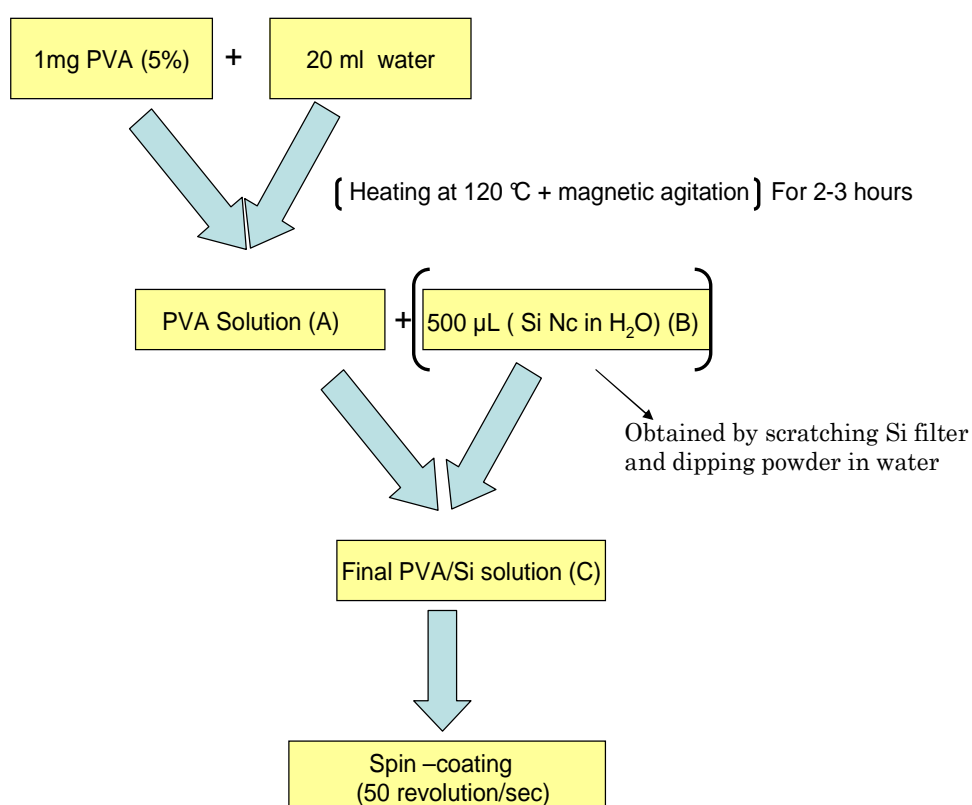
Figure IV- 7 preparation method for samples of PVA thin films, containing Si nanocrystals.

As we see, we first prepare the PVA solution (called solution A), where we place 1mg of PVA (in the form of powder) in 20 ml of water (since PVA is perfectly soluble in water), then simultaneously heat and agitate the solution with a magnetic agitator about 2-3 hours. The next step consists of adding Si Nc to solution A. As already mentioned, the Si nanocrystals were initially presented to us on a filter paper. We thus scratch the filter in

order to extract the Si powder and immerse the residue in water to get solution (B). 500µL of the obtained solution are then added to (A). The final solution (C) is spin cast on a silicon wafer.

Spin coating is a film deposition technique suitable for polymer films deposition, where it consists of spreading out an excess of a drop of solution placed on the surface of the substrate by the usage of a centrifugal force. In this context, its working principle can be summarized in four distinct steps:

1. A deposition of the drop from (C) on the substrate.

2. An acceleration of the rotation which provokes the formation of a meniscus at the centre of the drop, that extends by provoking the flow of the solution at the exterior of the substrate.

3. A rotation at constant speed permitting the ejection of the excess solution, which is accompanied by a uniform diminution of the thickness of the film.

4. An evaporation of the most volatile solvents, which diminishes the thickness of the thin film.
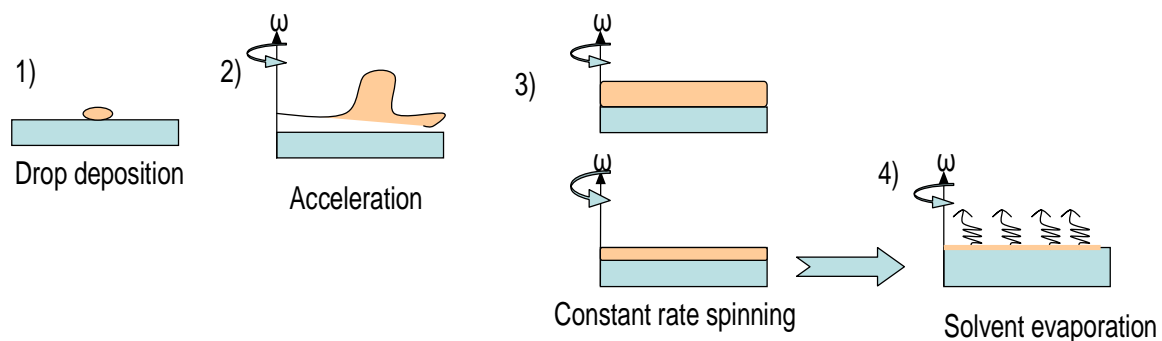
Figure IV- 8 Spin coating method overview

Many parameters have an influence on the thickness of the formed layer which can be either intrinsic to the solution (density, viscosity) or exterior (rotation rate, acceleration, temperature etc…). In our case, all the measurements were done at room temperature,

at an increasing rate until reaching about 30-50 revolutions per second (depending on the polymer in question). Ellipsometric measurements showed a thickness with an average of the order of few nanometers (2-3 nm) for the formed layer, which is a suitable depth for the kind of confocal setup that we used.

b) For PMMA:

For the PMMA sample, the preparation steps were a bit simpler since there was no need for any heating and stirring. The different fabrication stages are shown in the following scheme:
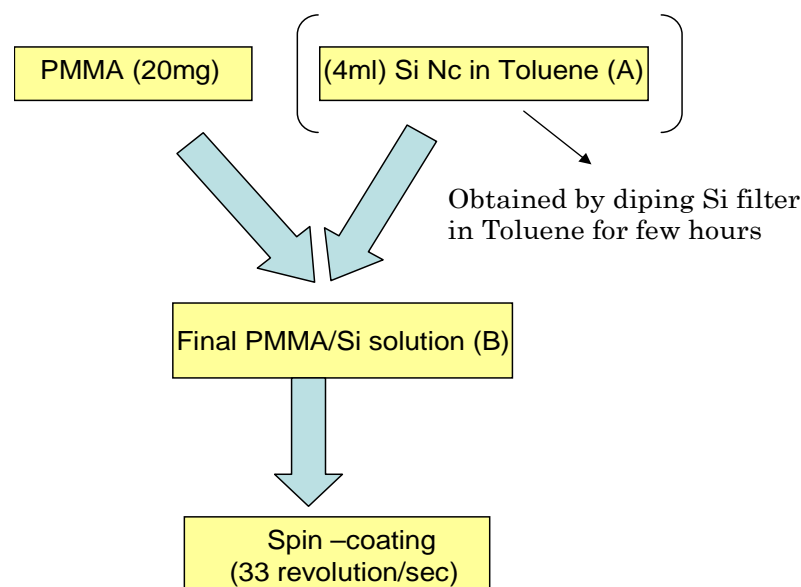
Figure IV- 9 preparation method for samples of PMMA thin films, containing Si nanocrystals

In this case, some differences can be found with respect to the PVA case: the solvent used is not water but Toluene, since PMMA in not soluble in the first, but can instead be dissolved in toluene at room temperature. The constitution of solution (A) was done by placing the filter in a Toluene containing recipient, and leaving it there for few hours. Due to the effect of their diffusion in a liquid, the Si nanocrystals disperse within the solution at a concentration which suits single confocal microscopy. 4 ml of (A) were added to 20 mg of PMMA and stirred for a few minutes. A drop of the resulting PMMA/Si solution (B) was then spin cast at room temperature for a few minutes on the Silicon/Silica substrate.

c) On SiO$_2$:

 Finally, we have also dispersed the Si nanocrystals on the substrate itself without the addition of any polymer in order to study their optical properties when left in air. In that

case, a drop of Si Nc in water solution was simply placed on the Si/SiO_2 wafer and spin cast for few minutes at a speed of about 50 rev/sec at room temperature, as was done for the hybrid nanoparticles (Chap III)

IV-3 Si nanoparticles Single Nanocrystal detection:

 The characterizing tool we referred to for studying the optical properties of the pyrolised nanocrystals is single molecule spectroscopy. Such a technique enabled the discovery of new phenomena dominating the optical properties of silicon nanostructures, such as the finding of several luminescence bands emanating from these nanocrystals. Also, such bands were not emitted continuously, instead, the fluorescence light was more in an on off regime, which was then referred to as 'blinking'. There still exists a lot of contradictory explanations that should be cleared out concerning the mechanisms taking place during the luminescence of Si nanoparticles, whether it concerns blinking phenomena or emission spectra; however we believe that a converging point can be reached with in depth studies concerning the different elements entering into action. In our case, the single molecule experiments that we performed consisted of gathering simultaneously two different kinds of information, the first was about the study of the variation of emitted light intensity from Si nanoparticles by recording different time traces after their excitation, the second considered the respective spectral responses with different emission spectra. First, we will study the time trace variation, and then we will look closer to the emitted light emission spectra.

These measurements giving the spectra were obtained using the spectroscopic setup described in chapter II, which we will illustrate again in Figure IV- 10.
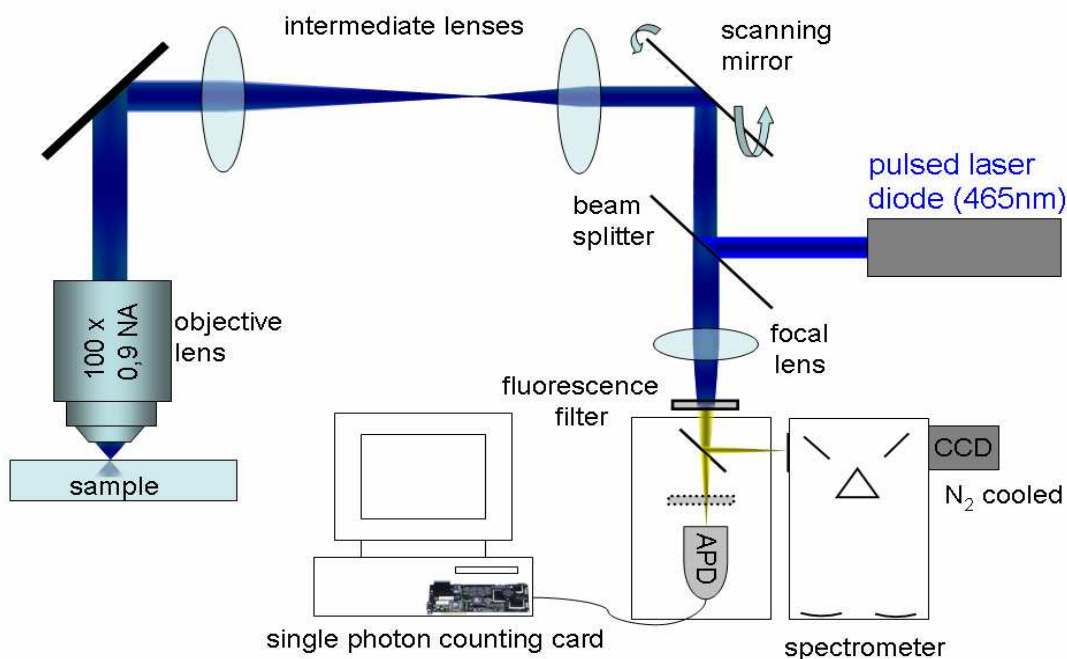
Figure IV- 10 Confocal microscope set up representation (Courtesy of Danny Kowerko- OSMP group – TU chemnitz Germany)

The lowest region of Figure IV- 10 shows two distinct parts: a single photon counting card on the left and and an N_2 cooled spectrometer on the right. Both of these functionalities work simultaneously during a measurement. The single photon counting card role is to provide emission time traces, which serve to show the variation of the intensity of the emitted light from an excited silicon nanocrystal. The spectrometer on the other hand defines the shape of the emited emission spectrum at the same time. Both kinds of information will be explained with more details in the coming sections.

IV-3.1 Emission spectra and time trace results

a) General view:

Figure IV- 11 shows the obtained spectra of emitted light from an Si nanoparticle which was studied for about a minute or two under a Single Nanocrystal Confocal microscope while it was being excited with a laser diode having λ_{ext}=475nm. The Si nanoparticles were dispersed on Si/SiO$_2$ substrates as previously explained in the previous section. An emission spectrum was recorded each second, so that in average 60 emission spectra were obtained with one single measurement. We can see different emission spectra of a Si Nc embedded in PMMA, which are presented at various times (4.89, 12.21, 13.47 and 16.45 seconds after excitation). Each one is composed of a main band (the most energetic one) which we will call a Zero Phonon Line band (ZPL) and of a side band, representing phonon line bands.
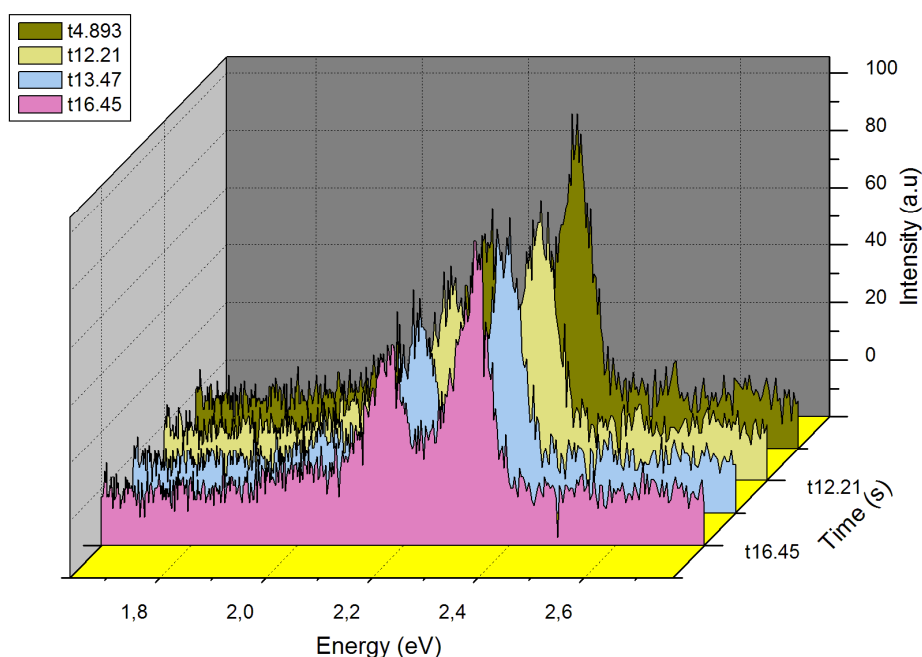
Figure IV- 11 An Si nanocrystal's fluorescence spectra, at different emission times

What attracts our attention in such a graph is the double peaked structure of each spectrum. Such a shape has been previously found in the emission spectra of Si nanocrystals, covered either by an SiO$_2$ shell or by another layer such as an organic monolayer, [174,175 ,176] and has been related to an electron-phonon coupling, which,

---

[174] Douglas S. English et al., "Size Tunable Visible Luminescence from Individual Organic Monolayer Stabilized Silicon Nanocrystal Quantum Dots," *Nano Letters* 2, no. 7 (Juillet 1, 2002): 681-685.

according to the separation between the two peaks has been assigned to Si-O-Si or Si phonon modes. In this figure, we only show a first phonon line band, however as we will show later, some emission spectra can also have second or third phonon lines. These phonon bands reflect the phonon assisted transitions which usually take place in Si nanocrystals; in the coming sections, we show how such sidebands will help us to have a clear idea about the optical mechanisms taking place in Si nanocrystals.

Using the confocal microscope setup described in chapter II, the time trace of the nanocrystal 's emission can be acquired during each measurement, it is defined as a plot of the variation of the emitted light intensity with respect to time. Figure IV- 12 represents the time trace of the spectrum shown in Figure IV- 11:
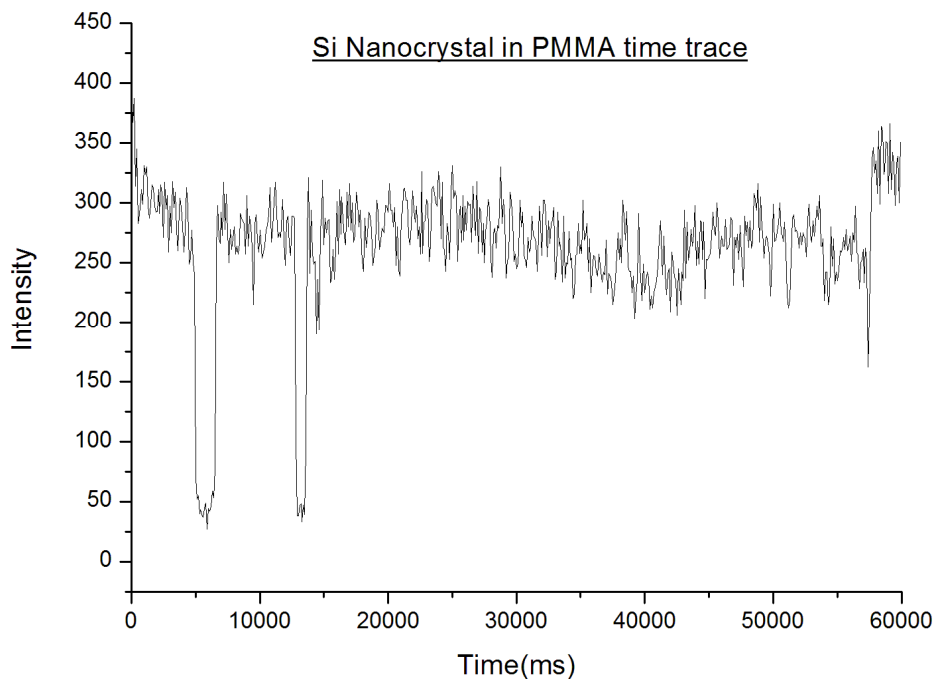
Figure IV- 12 Emission spectrum time trace for Si nanocrystals embedded in PMMA

We can understand by observing Figure IV-12 that during the 60 seconds in which the measurement had been taken, the emission of light could be described as 'blinking'; in

---

[175] Jorg Martin et al., "Electron–Phonon Coupling and Localization of Excitons in Single Silicon Nanocrystals," *Nano Letters* 8, no. 2 (Février 1, 2008): 656-660

[176] Ilya Sychugov et coll., "Narrow Luminescence Linewidth of a Silicon Quantum Dot," *Physical Review Letters* 94 (Mars 1, 2005): 87405.

fact, at time t=0 we could detect a high intensity emission (in this case we say that the nanoparticle is 'on'), which dropped after about 5 seconds (the nanoparticle is then 'off'), and was on again after few milliseconds. This intermitting cycle was repeated again with a little variation of intensity in the times where the nanoparticle was emitting. We sometimes also obtained other shapes of time traces, depending on the matrix which we were using. Figure IV- 13 – till Figure IV- 15 show different kinds of time traces which we also encountered, for Si nanocrystals embedded in PMMA, PVA and on an SiO_2 substrate.

b) Time trace of silicon nanoparticles:

i) In PMMA:
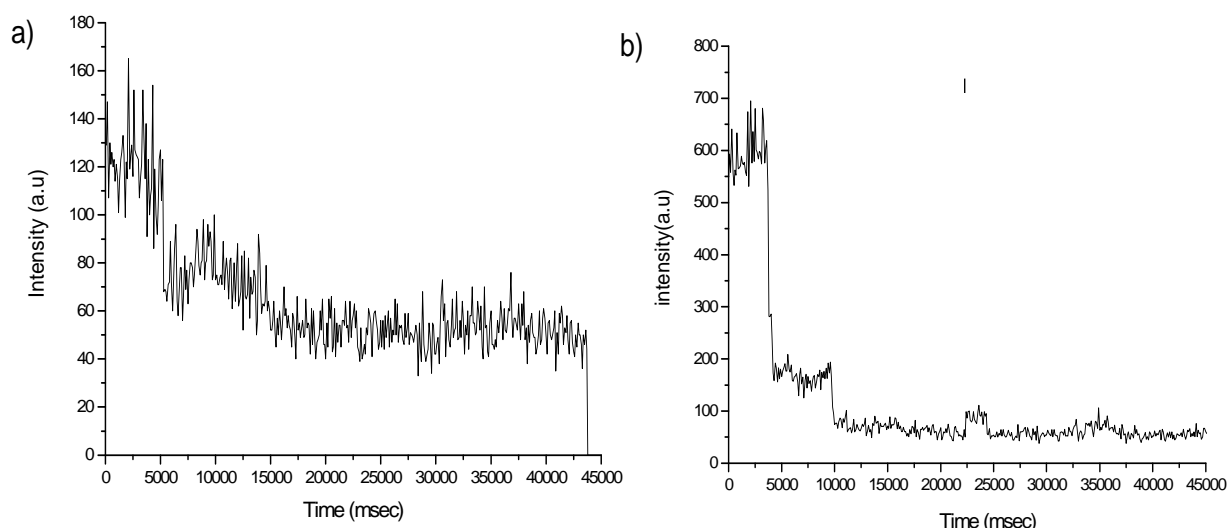
Figure IV- 13 Two different types of encountered time traces for Si nanocrystals embedded ,in PMMA

Part a) Figure IV- 13 exhibits an intensity blinking against a gradually decaying background signal. This behaviour could be attributed to an emission originating from a cluster of nanoparticles as have been considered by Korgel et al.[177] For our analysis, we disregarded the use of emission spectra corresponding to such time traces, since we are mostly interested in the study of the single silicon nanocrystals behaviour. Taking into consideration emission spectra emanating from such an aggregates would be leading us into erroneous results.

Part b) however, shows a different kind of time trace, where in this case the decaying background did not appear, but instead, we see blinking behaviour which exhibited

---

[177] Douglas S. English et coll., "Size Tunable Visible Luminescence from Individual Organic Monolayer Stabilized Silicon Nanocrystal Quantum Dots," *Nano Letters* 2, no. 7 (Juillet 1, 2002): 681-685

multiple intensity steps. Previous works have also treated with such a case,[178,179] but for Si nanocrystals which were directly observed on a substrate, without being placed in any polymeric medium. In such cases, this type of temporal features was attributed to the presence of a few particles within the studies region of the sample, each one emitting at a time in discordance with the other, resulting in a total superposed blinking producing the multilevel blinking which is illustrated. However, as we will show for PVA, the embedding matrix may also be involved in the time trace shape, whether it is for the chemical or dielectric nature of the Si nanocrystal surrounding. Thus, whether the hypothesis of such an assumption also holds for the PMMA case is still an open question, which may deserve a deeper investigation.

ii) On SiO$_2$:

Si Nc deposited on SiO$_2$ substrates also show the same kind of behaviour as that of nanoparticles embedded in PMMA. This is clearly seen in Figure IV- 14.
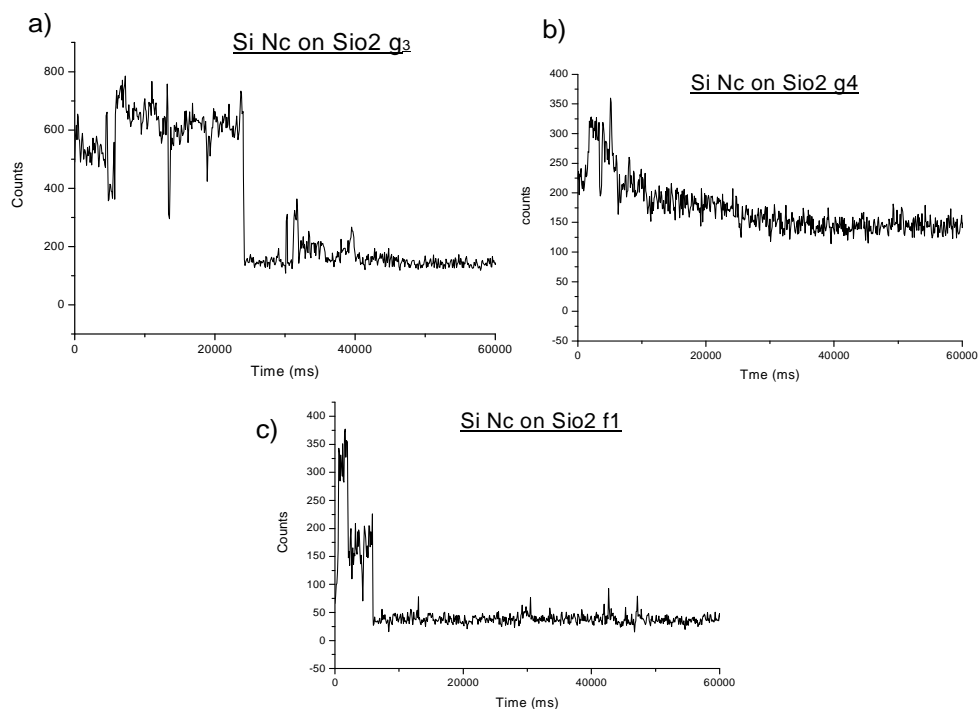
Figure IV- 14 Different kinds of time traces obtained from Si nanocrystals deposited on an Sio2 substrate.

We can clearly distinguish in Figure IV- 14 the three kinds of time traces which we discussed until now for PMMA: a) shows the double level time trace –b) the exponential decay time trace and c) the multiple step one. These results show that the dielectric

---

[178] Jan Valenta et coll., "Light-Emission Performance of Silicon Nanocrystals Deduced from Single Quantum Dot Spectroscopy," *Advanced Functional Materials* 18, no. 18 (2008): 2666-2672

[179] English et coll., "Size Tunable Visible Luminescence from Individual Organic Monolayer Stabilized Silicon Nanocrystal Quantum Dots."

nature of the environing media is an important factor in the emission properties of silicon nanoparticles. In fact, both PMMA and SiO_2 have a close dielectric constant, and they both seem to behave similarly concerning their time trace.

iii) In PVA:

Figure IV- 15 shows the time trace of Si Nc embeded in PVA. The left handed time trace (part a), features very sharp emission lines (very small ON times), that are spaced by a relatively long OFF times compared to the ON times. We exclusively have encountered these kinds of traits for numerous Si nanocrystal surrounded by the PVA media. This kind of behaviour has also already been previously reported in an experiment which was aiming to study the effect of the environment on the time trace shape of CdSe nanoparticles, at different conditions.[180] It was found that when CdSe-ZnS nanoparticles were placed in an O_2 rich environment, they had a much shorter time compared to when they were found in other environments. The presence of oxygen was thus found responsible for this time trace changing shape and was attributed to a photo-induced reaction with oxygen or the creation of additional traps by oxygen.
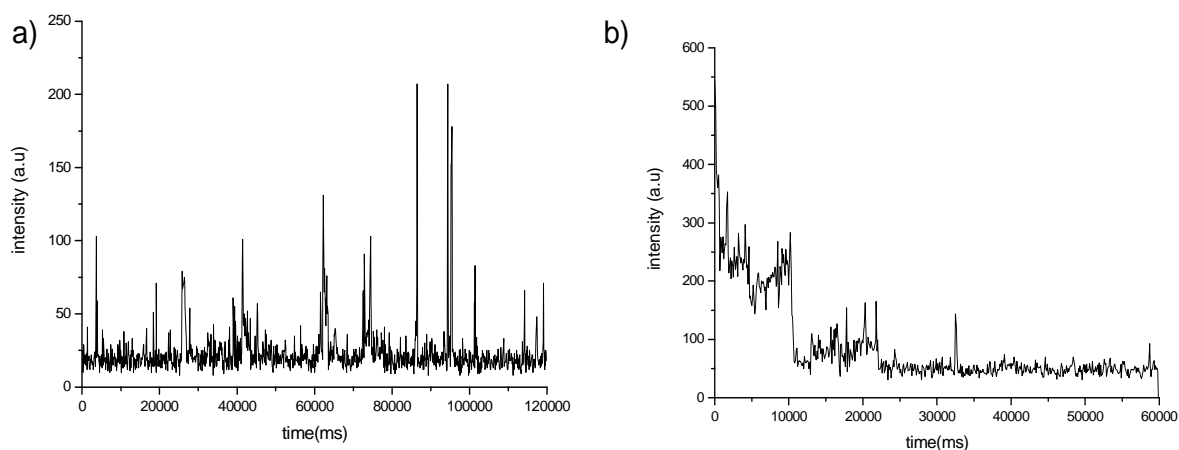
Figure IV- 15 Two different types of encountered time traces for Si nanocrystals in PVA

Now in our case, in order to prepare the PVA thin film, we had to mix water and PVA together and then place the nanoparticle in the formed solution. It thus may be a possibility that after the formation of the polymerised thin film, (which contains the Si nanocrystals), there has been a photoinduced reaction or the formation of additional traps leading to the observed time trace, coming from some remaining oxygen atoms, originating from H_2O molecules. Another possibility would be the polarisation of SiO_2

---

[180] F. Koberling, A. Mews, et T. Basché, "Oxygen-Induced Blinking of Single CdSe Nanocrystals," *Advanced Materials* 13, no. 9 (2001): 672-676

shell via PVA media, which will be an idea that we will discuss with much more detail in the coming results section.

Part (b) also shows multi step blinking, which may also originate either from the aggregation of a few nanocrystals, as has been the case in Figure IV- 13 (b), or from effects originating from the surrounding polymer film.

IV-3.2 Photoluminescence intermittency in Si nanocrystals (Discussion):

Such a behaviour, which is also described as photon bunching or fluorescence intermittency, is observed in all experiments with single fluorescent quantum systems,[181] but we should keep in mind that very different physical processes give rise to blinking in single particle studies; for example, it can be caused by single quantum transitions (between singlet and triplet states, for example for single Terrylene molecules[182]) by fluctuations of the particles nano-environement, which causes spectral diffusion at very low temperature(like a motion of the molecules surrounding the species),[183] or by spectral shifts at room temperature, which are thought to originate from fluctuations of the local environment of the fluorophore translating into fluctuations of the fluorescence emission.[184]

Different groups reported Single Nanocrystal Spectroscopic studies performed on single Si nanocrystals as the groups of Buratto,[185,186] Cichos,[187,188] Korgel's,[189] and Linros,[190] however each seemed to present different results and thus different explanations concerning the blinking of Si Nc. For example, if we compare between the Cichos (and co-workers) case with that of Linnros' we see that the first had found a blinking of porous Si grains obeying a power law statistics, and which was intensity

[181] Thomas Basché, "Fluorescence intensity fluctuations of single atoms, molecules and nanoparticles," *Journal of Luminescence* 76-77 (Février 1998): 263-269.

[182] Th. Basche, S. Kummer, et C. Brauchle, "Direct spectroscopic observation of quantum jumps of a single molecule," *Nature* 373, no. 6510 (Janvier 12, 1995): 132-134.

[183] W. P. Ambrose et W. E. Moerner, "Fluorescence spectroscopy and spectral diffusion of single impurity molecules in a crystal," *Nature* 349, no. 6306 (Janvier 17, 1991): 225-227.

[184] J. K. Trautman et coll., "Near-field spectroscopy of single molecules at room temperature," *Nature* 369, no. 6475 (Mai 5, 1994): 40-42.

[185] M. D. Mason et coll., "Luminescence of Individual Porous Si Chromophores," *Physical Review Letters* 80, no. 24 (Juin 15, 1998): 5405.

[186] M. D. Mason et coll., "Investigating individual chromopores within single porous silicon nanoparticles," *The Journal of Chemical Physics* 114, no. 18 (Mai 8, 2001): 8119-8123.

[187] Frank Cichos, Jorg Martin, et Christian von Borczyskowski, "Emission intermittency in silicon nanocrystals," *Physical Review B* 70, no. 11 (2004): 115314.

[188] Jorg Martin et coll., "Electron–Phonon Coupling and Localization of Excitons in Single Silicon Nanocrystals," *Nano Letters* 8, no. 2 (Février 1, 2008): 656-660.

[189] English et coll., "Size Tunable Visible Luminescence from Individual Organic Monolayer Stabilized Silicon Nanocrystal Quantum Dots."

[190] Jan Valenta, Robert Juhasz, et Jan Linnros, "Photoluminescence spectroscopy of single silicon quantum dots," *Applied Physics Letters* 80, no. 6 (Février 11, 2002): 1070-1072.

dependant; while the second indicated blinking On-OFF interval distribution which is mostly exponential, indicating random switching. The ON state was found to be shortened by the square of the excitation power.

In more detail, the intensity dependence of the blinking led Cichos et al.[45,46] to propose an assumption in order to explain such dark periods, and he suggested that the abrupt turning off of luminescence is caused by photo-ionization of the nanocrystal,[191] or more precisely quenching via an Auger process.[192] In such case, the electron of an excited electron hole pair would be ejected to trap states in the vicinity of the nanocrystal (or nanocrystal environment). The free carrier in the nanocrystal core could then efficiently quench further optical excitations by an Auger process until the particle is neutralized by the return of the electron. Since Auger process is much faster than the radiative lifetime, quenching via this process would be highly efficient and this mechanism is assumed to be responsible for the observed dark state of Si Nc. As seen, requirement for this dark state is the ejection of a charge out of the Si Nc core, i.e. nanocrystal ionisation, which is evidenced by spectral diffusion observations.

Statistical studies of the fluorescence intermittency in ensemble and single[193] semi conducting nanocrystal quantum dots (QD's) revealed a temperature-independent power-law distribution (which we already mentioned), in the histogram of these *on* and *off* times durations. That is, the probability density distribution of the on or off time is of the form:

$$p(t_{on,\ off}) = p_0 t^{-\alpha}$$

where p_0 is a constant and α the power law exponent.

Linros et al.[48] also indicated possible charging by Auger recombination due to the shortening of the on time interval with the square of the excitation power. By taking into account such behaviour, different models have been proposed in order to

[191] M. Nirmal et coll., "Fluorescence intermittency in single cadmium selenide nanocrystals," *Nature* 383, no. 6603 (Octobre 31, 1996): 802-804.

[192] Frank Cichos, Jorg Martin, et Christian von Borczyskowski, "Emission intermittency in silicon nanocrystals," *Physical Review B* 70 (Septembre 1, 2004): 115314.

[193] Frank Cichos, Jorg Martin, et Christian von Borczyskowski, "Characterizing the non-stationary blinking of silicon nanocrystals," *Journal of Luminescence* 107, no. 1-4 (Mai 2004): 160-165.

describe the process through which photo excitation takes place in Silicon nanocrsytals. For instance in one of them, if the charge is ejected to a trap state, it undergoes a random walk through this spatial distribution of trap states until it eventually returns to the nanocrystal to recombine with the hole;[194] another model assumes that the homogeneously distributed traps around the nanocrystal are populated or depopulated by electron tunnelling from or to the nanocrystal.[195] Thus, the difference between both models relies in the fact that in the first one many trap states are sampled during an off time, while in the second one, only one trap state is involved.[196]

Recently however, Valenta et al.[48] showed that the apparently contradictory results obtained with the different groups are due to the different experimental conditions in which each was performed.[197] In fact, considering the example of exponential and inverse power low dependence statistics of ON and OFF times, it was shown that the power law dependence with α close to 1.5 is observed for OFF and ON interval distribution at a short time scale. For longer dwell times, the distribution becomes exponential. The mentioned discrepancy has been proven understood by seeing that measurements on samples by Linnros et al.[48] addressed only the long part of the time scale (bin size is 15 s due to a slow detection system and low–emission rate under weak excitation) i.e., the exponential bending tail of the distribution. A theoretical model predicting exactly such kind of blinking distribution in semi conductor quantum dot was developed by Marcus and co, which was based on the diffusion-controlled-electron-transfer.[198] It lead to a 1.5 power law decay for both ON and OFF statistics as well as well as a breakdown of the power law with an exponential tail for the ON time distribution and eventually also for the OFF-time distribution at much longer times. The model that permits such a reconciliation between data, as presented by J. Valenta et al[199] would be the following :

[194] K. T. Shimizu et coll., "Blinking statistics in single semiconductor nanocrystal quantum dots," *Physical Review B* 63, no. 20 (Mai 2, 2001): 205316.

[195] Rogier Verberk, Antoine M. van Oijen, et Michel Orrit, "Simple model for the power-law blinking of single semiconductor nanocrystals," *Physical Review B* 66, no. 23 (Décembre 6, 2002): 233202.

[196] Cichos, Martin, et von Borczyskowski, "Characterizing the non-stationary blinking of silicon nanocrystals."

[197] Valenta et coll., "Light-Emission Performance of Silicon Nanocrystals Deduced from Single Quantum Dot Spectroscopy."

[198] "Diffusion-Controlled Electron Transfer Processes and Power-Law Statistics of Fluorescence Intermittency of Nanoparticles," *Physical Review Letters* 95, no. 10 (2005): 107401.

[199] Valenta et coll., "Light-Emission Performance of Silicon Nanocrystals Deduced from Single Quantum Dot Spectroscopy."

An electron hole pair is formed in a Si nanocrystal, after absorption of a photon. The exciton is at the same time strongly confined (in small nanocrystals), and feels strongly the amorphous-like interface between the Si core and SiO_2 shell and the related specific phonon vibrations that take part in recombination processes (thus influencing the spectral shape of the emission spectra). Such effects will be seen with more detail in the coming section.

The exciton can also diffuse in the complex energy landscape and meet a non-radiative centre that is reducing the average QE of radiative recombination. Because of a very slow photoluminescence decay typical for measurements in an ensemble of nanocrystals, and the very relatively high quantum efficiency of the radiative recombination of Si Nc in ON state, there a high probability of generation of a second exciton during lifetime of the first one. Exciton-exciton scattering is a crucial phenomenon in radiative and non radiative recombination processes of Si Nc's.

The inelastic scattering induces the non radiative recombination of one exciton and excitation of a second one. The same effect can be produced by Auger recombination of an exciton with a third quasiparticle. If the exchanged energy is high enough and the energy landscape is favourable, the scattering can lead to charge separation. In the charge separated state, the Auger recombination efficiently quenches created excitons, hence causing the nanoparticle to become dark until the charges recombine back.

IV-3.3 Emission properties (discussion):

b) Si nanocrystals (laser pyrolisis produced) emission variation with size:

As already explained, previous studies have been done concerning photoluminescence mechanisms of laser pyrolisis prepared Si nanocrystals[200] (covered by an Sio2 shell), having diameters varying from 2nm till 8nm.The main finding was an experimental correlation consisting of an inverse power law with an exponent of 1.39 between the average diameter of Si Nc and the photoluminescence peak energy they emitted; A good agreement is obtained by comparing such a behaviour with the quantum confinement theory[201] i.e. with the assumption of radiative recombination of electron-hole pairs confined inside the silicon nanocrystals. The inverse power law can also be explained in terms of electronic bands, where quantum confinement refers to a conduction band edge continually increasing in energy when the size of the Si Nc is being reduced, while the

---

[200] G. Ledoux et coll., "Photoluminescence of size-separated silicon nanocrystals: Confirmation of quantum confinement," *Applied Physics Letters* 80 (Juin 1, 2002): 4834-4836

[201] C. Delerue, G. Allan, et M. Lannoo, "Theoretical aspects of the luminescence of porous silicon," *Physical Review B* 48, no. 15 (Octobre 15, 1993): 11024.

opposite applies to the valence band edge. This result shows an increase of the band gap energy with decreasing size. Such a band gap increase can be reflected by a radiative recombination of the electron and hole showing an increase of the photoluminescence energy with decreasing size, which takes the form of the experimentally obtained inverse power law. In the following (Figure IV- 16), we show the graph in question, which has been obtained from Ref. 233.
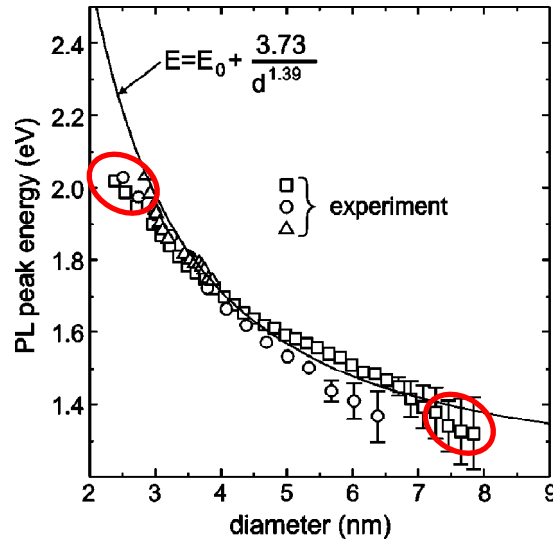

Figure IV- 16 Correlation between average diameter and PL peak energy of Si Nc's taken from reference 233 . Experimental data compares nicely with theory, but tends to diverge at the extremities of the curve (in red circles).

However, looking closer on each side of the measured range, one can find some small discrepancies between experiment and theory. For larger particles, this difference had been assessed by Ledoux et al.[58] as being due to maxima of PL curves which could not be accessed with the used detector. For particles with diameters smaller than 3nm, the deviation between measurement and theory had been attributed this time to two reasons: The first would be caused by the finite size distribution of the contributing particles to the signal at a given position of the sample: because of their absorption cross section and higher photoluminescence, the larger particles in the tail of the size distribution would be shifting the photoluminescence curve to smaller energies.

The second would be a phenomenon proposed by Wolkin et al.[65] which showed that for very small oxidized porous silicon nanoparticles (d<2.5nm), the photoluminescence energy would not increase anymore as would be expected from the quantum confinement model, due to the appearance of an oxide- related surface state within the band gap of the Si nanocrystal.[202] Other groups also reported such a deviation from quantum confinement for small Si nanocrystals.[203,204]

---

[202] M. V. Wolkin et coll., "Electronic States and Luminescence in Porous Silicon Quantum Dots: The Role of Oxygen," *Physical Review Letters* 82, no. 1 (Janvier 4, 1999): 197.

[203] J. von Behren et coll., "Quantum confinement in nanoscale silicon: The correlation of size with band gap and luminescence," *Solid State Communications* 105, no. 5 (Février 1998): 317-322.

[204] S. Schuppler et coll., "Size, shape, and composition of luminescent species in oxidized Si nanocrystals and H-passivated porous Si," *Physical Review B* 52, no. 7 (1995): 4910.

This last point has been recently treated by Martin et al.,[205] who investigated luminescence mechanisms within small nanocrystals, having Si diameters (d<3nm), and a total nanocrystal diameter of about 5.7nm, with the use of single nanocrystal spectroscopy. In his experiments, he had found photoluminescence spectra of single Si nanocrystals having at room temperature a zero phonon line width of about 100 meV and showed on the low energy side satellite bands with energy separations varying between 130 meV and 160 meV, which are separations clearly related to L-O or T-O Si-O-Si phonon modes of SiO_2.[206] By tracing the variation between the ZPL intensity with the emission energy, they obtained experimentally, contrarily to what would be expected by applying quantum confinement, a double peaked structure showing two maxima at 2.1eV and 2.325eV, instead of continuously increasing photoluminescence intensity with decreasing size. In order to explain such a behaviour, they decided to take into consideration a model which has been proposed by Wolkin et al.,[207] which consisted of dividing the electronic band structure into three regions as seen in the following image (Figure IV- 17) (the model was assumed as being due the formation of double bonds between Si and O atoms at the surface of the nanocrystal):
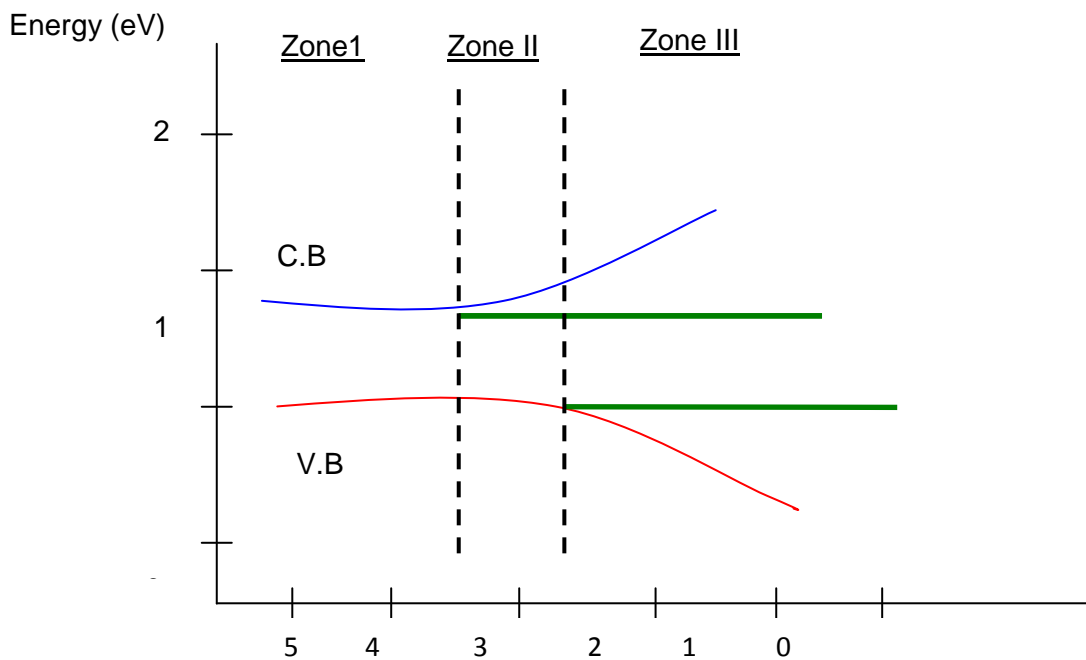
Figure IV- 17 Tentative illustration of the behaviour of electronic states of Si NC's (conduction and valence band energies) as a function of the cluster size and surface passivation, upon localization.

[205] Jorg Martin et coll., "Electron–Phonon Coupling and Localization of Excitons in Single Silicon Nanocrystals," *Nano Letters* 8, no. 2 (Février 1, 2008): 656-660.
[206] C. T. Kirk, "Quantitative analysis of the effect of disorder-induced mode coupling on infrared absorption in silica," *Physical Review B* 38, no. 2 (Juillet 15, 1988): 1255.
[207] Wolkin et coll., "Electronic States and Luminescence in Porous Silicon Quantum Dots."

We see that in a first region (Zone I) none of the carriers are trapped and quantum confinement applies, in Zone II (corresponding to the peak at 2.1eV) electron localisation occurs, and above this energy the corresponding conduction band energy level will become constant, finally in zone III, starting at 2.325eV both electrons and holes are trapped (where this time, the hole will be trapped in the valence band). Thus modelling the change of PL intensity with emission energy, based on the method proposed by Delerue et Al.[208] (by taking into consideration such electronic band structure) Martin et al.[46] were able to have an agreement between both the experimental and theoretical results concerning the obtained double peaked structure previously mentioned, confirming the electron-hole localisation hypothesis.

Also, another reinforcing argument to such an assumption would be considering the intensity of electron-phonon coupling in the localisation process. In fact, being able to extract the phonon lines from the emission spectra using SNS is extremely helpful, since it can allow us to have an idea about the strength of electron-phonon coupling taking place in the Si-SiO$_2$ separation, meaning the degree at which the Si-O-Si phonons at the Si-SiO$_2$ interface couple to the PL emission. This can be done through the calculation of the Huang Rhys-Factor, which can be approximated as the ratio of the intensity of the phonon band to that of the zero phonon line band. Phonon side bands involving n phonons ℏω have intensities: $I_n = S_n \exp(-S)/n!$ with S being the Huang-Rhys factor. Such an electron-phonon (Froehlich type) coupling is due to a phonon-induced deformation of the crystal lattice acting on the charge distribution of the exciton and resulting in a lowering of the excitonic energy. By calculating the H.R variation as a function of emission energy, a striking resemblance was obtained between S and PL variations. This was explained by the fact that as the electron and hole became sequentially localized (in the SiO$_2$ shell or at the (SiO$_2$-Si; SiO$_2$/PMMA) interface), the average distance between them would increase to $R \approx d/2$ (where d is the diameter of the Si no) in the first case, and thus S would also increase, and to $R > d/2$ in the hole localisation, causing the second peak to take place at 2.325 eV.

Having such a model in mind, it would be interesting to know if we can still talk about quantum confinement for nanoparticles having a diameter smaller than 3nm or whether it would be more appropriate to be talking about light emission from surface chemistry due to electron-phonon coupling with Si-O-Si phonons. Martin et al.[46] considered a break-down of the quantum confinement for small nanoparticles, in the sense of its being an increase of band gap for smaller nanoparticles, depending on the strength of electron phonon coupling.

Recently however, Sa'ar tried to explain the idea of electron-phonon localisation proposed by Wolkin et al. by considering a 'vibron' model,[209] which suggest that neither

[208] Delerue, Allan, et Lannoo, "Theoretical aspects of the luminescence of porous silicon."

[209] Amir Saar, "Photoluminescence from silicon nanostructures: The mutual role of quantum confinement and surface chemistry," *Journal of Nanophotonics* 3, no. 1 (Mars 12, 2009): 032501-42.

quantum confinement, nor surface state and chemistry alone can explain the entire spectrum of optical phenomena in silicon nanostructures.

c) The vibron model:

At first, Wolkin et al. [210] considered that the efficient light emission from Si nanocrystal was exceptionally due to slow nonradiative relaxation processes in the nanocrystal of the order of few milliseconds; thus excluding these channels could be the reason for a enhancement of the emitted intensity, which is what was found happening to small Si nanocrystals. To understand the triggering mechanism for such a non-radiative channel inhibition, he considered both the configuration space mode diagram for Si=O surface bonds (the variation of the potential energy versus the length of Si=0 bond), and the quantized electronic levels of the nanocrystal as the following (Figure IV- 18)
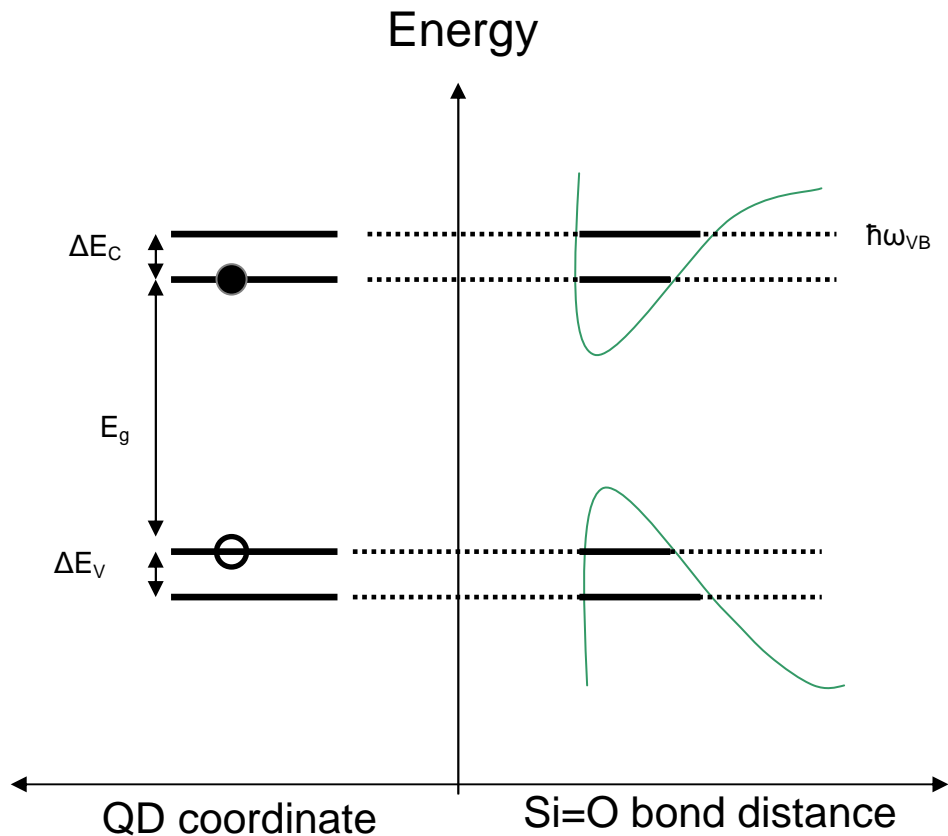
Figure IV- 18 quantized electronic levels of Si Nanocrystals and configuration space mode diagram for Si=O surface bonds. At left: ΔE_c and ΔE_v are the energy differences between lowest electronic sublevels of the conduction and valence bands. At right: Green lines represent the potential energy for surface vibrations (in the configuration space). The ground and first excited vibrational states are represented with the black lines. $\hbar\omega_{VB}$ is the vibrational energy. When $\hbar\omega_{VB=} \Delta E_c$ or $\hbar\omega_{VB=} \Delta E_V$, resonant coupling occurs.

It is important to note that the vibrational levels depend only on the type of bonding used to terminate the surface of the nanocrystal, while on the other hand, the quantized

---

[210] Ibid.

energy levels of the nanocrystal are size–dependant and should increase with decreasing size of the Si nanocrystal. Thus for relatively big Si nanocrystals the conduction/valence energy differences ΔE_c and ΔE_v (more specifically the energy difference between lowest conduction and valence sublevels respectively) are fairly small compared to vibrational energies. However, as the nanocrystal size decreases ΔE_c and ΔE_v increases until, for a given diameter of the nanocrystal, the two energies (electronic and vibrational) coincide. This is the condition for resonant coupling between surface vibrations and the electronic state of the nanocrystal, via a polarization field of the vibrations. Afterward, when this condition is fulfilled, the strong coupling between the core electrons and phonons of the crystalline shell give rise to a creation of a virtually everlasting mixed-electron phonon modes, called polarons, which themselves 'passivate' the surface against non radiative relaxation processes, meaning a decrease of intensity compared with respect to quantum confinement. The polaron state was thus seen as a 'dressed' state of the electron-phonon system, meaning that the electron and/or hole are coupled to the surface of the Si Nc. Thus we deduce with such an explanation, which is also in agreement with other similar experiments[211] (which also provides a better understanding of Martin et al. findings) that it is both quantum confined and surface chemistry state can simultaneously play a role in the photoluminescence of the Si nanocrystals at such small sizes.

c) Effect of medium on photoluminescence:

An important point which was mentioned in Martin's[65] work is the importance of a deeper understanding of the effect of the dielectric environment on the PL behaviour of Si Nc.

In fact, a correlation has already been found between photoluminescence intermittency and medium polarisability for CdSe quantum dots.[212] In this case, the power law exponent α of off time distribution noticeably changed to smaller values, when embedding the nanoparticles in polymers having higher dielectric constants. In reality, a response to the polarity of the surrounding medium is usually expected for systems which involve charged or charge separated states; such a behaviour was explained with a model which assumed that the charged quantum dot ejected the electron this time not to the SiO_2 shell, but to the outside matrix (the embedding polymer) inducing a reaction field (atomic and electronic relaxations of the surrounding material). The interaction of the charge with this reaction field would then fix the charge in the matrix, and thus stabilize the charge separated state against fast recombination. The stabilization energy E_{st} of a

[211] Douglas S. English, Lindsay E. Pell, Zhonghua Yu, Paul F. Barbara, et Brian A. Korgel, "Size Tunable Visible Luminescence from Individual Organic Monolayer Stabilized Silicon Nanocrystal Quantum Dots," *Nano Letters*, 2 (2002), 681-685

[212] Abey Issac, Christian von Borczyskowski, et Frank Cichos, "Correlation between photoluminescence intermittency of CdSe quantum dots and self-trapped states in dielectric media," *Physical Review B (Condensed Matter and Materials Physics)* 71, no. 16 (Avril 15, 2005): 161302-4.

charge q in a cavity of radius R surrounded by a homogeneous dielectric medium with a dielectric constant ε can be approximated by:

$$E_{st} = (q)^2/(8\pi\varepsilon_0 R)f(\varepsilon)$$

where the reaction field factor $f(\varepsilon)$ depending on the dielectric constant can be given by the expression:

$$f(\varepsilon) = 1 - 1/\varepsilon$$

Thus, as the dielectric constant of the medium increases, its reaction filed factor $f(\varepsilon)$ also increases, which implies the increase of the stabilisation of the energy. The ejected charges are then suggested to be self-trapped in mid-band gap states of the surrounding matrix during off times and are proposed to be the source of power law intermittency. Thus, an increase of ε, meant decrease of α_{OFF} because of the higher stabilisation energy, which is leading to an increase of OFF time probability.

In the case of Si Nc however, the previous studies, which used the same procedure, showed no dependence of α on the dielectric properties of the environment (which was varied from quartz to PMMA).[213] The reason for such behaviour might be related to the fact that the observed porous nanoparticles (prepared via electro-chemical etching followed by ultrasonic treatment) were covered by an SiO_2 shell which was much larger than 1 nm (about 10nm) and that in this case electron trapping occurred in the SiO_2 shell or at the Si/SiO_2 interface.

Thus an interesting idea would be to look deeper to such a configuration and to try to know whether there is really or not an influence of the surrounding medium on the emission properties of Si nanocrystals. This time however, we would be working with the same kind of pyrolised-nanocrystals having the same dimensions as those studied by Martin et al. since, the SNOM measurements that we have done have shown almost similar size in both cases (our measured nanocrystal diameter of 6 nm is very close to the 5.7nm measured by Martin. et al.[65]). Also we would be looking more into emission properties rather than blinking statistics. Such a goal could be realized by embedding the nanocrystals in different polymer films having different dielectric constants and studying the optical behaviour in each media.
It would be also interesting to see the effect of a larger or smaller SiO_2 shell on the nanocrystal's emission properties, which can be done by looking at the variation of their spectroscopic constants with increasing or decreasing size of Si nanoparticles. Such studies will be the subject of the coming section.

---

[213] C. von Borczyskowski et coll., "Common luminescence intensity fluctuations of single particle and single molecules in non-conducing matrices," *The European Physical Journal - Special Topics* 144, no. 1 (Mai 14, 2007): 13-25.

IV-4.Confocal spectroscopy results:

Now that we have a better idea about the time behaviour of the excited nanocrystals, a second important point would be to study the spectral shape of the emitted light during the ON time. This is also the subject of a lot of controversy since many groups tried to explain the mechanisms taking place during such a process in different ways. Having into consideration such different phenomena for Si luminescence investigations, the S band will be studied in order to find which model correspond the best to the luminescence features in the case of our pyrolised Si nanocrystals.

Thus, the main aim of our studies was about the processes that were taking place during the 'on' time, rather than studying the blinking of the nanocrystals; this has been done by placing Si nanocrystals in two different polymers having different dielectric constants;

Such measurements were repeated for three different situations: the Si nanoparticle where either embedded in PMMA (Polymethyl methacrylate)), in PVA (Polyvinyl alcohol) or simply deposited on the Si/SiO$_2$ substrate (ε_{PMMA}= 3.4 , ε_{PVA} =14 , ε_{Sio2} =3.7). Since most of our obtained spectra showed a relatively moderate signal to noise ratio, a fitting of each was done in the first place. We tried to fit each band with a Gaussian in order to include all the statistical variations and fluctuations which may have not been resolved with the experimental conditions (temperature, binning time etc…). We show in Figure IV- 22-Figure IV- 21) examples of emission spectra with the respective fittings obtained for the different studied particles at different times.

IV-4.1 Emission spectra of Si nanocrystals in different media

a) In PMMA:

Figure IV- 19 shows the emission spectra and respective time traces of two different nanoparticles which we called k1 and J1, in parts a and b. The upper part shows on the left a Si nanocrystal's time trace distinguished by two emission levels, characteristic of single nanoparticle spectroscopy. We see a maximum value of about 400 photon counts, when the particle is ON. On the left of the same graph, we depict the corresponding fitted emission spectrum which has been acquired 12.1 seconds right after the exciting laser has been turned on (Pointed at in the time trace scheme by a red arrow).The intensity of the collected emission signal is low, resulting in a blurred emission spectrum, drowned in an important background noise, this is typical of Si nanocrystals emission which have been excited at about 500 nm.
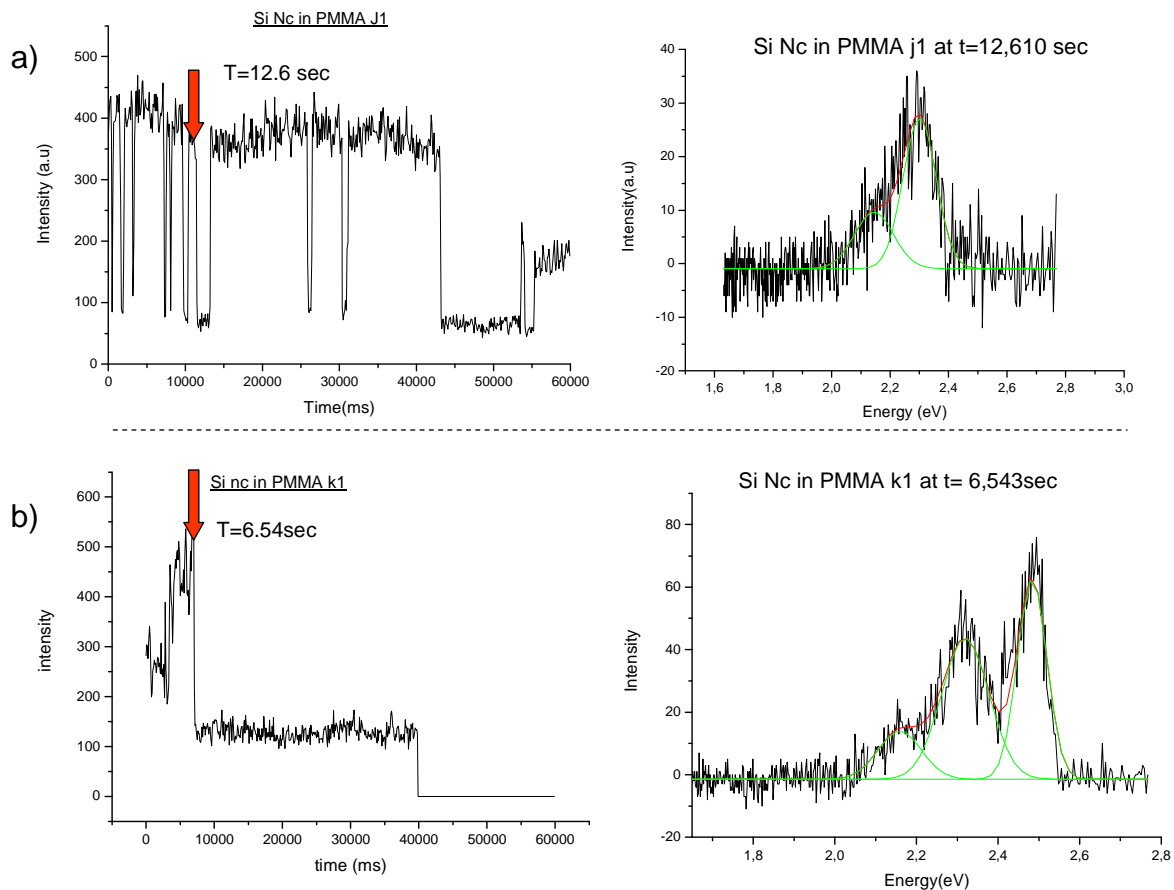
Figure IV- 19 Emission spectrum and corresponding time trace of silicon nanoparticles in PMMA

The lower part of the same figure shows a different time trace shape, which resembles to that of Figure IV- 15 b. In this case the photon counter shows an enhanced signal compared to that obtained in part a, thus resulting in an improved emission spectrum. What is interesting is the multiple peaks configuration that is clearly displayed in the spectrum. Such a shape represents the typical structure of a multiphonon mediated photon emission. Even thought the most energetic peak may seem sliced, which is probably due to the cut off filter, we can be sure about the existence of two phonon bands optical transitions in the silicon naocrystal that we study. We also show the perfect Gaussian fits that we can apply to such kind of transitions, it is very hard to predict whether the type of emission that will take place a single or multi-phonon. We should also note that silicon nanoparticles having a time trace resembling to that of part b, may have emission spectra like that of part a and vice versa. It is even possible to obtain emission spectra showing one or two phonon bands at different times, emanating from the same particle, as we will show in the following, for Si nanoparticles on SiO_2.

b) On SiO_2:

Figure IV- 21 shows different emission spectra, varying with time, for two silicon nanoparticles called nanoparticles (b1) and (f2). Their time traces are shown in Figure IV- 20
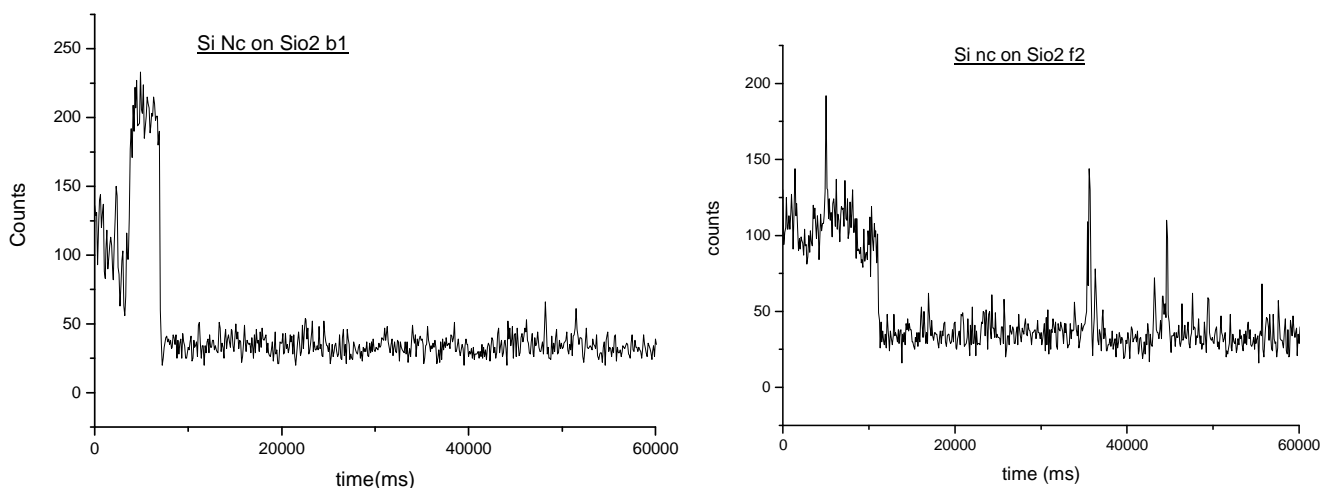
Figure IV- 20 Time traces of nanoparticles b1 and f2, which are deposited on an Sio$_2$ substrate.

For nanocrystal b1, the shown emission spectra (from the left to the right) have been recorded at t= 9.23, 9.85 and 11.25 seconds after the exciting laser has been turned on (that we will call a, b, c). For f2, this has been done after 10.9, 12.23 and13.64 seconds (called d, e, f). The signal may not appear very strong in this case also, but it is still interesting to notice the variation of both nanoparticle's spectra with time. We can see in each case a clear variation of the nanocrystal's spectral characteristics with time (this is also reflected in the fitted Gaussians). For example, b1 shows a clear increase of the signal's intensity when passing from time t= 9.23 sec to t=9.83 sec. There is also a difference in the side band's and zero phonon line band's dimensions (width-splitting between bands). Finally, a small shifting of the emission lines can also be noticed in the three cases.

The same kinds of variations take place for nanocrystal f2, but what is also interesting is an additional side band that we can depict (f, in the second row). In fact, at t=10.9 s we start with a spectrum showing a clear phonon side band, whose main characteristics begin to change at t=12.23s (e), and at t=13.64 s (f) a second phonon band begins to show. This is also seen through the use of the Gaussian fitting tool, which illustrates the new phonon line's formation. The conditions in which such a behaviour can take place is still unknown to us, however our main goal in this section is to show the diverse changes that take place with time in a nanocrystal's emission spectra and the numerous differences in the emission properties between two separate nanocrystals, excited exactly at the same conditions.
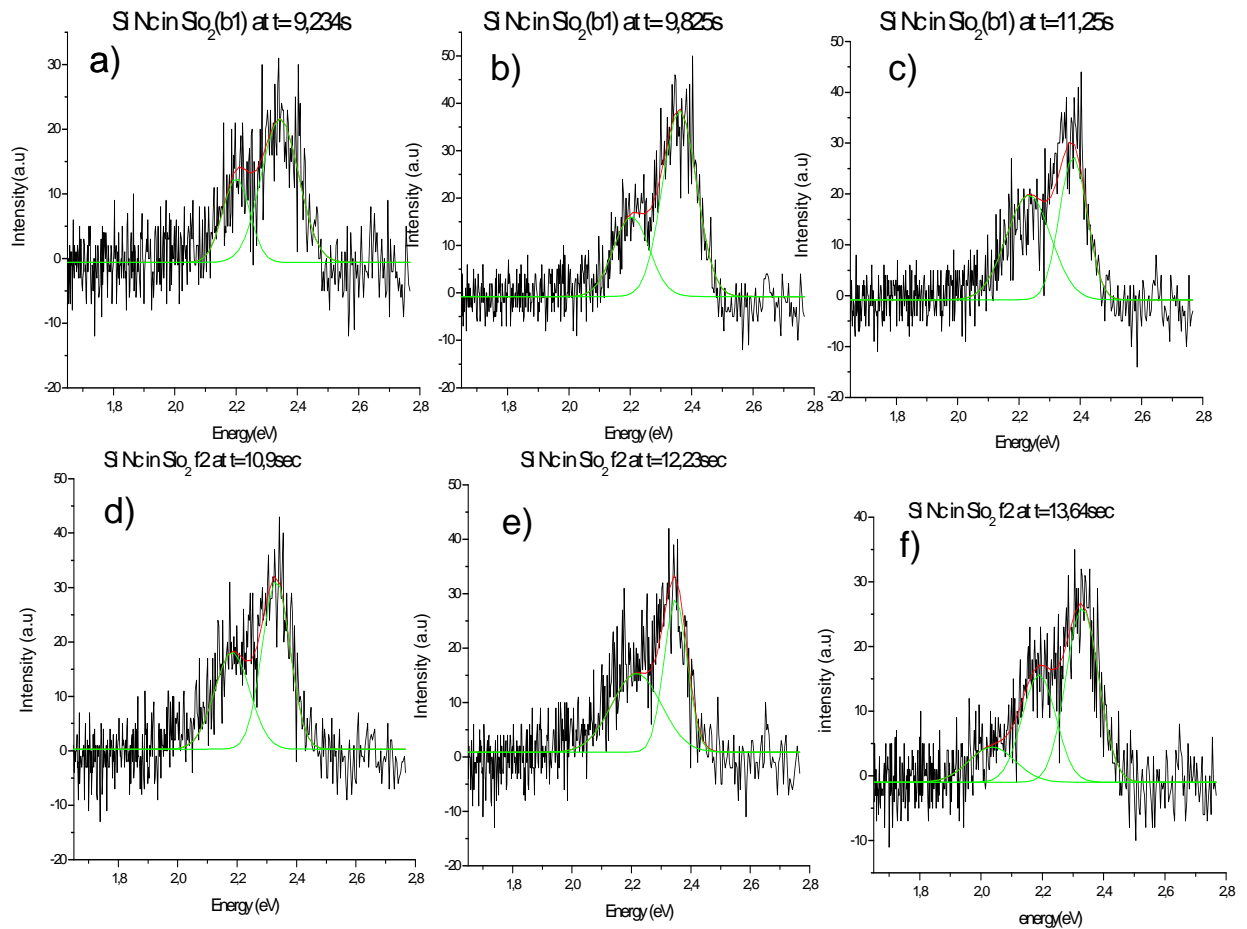
Figure IV- 21 Si Nc on Sio₂ emission spectra at different times, for two different nanoparticles

c) In PVA:

As we mentioned in Figure IV- 15, we have observed two different kinds of time traces for Si nanocrystals which are embedded in PVA. These can be either composed of sharp emission line showing photon emission for a very brief amount of time, or a multiple step time trace, having longer ON times. What would be interesting is to see the difference in emission spectra for each of these cases. Figure IV- 22 and Figure IV- 23 show the two kinds of emission spectra that we find for each time trace type. Figure IV- 22 shows the emission spectrum of a silicon nanoparticle having a sharp line time trace. The zero phonon line and first phonon line bands can be clearly seen and fitted. The origin of the small bump at about 2.55 eV is only of experimental nature (an external laser light of the same wavelength was present at the time of experiment). It is impossible to show spectra that are varying in time for this kind of emission since the ON time lasts for a very small period of time.
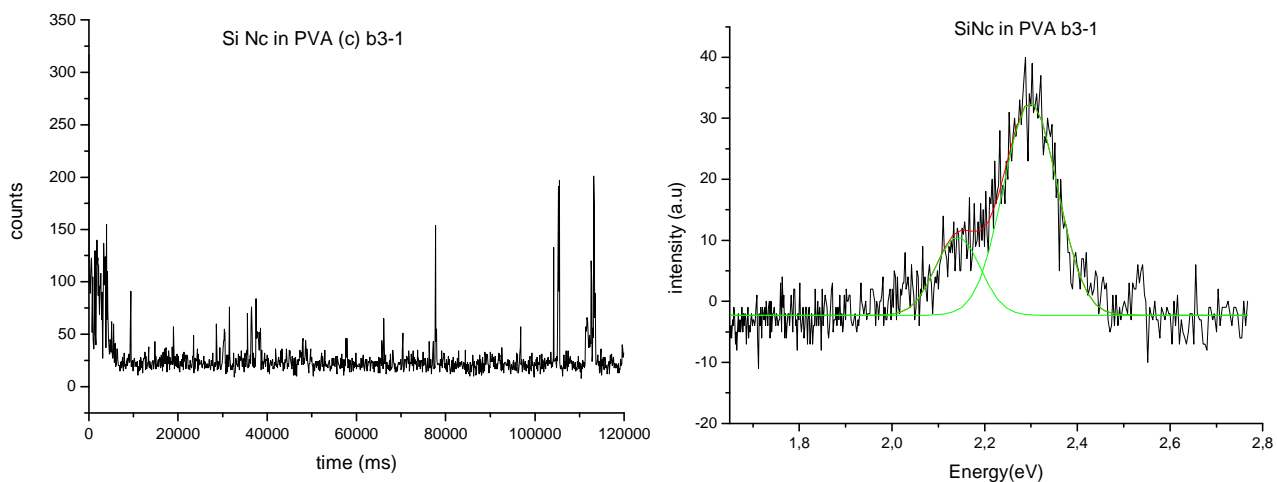
Figure IV- 22 Si nanocrystal in PVA sharped line time trace and corresponding emission spectrum.

Emission spectra originating from particles, whose time traces are composed by small steps, are shown in Figure IV- 23 and Figure IV- 24 (we will call these nanoparticles a7-a11). The time variation of each spectrum is also shown.
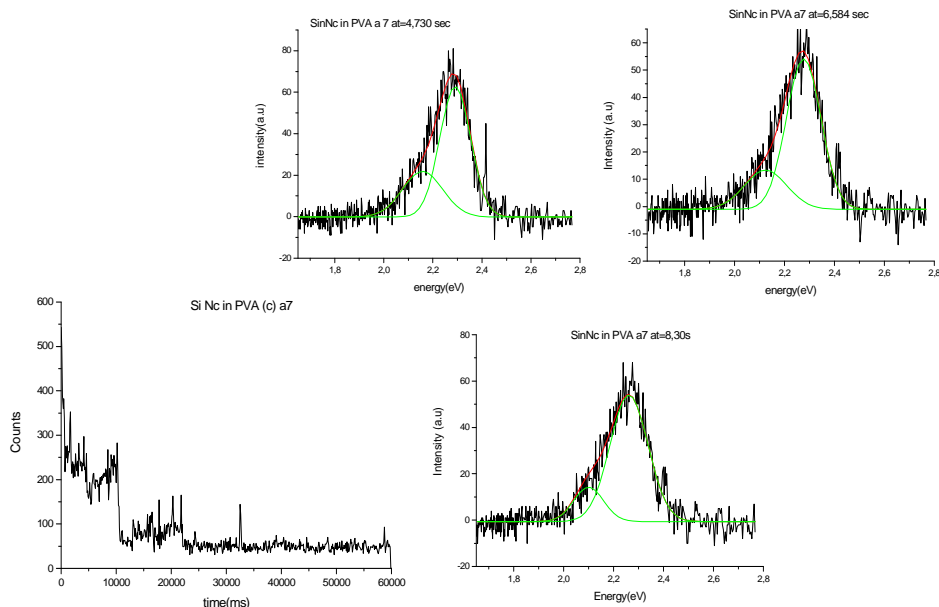

Figure IV- 23 Stepped time trace and corresponding time varying emission spectrum for a PVA embedded Si nanoparticle .
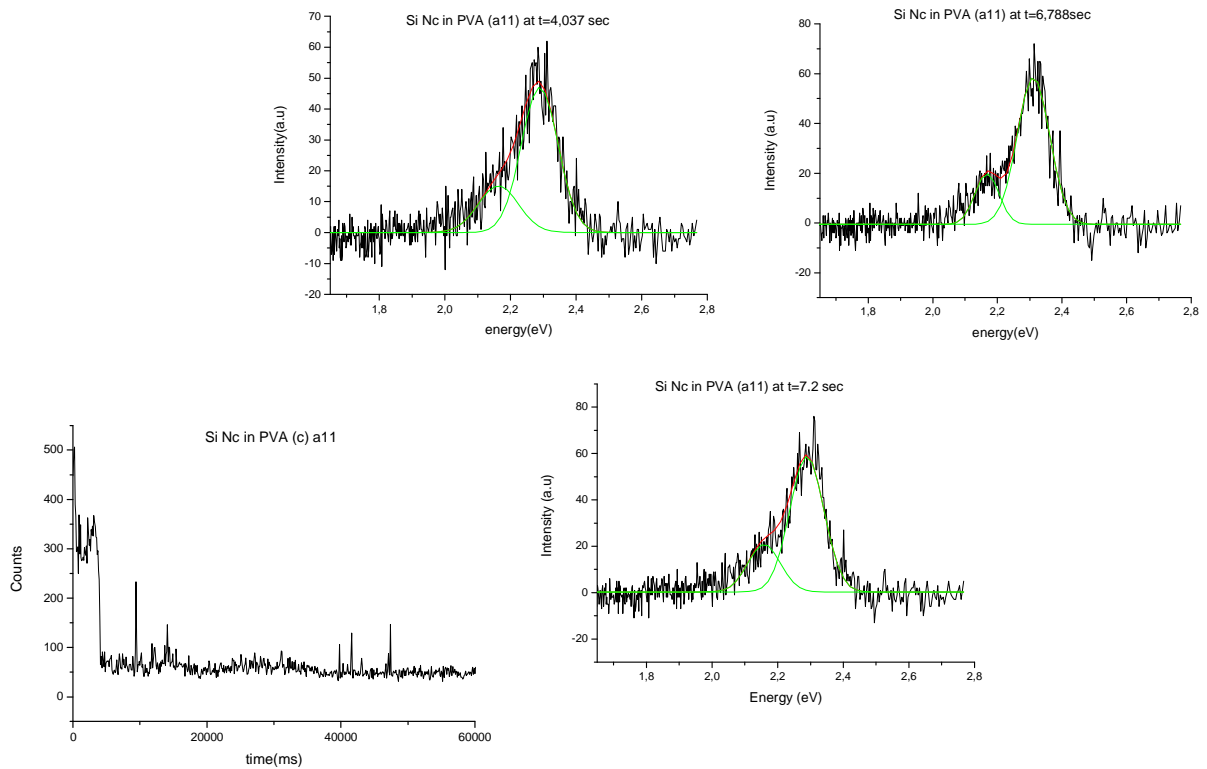
Figure IV- 24 Stepped time trace and corresponding time varying emission spectrum for a PVA embedded Si nanoparticle .

We see that eventhought both nanoparticles show similar time traces, the emission spectrum of each has different shapes. In the first case (nanoparticle a7), the side band is more or less seen, while for nanocrystal a11, the phonon line appears more clearly. As in the previous cases, we also notice a variation of their spectral characteristics with time, that is, the width, intensity and splitting of each emission spectrum changes as time passes.

Keeping in mind the multitude of different cases we encountered concerning the acquired emission spectra, we see ourselves exposed to an impossibility of having a clear understanding of the different phenomena taking place in the emission process of silicon nanoparticle, without performing a deeper study. In order to have a real comprehension of the diverse phenomena residing in the emission of nanocrystals, a more profound and precise study of specific parameters averred to be essential. An interesting investigation method would be to study separately the spectral features of each silicon nanocrystal spectrum by considering its different characteristics: Splitting-Width-Huang Rhys factor-Area, and then have a view of the general behaviour of all the nanocrystals, as we will show in the following.

IV-4.2 Method of Analysis:

As we just explained, in order to have a clearer idea about the behaviour of the nanocrystals, we had to consider different parameters in each spectrum and try to compare between the obtained values for each nanoparticle. We determined four parameters which are the following (Also illustrated in Figure IV- 25),

1° The splitting between the two bands

2° The Huang Rhys factor

3° The intensity of the zero phonon line band

4° The Width of the zero phonon line

The next figure (Figure IV- 25) is a representation of an emission spectrum, which would help to understand the different parameters:
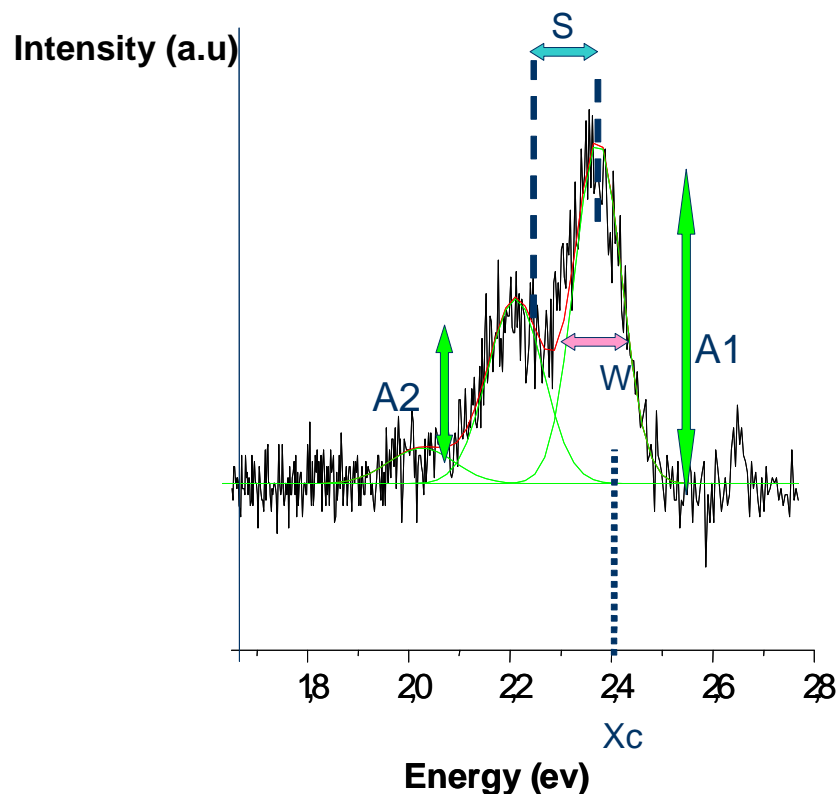

Figure IV- 25 Si Nc emission spectrum with the different elements used for its analysis.

In the following we will be giving an idea about the physical basics behind some parameter and the information it can bring us about the different mechanisms taking place in such a system.

139

a) Splitting between the two bands:

The phonon frequencies with which the coupling is taking place, is represented by *S* in Figure IV- 25

b) Huang Rhys factor:

Is commonly used to characterize linear vibrational coupling to electronic excitations through the difference between ground and excited state geometries. In molecular spectroscopy, Franck-Condon overlap factors, related to *S*, determine the probability of specific electronic-vibrational transitions that give rise to vibrational replicas in absorption and fluorescence spectra. Subsequently, *S* characterizes the strength of exciton-vibration coupling. It can be found by calculating the ratio of the intensity of phonon lines and the zero phonon line. (By calculating the ratio *A2 /A1*, where *A1* and *A2* are respectively the intensity of the Zero phonon line and first phonon band.)

c) Intensity of zero phonon line band:

Expresses the quantity of photons emitted in each emission (represented by *A1)*or degree of phonon coupling (A2).

d) Width:

When talking about the width of the ZPL, without the influence of the lattice, the natural line width (full width at half maximum) is $\gamma_0 = 1/T_{10}$, where T_{10} is the excited state life time. Above absolute zero however thermal motions will introduce random perturbations to the local environment, leading to a broadening of the FWHM. In general, the homogeneous width of a quantum dot is given by the inverse of the rephrasing time, which consists of the radiative lifetime and various scattering times (interaction of the exciton with phonons, interface states, defects, etc...)[214].

Then we plot a curve for each of these four parameters, in function of *Xc* and the abscissa of the zero phonon line. Thus, for each nanoparticle, at a given time, we had four different curves containing all the information obtained from each individual spectrum. Hr (Xc), S (Xc), W (Xc), A1 (Xc). We must remember however, that each nanocrystal was measured for a period of time (60s or 120s) so that for one nanoparticle we have the four differing parameters which change with time. Thus, for each parameter we obtained a series of 3 curves, representing Si nanocrystals in three different matrices. We will try to study each parameter alone, and try to compare the behaviour of such particles in the different media, and their variation with the nanocrystal's size change.

---

[214] T. Takagahara, "Theory of exciton dephasing in semiconductor quantum dots," *Physical Review B* 60, no. 4 (Juillet 15, 1999): 2638.

IV-4.3 Results:

a) Si nanocrystals phonon frequency variation with emission energy:

i) Previous results:

In their work, Martin et al.[65] presented a plot between phonon frequency variation and photoluminescence energy, obtained by taking into consideration the splitting between 55 individual pyrolised Si nanocrystals. It showed a linear increase from 130 to 170 meV upon increase of energy from 1.95 to 2.4 eV that was attributed to the existence of the surface phonons ω_S, and which have been predicted to be a mixture of LO and TO modes. Such a variation was in agreement with a model provided by Klein et al,[215] which permitted to confirm that decreasing the size of the Si nanocrystals would decrease the Si/SiO_2 ratio and thus the influence of Si.

ii) Si-O-Si phonon modes coupling hypothesis:

In our case, we apply the same method for the spectra obtained from different nanoparticles placed in the three different media. In other words, we tried to fit each spectrum by Gaussian LO or TO phonons and to look at the variation of phonon frequency with emission energy. Each nanoparticle is represented by a colour, and two dots of the same colour represent data taken from the same nanoparticle but at two different times. For example if we refer to Figure IV- 21, the upper row (nanocrystal b1) would be represented by 3 dots, all of them having the same colour, while the second row (nanocrystal F2) would be represented by three other dots having also the same colour, but which would be different from that used for b1. In a first trial, we obtained the graphs in Figure IV- 26, the right handed legend refers to a naming of the different nanocrystals and the word 'split' reminds us that we are taking into consideration the splitting in each graph. At a first glance, by taking into consideration the slope variation with scale, we have a similar relationship as that obtained with Martin et al.[65] for the three different cases (less Si impact for smaller nanocrystals); The emission energy is distributed in the case of PMMA at a larger energy scale than in PVA and on SiO_2 since two different filters were used: One for PMMA, the other for PVA –SiO_2 measurements. However both were prepared within the same conditions. Looking closer, we see that for PMMA and SiO_2, some of the splitting values are outside the barrier in which we normally would have obtained SiO_2 phonon coupling (130-160 meV); also, in the PVA case, much more points are outside the barrier.

A solution for resolving this problem would be not to consider only an SiO_2 phonon coupling in the fitting procedure, but instead (Si +SiO_2) phonons for nanocrystals whose splitting values are outside the range of (130-160 meV). We thought about such a solution based on the fact that the shapes of the ZPL were sometimes asymmetrically broadened to the low-energy side. Such shapes have also been found experimentally by

---

[215] M. C. Klein et coll., "Size dependence of electron-phonon coupling in semiconductor nanospheres: The case of CdSe," *Physical Review B* 42, no. 17 (Décembre 15, 1990): 11123.

Valenta et al., and have been assigned to unresolved phonons, or vibrational sidebands which would become clearly resolved at stronger pumping, or lower temperature.[216],[217,218,219]
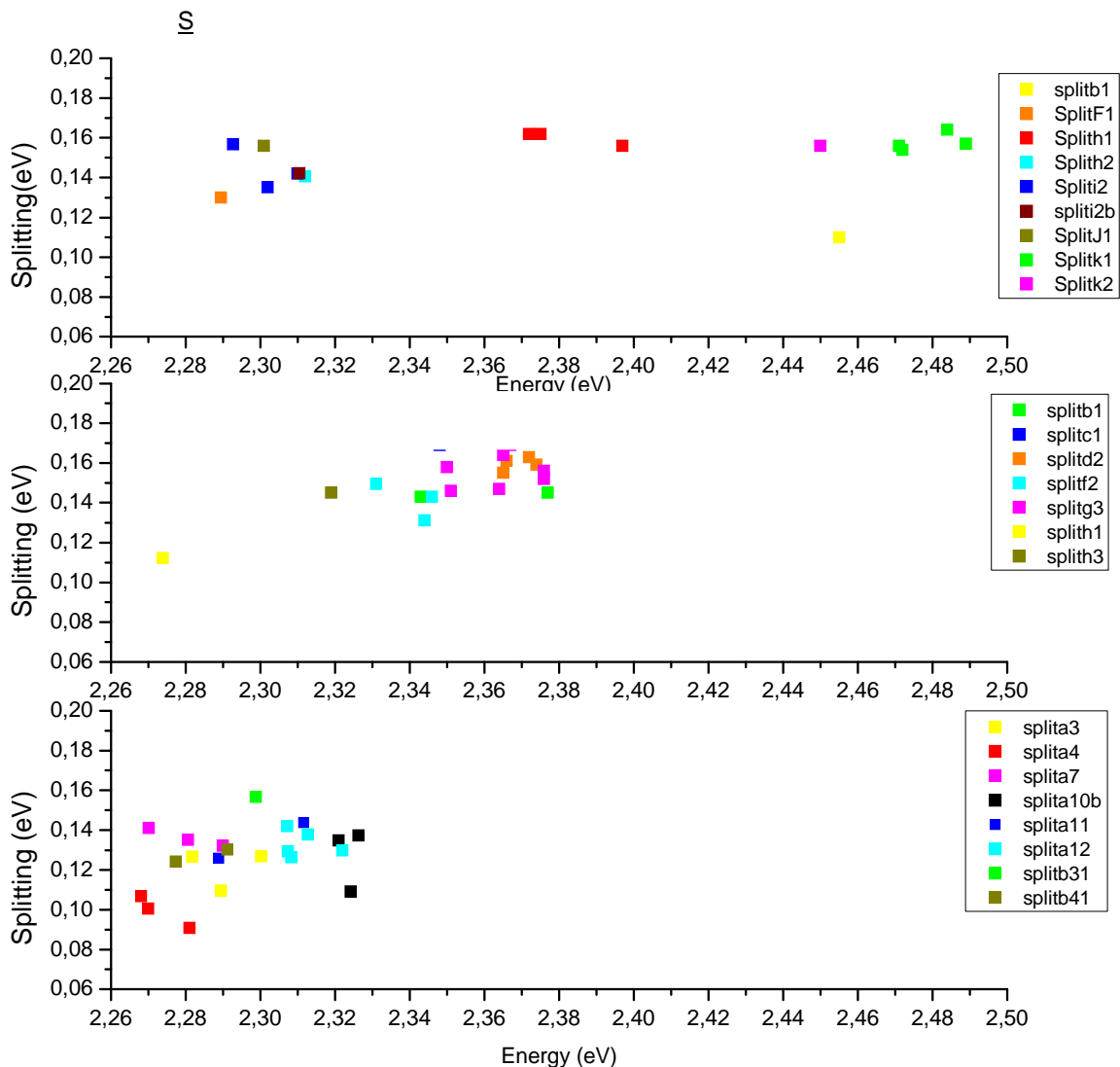

Figure IV- 26 Splitting variation in function of emission energy for Si Nc's fit with one SiO_2 phonon band in different media, at different times.

Different cases could be found, where such bands could be attributed to either coupling to Si-O-Si groups on the surface of the nanocrystal, to Transverse Optical (T.O) phonon

[216] M. D. Mason, G. M. Credo, K. D. Weston, et S. K. Buratto, "Luminescence of Individual Porous Si Chromophores," *Physical Review Letters*, 80 (1998), 5405

[217] M. D. Mason et coll., "Luminescence of Individual Porous Si Chromophores," *Physical Review Letters* 80, no. 24 (Juin 15, 1998): 5405.

[218] Ilya Sychugov et coll., "Narrow Luminescence Linewidth of a Silicon Quantum Dot," *Physical Review Letters* 94, no. 8 (Mars 4, 2005): 087405

[219] Jan Valenta et coll., "Light-Emission Performance of Silicon Nanocrystals Deduced from Single Quantum Dot Spectroscopy," *Advanced Functional Materials* 18, no. 18 (2008): 2666-2672

energy of bulk Si, or to spheroidal or torsion acoustic mode etc… . Thus, for our graphs, fixing an additional Si phonon at about 56 meV from the ZPL and trying to see if we can obtain a better fit would be equivalent to trying to illustrate the kind of phonons which would best present in the emission spectra if the experiment had to be done with a better resolution (with higher pumping, or lower temperature). Having a better fitting with such a method would thus encourage us to keep into consideration the $Si+SiO_2$ fitting and to continue the analysis with such a new fit. The two cases are represented in the following figure:
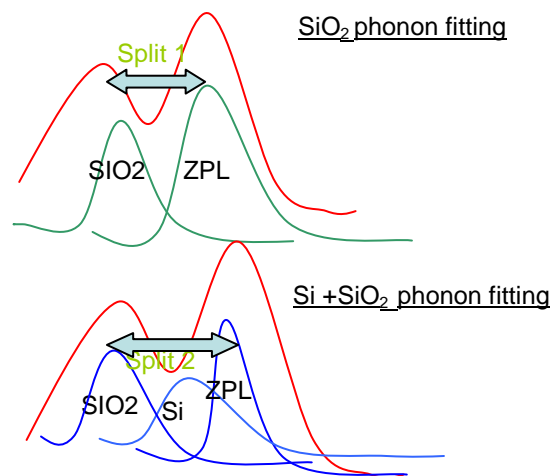

Figure IV- 27.Different fitting procedures used to study emission spectra of silicon nanoparticles

We give an example for the two different kinds of fittings, for the same spectrum, in Figure IV- 28:
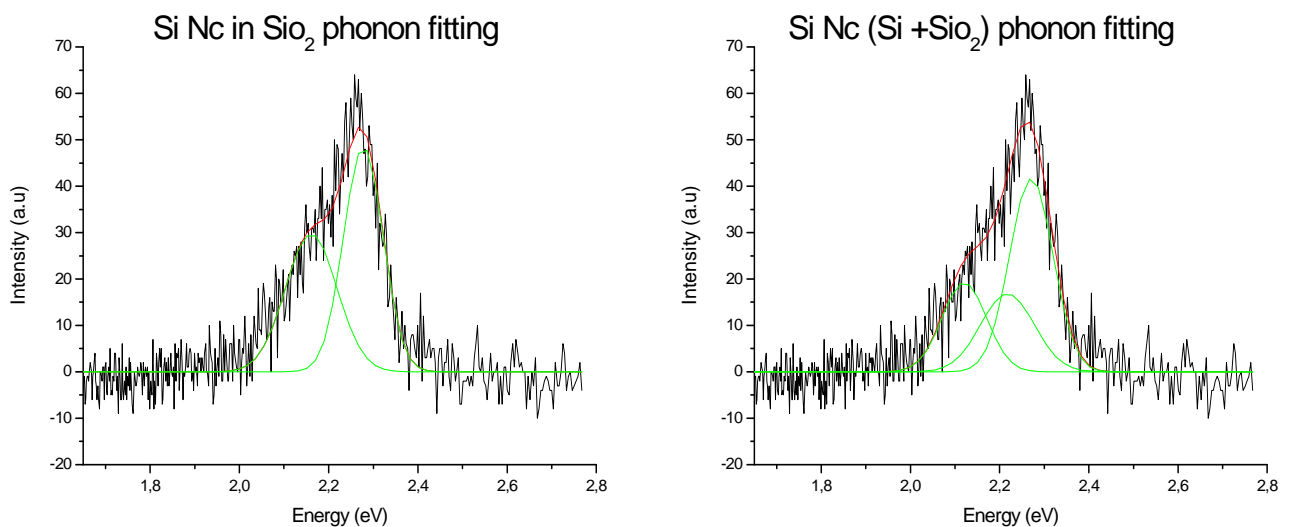

Figure IV- 28 Two different fittings of the same silicon nanocrystal emission spectrum.

This spectrum is an emission spectrum of a silicon nanocrystal embedded in PMMA. The left handed Gaussian fitting is done by taking into consideration one SiO_2 phonon, while the right one contains an additional Si band. The main conditions for such a fitting are three line fits with always fixing the Si phonon at about 53meV, no line width below 80 meV, that is a minimum of 80 meV for the Zero Phonon Line and 100meV for the others. The plan of the work has been first to fit all the spectra with two lines, keeping every parameter free. This is what we have done while fitting our spectra with only SiO_2 phonon lines. The next step has then been to fit the spectra again, but this time by taking into consideration 3 lines (The Zero phonon line, the Si band at 53 meV from the ZPL, and the SiO_2 line) and paying attention to the 53 meV splitting and lower limits to line widths. Then we would compare the overall better results in terms of fitting, and may decide to use either one method of fitting or the other, by judging individually the spectra.

iii) Si+ SiO_2 phonon modes coupling hypothesis:

If we now consider only one of the point in the set of points representing a nanocrystal at different times (the one with best looking fitting, or most energetic) and try to plot the new relationship between phonon frequency and emission energy, we would get the following Figure IV- 29 (triangles represent emission spectra who's best fitting was obtained by applying SiO_2 + Si fitting, while squares were best fit only with an SiO_2 phonons).
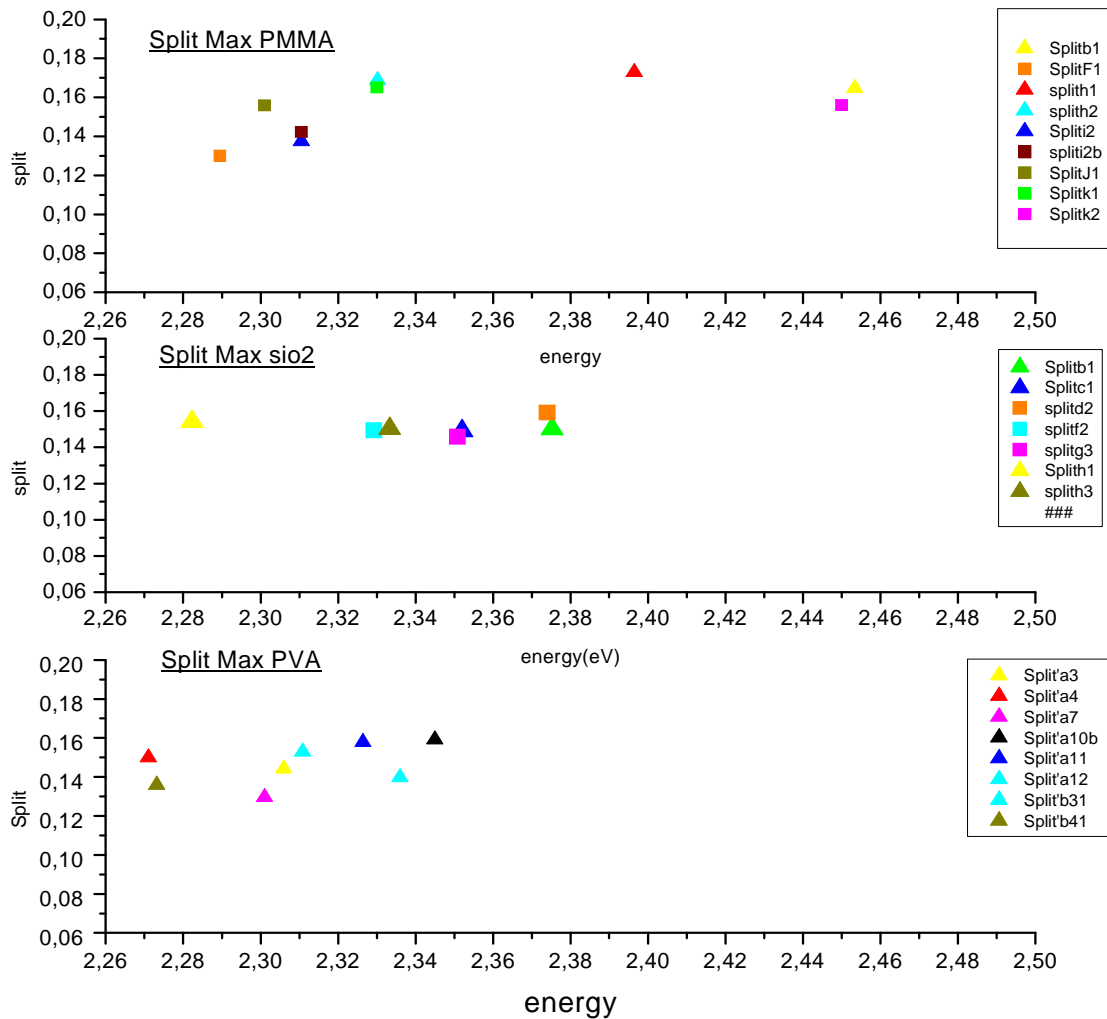
Figure IV- 29 Splitting variation in function of emission energy for Si Nc's fit with one Sio$_2$ phonon band(squares) or (Si+ Sio$_2$) phonon bands (triangles) in different media.

We thus now have a set of data with the splitting between the ZPL and SiO$_2$ phonon line in good agreement with theory whether by considering (SiO$_2$ + Si) or only considering Si phonons, where all the splitting are now between 130 meV - 160mev. A clear difference can be noticed for the PVA case, where we see that all the nanocrystals embedded in PVA tend to have an Si + SiO$_2$ fitting that is more suitable, while for the two other cases, better fittings were obtained with a mixture of both SiO$_2$ and Si+SiO$_2$ phonon fittings. The increasing tendency of phonon frequency with emission energy reflecting the Klein et al. model is however less seen in this case, than the one found with Martin et al. [220] This is because the scale which we are using and the number of studied nanocrystals is a much

---

[220] Ibid.

smaller, knowing that we studied about only 8 points whose emission energy extended from 2.26 eV to 2.46 eV, while in Martin's work, about 55 Nc were investigated extending on a scale going from 1.95 to 2.4 eV.

We can now start studying the different other parameters characterising the emission spectrum, and to compare what we obtain with and without Si coupling; we will first start with the width.

b-Width calculations:

i) Introduction and general idea:

Usually, the homogeneously broadened line width of Si Nc's is found to be about 100 meV at room temperature according to Sychugov et Al.[221,222] All other single Si studies showed either lines much broader than 100 meV, or Si-O-Si vibrational transitions between 130 or 160 meV. However what has been found at low temperature spectroscopy is the discovery of ZPL width which could reach values as small as 25 meV, when the emission was a No-Phonon line emission (meaning that we do not see any phonon side band accompanying the spectrum main band); and 35 meV ZPL, when an Si TO phonon band was present within the spectrum. Thus, the ZPL width band varied whether or not the emission under study was accompanied by a phonon side band or not. What we would like to show in our case is that the decrease of the size, meaning the decrease of the Si/SiO_2 ratio does not only have an influence on the phonon frequencies of the Si nanocrystals, but also on the width of the ZPL of the emitted spectra. To do that, we will take into consideration only fittings with SiO_2 phonons, and look at the general tendency or behaviour of the emitted light. We will then try to see how the situation would change with respect to a different fitting compromising this time both $Si+SiO_2$ phonons. From the comparison between both cases, we will see how we could understand why such changes would take place.

ii)ZPL width with Sio2 phonon fitting

Without taking any Si phonon into consideration, that is, only working with SiO_2 phonons, we trace the variation of ZPL width with ZPL emission energy for the different nanocrystals in different media, at different times, we have the graph inFigure IV- 30, we

---

[221] Ilya Sychugov et coll., "Narrow Luminescence Linewidth of a Silicon Quantum Dot," *Physical Review Letters* 94 (Mars 1, 2005): 87405.

[222] Ilya Sychugov et coll., "Single dot optical spectroscopy of silicon nanocrystals: low temperature measurements," *Optical Materials* 27, no. 5 (Février 2005): 973-976.

see that, we have a variation of the ZPL width from about 0.08 till 0.15 eV, which is in the range of usually obtained spectra.
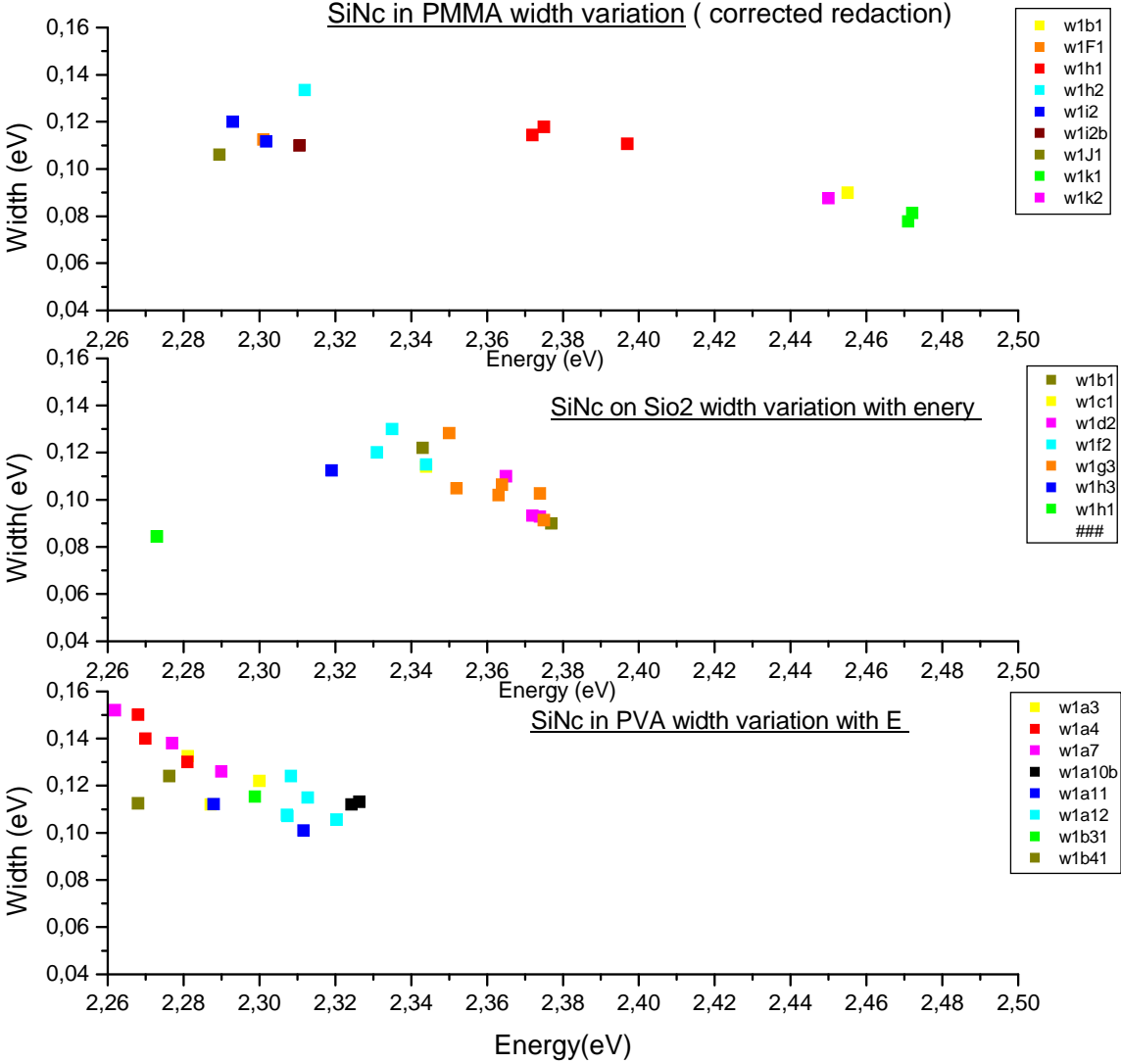

Figure IV- 30: ZPL width variation in function of emission energy for Si Nc's fit with one SiO_2 phonon band in different media, at different times.

We can distinguish a linearly decreasing relationship at a first glance, that is, with decreasing size of Si Nc, the width of the considered ZPL is decreasing. If we consider only one point of each set of points, obtained at different times, we still have the same kind of behaviour as we see in the following
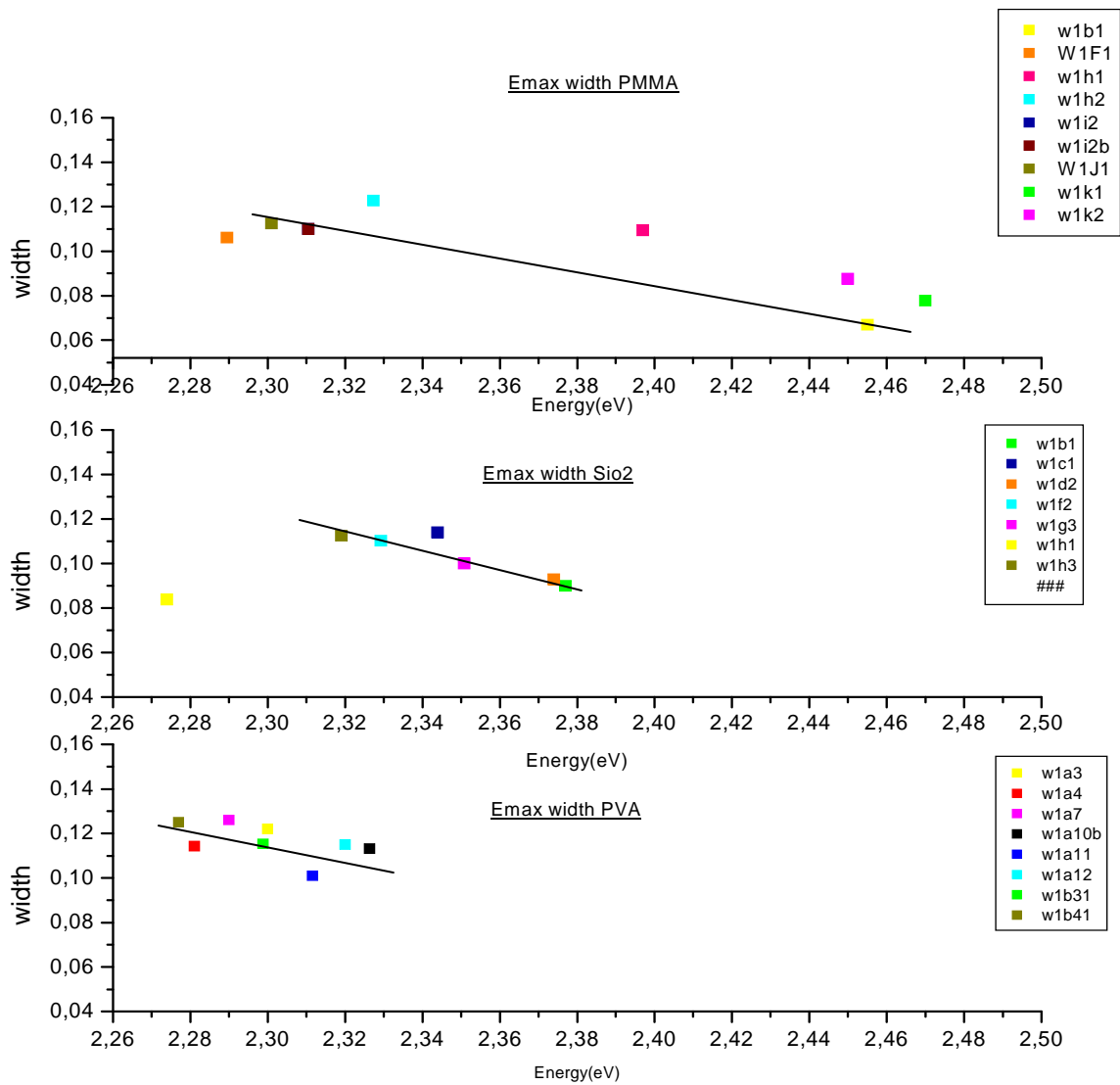
147

Figure IV- 31 ZPL width variation in function of emission energy for Si Nc's fit with one Sio2 phonon band in different media.

iii) ZPL width with (Si+Sio$_2$) phonon fitting:

To understand this behaviour, we must remember that this fitting corresponds to that of SiO$_2$ phonons only. But for some of the nanoparticles (which, in reality can be better fitted by a Si+SiO$_2$ fitting) the ZPL width that we are considering is actually a combination of Si and ZPL (not only a ZPL width), the Si corresponding to the 'intrinsic' Si phonon. In fact, if we now replace the points which can be fit with Si+SiO$_2$ phonon in Figure IV- 31 and consider their ZPL width (represented by triangles) we obtain the following:
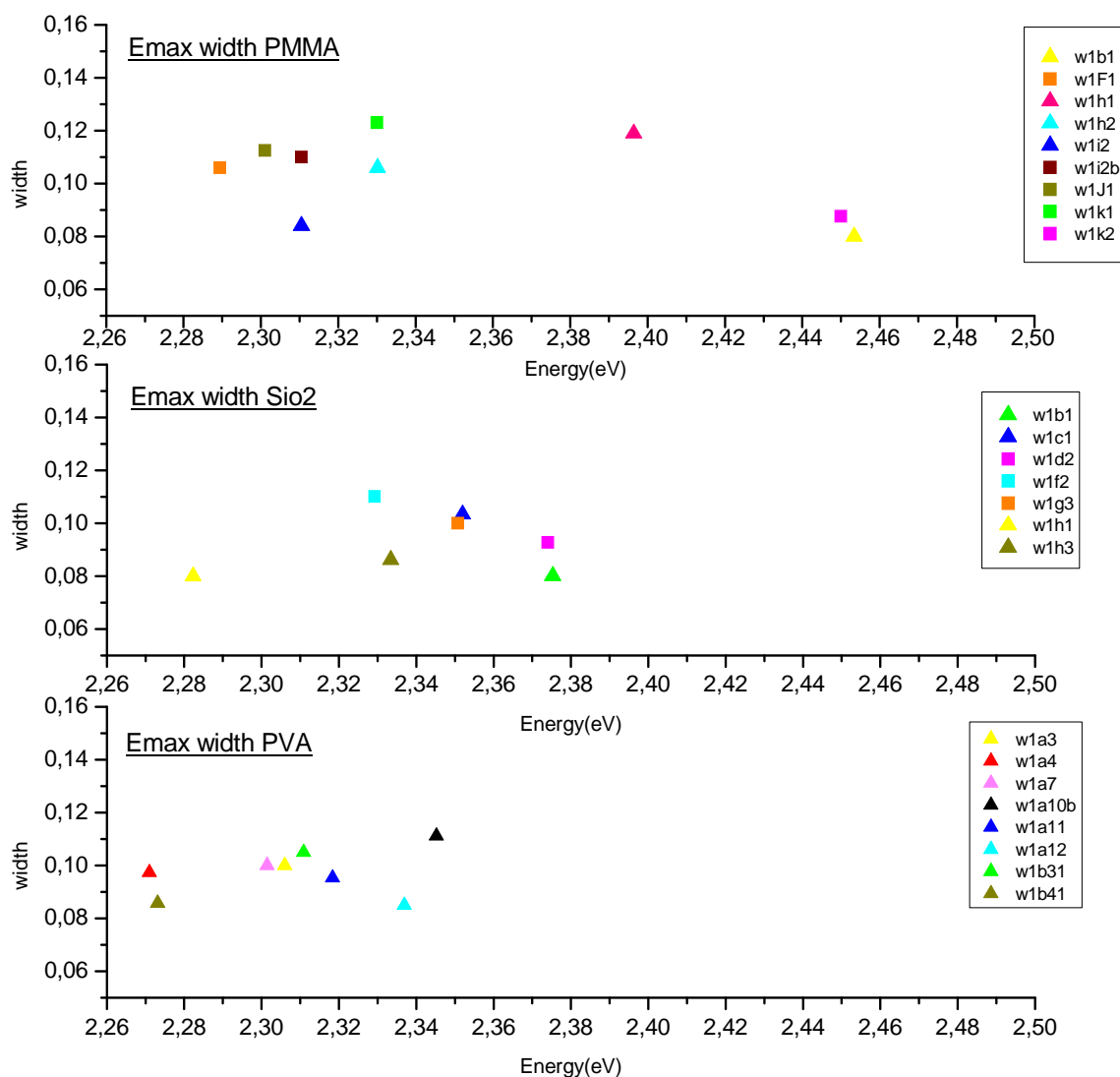
Figure IV- 32 ZPL width in function of emission energy for Si Nc's fit with one Sio_2 phonon band(squares) or (Si+ Sio_2) phonon bands (triangles) in different media.

We see that the systematic feature of decrease of width with increasing energy has become much less visible by considering the ZPL obtained with Si+SiO_2 fittings. This 'non feature' shape has also been proven experimentally, when Sychugov et al. confirmed having found no relationship between width and energy for ZPL at very low temperatures.[223]

iv) Si phonon width:

The difference between Figure IV- 31 and Figure IV- 32 may be understood if we take into consideration the variation of Si phonon line width with energy (and not the ZPL one). In

---

[223] Sychugov et coll., "Narrow Luminescence Linewidth of a Silicon Quantum Dot."

fact if we come to trace the widths variation of the Si phonon respectively for each nanocrystal, we obtain the following:
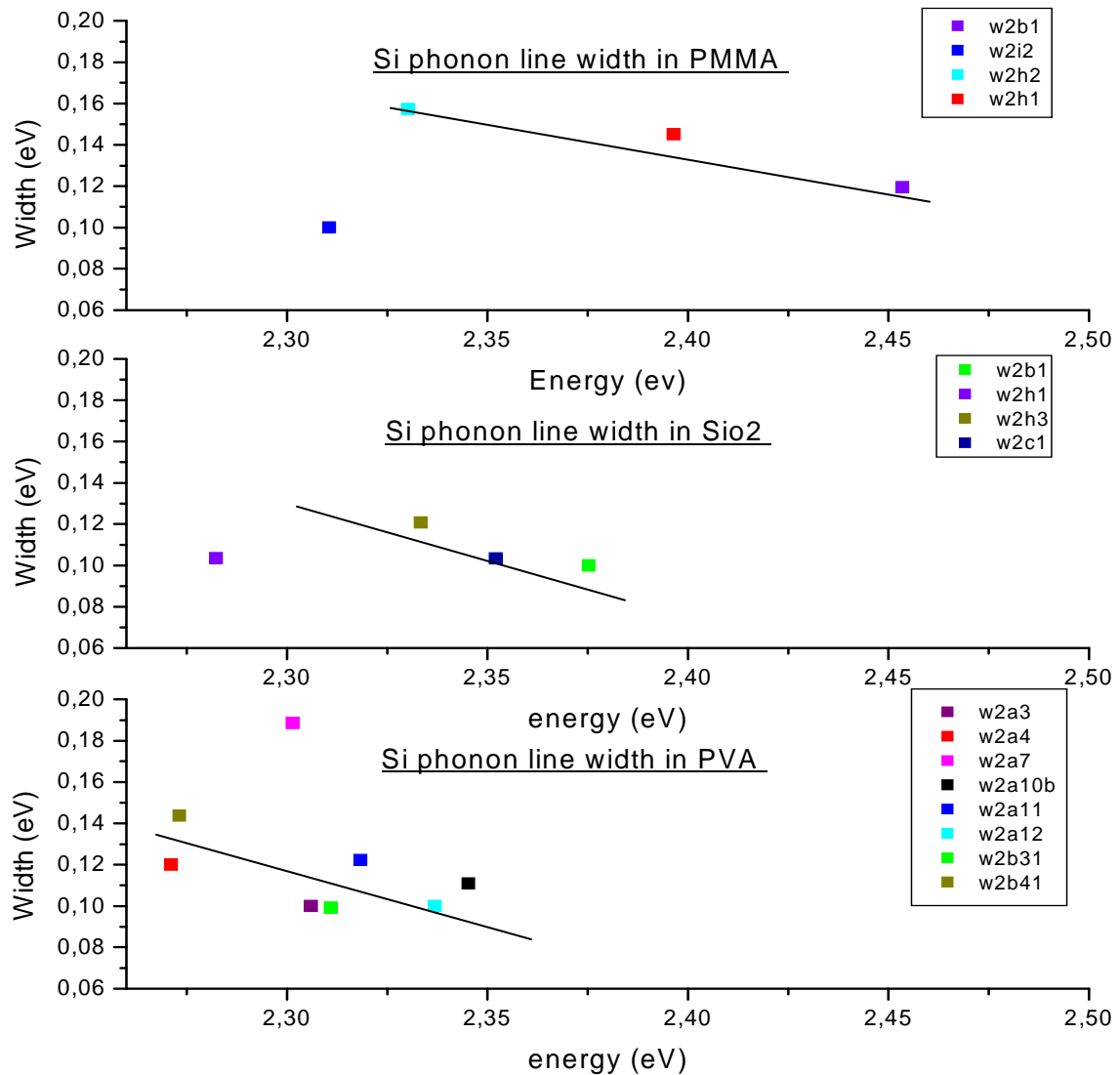

Figure IV- 33: Si phonon line width in function of emission energy for Si Nc's fit with (Si+ Sio₂) phonon bands (triangles) in different media.

v) Relating width behaviour to nanocrystal size

We see that the general tendency or behaviour (and mostly in PVA) is a decreasing relationship with increasing energy (the lines have been place for eye following) resembling to that obtained only by considering SiO_2 phonon fitting in figure 5. This kind of relationship is in agreement with the model of $Si+SiO_2$ phonon coupling, since, in this case, as the emission energy increases, the size of the nanoparticle will decrease, and

so will the Si core size and thus contribution (we feel more the effect of the shell).Its influence is reflected by the Si phonon width, which decrease as seen in Figure IV- 33.

Also, another explanation for such behaviour can be considered when looking at resonant photoluminescence studies. In fact, these have proven an increased probability of no-phonon transition probability with a decrease size of the Si nanocrystal.[224] In other words, with increasing energy, electron-phonon coupling to the intrinsic Si phonon is going down since the transition becomes optically more allowed, and this is also what we see in figure IV-17 since we explicitly have a decreasing Si phonon line going down as the size of the nanocrystal increases. If we try to do a little scheme to this, the following would be happening:
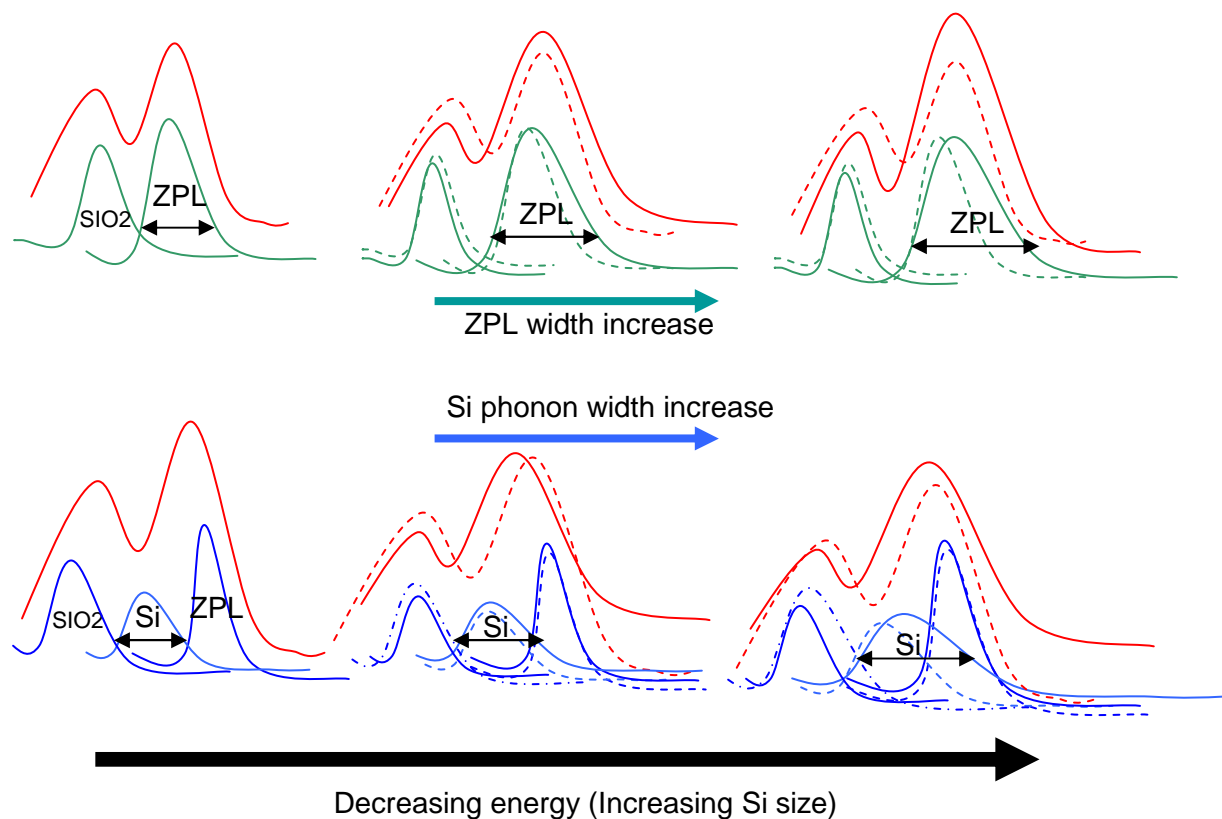

Figure IV- 34 : Comparison of different width variations with increasing Si size for the two fitting procedures

[224] Johannes Heitmann et coll., "Excitons in Si nanocrystals: Confinement and migration effects," *Physical Review B* 69, no. 19 (Mai 21, 2004): 195309

The first row would represent what we are seeing inFigure IV- 30 (Without considering explicitly the coupling with Si phonons). The second one would represent what is happening Figure IV- 32 (after seeing explicitly the effect of Si phonon coupling).

Also, if we look at the range of the two different measures we obtain (with and without Si phonons) the following: The range of width of Si phonons is broader than that of the ZPL after applying (Si+SiO$_2$) fitting, and so would their influence be more important on width variation.

	ZPL width (Si+SiO$_2$ fitting)	(Si width)
PVA	0.08-0.11	0.09-0.14 eV
SiO$_2$	0.08-0.11	0.08-0.14 eV
PMMA	0.08-0.12	0.09-0.16 eV

The range of width of ZPL considering Si + SiO$_2$ fitting is smaller than that while considering SiO$_2$ fitting only, since in the last one we are implicitly also considering the Si phonon into consideration. However for PMMA, this is more or less visible since the number of points which can be fit with Si+SiO$_2$ is less.

	ZPL (with SiO$_2$ fitting)	ZPL ((Si+SiO$_2$) fitting)
PVA	0.10-0.14	0.08-0.11
SiO$_2$	0.08-0.12	0.08-0.105
PMMA	0.08-0.125	0.08-0.12

If we now look at the SiO$_2$ phonon line by itself, we see that an increase in the size of Si nanostructure implies a decrease of the effect of SiO$_2$ shell, and thus a decrease of the width of the SiO$_2$ phonon itself. This is actually what we observe when we plot the variation of SiO$_2$ phonon width with emission energy.
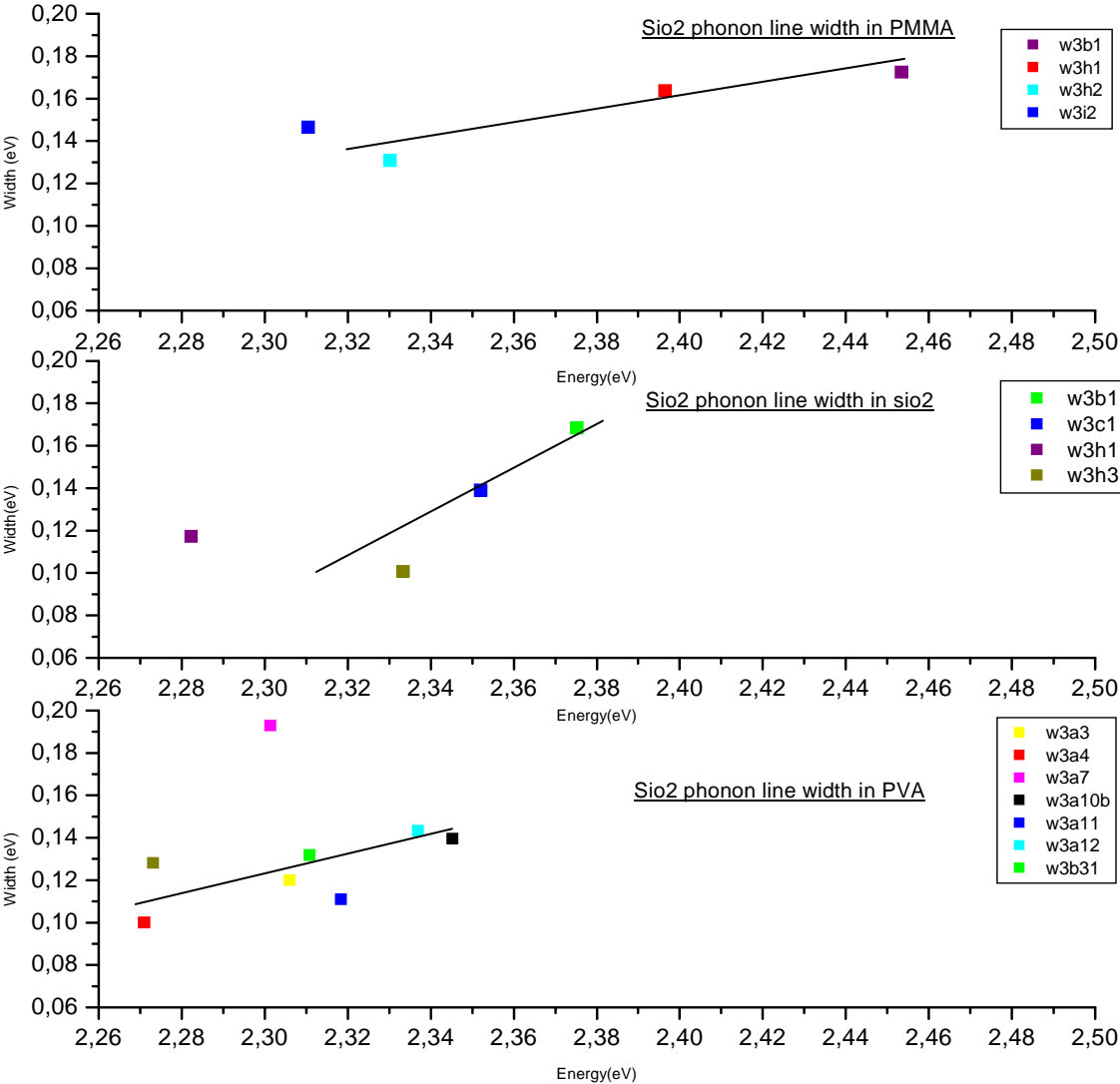

Figure IV- 35 Sio$_2$ phonon line width in function of emission energy for Si Nc's fit with (Si+ Sio$_2$) phonon bands (triangles) in different media

In the following we illustrate a summary for all previous explanations in the following: the main idea to be concluded about this part would be that, we have explicitly shown that for nanoparticles having a coupling involving Si phonons (better fitting with SiO$_2$+Si than only Si) the decrease of the ZPL line width with energy is due to that of the Si phonon, which itself is due to the fact that smaller nanocrystals have less Si influence, and thus a smaller width; SiO$_2$ phonons width, on the contrary, increase with energy at the same time. This also reinforces the statement that we obtained through the Klein et al.

relationship with phonon frequencies variation with emission energy, concerning the importance of the influence of Si core as the nanocrystal size increases. It indirectly also confirms again the importance of the roles of both quantum confinement and surface chemistry in the emission properties of light from Si nanocrystals.
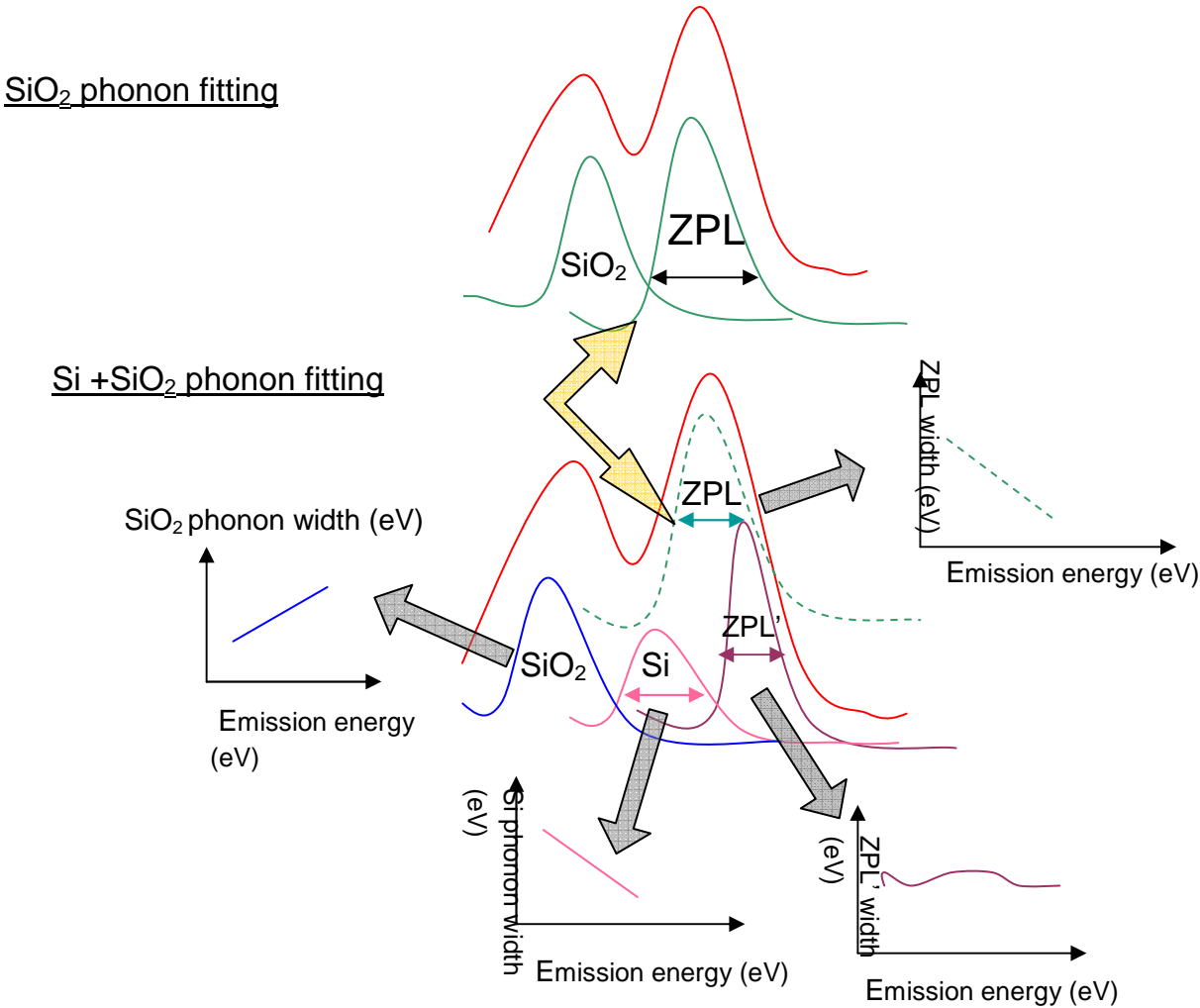

Figure IV- 36 Summary of different widths variation taking place in function of Emission energy

We have also seen that Si nanocrystals surrounded by a highly localised electric environment would be 'encouraged' to have more coupling with both Si and SiO_2 phonons rather than only SiO_2, since the nanoparticles embedded in PVA, which is the material having the highest dielectric constant among the rest tend all to a better fitting while taking into consideration both Si and SiO_2. An essential point would be to understand why it behaves in this way, and the different elements entering in action.

d) Huang-Rhys variation:

As we previously explained, the Huang-Rhys factor(S) calculation is of essential importance for understanding the different processes taking place in the nanocrystals structure, since it provides an idea about its electron-phonon coupling. Martin *et.al*[225]. previously plot the variation of Huang Rhys factor with ZPL emission energy. From their results they had drawn an important conclusion concerning the variation of the Huang-Rhys factor with nanocrystals size[226], especially in the special case of a localisation, which can be approximately summarized from larger crystals to smaller ones as in the following (The absolute values of H.R factor are not considered) :

At first, HR is strong for large crystals since the electron and hole are at a large distance one from another. Then, as the nanocrystal gets smaller, the distance between electron and hole decreases, and so will the Huang Rhys factor. However, at the localisation of the electron, the average distance R between the electron and hole will be suddenly increased to about half the diameter of the nanocrystal. At the same time, (S) will also rapidly increase. Then, as we continue decreasing the size, (S) will again decrease, until the second localisation : that of the' hole ', will take place again, where this time, the average distance R (and thus S) will increase to a distance larger than d/2 (d being the radius of the silicon nanocrystal). Finally, as the size is further decreased, the phonon coupling will also decrease, and so will the H.R.

We tried to follow the same scheme as that pursued by Martin et Al, in order to see whether we also had a similar behaviour with our PMMA, Sio_2 and PVA samples. We thus decided to plot the variation of the Huang –Rhys factor with respect to the emission energy, for the different emission spectra we obtained. Figure IV- 37 corresponds to the scheme we obtain by considering only SiO_2 phonon lines for each spectrum. One may discern two kinds of tendencies, either one in which there is only a constant increase of the HR factor with increasing energy, or one in which we have both its increase and decrease, as shown in the drawn lines. The difference is most probably due to a different view in range variation. The lines within the figure only serve as a follow up for the eyes to denote this last tendency in the behaviour of the Si nanocrystals, and the coming discussion will be based upon it .

[225] Martin et coll., "Electron–Phonon Coupling and Localization of Excitons in Single Silicon Nanocrystals."
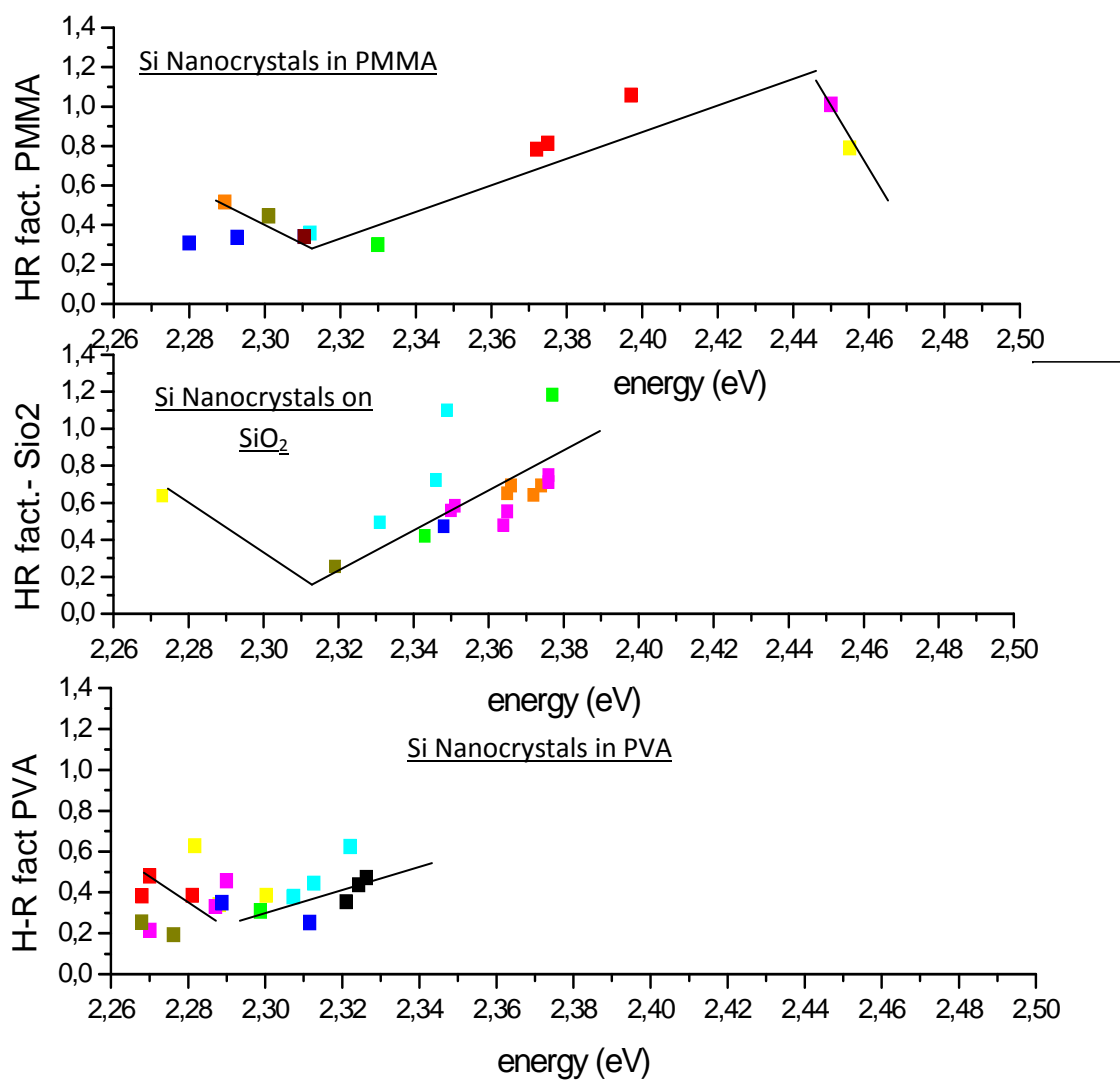[226] Ibid.

Figure IV- 37 Si0₂phonon Huang-Rhys for Silicon nanocrystals in PMMA, Sio₂, PVA with (Sio₂) fitting

We can already discern a general tendency in the three cases which resembles that of the previous discussion. If we now consider the different fittings we obtained, that is, spectra having (Silicon +Sio₂) phonons (represented by triangles) or (2× Sio₂) phonons (represented by squares) as in Figure IV- 32, but with only one point in time for each . We obtained the following:
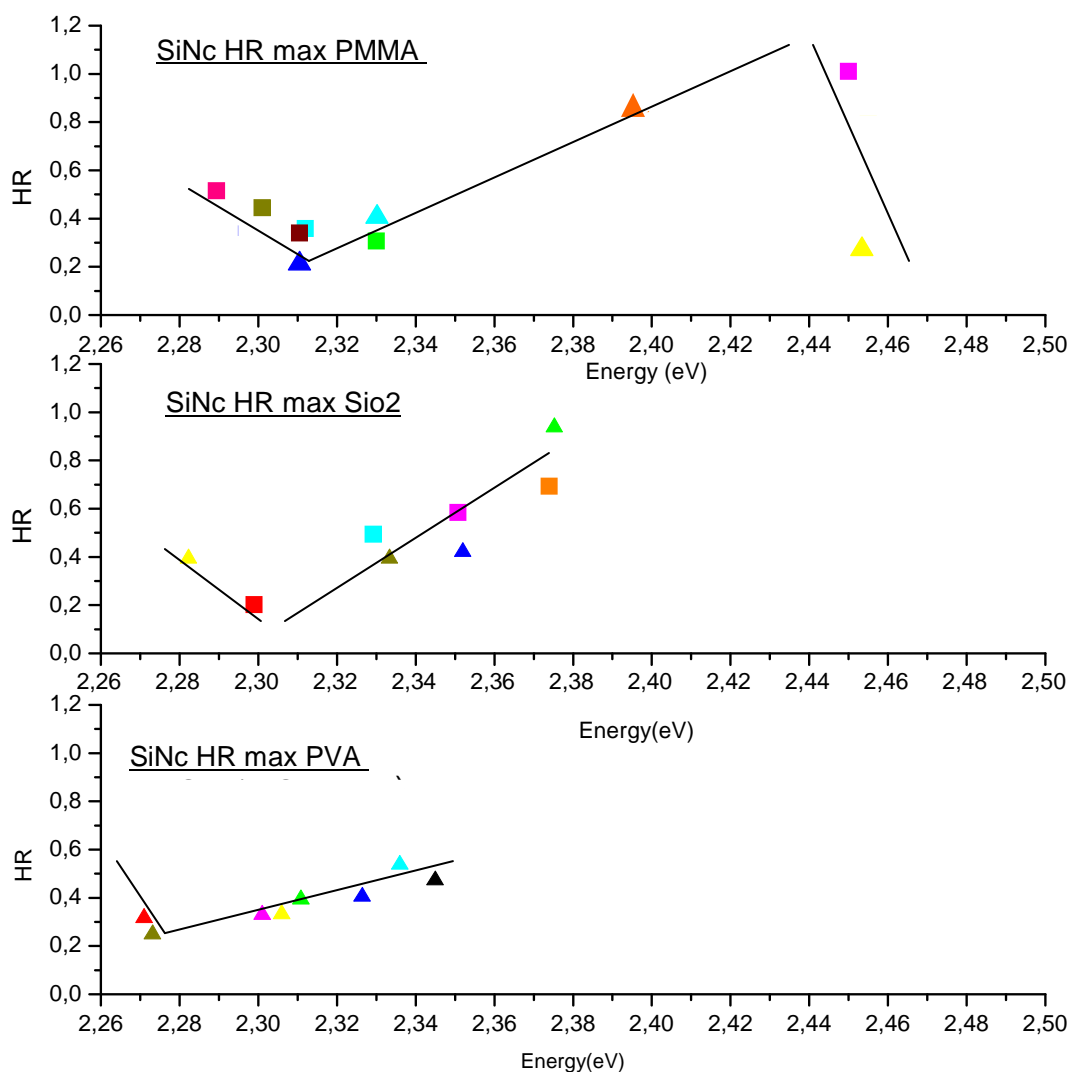
Figure IV- 38 Si0$_2$phonon Huang-Rhys for Silicon nanocrystals in PMMA, Sio$_2$, PVA with (Si+Sio$_2^)$ and Sio$_2$ fitting

The same kind of behaviour is almost obtained as that of Figure IV- 37: For PMMA, we see in Figure IV- 38 that as the nanocrystal size decreases (emission energy increases), the Huang-Rhys factor first decreases, then increases and decreases again. On Sio$_2$ and in PVA it is mostly a decrease followed by an increase. Even thought we can discern such tendencies with the follow up lines we draw on the graphs, we must remember that the Huang-Rhys factor value at certain energy is somewhat more or less precise, and is exposed to a large amount of fluctuations, as has been already mentioned by Martin. *et.al.* In fact as they already precised [227], determining an accurate value of (H.R*)* factor can be hampered by distorted spectral line shapes. Also, large fluctuations of the (H.R) factor at certain photoluminescence energy were found as being assigned to variations of

---

[227] Ibid.

(S) from nanocrystal to nanocrystal and time dependant spectral fluctuations. The first (variation of H.R) is due to the difference of the SiO_2 shell's inhomogeneous structure from nanocrystal to nanocrystal, while the second (spectral variations) been assigned assigned to a charging of the Si nanocrystals. The graphs in Figure IV- 37 and Figure IV-38 compromise such fluctuations for the reasons cited above, but the general behaviour can still be seen by the guiding lines. We see that for PMMA we are in the range where the electron has already localised, and the hole localisation would be staring soon. The same minimum has been found for Si nanoparticles embedded on SiO_2, and a bit smaller one for PVA (about 2.27 eV). We must precise that the number of studied points in our context could not allow us to see the entity of the behaviour which is illustrated in *Martin's* work. In fact in our case, for each kind of media we had about 8-9 nanocrystals that were studied while in *Martin's*, the Huang Rhys factor was calculated for about 55 nanocrystals in PMMA, making the studies scale a much larger one. For the cases of PVA and SiO_2, the decrease after hole localisation isn't reached yet. However one special point attracts our attention concerning the PVA media: The Huang-Rhys values for the PMMA and SiO_2 cases appear to reach values close to 1 upon hole localisation, however in the PVA media, it seems as if hole localisation is retarded, since the corresponding Huang-Rhys is moderately smaller than in the other two matrices (it reaches a maximum of 0.6). Such behaviour can be explained in terms of the effect of the dielectric environment on the emission of the silicon nanocrystals as in the following: The high value of the dielectric constant of the PVA matrix results in larger polarization of the SiO_2 shell, with a more negative outer shell (or boundary) PVA/ SiO_2 and a more positive inner shell SiO_2/Si as seen in the following figure.
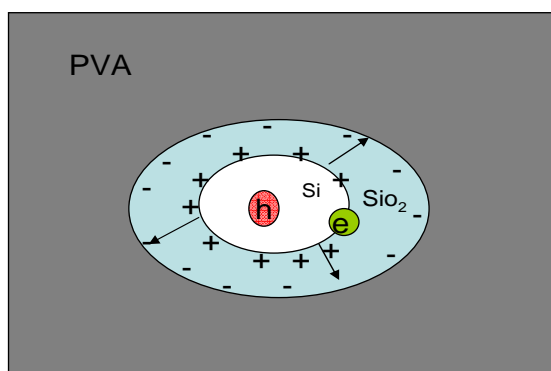
Figure IV- 39 Representation of electric behaviour of Silicon nanoparticles in PVA

This would thus prevent the hole to become localised in the shell, and will keep the exciton on average more in the Si core, leading to a smaller value of the HR (SiO_2) upon

hole localisation. At the same time, an increase of the HR of the Si phonon is expected. In fact, if we now try to look at the Huang- Rhys variation of the Si phonon line with energy, we have the following Figure IV- 39.
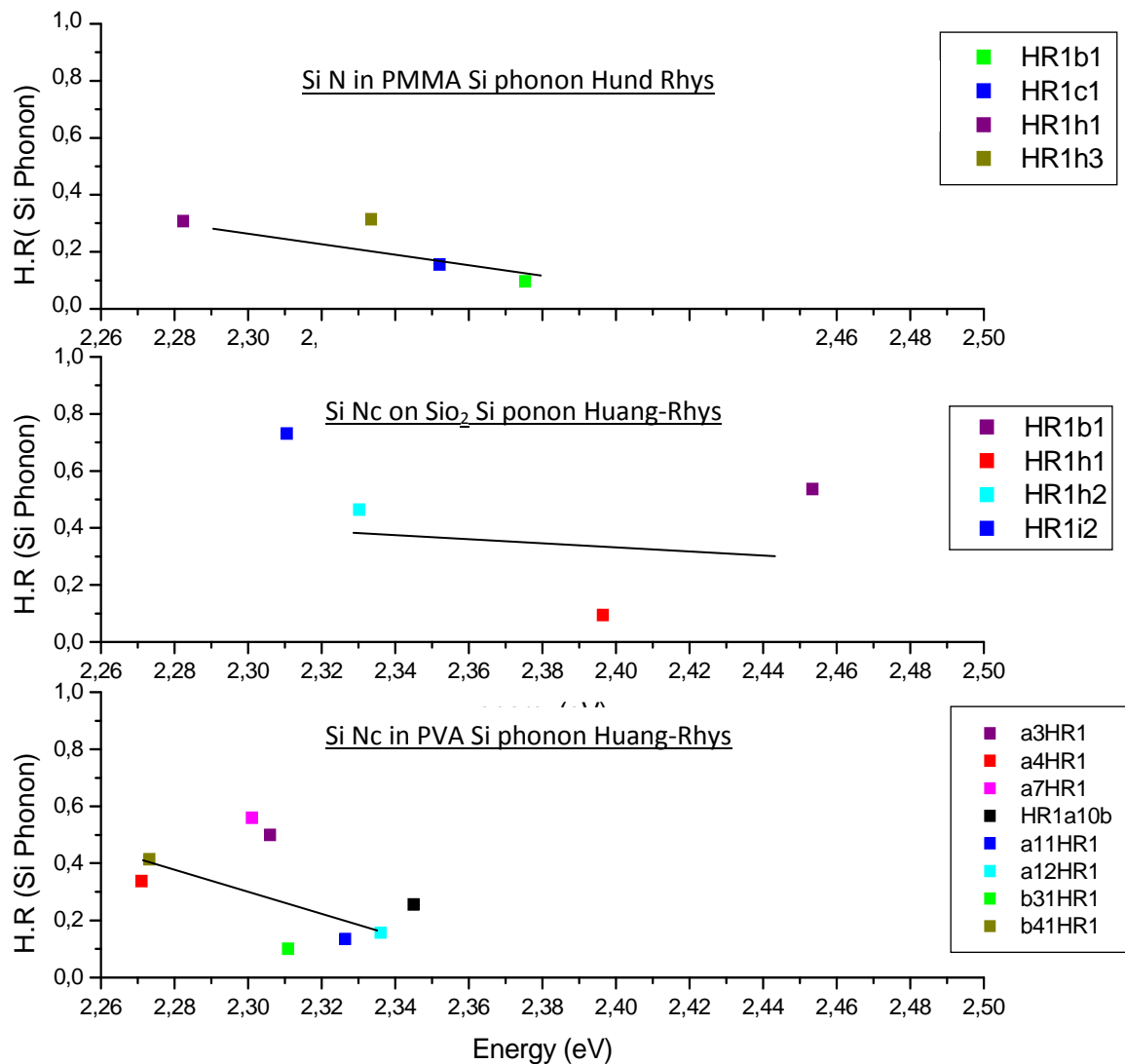

Figure IV- 40 Si phonon Huang-Rhys for Silicon nanocrystals in PMMA, Sio$_2$, PVA

In all of the three cases, we see in general a decreasing Huang-Rhys factor value with increasing energy. Such a relationship is already expected, since in this case, the main factor we consider is the distance between electron and hole, which is directly related to

the size of the nanocrystal.. For larger nanocrystals, the distance between electron and hole increases, what usually happens is that the more we have increasing field strength due to a separation of electrons and holes, the stronger are the lattice distortions and thus the bigger is the Huang Rhys factor. Such kind of behaviour has already been observed by Heitmann *et.al* [228]. This is the tendency which appears to be the most present in our graphs, where as the Huang-Rhys factor seems to diminish as the energy increases (or as the size decreases). For PVA however, the slope of the plotted line seems to be steeper than that in the other two media, referring to the property we last talked about, of a higher Si phonon coupling in PVA due to a higher polarisability.

It is important to note that it is this same effect which can be the cause of the typical emission time trace of Si nanocrystals in PVA (sharp on time traces with longer off times) as in Figure IV- 15. In fact, what would be happening is that as the shell is more polarized, the electron of the electron-hole pair would be more easily trapped in the shell, while the whole would be repelled. This would be the cause of a longer OFF times and much shorter ON ones; just like the ones resembling what we obtained in the PVA case.

d) Stark effect:

An interesting subject which we would like to mention quickly is the ZPL width fluctuations in time of a single nanocrystal when it emits. Even though such an area is worthwhile a deep investigation, we will present here some short results about the emission characteristics of a single crystal, which would help us have an idea about the Stark effect, and its consequences on the emission properties of silicon nanocrystals.

If we take a look at Figure IV- 30, we see a certain tendency of width variation with time for each of the colored spots, i.e for each one of the nanocrystals.. We will separately take few spots from each case and represent them in the following figures:

---

[228] Johannes Heitmann et coll., "Excitons in Si nanocrystals: Confinement and migration effects," *Physical Review B* 69, no. 19 (Mai 21, 2004): 195309
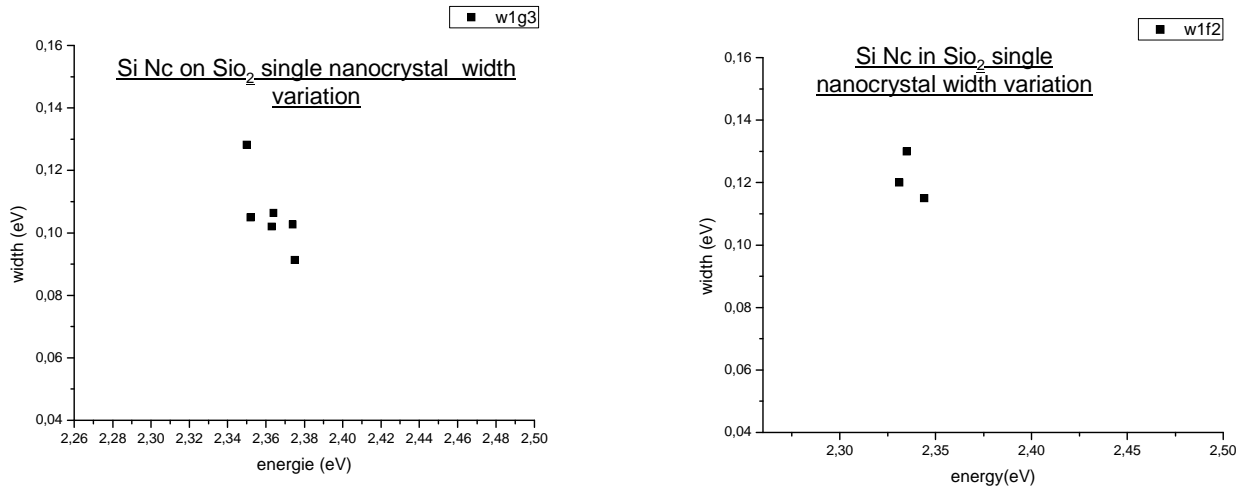
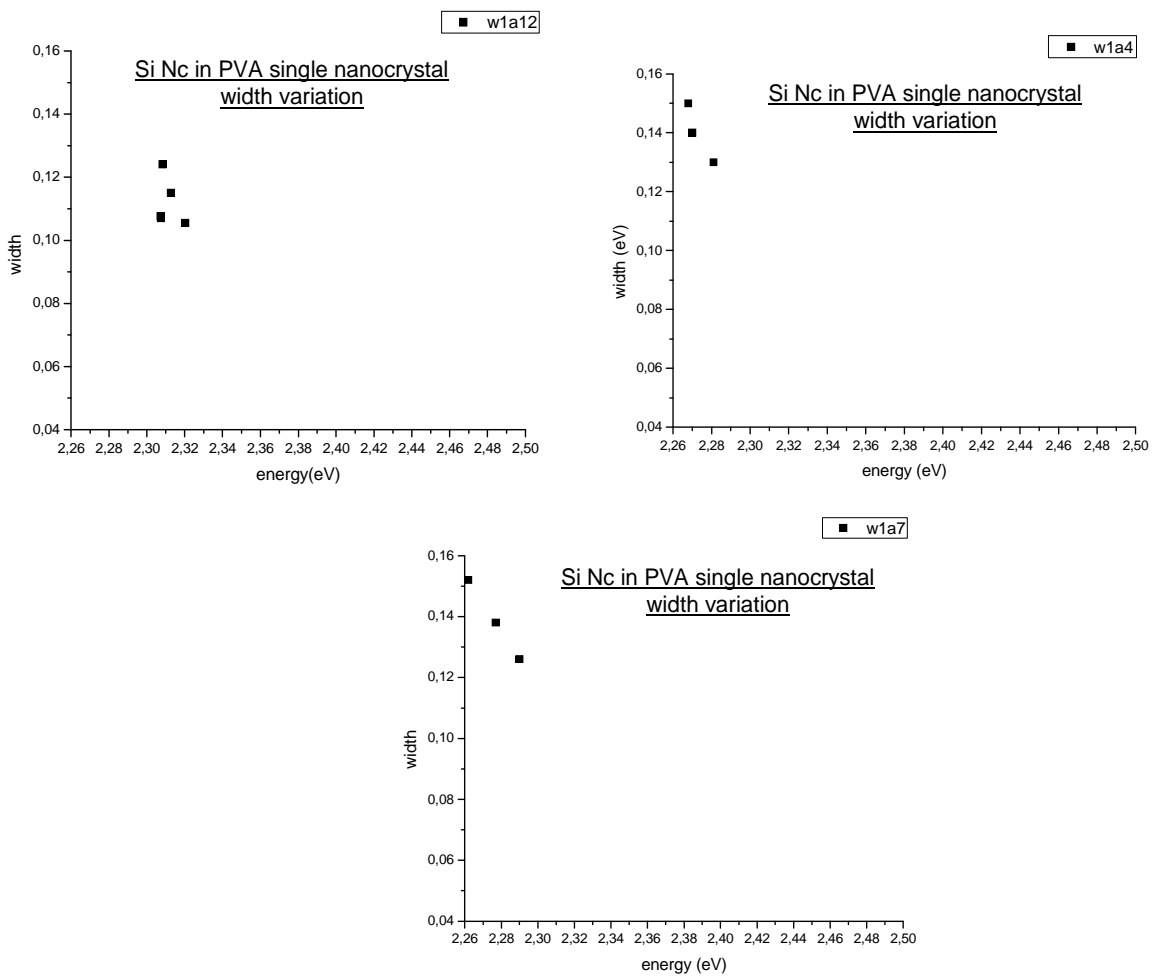**Figure IV- 42 Width variation in function of energy for different single nanocrystals on Sio₂**

Figure IV- 41 Width variation in function of energy for different single nanocrystals in PVA

Each graph in Figure IV- and Figure IV- 41 represent the variation of the width of the ZPL of one single Si nanocrystal as its emission energy peak increases. In the first case we deal with Si nanocrystals on SiO_2 , while in the second the nanocrystals are embedded in PVA. The PMMA case has too few points, so that a single nanocrystal spectral diffusion study of Silicon in such a medium seemed to be very hard for drawing effective conclusions. We have only chosen a few points for each case as an illustration, but the tenancies are generally the same for all the nanocrystals of the same medium. What we notice by looking at the different graphs is that the widths of the zero phonon lines seem to decrease as the emission energy of the nanocrystal increases. Such a behaviour has been previously found for semi conductor nano-objects and has been assigned to stark effect (or quantum confined stark effect)[229],[230]. This phenomenon happens when the Si nanocrystal is surrounded by an electric field, may it be an external one (by using electrodes on the sample) or an internal one (due for example to net surface charges on the surface of a nanocrystal). In our case, as we explained in the Huang-Rhys factor section, the polarisation of the nanocrystals may be arising from the interaction of the non uniform charge density distribution of the electron and hole and the dielectric nature of its environment. Even thought the data we have are still too scarce to draw a final conclusion about the different emission mechanisms taking place, we can however be sure that the spectra red shifted variation are related to an increase of the Huang –Rhys factor, which itself causes the broadening of the phonon line. An interesting suggestion for further studies would be to look closely at the differences between these effects in the PVA media or on the SiO_2 substrate, which would help us understand the influences of the Si nanocrystals environing media with much more detail.

Conclusion:

In this chapter, we have presented results concerning optical characterization of pyrolised silicon nanocrystals. After a topographic and crystallographic characterization, a clearer idea could be assessed about their dimensions, where the measures done showed that the nanocrystals were so small (Si core about 3nm) that an assumption of breakage of quantum confinement rule could not be excluded from the mechanisms contributing to their emission. A possible case of electron-phonon localization in the shell of the nanoparticles could be indeed considered. In fact, we proposed a new mechanism taking place during the emission of a nanoparticle, which would take into consideration a

---

[229] "Monitoring surface charge migration in the spectral dynamics of single CdSe∕CdS nanodot/nanorod heterostructures," *Physical Review B* 72, no. 20 (2005): 205339

[230] S. A. Empedocles et M. G. Bawendi, "Quantum-Confined Stark Effect in Single CdSe Nanocrystallite Quantum Dots," *Science* 278, no. 5346 (Décembre 19, 1997): 2114-2117

coupling with both Si and SiO$_2$ phonons, instead of only Si or SiO$_2$ phonons. The nanocrystals were placed in media having different electronic constitutions, and it was found that the dielectric neighbouring of each nancrystal affected its emission properties, whether concerning the time trace shape or emission characteristics, through a depicting of the Huang-Rhys factor variation. Finally, concrete evidence of stark effect presence could be confirmed through the variation of the ZPL width for a single nanocrystal, through time. A final important note to take into consideration is the fact that due to the very low signal emitted by the Si nanocrystals, a difficulty was encountered in collecting a significant number of data points. More profound studies and a bigger number of data points would surely help into knowing more about the emission properties of the nanocrystals and the effect of the environement on them.

The present work can be divided into two distinct parts, according to the type of nanoparticles investigated and the tool which was used to study them. The first kind of studies concerning nanohybrid particles, which can be considered as a demonstration for the applications of physics in biosciences has taken place in France at the LPCML laboratory and Nanoptec center in Lyon. The second kind, more of a fundamental nature, and treating with silicon nanocrystals, resulted from a collaboration which has taken place through the European Research Network 'NANOLUM'. This time the nanoparticles were produced at 'Jena University'(Jena-Germany) and were studied by confocal microscopy at 'Chemnitz Technical University' (Chemnitz- Germany). Even though seemingly far from each other, both subjects show the considerable importance of nanoparticles, and the impact they can have on the advancement of science, and technology.

We have acquired an idea about the importance of the intercrossing of different types of sciences while studying the nanohybrids in near field optical microscopy. For example, a first technical difficulty consisted of finding an easy, fast and reliable way to study nanoparticles which were initially presented to us in the form of a solution. Our referring to surface science helped to resolve the problem, by opting for the spin coating deposition method and trying to reach the optimum condition for the homogeneous dispersion of the nanohybrids on a substrate. The near field microscope also showed once again itself to be an essential tool for bioscience investigations. Where, after having studied the attainable resolution (about 50nm) of the near field setup we were using, and having proven the genuine nature of the optical images we acquired, we validated the importance of such a tool for bio sensing applications. In a first case, we proved possible the detection of streptavidin proteins on a gold substrate, after their binding to biotin molecules (which were attached on the surface of the gold plots), and studied the effect of excitation wavelength variation on the emitted light. We also observed localisation of Surface Plasmon Resonance hot spots on the peaks of the hemispheroidal shaped gold nanoplots. This has been done by referring the SNOM illumination reflection mode configurations. Also, we demonstrated the ability of the SNOM tool to detect the luminescence of hybrid nanoparticles by using the guided mode excitation configuration. We were able to attain small scale resolutions with this method, were nanoparticles aggregates in the order of 100 nm were easily detected on the surface of the waveguide. This constitutes an essential opening to a new evanescent wave biosensors tool. However, even though we proved successful the considerations of near field optical microscopy as an means for attaining a bio sensing detection role, one must say that we were faced to many difficult technical problems which hindered the advancement of the

work; Trying to surmount them lead to a drastic improvement of the results. For example, as we showed it chapter III, the rough topography of the channel glass waveguide prevented us to obtain clear images, and we had to opt for the planar waveguide excitation in order to resolve such a problem. Of course other technical problems related to the setup itself were encountered, and mostly concerning the fabrication and manipulation of SNOM tips, however those constitute the general main problem in aperture SNOM imaging. We should finally take notice that much more improvements and many new configurations could open the road for a perfection of the obtained results. For example, different types of waveguides having a smoother topography and better optical properties could be used. Other new configurations such as the total internal excitation of the gold plots through their deposition on the surface of the waveguide, or even using other kinds of nanohybrids can also contribute to a wide range of new possibilities and an improvement of the results.

The Silicon nanocrystals studies were experimentally performed in Germany. In this case, the utilisation of the confocal microscope helped elucidate many optical aspects of silicon nanocrystals emission. The single nanocrystal studies allowed us to examine the properties of separated silicon nanocrystals, and to have an idea about the impact of the nanoparticles environment on its emission response. A clear impact of the dielectric nature of the embedding medium on the nanoparicles was figured out through time trace and emission spectra examination. Also, a new kind of coupling involving both Si and SiO_2 phonons was proposed and seem to be eligible with the obtained results. Finally stark effect impact was clearly seen on the width variation of the zero phonon line of the emission of single nanocrystal spectra. As for the near field measurement case, the confocal measurements also presented technical difficulties which were, this time, related to the low emission yield of such silicon structures. This resulted in a low number of data point, which, however showed well specific tendencies that are characteristic to silicon nanoparticles. New ways of improving the obtained results can be done by utilising new experimental tools, for example changing the excitation wavelength into more blue shifted values, or more sensitive detectors. Also, an interesting point would be to perform near field optical spectroscopy on silicon nanoparticles, since new kind of pertinent information could be obtained with such a tool, with probably a better resolving power. Excitation of the nanocrystals through waveguide mode configuration is also an important alternative to be considered. Even thought there still exist an important controversy in the scientific society concerning the emission mechanisms which are ruling silicon nanoparticle excitation, we believe that our results may lead to an improvement in the understanding of such phenomena.